University of Strathclyde

Department of Naval Architecture and Marine Engineering

A RISK-BASED SHIP DESIGN APPROACH TO PROGRESSIVE STRUCTURAL FAILURE

Seungmin Kwon, MSc. BSc.

Thesis submitted to the University of Strathclyde in fulfilment of the requirements for the degree of Doctor of Philosophy

Glasgow, May 2012

COPYRIGHT STATEMENT

ACKNOWLEDGEMENTS

I would like to express my heartfelt gratitude to Prof. Dracos Vassalos, the supervisor of this thesis, for his support, guidance and encouragement throughout the course of this study. His insight and inspiration on the topic have been precious.

I also want to express my appreciation to Dr. George Mermiris for his continuous help and advice. The discussion we had on the topic has been served as a solid foundation until finalising this thesis.

Mr. Nan Xie has provided wave loading calculation with respect to the provided wave data. His support on this and general discussion are highly appreciated. I am also thankful to colleagues at the Ship Stability Research Centre (SSRC), Dr. Andrzej Jasionowski, Joonyun Kang, Nikolaos Tsakalakis, Wenkui Cai, Qi Chen, Przemyslaw Zagorski, Romanas Puisa, Jakub Cichowicz, Khaled Mohamed, Yasmine Hifi, Susan Hamilton for their hospitality and friendship during my study.

It is a pleasure to thank to Mrs. Thelma Will for her help with the administrative work from the application for the degree to the preparation and submission of my thesis.

Best of all, I am deeply indebted to my wife, Yoonjeong, my children, Sarah and Eunwoo, and my parents for their support, endurance, encourage and love in the course of my study. I should stress that this achievement would have never been successful without them.

The financial support of Daewoo Shipbuilding and Marine Engineering Co. LTD. (DSME) is highly acknowledged.

ABSTRACT

Although substantial effort has been devoted in the design process of ships to reduce the operational risk level by preventing and mitigating accidental events, the societal expectation on the safety at sea is growing faster than ever. The framework of the *safe return to port* for passenger ship safety reflects this trend in pursuance of zero tolerance to loss of human life in the event of an accident. Along these lines the emphasis of the survivability of a damaged ship is placed on the damage stability and the hull girder collapse under the explicit assumption that the initial damage extent is fixed. However, in practice it is often observed that progressive degradation of the damaged structure threatens the survival of a ship by causing significant reduction of its strength, as it was witnessed in the loss of *MV Prestige*.

Hence, the information of progressive structural failure in timeline and its effect on the hull girder residual strength is of paramount importance in the course of evaluating survivability of a damaged ship and mitigating the ensuing consequences. This provides an obvious objective for this study, which is the elaboration on a method for progressive structural failure analysis under time varying wave loads and the development of a parametric tool for fast and reliable assessment of the structural survivability of a damaged ship with respect to the damage propagation.

The developed tool provides the probability of unstable damage propagation over time, from which the window of safe intervention in emergency operations can be extracted and support the decision-making process in the course of the rescue and salvage operation. Moreover, this work also sets the foundation of a new dimension in the early ship design phase, namely the structural survivability with respect to the progressive structural failure. In this way, it contributes to the holistic safety assessment approach advocated by the *design for safety* philosophy and the *risk-based ship design* methodology. The developed tool is fully parametric so as to support decision-making both in the emergency operations, where fast and reliable information is required, and in the early design stage, where various damage cases need to be assessed in order to administer appropriate structural design solutions.

TABLE OF CONTENTS

ABBREVIATIONS

ABS	American Bureau of Shipping
A/B	Above Baseline
ALPS/ISUM	Analysis of Large Plated Structures using the Idealized Structural Unit Method
A.P.	After Perpendicular
ASTM	American Society for Testing and Materials
BM	Bending Moment
BS	British Standard
CCT	Centre Crack Tension
CDF	Cumulative Distribution Function
CFD	Computational Fluid Dynamics
CG	Centre of Gravity
C.O.T.	Cargo Oil Tank
COV	Coefficient of Variation
CSR	Common Structural Rule
DEXTREMEL	Design for Structural Safety under Extreme Loads
DWT	Deadweight Tonnage
FE	Finite Element
F.P.	Forward Perpendicular
FPSO	Floating Production, Storage and Offloading
GM	Metacentric height

HSLA	High Strength Low Alloy
IACS	International Association Classification Societies
ISSC	International Ship and Offshore Structures Congress
ISUM	Idealized Structural Unit Method
JBP	Joint Bulker Project
JTP	Joint Tanker Project
LBHD	Longitudinal Bulkhead
LEFM	Linear Elastic Fracture Mechanics
MC	Monte Carlo
MPC	Multi Points Constraint
N.A.	Neutral Axis
QT	Quenched and Tempered
RAO	Response Amplitude Operator
RP	Reference Point
SAFEDOR	Design, Operation and Regulation for Safety
SIF	Stress Intensity Factor
VCCT	Virtual Crack Closure Technique
VLCC	Very Large Crude Carrier
VOF	Volume of Fluid
WBM	Wave Bending Moment

NOMENCLATURE

a	Half crack length
a_0, a_f	Initial and final crack sizes
a_i, a_j	Sizes of shorter and longer asymmetric cracks in an L-shaped finite plate
a_P, a_S	Primary and secondary crack size including opening size in asymmetric propagation
$a_{0,P}$, $a_{0,S}$	Initial crack sizes of Primary and secondary cracks in asymmetric propagation
a_v, a_h	Vertical and horizontal crack size in an L-shaped finite plate
da/dN	Crack propagation rate
Δa	Length of the element
b	Radius of an elliptical opening perpendicular to cracks
b_e'	Tangent effective width of the plate
b_f	Width of the flange of the stiffener
b_p	Width of plate associated with the stiffener
b_{DS}	Width of double side
Δb	Width of the element
c	Radius of an elliptical opening parallel to cracks
d_w	Depth of the web of the stiffener
f_k	Koiter's finite width correction
h_{dam}	height of damage at side shell
h_{DB}	Height of double bottom

l	Span of the element
p	Uniformly loaded internal pressure in a centre cracked plate
r_{ce}	Equivalent radius of inertia of the element
r_p	Plastic zone size
s	Half of the stiffeners' space
s_i	Half stiffener space of *i*-th stiffener
s_c	Ratio of initial crack size to half of the total damage size of a circular opening, $S_c = a_0/(a_0 + R)$
s_e	Ratio of initial crack size to half of the total damage size of an elliptical opening, $S_e = a_0/(a_0 + c)$
s_L	Ratio of length to the sum of length and width in a finite plate, $s_L = L/(L + B)$
t_f	Thickness of the flange of the stiffener
t_w	Thickness of the web of the stiffener
t_p	Plate thickness
$t_{pl,i}$	Plate thickness relevant to *i*-th stiffener
u_{Ll}, v_{Ll}, w_{Ll}	Corresponding displacements behind the crack at the top face node row *l*
u_{Ll*}, v_{Ll*}, w_{Ll*}	Corresponding displacements behind the crack at the lower face node row *l**
x_i	Distance to *i*-th stiffener from centre of crack
x_i'	Distance to *i*-th severed stiffener from centre of crack
y_{ij}, z_{ij}	Horizontal and vertical distance from the origin of the section under the *i*-th curvature to the centre of the *j*-th element
$y_{g,ij}$, $z_{g,ij}$	Horizontal and vertical distance from the instantaneous centre of gravity of the section under the *i*-th curvature to the centre of the *j*-th element

A_j	Sectional area of j-th element
A_s	Sectional area of stiffener
$A_{st,i}$	Sectional area of i-th stiffener
ΔA	Virtually closed area of elements
B	Half width of a finite plate
B_{hull}	Breadth of ship
B_i, B_j	Widths of plates where the shorter and longer asymmetric cracks are embedded in an L-shaped finite plate
B_v, B_h	Vertical and horizontal width of an L-shaped finite plate
BM_y	Maximum yield bending moment
C, m	Material constants for crack propagation equation
ΔCG	Shift of the centre of the gravity required for force equilibrium in the section
D_{hull}	Depth of ship
E	Young's modulus of material
E_j	Young's modulus of the j-th element
$E_{st,i}$, $E_{pl,i}$	Young's modulus of stiffener and plate respectively
F_i	Total axial force of the section under i-th curvature
G	Strain energy release rate
G_I, G_{II}, G_{III}	Mode I, II and III components of strain energy release rate due to opening, sliding and tearing modes of fracture respectively
Hs	Significant wave height
I	Hull girder moment of inertia

I_{ce}	Moment of inertia of the element
I_P	Polar moment of inertia of the stiffener
I_T	St. Venant's moment of inertia of the stiffener
I_ω	Sectorial moment of inertia of the stiffener
K	Stress intensity factor
ΔK	Range of the stress intensity factor
ΔK_{th}	Threshold range of the stress intensity factor
ΔK_{th0}	Threshold range of the stress intensity factor at $R = 0$
ΔK_{eff}	Effective range of the stress intensity factor
ΔK_{eff_th}	Effective range of the stress intensity factor at the threshold level
K_{max}	Maximum stress intensity factor
K_{min}	Minimum stress intensity factor
K_R	Residual stress intensity factor
K_{op}	Crack opening stress intensity factor
K_{cl}	Crack closing stress intensity factor
K_C	Fracture toughness of materials
K_{IC}	Plane strain fracture toughness of materials
L	Half length of a finite plate
M_i	Total bending moment under i-th curvature
$M_{y,i}$,$M_{z,i}$	Total vertical and horizontal bending moments of the section under i-th curvature
$M_{y,ij}$,$M_{z,ij}$	Horizontal and vertical bending moments of j-th element under i-th curvature

N	Number of loading cycles
N_r	Required number of cycles
Q	Material constant related with yield strength
R	Radius of a circular opening
R_σ	Stress ratio
$R_{\sigma,eff}$	Effective stress ratio
SIF_0	SIF for centre cracked infinite plate, $SIF_0 = \sigma\sqrt{\pi a}$
$SIF_{geometry}$	SIF including the effect of 'geometry'
Tz	Zero-crossing wave period
U	Effective crack opening ratio
X_{Li}, Y_{Li}, Z_{Li}	Forces in X, Y and Z directions at the crack front in column L and row i
$Y_{geometry}$	Correction factor for the specific 'geometry' effect
Z	Section modulus
Z_{dk}, Z_{btm}	Section modulus at deck and bottom, respectively
α	Ratio of the secondary crack size to the primary crack size in asymmetric propagation
α_1, α_2	Constants characterizing the magnitude of the edge stiffener's restraint
α_r	Residual stress coefficient
β_i	Axial stiffness ratio of i-th stiffener to relevant plate
β_p	Plate slenderness
β_w	Slenderness ratio of web
ε	Element strain

ε_y	Yield strain
ε_{ij}	Average strain of *j*-th element under *i*-th curvature
$\bar{\varepsilon}$	Average strain of the element
$\overline{\varepsilon_{ij}}$	Average strain of *j*-th element under *i*-th curvature normalised by yield strain, ε_y
ϵ_{dof}	Degree of fixation
θ	Angle between the neutral axis and the x-axis of the hull cross section
κ_i	Curvature of the inter-frame section
$\kappa_{y,i}$, $\kappa_{z,i}$	Component curvature in the *y*- and *z*-directions respectively
κ_{max}	Estimated maximum required curvature
$\Delta\kappa$	Curvature step size
λ	Slenderness of the column
μ_i	Ratio of *i*-th severed stiffener's area to area sum of *i*-th severed stiffener and its associated plate
ν	Poisson's ratio
σ	Applied uniform stress
σ_0	Linear varying component of the applied stress
σ_{ET}	Euler torsinal buckling stress
σ_{max}	Maximum applied stress
σ_{min}	Minimum applied stress
σ_{res}	Residual stress
σ_y	Yield stress

σ_{ij}	Average stress of the j-th element under i-th curvature, κ_i
χ_i	Crack distance normalised by i-th stiffener
χ_i'	Crack distance normalised by i-th severed stiffener
$\Phi(\overline{\varepsilon_{ij}})$	Average stress of j-th element under i-th curvature normalised by yield stress, σ_o, at a normalised average strain of $\overline{\varepsilon_{ij}}$
Φ_{cb}	Load-end shortening curve for the beam column buckling
Φ_{cr}	Critical stress ratio of stiffener
Φ_{cw}	Critical stress ratio of web
Φ_{dw}	Ratio of the effective depth of the web
Φ_e	Edge stress ratio
Φ_{pb}	Load-end shortening curve for the plate buckling
Φ_{tc}	Load-end shortening curve for the torsional buckling
Φ_w	Ratio of the effective plate width
Φ_{wb}	Load-end shortening curve for the web local buckling
Φ_{EC}	Euler column buckling stress ratio
Φ_{EL}	Euler local buckling stress ratio of web
Φ_{ET}	Euler torsional buckling stress ratio
Φ_{JO}	Johnson-Ostenfeld stress ratio

1 INTRODUCTION

1.1 Preamble

This chapter introduces the subject of the research especially the background, the motivation of the work. It addresses an issue that has not received sufficient attention in the survivability assessment of damaged ships although its importance is continuously growing in the maritime industry for ships' survivability with respect to the emergency salvage operation and design aspects. Also, the description of the objectives of this research is presented followed by the scope of work.

1.2 The loss of *Prestige*, how it happened?

On Tuesday, 19th November 2002, the Bahamian registered tanker *Prestige* (Figure 1-1) split into two and sunk with a large amount of heavy fuel oil (76,972 tonnes) in her cargo holds. The vessel was sailing from Ventspils in Latvia to Gibraltar when it sustained hull damage on starboard side on 13th November 2002 because of large wave impact during stormy weather conditions. When she rapidly developed list of 20 degrees to starboard, two wing tanks of port side were intentionally flooded in order to correct the list, which was slowly reduced to around 5 degrees.

Figure 1-1: Sink of Prestige, the Guardian (www.guardian.co.uk)

Having lost her main engine power, she began taking on water and drifted towards Finisterre, Spain. The Master asked to take her to a place of refuge, however, the Spanish authorities ordered the vessel to be towed in a North-West direction away

from the coast. The repeated requests by the engaged salvage team for permission from the Spanish authorities to take the ship to a sheltered area were all denied as well. After 6 days of towing operations the ship was 130 miles away from the Spanish-Portuguese coastline when she broke in two and sank in deep waters.

It is believed that an estimated 63,000 tonnes of cargo has been released during the break up and the subsequent sinking of the tanker. Although the oil spillage took place in a deep sea far from the coastline, the spilled oil washed up to the coastline of Spain and Portugal causing an ecological disaster at the affected areas.

1.3 Survivability of ships in the emergency operation and design

Although nine years have passed since the disastrous loss of *Prestige*, debates on the decision to tow the tanker to the open sea still remain. It was argued that the vessel would have been saved and the environmental damage could be minimised if she was towed into a sheltered area. Others argued that a much greater catastrophe at the coastlines has been avoided with the decision made at the time by towing the vessel out to the open deep sea.

Considering the situation that the ship was damaged in severe weather condition, her breakup could have been anticipated and brought the eventual environmental damage to the highest concern. Being supported by the above information, the decision-making that took the tanker off away from the coastline could be justifiable. The information which predicted the breakup was correct but insufficient to support the decision-making for the best conclusion as it could not provide any relevant answer on the question, “When the breakup would take place?” It is no doubt that such information would have been crucial in the process of the salvage operation. Because the decision made on the *Prestige* case would have been different if it were predicted to survive for 6 days in the open sea as it did and even more if it were expected to survive in a sheltered area.

The survivability of ships has been the prime concern when the ships are damaged due to accidental events like collision, grounding and structural failure in severe weather conditions. The assessment deals with the chance whether the damaged hull structure would collapse (residual strength analysis) and whether the ship would

capsize if flooding is involved (damage stability analysis). Traditionally, these two analyses have been carried out independently with a strong assumption that the initial damage extent remains stable.

According to this approach, *Prestige* would have survived because i) her stability was improved when the port wing tanks were deliberately flooded and this could be supported by the fact that capsize, which should have taken place in the early stage, did not happen eventually, and ii) the residual strength of the ship was sufficient at the moment of the initial damage as she broke up after six days even though the wave conditions in the final two days were calmer than before. At this point, the loss of *Prestige* is attributed to the structural degradation, which progressively accumulated from the initial damage. This realisation added another dimension to the approach for the structural survivability assessment of damaged ships, that is, the progressive structural failure analysis, which predicts damage propagation in time domain under varying wave loads. Hence questions on whether the damaged ship could survive, and if not, for how long it could stay afloat should be answered. However, this requirement has not been discussed properly in the overall survivability assessment procedure e.g. Lee, Lee, Park and Kim (2005), although it is certainly a strong requirement of the field. The reason for this is attributed to the fact that survivability assessment primarily pertains to passenger ships, which are inherently much less susceptible to structural degradation than cargo ships like tankers.

It is believed that with a tool enabling estimation of the progressive structural failure in the emergency operating situation, the timeline information on the structural survival (time to break) of a damaged ship under forecasted weather conditions could be obtained and used to support the decision-making process, which always aims at the most desirable conclusion. It should be noted that in emergency situations where decision-support information is crucial requires a fast, and reliable tool that can be implemented in timeline basis and embrace uncertainty (regarding the damage itself) , as well as environmental prediction so that the decision-making process is well-informed and draws the best decision with sufficient confidence.

The importance of the progressive structural failure as a part of the survivability assessment of a damaged ship in the course of the salvage planning and operation is obvious. At the same time, it is natural to bring it into the ship design process so as that the structural survivability of ships following accidental events is guaranteed in terms of the progressive structural failure at the earliest design stage by maximising the safe rescue and salvage operation time in order to achieve zero tolerance to loss of life and to minimise environmental pollution and loss of property.

Stemming from this, the structural survivability of a damaged ship needs to be quantified so that it can be managed in the design stage with consideration of the all loading conditions that the ship is intended for, various damage conditions that the ship would experience from the possible accidental events, and the wave conditions (including extreme ones), which are expected to be encountered in the planned routes during her service life.

The traditional rule-based design approach cannot cater for this requirement as safety is considered as a constraint rather than an objective and assessment of the absolute safety level of the designed ships is missing.

In response to this, the *Risk-based ship design* methodology that has been developed is based on the *Design for Safety* philosophy, (Vassalos, 1999). This philosophy treats safety in its rightful place as a design objective (i.e. integrating it into early design process) rather than mere rule compliance as addressed in Vassalos, Oestvik and Konovessis (2000a, 2000b), Konovessis (2001), Vassalos, Konovessis and Vassalos (2003), Vassalos, Konovessis and Guarin (2005), and Vassalos, Guarin and Konovessis (2006). In this manner, absolute levels of safety for each ship can be obtained for example, how long it would take to capsize or collapse for a given damage, loading condition and sea state?; how long it would take to evacuate people on board?

1.4 Risk-based ship design and the structural survivability

The risk-based ship design framework as shown in Figure 1-2 methodically integrates risk assessment in the conventional ship design process in order to evaluate and reduce risk to life, property and environment by balancing design

parameters pertinent to safety with others related to the conventional design objectives such as cargo carrying capacity, structural strength, speed, etc.

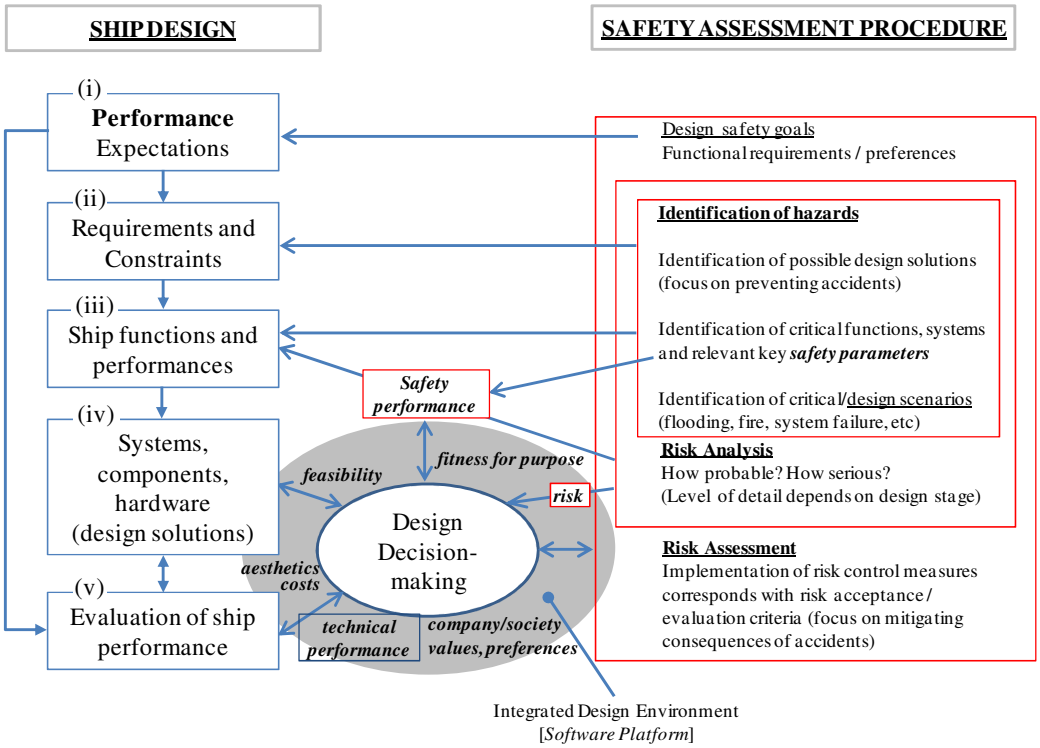

Figure 1-2: High level framework for risk-based design, Vassalos, Guarin and Konovessis (2006)

According to Vassalos, Guarin and Konovessis (2006), addressing safety explicitly indicates the need to measure it and in this respect, *risk* is considered as the means to measure safety, which is necessary to evaluate in the early design phase where most of the fundamental characteristics of the ship are generated and easily altered with the minimised cost incurred (Figure 1-3).

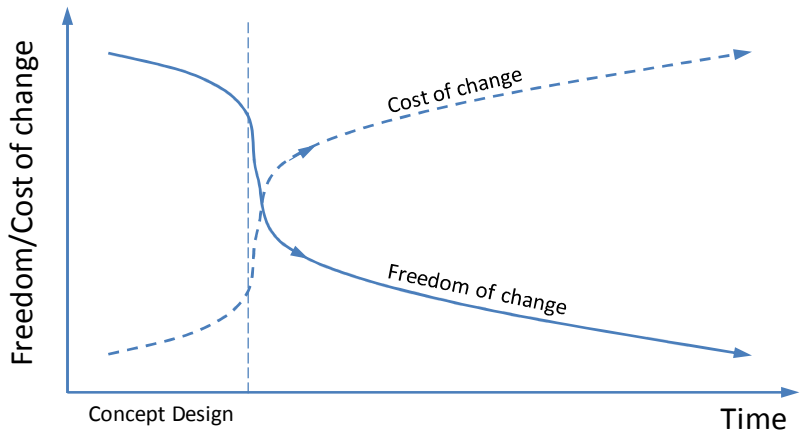

Figure 1-3: Freedom and cost of change in design timeline

The principal advantage that the risk-based design methodology has in comparison to the conventional design process is the explicit, rational and cost-effective treatment of safety. To achieve this, the following principles need to be considered as covered in Vassalos (2009), Vassalos, Guarin and Konovessis (2006):

- A consistent measure of safety should be obtainable with a formalised risk analysis that focuses on key safety drivers (major accident categories, Figure 1-4) but their portion to the total safety of the target vessel should be enough to cover the total safety.
- Risk analysis should be included in the design process by providing safety-related information needed for design-decision making and design optimisation in order for the most cost-benefit design solution to be identified.
- Use of reasonably accurate parametric models is preferable in dealing with safety as they would be fast and easily applied in order to allow trade-offs among all design objectives.

The major accident categories of a specific vessel type can be selected either by hazard identification (HAZID) sessions with experts, or available historical data, from which the corresponding design scenarios would be defined by sequentially occurring events. The generic design scenarios advocated by Vassalos and Konovessis (2003) and shown in Figure 1-4 can be used for this purpose for a specific vessel. It should be noted that human element is another important source of the major accidents and it is combined in 'System Hazard'.

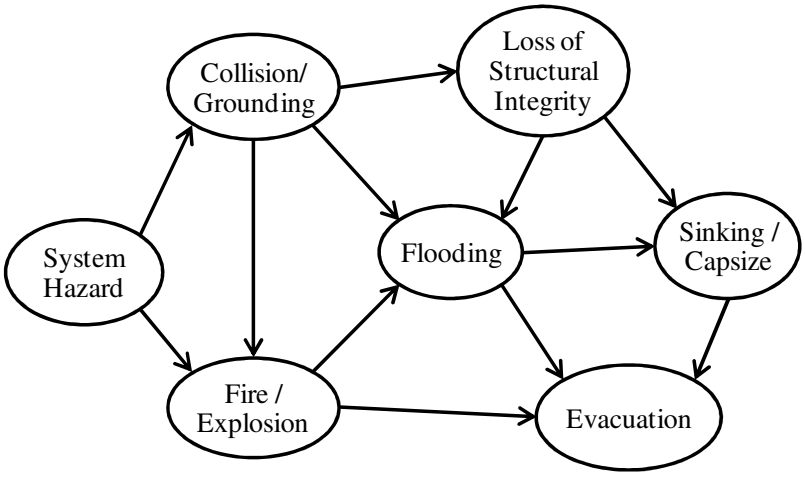

Figure 1-4: Typical structural links of design scenarios, Vassalos and Konovessis (2003)

The current status of developments of the risk-based design implementation for passenger ships focuses mainly on the flooding survivability analysis (with respect to collision and grounding accident) and the fire safety analysis as reported in Vassalos (2009).

One missing subject among the components of the above design scenarios is *the loss of structural integrity* (in other word, *structural survivability*). This is contributed to the historic data that over 90 % of risk regarding loss of life is from flooding and fire-related scenarios in passenger ships and also to the fact that the passenger ships are inherently more robust in their longitudinal strength. However, the recent framework of the *Safe Return to Port* for passenger ship safety (Figure 1-5) has opened the way for *zero tolerance* to loss of life even in the regulatory requirement and has questioned the presumption of structural stability and emphasis on the damage stability assessment alone. That is, under the premise that the ship should be designed to be its own life boat, the ship is, if the casualty threshold is not exceeded, expected to remain afloat, upright and habitable for as long as necessary (infinitely but 5 days recommended) until it can return to port under its own power or until assistance has arrived (IMO, 2004).

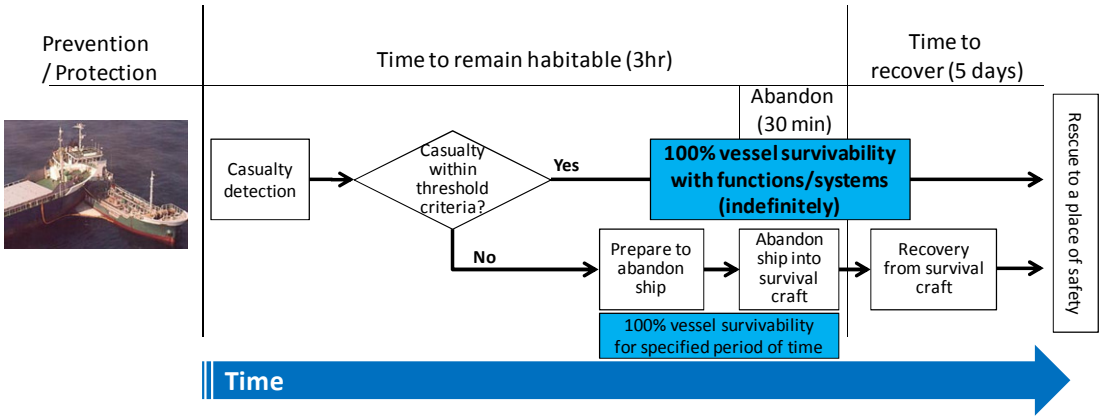

Figure 1-5: The concept of the Safe Return to Port, IMO (2004)

As the focus of the framework is clearly on the timeline development of different events, it is not only important to know whether the vessel will survive under the casualty with the given loading and environmental conditions but also the time the vessel will remain habitable in order to return to port or wait for assistance. Although achievement of these goals is already implemented by direct deployment of risk-

based design methodology including flooding survivability analysis, fire safety analysis, post-accident system availability analysis and evacuation analysis, (Vassalos, 2009), taking into consideration the structural survivability with the progressive structural failure in the time domain is a step ahead for achieving the ultimate safety goal.

Aside from the passenger ships' safety, the importance of evaluation of the structural survivability of ships in the implementation of risk-based design methodology becomes larger for other types of ship e.g. tankers, which are critical to environmental impact. As it is previously explained, the loss of *Prestige* is a prominent accident that signifies the importance of a methodology and a tool for the quantification of risk pertinent to the structural survivability with respect to the progressive structural failure and its integration in the risk-based ship design framework in order to guarantee efficient mitigation action in emergency operations following any possible accidental events during the ship's service life.

1.5 Thesis objectives

The work addressed in this research targets the establishment of a methodology and development of a tool for evaluating the structural survivability of damaged ships by taking into account the progressive structural failure in the time domain and support i) achievement of safety goals by pursuing zero tolerance to loss of life as well as the minimal environmental impact and loss of asset, and ii) emergency decision-making that should be immediate and decisive within limited time intervals for rescue and salvage operations. For the purpose, the tool is required to be fast, reliable and to cater for all levels of uncertainty in the process.

In light of the above the objectives of this work are:

- The development of a methodology for the analysis of progressive structural failure in the time domain;
- The development of knowledge-intensive (parametric) models for analysing the progressive structural failure under time-varying environmental conditions so that they can be implemented fast with appropriate accuracy

both in the *risk-based ship design* context and in the emergency operations; and

- The implementation of the methodology in a software tool.

It should be noted that it is not the purpose of this research to carry out a risk analysis study but to provide an analysis tool and methodology that can be used in the analysis of risk pertinent to structural survivability that can be integrated in the implementation of *risk-based ship design* and implemented in the emergency rescue and salvage operations.

1.6 Scope of work

To achieve the objectives of the current work and to check the applicability of the developed models and methodology, the following scope of work is defined:

- Defining approaches for progressive structural failure analysis
- Defining crack growth models
- Conducting FE analysis and developing knowledge-intensive models for determining the stress intensity factors and their validation studies
- Development of a method to calculate residual strength capacity of damaged hulls and its validation studies
- Consideration of environmental loads into the damage propagation analysis
- Develop a tool that combines the progressive structural failure analysis with the residual strength assessment
- Application of the developed tool through case studies
- Sensitivity and probabilistic analysis

1.7 Thesis structure

Starting with the introductory chapter, the thesis will continue on the critical review of literatures regarding development of progressive structural failure analysis especially in terms of crack propagation and development of residual strength assessment, which will be elaborated separately in the Chapter 4 and 5 respectively after addressing the method proposed to evaluate the survivability of damaged ships. The applicability of the models developed is tested in case studies that are followed

by sensitivity and uncertainty analysis. The thesis concludes with a summary and discussion of the work carried out and some suggestions on the way forward. The structure of the thesis is outlined in Figure 1-6 with chapter references.

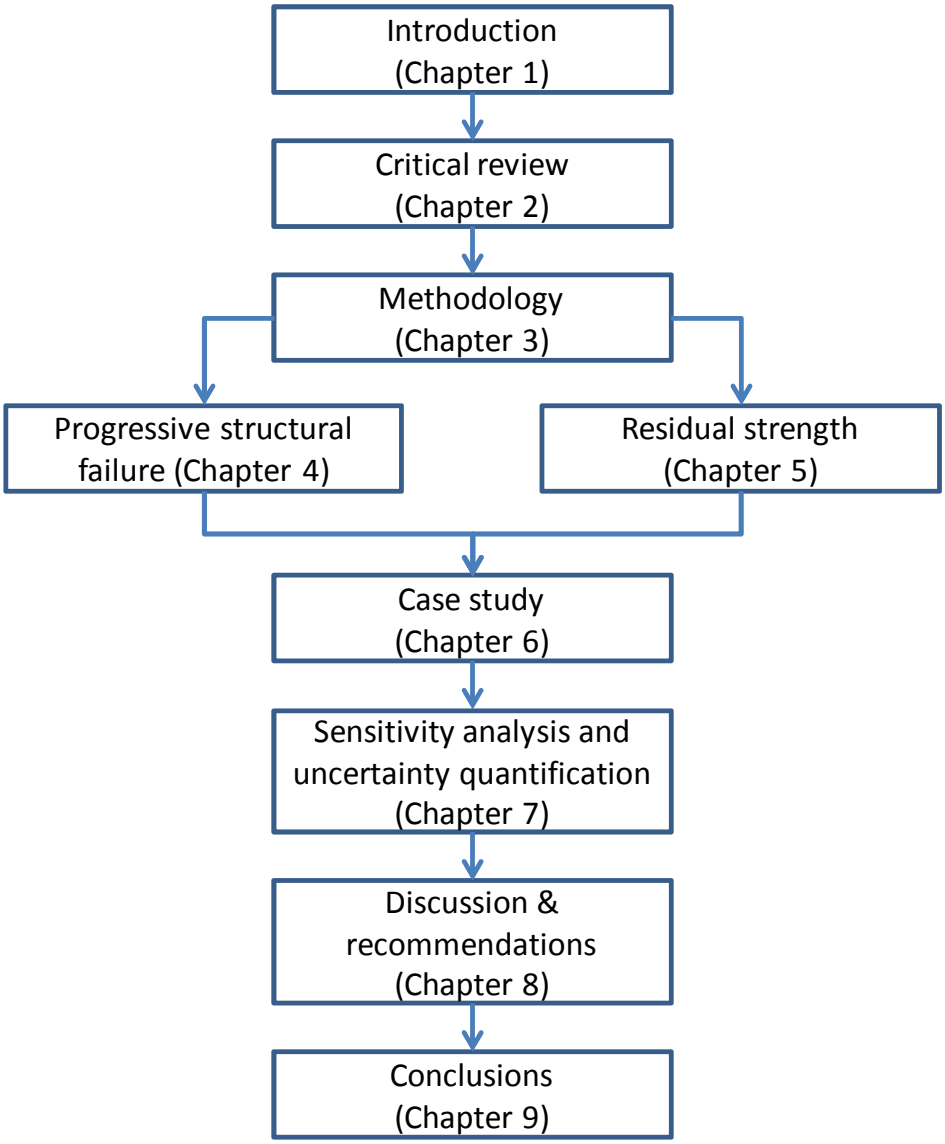

Figure 1-6: Structure of the thesis

2 CRITICAL REVIEW

2.1 Preamble

In this chapter the methods and approaches that have been suggested and established in the past few decades for the study of the crack propagation analysis and the residual strength assessment are critically reviewed. The field of progressive structural failure from damage openings has not been studied to a sufficient extent, hence this chapter starts from the fatigue crack propagation analysis approach, which will be combined with the accidental damage openings. Due to the complementary character of the crack propagation and the ultimate strength in this research, a section is devoted to each topic respectively.

2.2 Fatigue crack propagation

In this section the study on crack growth models that have been proposed, applied and compared with experimental data is reviewed. This includes determination of material constants for the basic *Paris* equation and various modifications of it. Also the methods for the determination of the Stress Intensity Factor (SIF) that should be used with the crack growth models in order to obtain the crack propagation rate are addressed.

2.2.1 Crack growth models

Since it was hypothesised by Paris and Erdogan (1963) that the range of the SIF, ΔK, governs fatigue crack growth, the empirical expression of *Paris Law,* which shows that the crack growth rates are proportional to ΔK when plotted on a log-log scale, has been the basic model of crack propagation.

However, experimental data shown in literature, e.g. Donahue et al. (1972), Hirt and Fisher (1973), Klingerman (1973), Yazdani and Albrecht (1989), Farahmand, Saff, Xie and Abdi (2007), etc., generally showed a sigmoid shape on a log-log scale (Figure 2-1). This is attributed to the threshold value, ΔK_{th}, below which crack propagation does not occur, and the maximum value, ΔK_{max}, at which crack propagation will be accelerated and either a ductile tearing or a brittle fracture would follow. Hence, the *Paris Law* in Equation (2-1) is applicable only when the range of SIF is between ΔK_{th} and ΔK_{max}.

$$\frac{da}{dN} = C \times \Delta K^m \quad \textbf{(2-1)}$$

where, $\frac{da}{dN}$ is crack propagation rate in units of [metres/cycle]

ΔK is range of SIF in the unit of [MPa$\sqrt{m}$],

$\Delta K = K_{max} - K_{min}$

C and m are material constants for crack propagation

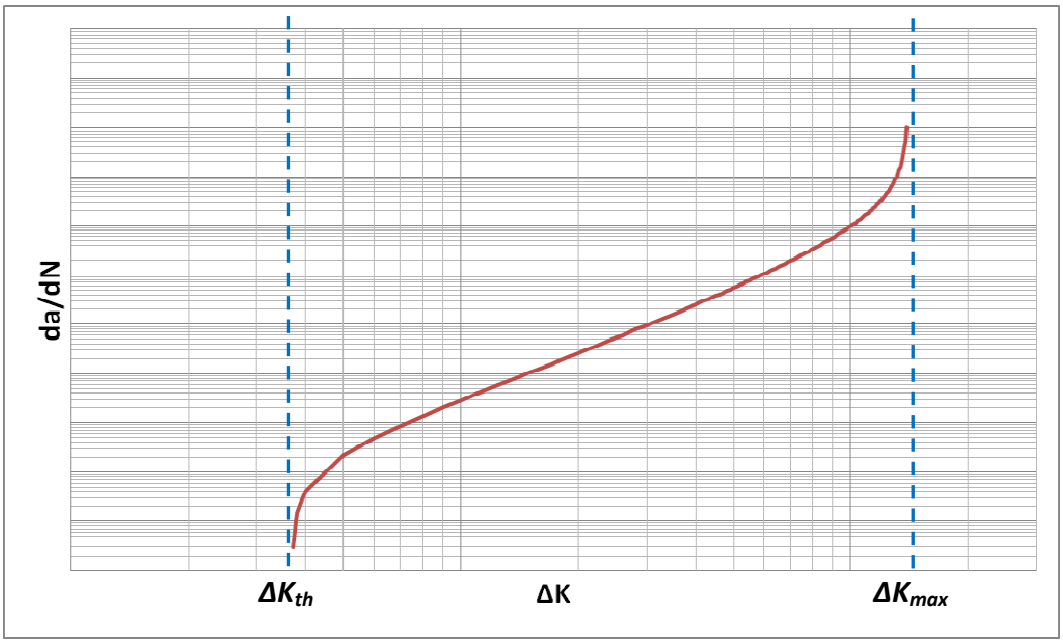

Figure 2-1: Typical plot of crack growth rates

Material constants for Paris Law

Based on the *Paris Law* a number of tests were carried out to obtain the material constants of steels. Regression analysis of the measured experimental data enabled the constants to be evaluated by tests. Although these tests have been carried out by focusing on the middle range of ΔK that is expressed as a straight line, the induced set of material constants vary as the experimental conditions and the material types have not been the same. Also various sources of uncertainty during the experiments and measurements contribute as well.

The A36 steel, which is a standard structural carbon steel identified and specified by American Society for Testing and Materials (ASTM), was used in the test carried by

Hirt and Fisher (1973) and a set of material constants based on the experimental data was derived as C and m to be 3.925×10^{-12} and 3.0 for units of MPa and metres. However, further fatigue crack growth tests conducted by Klingerman (1973) for the same material suggested a value of $C = 1.859 \times 10^{-12}$ and $m = 3.1$. The difference of material constants between two tests is attributed to the fact that the former test was carried out in the high fatigue crack growth region while the latter test was conducted with inclusion of the low fatigue crack growth just above the threshold region. Hence, the latter case has the lower value of C but the higher value of m. One noticeable thing from both tests is that the suggested set of material constants has been derived based on the mean line of each test data.

The use of upper bound of the test data rather than the mean line was accepted later as this gives higher value of C hence a conservative result is obtained in predicting crack propagation. Barsom and Rolfe (1987) established an upper bound for various steels. They suggested values of C and m as 6.8×10^{-12} and 3.0 respectively for units of MPa and metres. Also the test performed by Fisher et al. (1993) with High Strength Low Alloy (HSLA) steels showed that the upper bound value of C was 9.0×10^{-12} with a constant value of $m = 3.0$. As the values of C from the upper bound are higher than those from the mean line, using the upper bound of the test data for design purposes is preferable.

In addition, the material constants for crack propagation were found to vary for different types of steels and affected by environmental conditions. According to Yazdani and Albrecht (1989) who have gathered crack growth rate data from published plots in the literature and derived material constants, the quenched and tempered (QT) steels have higher value of C but lower value of m when compared with the mild and HSLA steels. Also the crack growth rate in seawater conditions is about twice as high than in the air conditions resulting to higher value of C but similar value of m. The effect of seawater on crack growth of steels also has been reported in Burnside et al. (1984) and Dexter, Norris, Schick and Watson (1990).

The best way to select the material constants for each purpose would be to carry out experiments with the target materials under the required or expected conditions of loading and environments. However, if all the required tests are not viable, using the

data from the available regulations or standards could be the best alternative. The British Standard Institute has published its guidance on this. In BS PD6493 (1993), it was recommended to use an upper bound of 9.5 x 10^{-12} for *C* while BS 7910 (1999), which is a later version, recommends to use an upper bound of 16.5 x 10^{-12} for *C* for steels in land-based applications with units of MPa and metres. A value of 3.0 was recommended for *m* in both cases. According to BS 7910 (1999), in dry air environments, fatigue cracks are observed to grow at closely similar rates for a wide range of steels. This supports the argument that a single crack growth law can be used regardless of different grades of steels.

Models with the effective range of SIF

Although the upper bound of various test data could be used, the scattered pattern of data under different test environments has been examined and the effective range of SIF, ΔK_{eff}, was introduced and substituted for ΔK to enhance the regression analysis. However, the way to define the effectiveness of the range of the SIF has been treated in various approaches.

The effect of the stress ratio has been included in defining the effective range of the SIF. Yazdani and Albrecht (1989) gathered crack propagation rate and carried out a linear regression analysis by utilising the modified *Paris Law*, where the effective range of the SIF is expressed in Equation (2-2) as a function of stress ratio as well as steel grades (yield strength of the materials).

$$\Delta K_{eff} = \frac{\Delta K}{1 - R_\sigma / Q} \qquad \textbf{(2-2)}$$

where, R_σ is the stress ratio, $R_\sigma = \sigma_{min} / \sigma_{max}$

Q is a parameter related with the yield strength of the material, 4.0 for A36 steels (carbon steels), 4.6 for A588 steels (HSLA steels) and 9.1 for A514 steels (quenched and tempered steels) are recommended

This model has the benefit that all ranges of stress ratio, even the negative ones, can be applicable but contrasts with the opinion of other literature, e.g. Hirt and Fisher (1973), Barsom and Rolfe (1987), Dexter and Pilarski (2000), that steels have similar crack behaviour regardless of their grades.

Elber (1970) introduced the effective crack opening ratio, U, describing the effectiveness of the applied loading cycle with the crack opening SIF, K_{op}, is defined as the amount of SIF required to open the crack front tip.

$$U = \frac{\Delta K_{eff}}{\Delta K} = \frac{K_{max} - K_{op}}{\Delta K} \quad \textbf{(2-3)}$$

Later, Kato, Kurihara and Kawahara (1983) proposed the effective crack opening ratio as a function of the stress ratio which included the residual stress effect. In their approach the effective range of the SIF was defined as Equation (2-4).

$$\Delta K_{eff} = U \Delta K \quad \textbf{(2-4)}$$

where, U is the effective crack opening ratio,

$$U = \begin{cases} 1/(1.5 - R_\sigma), & for\ 0 < R_\sigma \leq 0.5 \\ 1.0, & for\ R_\sigma > 0.5 \end{cases}$$

R_σ is the stress ratio included the residual stress effect,

$$R_\sigma = \begin{cases} (K_{min} + K_R)/(K_{max} + K_R), & K_{min} + K_R > 0 \\ 0, & otherwise \end{cases}$$

ΔK is the range of the SIF

$$\Delta K = \begin{cases} K_{max} - K_{min}, & K_{min} + K_R \geq 0 \\ K_{max} + K_R, & K_{max} + K_R \geq 0\ and\ K_{min} + K_R \leq 0 \\ 0, & otherwise \end{cases}$$

K_{max} and K_{min} represent the maximum and minimum SIFs

K_R is the SIF due to residual stress

This approach was used later by Sumi (1998) who proposed a crack growth model by taking into account the threshold range of SIF. Although taking into account the effect of the residual stress is the advantage of this approach, its practical use with the real structures, e.g. ship hull, is questionable as the determination of the residual stress distribution in the structures is uncertain and redistribution of the residual stress is expected when accidental events take place. Also, the negative stress ratio,

which effectively reduces the full range of applied stresses as addressed by Yazdani and Albrecht (1989), is not properly taken into consideration in the model.

Another effective range of SIF was proposed by Dexter and Pilarski (2000) who have included the crack closure effect due to stress ratio and residual stress in defining the crack opening SIF, K_{op} for the effective range of SIF expressed in Equation (2-5). The concept of the crack opening SIF was introduced by Elber (1970) and already adopted in the literature e.g. McEvily and Yang (1990) to define the effective range of the SIF, although its definition was not clearly explained.

$$\Delta K_{eff} = K_{max} - Max\left(K_{op}, K_{min}\right) \quad \textbf{(2-5)}$$

where, K_{max}, K_{min} are the maximum and the minimum applied SIF using σ_{max} and σ_{min}

K_{op} is the crack opening SIF,

$$K_{op} = -K_{cl} - K_R = Min\left(\frac{0.2}{(1-R_{\sigma,eff})}, 0.28\right) \cdot (K_{max} + K_R) - K_R$$

K_R is the SIF due to residual stress σ_{res}

$R_{\sigma,eff}$ is the effective stress ratio, $R_{\sigma,eff} = (\sigma_{min}+\sigma_{res})/(\sigma_{max}+\sigma_{res})$

The SIF due to residual stress, K_R, was borrowed from the work by Nussbaumer, Dexter, Fisher and Kaufmann (1995) who proposed an analytical expression based on Green's function.

However, this model has the same concern regarding the residual stress distribution. In addition, the effect of the stress ratio becomes negligible when the stress ratio is larger than 0.28, which is different from the general opinion that the effect of the stress ratio would decrease with the high stress ratio, e.g. above 0.5, as adopted by others, Kato, Kurihara and Kawahara (1983), Sumi (1998) etc. Despite of the pitfalls, this approach has also been used in the subsequent test and analysis carried out by Dexter and Mahmoud (2004) and its effect is shown in Figure 2-2.

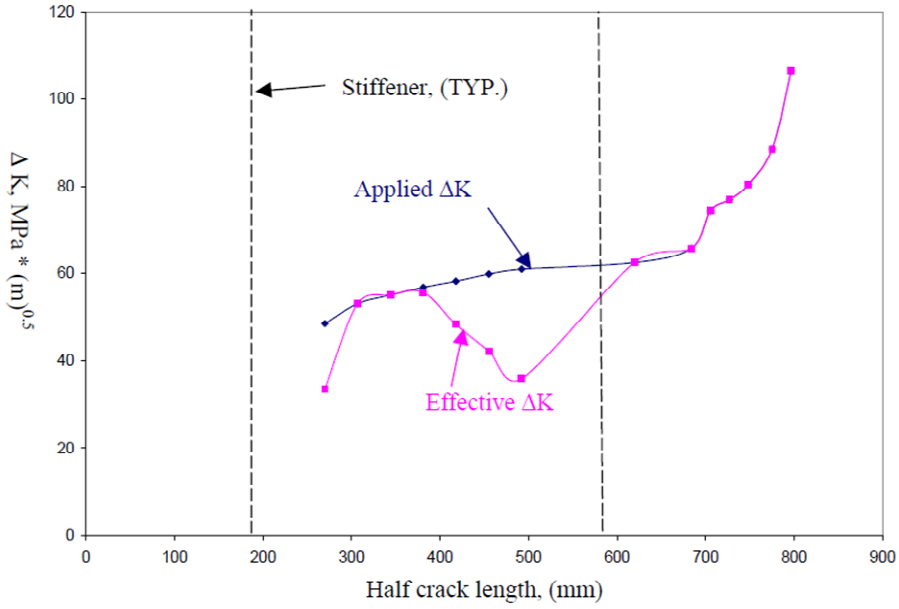

Figure 2-2: Difference between ΔK_{eff} and ΔK due to residual stress of -100 MPa between stiffeners in a stiffened panel, Dexter and Mahmoud (2004)

Models with the threshold range of SIF

Alongside the development of the model taking into account effectiveness of the SIF, effort to cover the effect of the threshold SIF was devoted in the field. A common weak point that the models of this category have is that they are valid up to the crack growth rates above which an accelerated growth or tearing is expected.

The very first crack growth model for the region of the threshold SIF was suggested by Donahue et al. (1972) who gathered various experimental results at the stress ratio $R_\sigma \approx 0$ and introduced a range of threshold SIF, ΔK_{th}, in the model expressed in Equation (2-6).

$$\frac{da}{dN} = C \times \left(\Delta K^2 - \Delta K_{th}{}^2\right) \quad \textbf{(2-6)}$$

where, C and m are material constants

ΔK is the range of the SIF due to applied load

ΔK_{th} is the range of the threshold SIF

As the above model was based on the data with the stress ratio of zero, its generalisation would require the effective range of the SIF by taking into

consideration various stress ratios as well as use of the general power than the fixed one with 2.0.

The use of effectiveness of SIF in defining a model for the threshold range of SIF is proposed by McEvily and Yang (1990). They included the effect of opening SIF which is required to overcome crack closure phenomenon due to an overload into the above Equation (2-6) by introducing the effective range of SIF. Hence, the crack growth model proposed is expressed as Equation (2-7). The validity of the model was carried out later by Makabe, Purnowidodo and McEvily (2004) by representing their test results under various overload-underload sequences (Figure 2-3).

$$\frac{da}{dN} = C \times \left(\Delta K_{eff} - \Delta K_{eff\_th}\right)^2 \quad \textbf{(2-7)}$$

where, C is a material constant

ΔK_{eff} is the effective range of the SIF, $\Delta K_{eff} = K_{max} - K_{op}$

K_{op} is the crack opening SIF level

K_{eff_th} is the range of the effective SIF at the threshold level

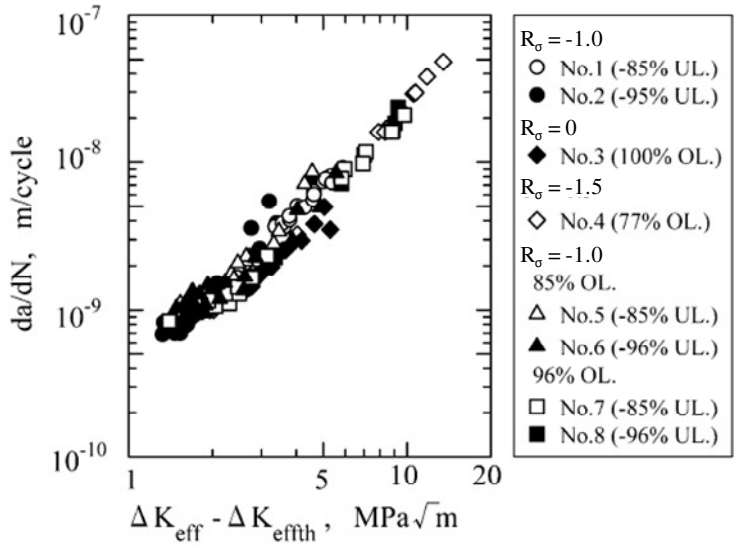

Figure 2-3: The generalised crack propagation rule of Equation (2-7) from Makabe, Purnowidodo and McEvily (2004)

It should be noted that as the tests are based on the single overload and underload within a constant loading, the validity of ΔK_{eff} under the multiple occurrence of load variation and their combinations is not fully guaranteed.

A more generalised form of the model to include the effect from the threshold SIF as well as compressive residual stress was suggested by Sumi (1998) who adopted the effective crack opening ratio proposed by Kato, Kurihara and Kawahara (1983). The crack growth model expressed in Equation (2-8) was shown to give a good agreement with his experimental results.

$$\frac{da}{dN} = C \times [(U\Delta K)^m - \Delta K_{th0}{}^m] \quad \textbf{(2-8)}$$

where, C and m are material constants

U and ΔK are defined in Equation (2-4)

ΔK_{th0} is the threshold range of the SIF at $R_\sigma = 0$, $\Delta K_{th0} = 2.45$ MPa$\sqrt{\text{m}}$

Model with unstable crack growth

Effort had been made by Foreman, Kearney and Engle (1967) to represent a curve that exhibits a rapidly increasing crack growth towards ductile tearing and brittle fracture in the high SIF region. They proposed a formulations that covers high and medium range of the SIF involving the fracture critical condition for $K_{max} = K_C$ as expressed in Equation (2-9), where the effectiveness of the range of SIF is implicitly included by using the stress ratio.

$$\frac{da}{dN} = \frac{C \times \Delta K^m}{(1 - R_\sigma)K_C - \Delta K} \quad \textbf{(2-9)}$$

where, C and m are material constants

ΔK is the range of the SIF

R_σ is the stress ratio

K_C is the fracture toughness of the material

Model including threshold and unstable regions

Combinations of high, medium and low range of the SIF also had been studied. McEvily and Groeger (1977) have proposed an equation including both the range of threshold SIF and the fracture toughness of the material as expressed in Equation (2-10) by adopting a similar concept of the unstable crack growth proposed by Foreman, Kearney and Engle (1967).

$$\frac{da}{dN} = C \times (\Delta K - \Delta K_{th})^2 \times \left[1 + \frac{\Delta K}{K_C - K_{max}}\right] \quad \textbf{(2-10)}$$

where, C is the material constant

ΔK is the range of the SIF due to applied loading

ΔK_{th} is the range of the threshold SIF

K_C is the fracture toughness of the material

K_{max} is the maximum SIF due to the maximum loading

It should be noted that in the above equation the model uses power of two but change of it by a general form of m would make the model to be used in more general purpose. Also it is preferable to include the effectiveness of the SIF by including the effects of stress ratio, residual stress, etc. A proper modification of this model can be used to represent the crack growth model covering all the region of ΔK, which is a requirement for this research.

2.2.2 Stress Intensity Factor (SIF)

The Linear Elastic Fracture Mechanics (LEFM) approach is used to predict the growth of fatigue cracks under conditions where the relatively little plastic deformation around the crack tip is expected as stressed by Irwin (1957). The formulation is based on SIF (K), which describes the magnitude of the stress field at the crack tip and is related with the applied stress remotely and the crack size. The determination of SIFs is available in theoretical solutions, e.g. Isida (1973), but is limited to the relatively simple cases, in numerical solutions by use of a series solution, e.g. Newman (1971), and in empirical solutions based on the results of both the theoretical and numerical solutions, e.g. Tada, Paris and Irwin (2000). Recently,

the use of the Virtual Crack Closure Technique (VCCT) has been focused for the purpose as the complicated structures of 2D and 3D can be involved in the analysis, e.g. Leski (2007).

Theoretical solutions

The SIFs for cracks propagating near stress concentration areas, e.g. cuts, geometric changes or boundaries, have been obtained based on the theoretical approach. However, due to the difficulty of deriving the solutions of closed form and the lack of theoretical supports for the complicated structures, there have been limited applications for limited boundary conditions.

Some examples of the theoretical solutions can be found in the literature such as Bowie (1956) for cracks emanating from an opening, Paris and Sih (1965) for edge cracks emanating from an elliptical opening, Isida (1973) for a centrally cracked strip reinforced with stiffeners and Watanabe, Yajima and Kawano (1979) for the crack propagation in a welded, stiffened panel.

Although the theoretical approach has limited applications for the further development, the developed solutions of SIFs in the closed form are of great help in establishing the parametric models for determination of SIFs in this research where the method of superposition is adopted.

Numerical solutions

The numerical approaches to obtain solutions for SIFs have been developed in cases where theoretical solutions were not feasible. The numerical solutions have been obtained using methods such as the boundary collocation method, Mellin transform technique, FE analysis, etc.

The *boundary collocation* method is a numerical way to evaluate the unknown coefficients in a series of stress functions. A general series solution of the governing linear partial differential equation would be truncated to a specified number of terms then the coefficients are determined with the satisfaction of the prescribed boundary conditions. The obtained solution would satisfy the used boundary conditions in the exact ways but others in approximate ways. The use of this method can be found in literature e.g. Gross, Srawley and Brown (1964) for single edge crack case, Newman

(1971) for cracks emanating from circular and elliptical openings in an infinite plate and in a finite plate and Wang, Cheung and Woo (1990) for a single crack emanating from a circular opening in a finite plate. Among the results of Newman (1971), correction factors of cracks from a circular and an elliptical opening (Figure 2-4) would be a good reference for investigating crack behaviours from collision or grounding damages of ships.

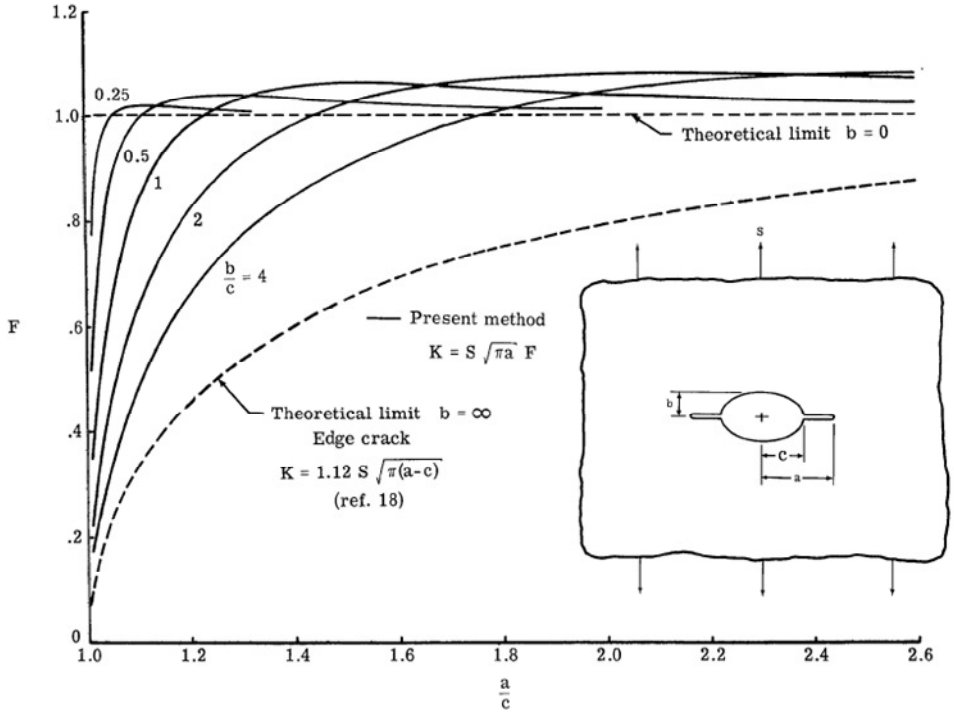

Figure 2-4: Correction factors for cracks emanating from an elliptical opening in an infinite plate subjected to uniaxial stress, Newman (1971)

Other types of methods have been used in developing the numerical solutions of SIFs. Tweed and Rooke (1973) used the *Mellin transform*[1], which is an integral transform regarded as the multiplicative version of the two-sided Laplace transform, to obtain SIF solutions of cracks from a circular opening in an infinite plate. Lai, Zhang and Schijve (1991) have developed solutions of SIFs for cracks of different lengths emanating from a circular opening edge based on the complex variable method, which uses complex series expansions to solve the stress functions. Nussbaumer, Dexter, Fisher and Kaufmann (1995) proposed a solution for SIF of the residual stress using the Green's function technique. An example of the use of *FE analysis* in

[1] http://en.wikipedia.org/wiki/Mellin_transform

obtaining SIFs of cracks is found in work by Sumi, Iyama, Bozic and Kawamura (1996) who used ANSYS, a FE code, to calculate the equivalent SIFs of cracks in stiffened panels.

Empirical solutions

A number of handbooks containing SIFs as numerical result forms and empirical expressions are available for various geometrical configurations and loading conditions, e.g. Tada, Paris and Irwin (2000), Murakami (2005), etc. The following descriptions are about the analytical or empirical solutions on the SIF especially related with ship structures and damage openings. They include the effect of circular or elliptical openings, stiffeners and arbitrary distributed stresses.

- **Cracks emanating from openings:** The numerical solutions of Newman (1971) are well established by an empirical expression for a circular opening but need a development of an empirical expression for an elliptical opening.
- **Cracks in stiffened panels:** The effect of the welded stiffeners on the SIFs of cracks in the panels was initially studied by Poe (1971) with experiments. According to the experimental results of panels with integral stringers it was noted that the crack growth rates decreased before stringers and retrieved sharply after stringers with higher crack growth rates than those of plain plates. A curve of SIF against half crack length in stiffened panels with integral stringers was proposed (Figure 2-5) based on his experimental results. The analytical solution of SIFs obtained by Isida (1973), who has used a series of the complex stress potentials of which coefficients were determined by satisfying the boundary conditions, has been expressed in the form of power series with 36 terms of a/B, the ratio of the crack length to the plate width, and follows the tendency of the effect of stiffeners proposed by Poe (1971). The solution of Isida has been proved to give practically exact values for $a/B < 0.95$. The proposal of Poe (1971) and the analytical solution of Isida (1973) have been used as a reference for obtaining the effect of stiffeners in literature, e.g. Dexter and Pilarski (2000), Dexter and Mahmoud (2004) and also are the reference for the current research in developing the correction factor for stiffeners.

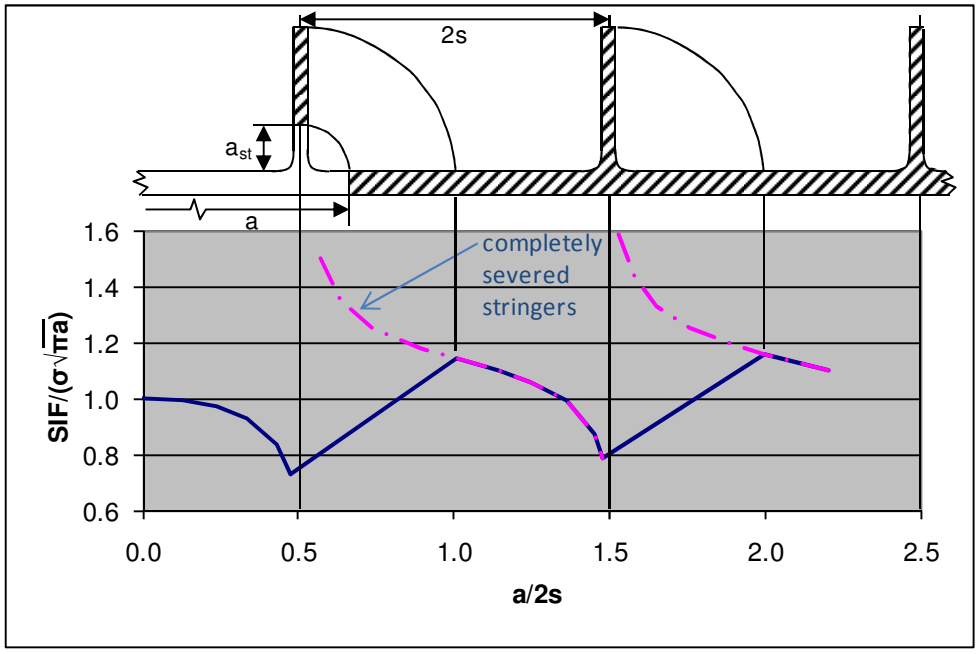

Figure 2-5: Relationship between SIFs and crack length for panels with integral stringers, Poe (1971)

- **Cracks in plates under non-uniform stresses:** Regarding the non-uniform stress effects on SIF, Chell (1976) proposed semi-empirical expressions for centre and edge cracks in plate by simple polynomial equations. The validity of the solutions was proved from comparison with other literature's results and FE simulations.

The solutions of the handbooks, which are generic, may be extended to more complex cases through the principle of superposition and also are quite useful for determining solutions of complex structures with simplified assumptions.

Virtual Crack Closure Technique (VCCT)

To cope with the limitation from using handbook or simple numerical approach for determining SIFs of cracks in very complex structures, some effort has been made to use FE method to calculate SIFs. Recently, the VCCT has been widely accepted in conjunction with LEFM and normally involves FE methods.

The VCCT is a well-known public domain post-processing and re-meshing technique that provides progressive crack growth between bonded surfaces based on the fracture toughness of the bond and the strain energy release rate at the crack tip

(ABAQUS, 2005). Since the idea of VCCT was proposed in 1977 by Rybicki and Kanninen (1977), VCCT has been a very attractive technique to extract SIFs because its algorithm of application is relatively easy and its results are in a good accuracy.

The original technique has been elaborated and extended to three dimensional bodies which have been introduced by Shivakumar, Tan and Newman (1988), Chang, Choi, Kim and Yagawa (2004) and Leski (2007). Although the VCCT has been useful to determine SIFs, its implementation into the commercial, general purpose FE codes has been only recently reported. Xie and Biggers (2006) have developed an interface element of which implementation has been carried out into ABAQUS using the user defined element subroutine. Implementation of VCCT into another commercial FE code, MSC/Patran, also has been conducted by Leski (2007) through a user subroutine using the Patran Command Language (Figure 2-6). These techniques have been applied as a post processing routine using the FE analysis results hence have required much time in the iterative process of the information between the module of VCCT and FE results.

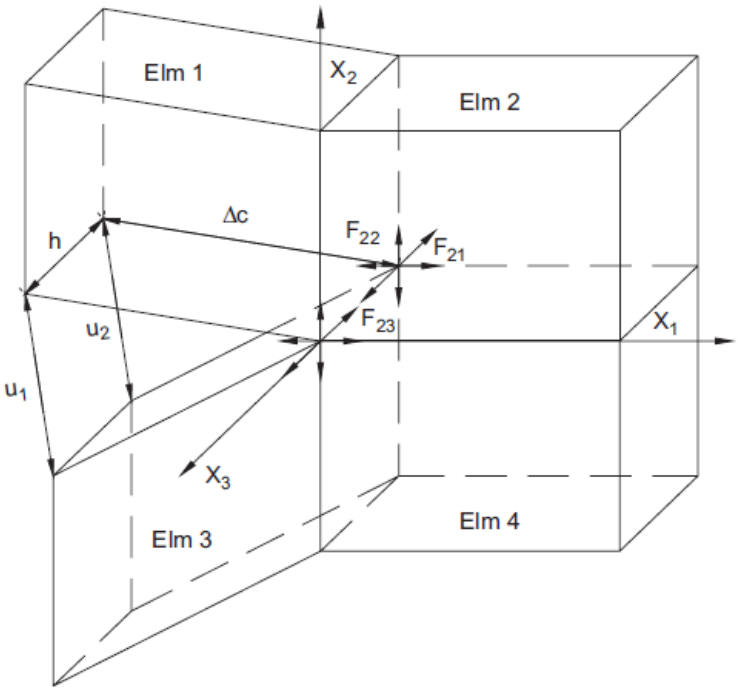

Figure 2-6: Configuration of VCCT in 3D FE model, Leski (2007)

An enhanced implementation of VCCT with the general FE codes has been allowed as some of the general FE codes have recently started to include the VCCT as an

intrinsic feature, which means no more user subroutine to combine the result from FE analysis with VCCT is required but the strain energy release rate, which can be easily converted to the SIF, can be obtained directly from the FE analysis. This provides convenience in simulation as well less analysis time than the use of VCCT in the isolated form. This enables that empirical expressions of SIF for any geometric feature may be established based on the results solved by it. The feature of VCCT embedded in commercial software can be found in Simulia (2008), MSC Sofware (2008) and ANSYS (2010).

2.3 Ultimate strength

The second section includes critical reviews on the approaches and development of methods for the calculation of the ultimate strength of the hull girder and the residual strength capacity of the damaged section. In the following sub-sections, research on experimental tests and development of simplified and analytical models for ultimate ship hull girder strength is reviewed followed by reviews on the numerical approaches and the extended applications to the assessment of the residual strength of damaged ships.

2.3.1 Experimental tests

Experimental tests provide the basic but reliable information for understanding the collapsing behaviour of the ship's hull girder or the ship-like structures. Due to the practical difficulties associated to model preparation, the measurements and finance, a limited number of full scale tests have been carried out whilst experiments with scaled models and box girders have been more popular. The results of the experimental tests have been the basis for validation purposes of the developed methods by many researchers and also been used for benchmarking studies.

The first full scale test has been conducted with a destroyer, *HMS Wolf*, the sister ship of the *HMS Cobra* that sank in 1901 to investigate the cause of the casualty. The findings from the test which measured elastic deflection of the ship were reported in Hoffmann (1925). He reported that some structural members could not carry loads effectively due to local buckling of the panel and shear lag. Another full scale test was carried out with two destroyers of the US Navy in 1930 and 1931. This time the

ships were loaded until they collapsed under the sagging and the hogging condition, respectively. It was reported by Kell (1931) and Kell (1940) from the test results that the overall collapse of the hull girder was led by the buckling collapse of the deck and bottom structure respectively. Other full scale tests have been carried out and findings from the test results were found in the reports of Vasta (1958), Lang and Warren (1952), etc.

Instead of using the full scale tests, collapse tests have been conducted with scaled models of ship hulls. Mansour, Lee and Thayamballi (1990) carried out an experimental investigation on the ultimate strength of ship hull girders with two large scale models. A stiffened steel hull model representing a tanker was subjected to a sagging moment and another open deck ship model was tested under hogging loads along with lateral pressure on the bottom. A comparison between simple theoretical analyses using the effective section modulus concept and experimental results was made with the effects of residual stresses and initial distortions included in the approximate methods, which was concluded to offer a promising and practical method for estimating the collapse bending moment. Another scale model test was performed by Dow (1991), who carried out a collapse test on a 1/3-scale welded steel frigate model representing a typical warship hull structure subjected to sagging bending loads. The overall collapse of the section led by the buckling of the deck and the upper part of side shell plating was discussed and compared with theoretical strength predictions. The test results of Dow have been used for the verification of the models developed by Paik and Mansour (1995), Gordo and Soares (1996), etc.

Experimental collapse tests with the box girder models have also been conducted. Dowling, Chatterjee, Frieze and Moolani (1973) tested a number of different steel box girder models subjected to different load conditions. They conducted point load tests and pure bending tests of which structural responses were obtained and compared.

Later Dowling, Moolani and Frieze (1976) carried out tests to investigate the effect of shear lag on the ultimate strength of box girders and concluded that the presence of shear and shear lag has no significant effect on reducing the ultimate strength of the stiffened compression flanges. Nishihara (1984) carried out experimental work

with eight box girder models representing conventional types of ships such as a tanker, a bulk carrier and a container ship. A pure bending moment was applied to each specimen and a method to predict the ultimate bending strength of hull girder structures was proposed with a successful application to midship sections of actual ships. The results of these tests on the ultimate strength of the simple box girders have been used for the validation of their own developed methods as well as methods developed in other research e.g. Frieze and Lin (1991), Paik and Mansoure (1995), Gordo and Soares (1996). More experimental tests on the ultimate bending strength of the box girders can be found in literature, for example Gordo and Soares (2004), and Qi, Cui and Wan (2005). Gordo and Soares (2008) carried out the experimental test in order to obtain collapse behaviour of the box girder made of mild steel, while the collapse behaviour of the box girder made of high tensile steel (Figure 2-7) was experimentally obtained later in Gordo and Soares (2009).

Figure 2-7: General deformation of box girder of high tensile steel after the collapse load, Gordo and Soares (2009)

2.3.2 Simplified analytical approaches

The ultimate strength of the hull girders under bending has been calculated analytically in three ways: (i) the yield moment approach, (ii) the fully plastic moment approach, and (iii) the progressive collapse moment approach.

Yield moment approach

The yield moment approach is based on the simple beam theory which considers the hull girder as a single beam and explains that the ultimate strength of the hull girder is reached when either the deck or the bottom plating reaches yield condition. In this approach, it is assumed that buckling in the compressive flange does not occur before yielding hence, the ultimate bending strength is expressed as a function of the elastic section modulus and the yield strength of the deck and bottom plating. Due to its simplicity, this approach has been widely used and modified, although it does not account for the buckling of the individual structural members.

The drawback of the yield moment approach has been taken into account by Vasta (1958) who has found from the full scale tests that the ultimate bending strength of the hull is correlated with the buckling strength of the compressed parts of the hull plates. He proposed that the ultimate bending moment of longitudinally framed hull structures would be obtained from the product of the elastic section modulus and the ultimate strength of the compressive flange. That is, the yield strength of the deck and bottom plating is replaced by the ultimate strength of the deck and bottom plating.

A modification of the Vasta's approach has been made by Mansour and Falkner (1973) in order to take into account the shift of the neutral axis when the buckling of the compressive flange occurs. They introduced a constant expressed as a function of the ratio of the areas of the side shell to the compressive flange. Further improvement of this approach (which uses the elastic section modulus) is made by Faulkner and Sadden (1979), and Valsgard and Steen (1991).

Fully plastic moment approach

On the other hand, the fully plastic moment approach has been adopted by Caldwell (1965) who has derived analytical formulations of the ultimate strength of the hull structures taking into account both buckling failure in compressive parts and yielding failure in tensile parts. He idealised the hull section of plates and stiffeners as an equivalent section of plates with average thickness to meet the total area in deck, bottom and side shell, respectively. He assumed that each plate of the equivalent section has the same ultimate strength as well as yield strength. In the state of

ultimate strength, he assumed that the structural members in compression reach their ultimate buckling strength while the structures in tension are in fully yielding condition. The ultimate moment strength of the hull structure was calculated by summing up each plate's moment induced by the axial force (product of stress and area) with respect to the distance to the neutral axis, which could be defined by the fact that the sum of the axial forces is zero.

The maximum capacity obtained by this method is overestimated as the strength reduction of structural members beyond their ultimate strength is not taken into account. In addition, the assumed situation that all the members reach their ultimate strength state is not viable because in reality the bending strain is linearly distributed along the depth of the cross-section so the individual element reaches its ultimate strength in the different time scale.

Based on the fully plastic moment interaction, Mansour and Thayamballi (1980) analysed the ultimate strength of a hull girder in plastic and buckling modes. They considered a ship subjected to a realistic loading of vertical and lateral bending and torsional moments. In the process for estimating the ultimate capacity of the hull, buckling and instability of the hull stiffened plates (i.e. flexural buckling of stiffeners, tripping of stiffeners), the fully plastic collapse moments and the shakedown moments (the effect of the alternating bending moment between hogging and sagging) were further developed. Also, they developed a set of interaction relationships for the ultimate strength of ships subjected to combined moments.

The weakness identified in the Caldwell's approach has been modified by Paik and Mansour (1995), who developed a simple analytical formula to predict the ultimate collapse strength of ships with single and double hull. They observed that side shell near the compressive and the tensile flange would fail also but the remained parts in the vicinity of the final neutral axis would remain in the elastic region of the material. Based on this observation, they assumed a longitudinal stress distribution of a hull section at the state of overall collapse (Figure 2-8) and obtained an explicit analytical formula for calculating the ultimate strength of the hull section. The adequacy of the proposed method was checked with applications to box girder models, a frigate model and a VLCC. However, the drawback of not taking into consideration the

reduced strength of the individual structural members beyond their ultimate strength remains. Also several grades of steel in a single member, e.g. side plating is not taken into account.

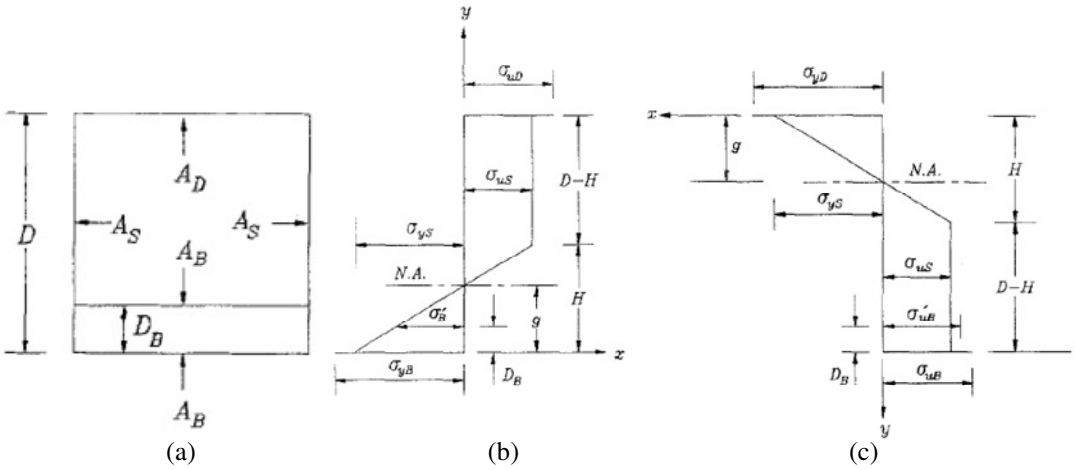

(a) (b) (c)

Figure 2-8: A hull cross-section of a equivalent double hull configuration (a) and assumed distribution of longitudinal stresses in at the overall collapse state in sagging (b) and hogging (c), Paik and Mansour (1995)

Progressive collapse moment approach (beam-column method)

The above-mentioned problem could be solved with the progressive collapse moment approach, which includes buckling and post-buckling behaviour of the individual structural members. Smith (1977) proposed a simplified method to derive the moment-curvature relationship of a hull girder cross-section. He demonstrated that the reduced strength of stiffened panels above the ultimate load plays an important role in the ultimate strength of the hull girders. In this method, a cross-section of the hull girder was divided into small elements composed of a stiffener and associated plate. He introduced an average stress-strain relationship of each element by taking into account yielding and buckling. A progressive collapse analysis was carried out assuming that a plane cross-section remains plane and each element behaves independently according to the corresponding average stress-strain curve.

This approach is commonly known as the *Smith's method* or *beam-column method* because each element constituting the hull cross-section behaves like a beam-column. The accuracy of the Smith's method was investigated by Dow, Hugill, Clark and Smith (1981) through correlating the analysis with various collapse experiments on

longitudinally stiffened steel box girders, from which satisfied agreement was obtained. They also extended the analysis method to deal with dynamic responses such as whipping of hull girder caused by bow slamming or underwater explosions. In the method, the influence of imperfections such as initial deformations and residual stresses were accounted for by modifying the initial structural geometry and by imposing the initial stresses, respectively.

This method has been used by other researchers with some differences and modifications for improvements. The effect of the flexural-torsional buckling has been formulated by Adamchak (1984) who developed a simple method which was implemented in a computer program based on the Smith's method. In the application by Rutherford and Caldwell (1990), they compared their results of strength of a VLCC *Energy Concentration* with the ultimate bending moment experienced by it. The calculation was made by a simplified approach based on the Smith's method using stiffened plate's strength without considering post-buckling strength. They investigated the importance of lateral pressure, initial deformations and corrosion rates and the validity of the method was compared with the results obtained by a nonlinear FE program.

An approximated method for the load-end shortening curves of stiffened panels was proposed by Gordo and Soares (1993), who included the post-buckling behaviour, the effects of residual stresses and the initial deformations. In the load shortening curve of a stiffened plate, they included plate induced failure, flexural buckling of column and tripping of stiffener. The validity of the method was checked by comparison of the results with a series of numerical analyses results using an FE program for the relevant range of plate and column slenderness. Further validation of the proposed method was made by Gordo and Soares (1996) using the small scale box girder models of Dowling, Chatterjee, Frieze and Moolani (1973) and the 1/3-scale frigate model of Dow (1991). Later, the proposed method enabled the evaluation of the strength of the hull girder at several heeling conditions (Figure 2-9) in the work of Gordo, Soares and Faulkner (1996).

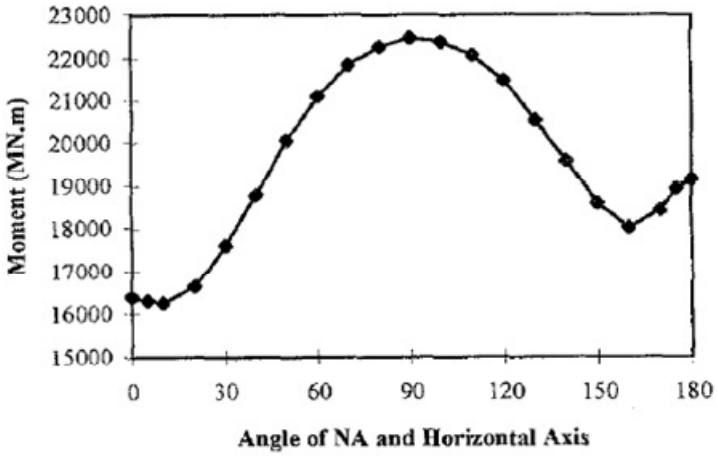

Figure 2-9: An example of combined bending moment against heeling angle, Gordo, Soares and Faulkner (1996)

It is required by rules that the hull girder ultimate strength should be checked. The criteria for ultimate strength assessment as well as methods for calculation of hull girder ultimate capacity is presented in the structural rules such as the Common Structural Rules for Oil Tankers required by IACS (2008). Although other alternative methods are accepted, the single step method based on section modulus and the simplified method based on an incremental iterative approach, which uses the moment-curvature curves are addressed to help calculating the ultimate strength of hull girders.

The accuracy and the usefulness of the Smith's method can be found in the benchmark investigations of ISSC (1994a), ISSC (1994b), and Wang, X. et al. (2008). In the comparison analysis by Wang, X. et al. (2008), three different methodologies of hull girder ultimate strength were presented and numerical calculations of hull girder ultimate strength of six different FPSO designs were carried out. The used methodologies included an incremental-iterative approach, an in-house code, HULLST, based on Smith's method and an application of Idealized Structural Unit Method (ISUM) by Ueda and Rashed (1984). According to the results, all three methods showed good agreement. They found that the in-house code based on the Smith's method and ISUM were almost identical for most of the cases, while the incremental-iterative method showed slightly conservative results in some of them. Hence, it was concluded that all three methods could be applied for hull girder ultimate strength calculation of FPSOs.

2.3.3 Numerical approaches

Numerical approaches are powerful computational methods to perform the progressive collapse analysis of the hull girder by taking into account the elasto-plastic properties of the material, the non-linear geometric aspect of structural members, the buckling and post-bucking behaviour of the elements, and the residuals stresses. In general, these approaches are extremely time-consuming as they require vast man-hours for creating models and computer resources for solving the problem. The general FE methods as well as other simplified numerical methods, like ISUM, belong to this type of approach. In this review, the simplified numerical approaches are mainly addressed as they have the reduced drawback as well as the merits mentioned. The ordinary FE method is considered difficult to deploy in the emergency situation as well as in the early design stage because the hull girder is too huge to carry out the progressive collapse analysis despite the hugely advanced computer capacity.

One of the alternative methods to perform the progressive collapse analysis is developed by Ueda and Rashed (1984) is ISUM, which is used for the analysis of the nonlinear behaviour towards collapse of large size structures. In this method, a structure is divided into the biggest possible structural units of which geometric and material nonlinearities can be idealised and expressed in a concise analytical-numerical form. The ultimate strength of the structure is obtained with incrementally applied loads. With the efficient division of the structure, the ISUM could eliminate some effort required in conventional FE methods such as choice of element types and size of mesh. In addition, this method requires less number of structural units and overall degrees of freedom than those required for a conventional FE analysis. Application of the method was made to structures built up deep I girders (Figure 2-10) and the benefit of the method as well as its accuracy were verified.

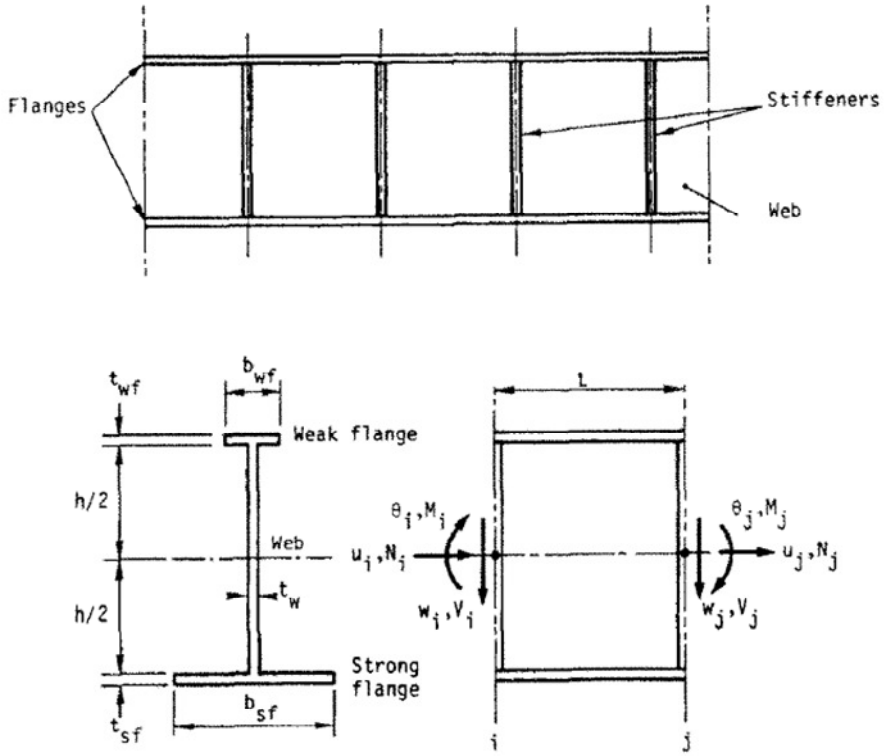

Figure 2-10: The girder structural unit: nodal points and degrees of freedom, Ueda and Rashed (1984)

A similar approach was followed by Bai, Bendiksen and Pedersen (1993) who developed an FE procedure for the collapse analysis of ship hull under complicated loads. They developed a set of finite elements, such as beam-column elements, stiffened plate elements and shear panel elements (Figure 2-11), directly accounting for the geometrical and material nonlinearities as well as initial imperfections. They derived elastic-plastic stiffness matrices for elements and included the buckling and post-buckling behaviour of plates. Fracture mechanics criteria were also introduced to account for tension tearing rupture and brittle failure of the material.

A numerical tool was developed based on the ISUM. Paik, Wang, Kim and Thayamballi (2002) studied the ultimate limit state design of ship plating and stiffened panels and developed a numerical tool called ALPS/ISUM (Figure 2-12), which enables the progressive collapse analysis of ship hulls in an efficient and accurate way. The validation of this approach has been made by further research effort of Paik and Kim (2008).

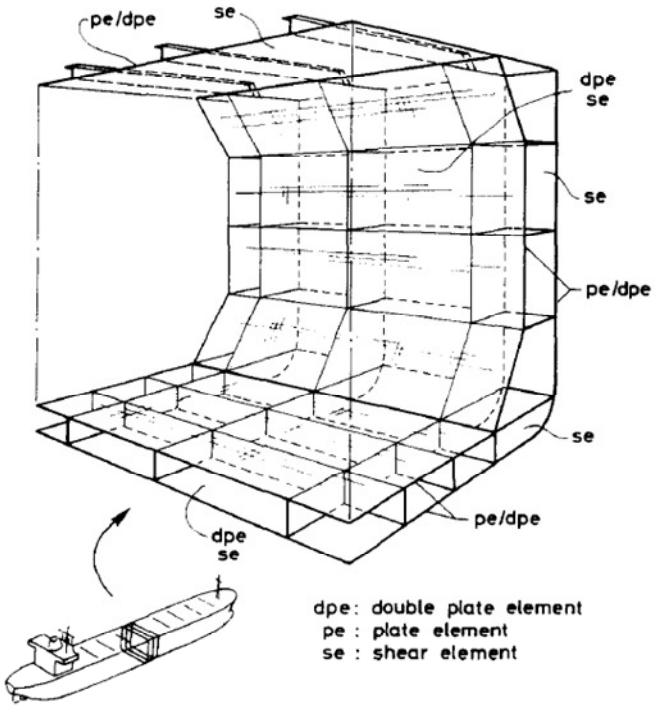

Figure 2-11: Extent of the FE model, Bai, Bendiksen and Pedersen (1993)

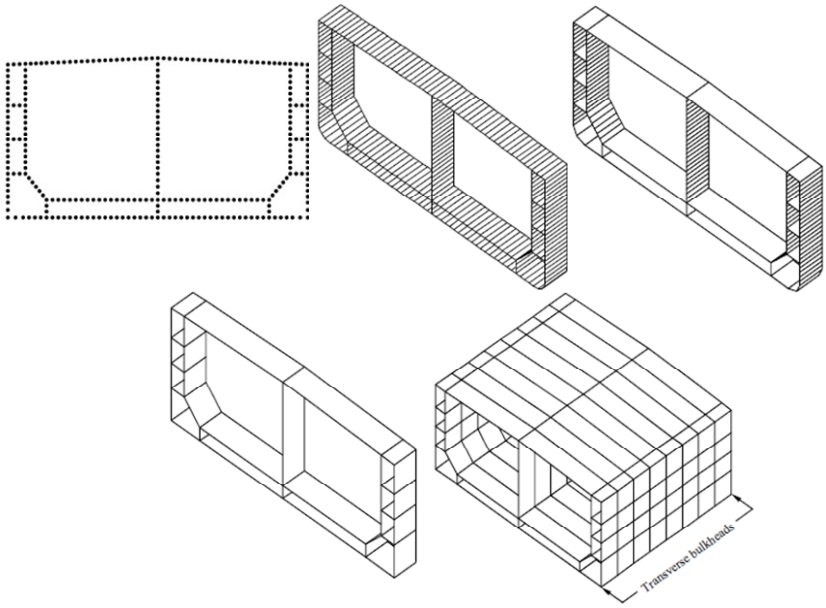

Figure 2-12: Various types of ALPS/ISUM model, Paik, Wang, Kim and Thayamballi (2002)

Other than the ISUM, a numerical program was developed by Kuo and Chang (2003) to calculate the ultimate longitudinal strength of the ship hull. The adopted method was similar to the approach of Caldwell (1965) or Paik and Mansour (1995) but was based on individual components of ship structures (Figure 2-13). The reduction factor of ultimate strength of the stiffened panels was obtained using empirical

formulae from the literature like the one of Paik and Mansour (1995). In addition to the ultimate vertical bending strength, they formulated ultimate horizontal bending strength as well as ultimate shear strength of ship the structures.

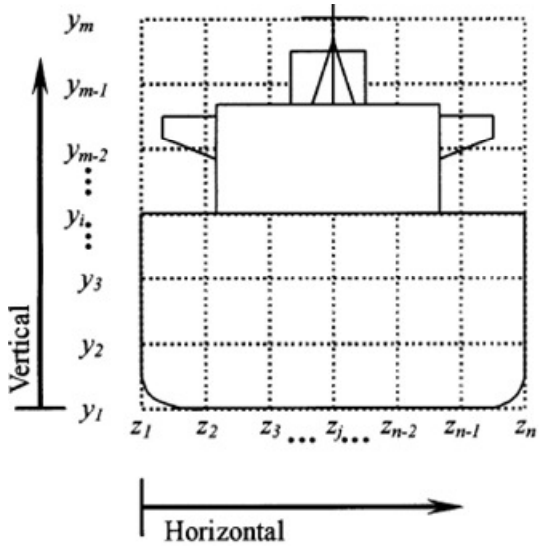

Figure 2-13: Hull section divided into several components, Kuo and Chang (2003)

Karvinen and Pegg (2006) proposed a simplified analysis method for nonlinear failure of stiffened plates using a FE method. Their approach utilises pre-determined failure equations derived from nonlinear FE analysis. For each component of a large structure, the failure load was determined under nonlinear FE analysis. Then a representative failure stress of each component would be obtained under linear FE analysis with the failure load. The representative failure stress of each component was used in simpler linear analysis to provide a representative failure limit of the large structure.

Naar (2006) investigated the ultimate strength of the hull girder for large passenger ships. Assuming that a ship structure can be modelled as a set of coupled beams, he developed a theory of a nonlinear coupled beam method which enables estimation of the nonlinear response of a passenger ship with multi-deck superstructures subjected to longitudinal bending load (Figure 2-14). In the method, each deck of the superstructure as well as of the main hull was considered as a thin-walled beam with nonlinear structural behaviour, for which load-end shortening curves under axial load were taken from the literature. The beams were coupled to adjacent beams with nonlinear springs, which have the stiffness properties of the vertical and shear

members, of which load-displacement curves were developed by nonlinear FE analysis. The ultimate strength of a post-Pamamax passenger ship was calculated and verified with the result of FE analysis.

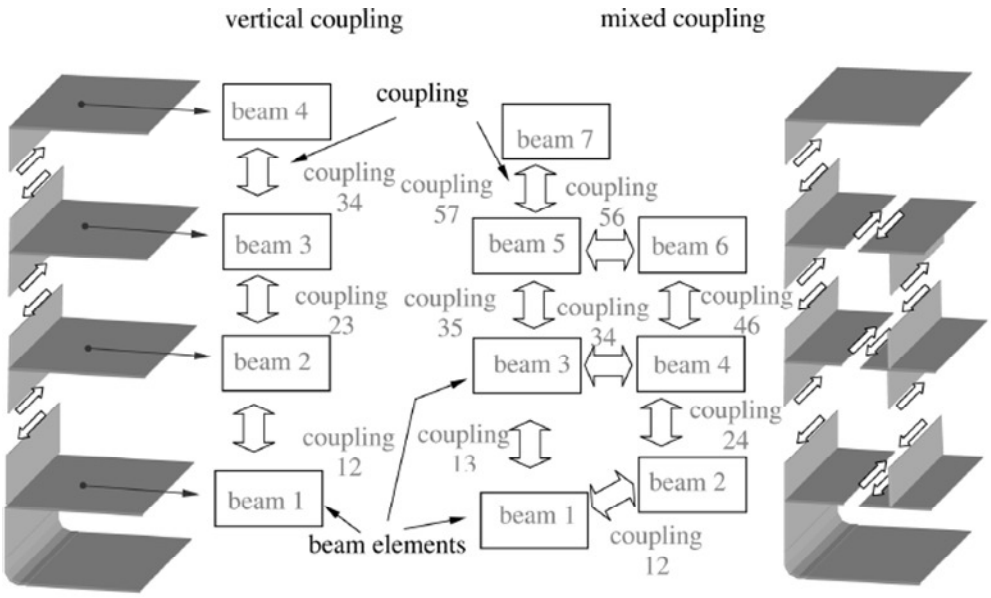

Figure 2-14: Types of coupling between beams, Naar (2006)

Although the simplified numerical approaches are developed in order to reduce efforts required for modelling the hull girder and solving the matrix, it should be noted that in the context of risk-based design and the emergency response, where reliable decision-making is required (through fast uncertainty quantification), they have disadvantage compared by the analytical approaches. Also the accuracy which is considered to be their most powerful arsenal has been faded by the increased accuracy of the analytical approaches. Most of all, the limited application and expansion of these numerical approaches in conjunction with other tools prohibits the joint analysis in a fast way.

2.3.4 Residual strength analysis

This section discusses a critical review of the methods for the calculation and determination of the residual strength capacity of a damaged hull structure. Most of the literature has addressed damaged hull sections from grounding and collision accidents but some of it elaborates on the corrosion- and crack-induced reduction of the ultimate strength capacity against the life span of the target ship. Due to the requirement of the fast application in emergency situations following accidental

damages or in the early design stage pursuing guaranteed safety performance against such accidental damages, it is understood that the analytical methods have been preferred to the numerical methods.

Based on the section modulus approach, Zhang, Yu and Mu (1996) proposed a semi-analytical method for assessing the residual longitudinal strength of damaged ship hulls. According to the definition of the effective area coefficient of damaged ship structural components, the effect of the initial deformation on the longitudinal strength was taken into account as the reduced section modulus of the damaged ship hull. They investigated plates with both longitudinally and transversely stiffeners.

The residual collapse analysis with the location and amount of collision and grounding damage was carried out by Paik, Thayamballi and Yang (1998) who developed a simplified method for assessing the residual collapse of the hull girder in the damaged condition after collision and grounding based on the approach proposed by Paik and Mansour (1995). With the prescribed damage definitions, the possibility of hull collapse was examined by a comparison of the applied extreme bending moment and the ultimate residual hull strength estimated using design oriented methods and formulas. They defined two types of residual strength index based on (i) the section modulus, and (ii) the ultimate bending strength. It was claimed that the developed method would be useful for preliminary structural design of a ship hull in accidental situations as well as for decision-making process related to salvage and rescue.

A further development of the method has been made by Mansour, El-Kilani and Abdel-Malek (2003) who carried out residual strength assessment of a ship after grounding by the approach of Paik, Thayamballi and Yang (1998) except bottom girders treated separately from bottom plates. A typical single hull tanker was analysed for the residual strength index with two grounding accident scenarios, in which the proposed method showed an enhanced accuracy when compared with the results obtained by the previous approach especially in terms of section modulus.

The method based on the calculation of the section modulus is very fast and useful in the emergency situations however, as it was addressed in the previous section, its

accuracy is less than other methods as it does not account for the different capacity of each element. Also, the maximum capacity of the residual strength from this method is hardly achieved in reality as all the structural members are assumed to reach their ultimate strength at the same time.

The use of *Smith*'s method in the evaluation of the residual strength capacity of the hull girder has been investigated by many researchers. Various types of structural damage in ships and offshore structures were reviewed by Smith and Dow (1981) with focus on the influence of such damage on stiffness and ductile strength – especially hull girder bending strength for ships. The method was suggested for evaluation of the damage effects quickly and economically for the early assessment of damage consequences.

The usefulness of the method has also been presented by Gordo and Soares (2000), who investigated the structural behaviour of several damaged hull girders of tankers and container ships by a method that tested in undamaged hulls with good results as reported by Gordo, Soares and Faulkner (1996) and Gordo and Soares (1996). Tankers of single skin and double skin as well as two container ships were analysed under different damaged situations and the degradation of the ultimate carrying capacity under longitudinal bending moments was evaluated. Further application of the method can be found in the projects partially funded by the European Commission, e.g. SAFEDOR (2006), in which the ultimate bending strength is expressed as a probabilistic model by accounting for the uncertainty in the geometry and material properties as well as in the model itself.

The collision resistance of single- and double-skin bulk carries subject to collision damage has been investigated by Ozguc, Das and Barltrop (2005) followed by residual strength analysis. For the evaluation of resistance forces, energy absorption and penetration depth, impact dynamic analyses simulating collision accidents were carried out using ANSYS LS-DYNA (Figure 2-15). Residual strength analysis against each collision damage scenarios was conducted using *Smith*'s method. By comparing the ultimate hull girder strength of the damaged vessels with hull girder bending moment predicted by the Joint Bulk Carrier Project (JBP) Rules, the safety of vessels in damaged conditions was determined.

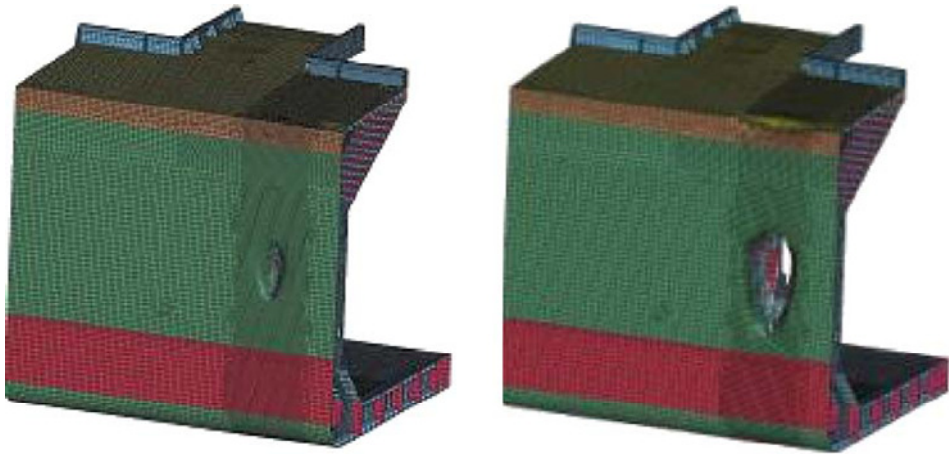

Figure 2-15: An example of collision damage simulation of double side skin bulk carrier, Ozguc, Das and Baltrop (2005)

The efficiency and accuracy of the *Smith*'s method in the use of the calculation of the residual strength capacity of the damaged hull girder has been investigated by Soares et al. (2008), who have conducted a benchmark study on the use of simplified structural analysis methods based on the *Smith*'s approach to predict the ultimate strength of a damaged ship. A number of different simplified methods were taken into account for comparison of the predicted ultimate strength both in intact condition and damaged condition of a Ro-Ro ship. The damaged section modelled by removing the structural elements from the affected areas. Results obtained for the ultimate strength were compared against each other and with the results of the FE analysis. It was found that with a few exemptions, the results of the approximate methods agreed well with each other for the intact and damaged conditions. The simplified methods were more conservative than the FE analysis in hogging while they seemed to give a very good approximation to the result for sagging with some of them overestimating this value. However, it was stressed that without experiments, accuracy of both analyses could not be rated.

The effect of the fatigue crack propagation on the degradation of the residual strength capacity of the hull girder has been addressed in the report of Ghose, Nappi and Wiernicki (1994). In the report, they reviewed the state of the art of the residual strength analysis methods used by marine industry and introduced the subject of the residual strength assessment of the damaged marine structures due to normal operating loads. While summarising the state of the art technology and methods

available in the industry for quantifying residual strength in terms of fatigue crack propagation and ultimate hull girder strength, they recommended further steps to integrate existing engineering procedures in the fields of crack growth, permanent deformation and ultimate strength in cost effective ways.

Later, the effect of the crack presence in a steel plate on the reduction of the ultimate strength of the steel plate has been investigated by Paik, Kumar and Lee (2005). They carried out an experimental and numerical study on the residual ultimate strength of transversely cracked steel plate subjected to axial compressive or tensile loads. The ultimate strength reduction due to cracking damage was investigated with various sizes and locations of cracking damage (Figure 2-16). Based on the experimental and numerical results, theoretical models for predicting the ultimate strength of cracked plate under axial loads are developed.

A further study was carried out by Paik (2008) for the steel plate with longitudinally cracked damage under axial compressive loading. It should be noted from the results that cracks as well as damages on the plating reduces the ultimate strength capacity hence the accidental damage opening on the hull plating and its propagation due to dynamic external loadings are of importance in evaluating the residual strength capacity of the damaged hull girder.

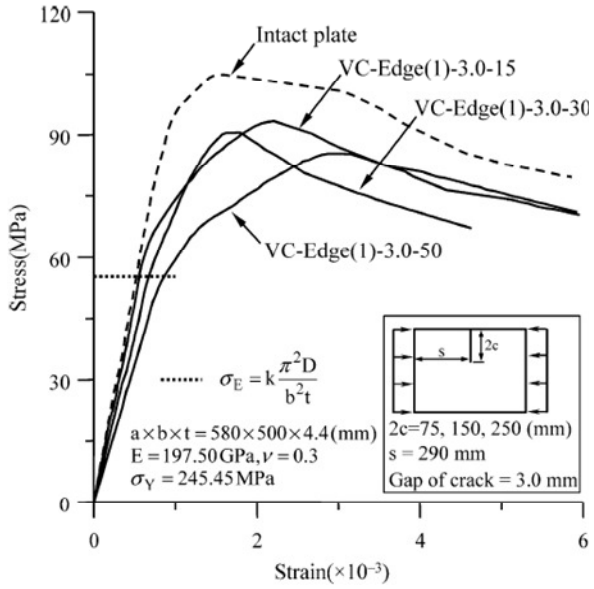

Figure 2-16: Average axial compressive stress-strain curves of specimens with one side crack of varying crack sizes, Paik, Kumar and Lee (2005)

Paik et al. (2003a) also investigated the effect of time-variant corrosion wastage on the ultimate hull girder strength as well as the section modulus of bulk carriers. They used a set of the time-dependent corrosion wastage models for 23 different member locations/categories of bulk carriers based on the available corrosion measurements for existing large bulk carrier structures. The reduction of the ultimate strength of a bulk carrier due to the corrosion effect was identified (Figure 2-17). Other studies on the effect of the corrosion on the reduction of the hull girder strength can be found in Wang, Spencer and Sun (2003), and Wang, G. et al. (2008).

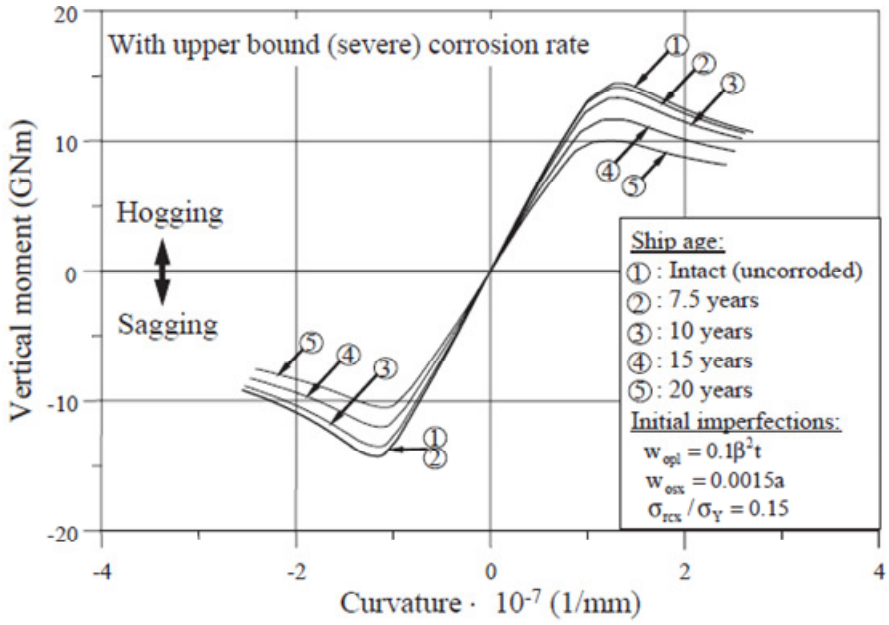

Figure 2-17: Comparison of the progressive collapse behaviour of the corroded bulk carrier hull under vertical moment varying the ship ages, Paik et al. (2003a)

The effect of the corrosion wastage and fatigue cracking as well as the local denting damage on the reduction of the ultimate strength of aging ships has been investigated by Paik et al. (2003b). Each effect was determined by an ultimate strength reduction factor and extended in a time dependent model. Also their combined effect is proposed by a multiplication. The decrease of the ultimate strength of the three ships i.e. a double hull tanker, a single sided bulk carrier and a single hull tanker-type FPSO is assessed against the ship's age and a reliability index is calculated with the probabilistic characteristics of the random variables considered for the analysis. Based on the degrading ultimate strength results, the authors proposed a repair scheme in order to keep the longitudinal strength of the aging ship within the criteria.

It seems that this was the first research that the effect of the fatigue crack propagation was explicitly considered in the calculation of the ultimate strength of the hull girder in time domain even though the crack growth model was very simple ignoring the effect of the threshold and accelerated region. Also the main objective of the study lay on the proposal of the maintenance scheme for the aging ships.

Aside from the calculation of the residual strength, an approach enables a fast estimation of the residual strength using the simple analytical equations or the pre-calculated information has been explored. Wang, Chen, Zhang and Shin (2000) investigated residual strength of hull girder after grounding of four double hull tankers, three bulk carriers and one single hull VLCC. It was noted that the loss of section modulus (to the deck and to the bottom) and the loss of ultimate strength (sagging and hogging conditions) are approximately proportional to the transverse damage extent at the bottom but has a poor relationship with the ship's length. Hence, they were approximately expressed as simple equations. It was revealed from the results that when damaged to the same proportion of the ship's breadth, a double hull tanker and a bulk carrier have comparable hull-girder residual strength, and are better than a single hull tanker.

A further study was carried out by Wang, Chen, Zhang and Peng (2002) who investigated the longitudinal strength of ships with damages due to grounding or collision accidents. They developed analytical equations for residual hull girder strength analysis and verification was made for a broad spectrum of accidents of 67 commercial ships including double hull tankers (Figure 2-18), single hull tankers, bulk carriers and container carriers. Based on the results of the commercial ships, new proposed equations for residual section modulus were derived for each ship type regardless of ships' dimensions and its use in the emergency or salvage operation is claimed. However, in this study, the residual strength was based on the section modulus rather than the ultimate strength. Further development of similar analytical equations for ship types other than those used in the analysis may be recommended.

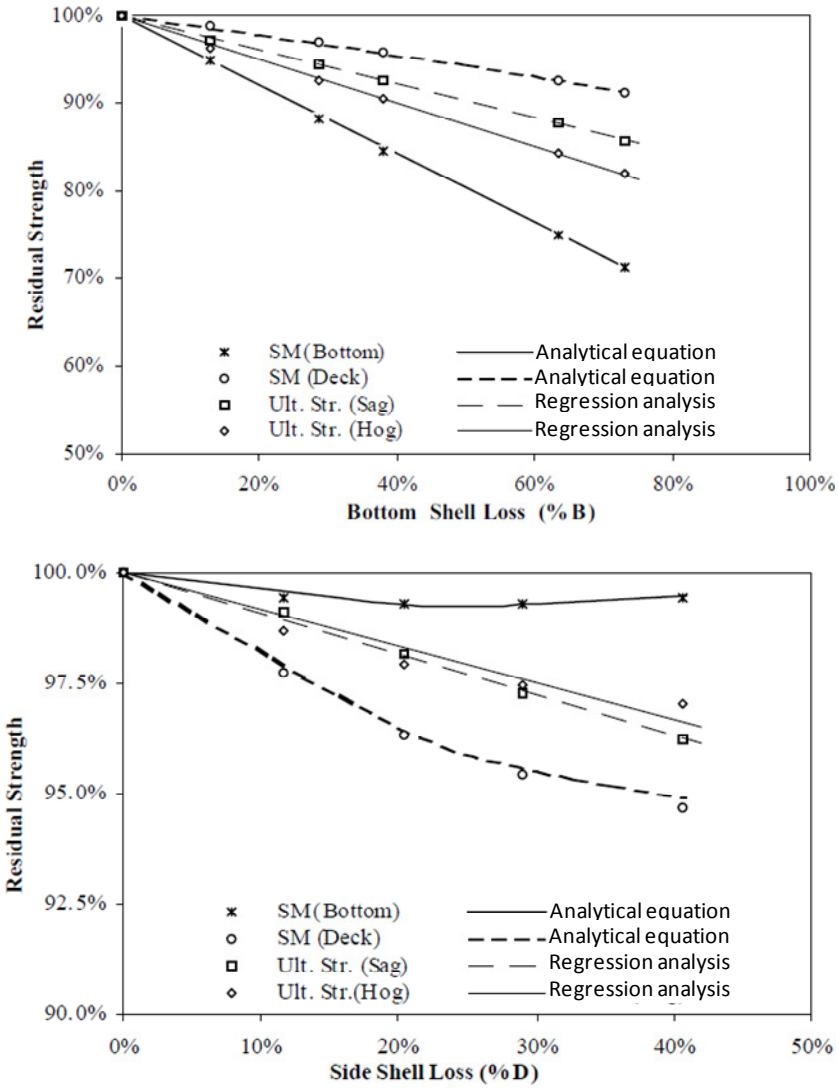

Figure 2-18: An example of residual strength of double hull tanker with grounding damages (upper), and collision damages (lower), Wang, Chen, Zhang and Peng (2002)

Another effort on the pre-calculation approach could be found in the work of Ziha and Pedisic (2002), who investigated the effect of different damage modes of a hull section on the residual longitudinal strength of an impaired ship based on elastic theory, fully plastic resistance moment theory and ultimate bending moment approach then produced a residual strength contours. The practical application of the computational link between the residual strength contours and a ship's survivability was graphically represented in an example (Figure 2-19). It is understood that the use the residual strength contours of damaged hull girder sections would enhance assessment of a ship's survivability when exposed to longitudinal vertical bending after an accident.

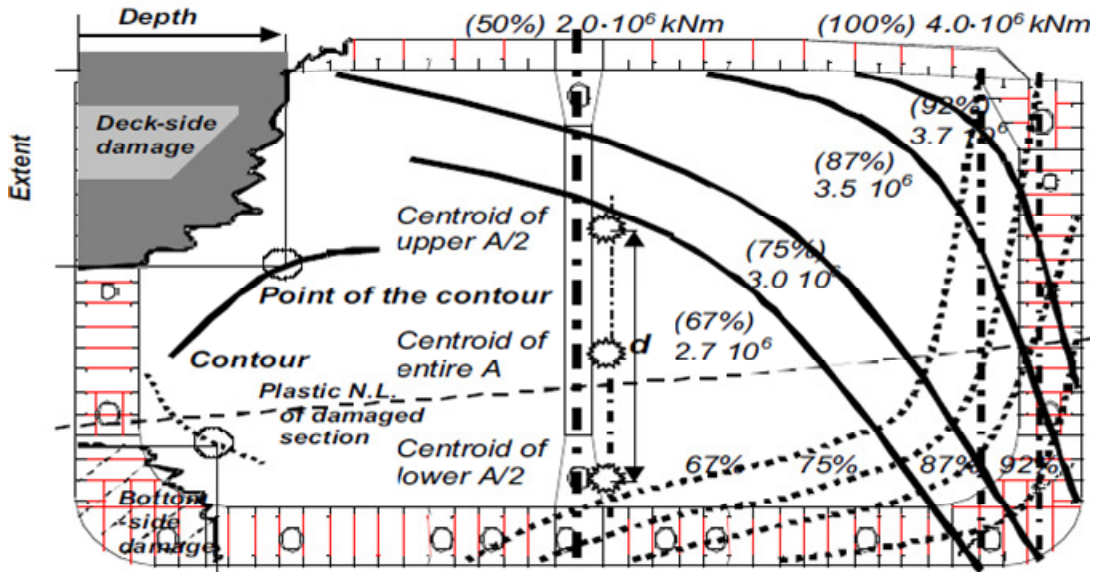

Figure 2-19: Definition of damaged areas and contours of constant residual strength (left), an example of fully vertical plastic resistance moment contours in a hogging condition with an upright position (right), Ziha and Pedisic (2002)

2.4 Chapter summary

The critical review of the fatigue crack propagation and the methods for calculating the ultimate (residual) strength capacity of the hull girder presented in this chapter indicates that each discipline has been researched broadly and deep. Although some study has addressed the necessity of combining the two subjects and effort has been devoted to solve the problem e.g. Paik, Kumar and Lee (2005) and Paik (2008), it is clearly understood that the realistic phenomenon of crack propagation from the accidental damages has not been treated at all and that an elaboration devoted to combining the damage propagation with the assessment of the structural survivability of damaged ships in time domain is of importance at the emergency situations or at the design stage. A detailed explanation of the approach and methodology to solve the coupled problem where the time-varying damage propagation from the initial accidental damages affects the survivability of the damaged ships will take place in the following chapter.

3 METHODOLOGY

3.1 Preamble

The methodology for assessing the survivability of a damaged ship in terms of loss of structural strength and damage stability under time-varying weather conditions is proposed in this chapter. Considering the matured effort on the damage stability aspects, the progressive loss of structural integrity and the residual strength assessment in time domain are focus points of the current research.

3.2 Framework of development

In case of accidental loadings or structural failure in severe environments emphasis is placed on the survivability of the ship in terms of damage stability and residual strength assessment.

The ensuing loss of stability and potential for capsizing or foundering of the damaged ship have been covered extensively and to great depth in the literature for passenger ships, Vassalos, Jasionowski and Guarin (2005), Vanem, Rusas, Skjong and Olufsen (2007), etc. On the other hand, assessment of the residual strength of the ship has been carried out by calculating the residual bending moment capacity and ultimate bending strength of the damaged hull girder. Applications can be found in Paik, Thayamballi and Yang (1998), Soares et al. (2008) and also in some jointly funded research projects by the European Commission and the industry such as DEXTREMEL (2001), and SAFEDOR (2006).

As it was discussed in Chapter 2, the assessment of stability and residual strength in the context of accidental scenarios have been carried out independently with a strong assumption that the initial damage extent remains stable. Quite evidently this is not the case considering that the initial damage can propagate as dynamic loads are continuously imposed by the environment and accumulate until a limiting state is reached after which total failure is observed. The progressive structural failure during these complex situations may threaten the survivability of the damaged ship by reducing the hull girder structural capacity and/or by increasing the chance of loss of the damage stability from the exaggerated flooding. That is, any cases where flooding contribution is important (e.g. passenger ships).

In direct response to the clear gap between reality and the conventional way of treating situations like these, this research elaborates on a methodology that combines both environmental (global) and flooding (local) loads, determination of damage propagation and assessment of residual strength and damage stability. A high level description of the proposed methodology is shown in Figure 3-1.

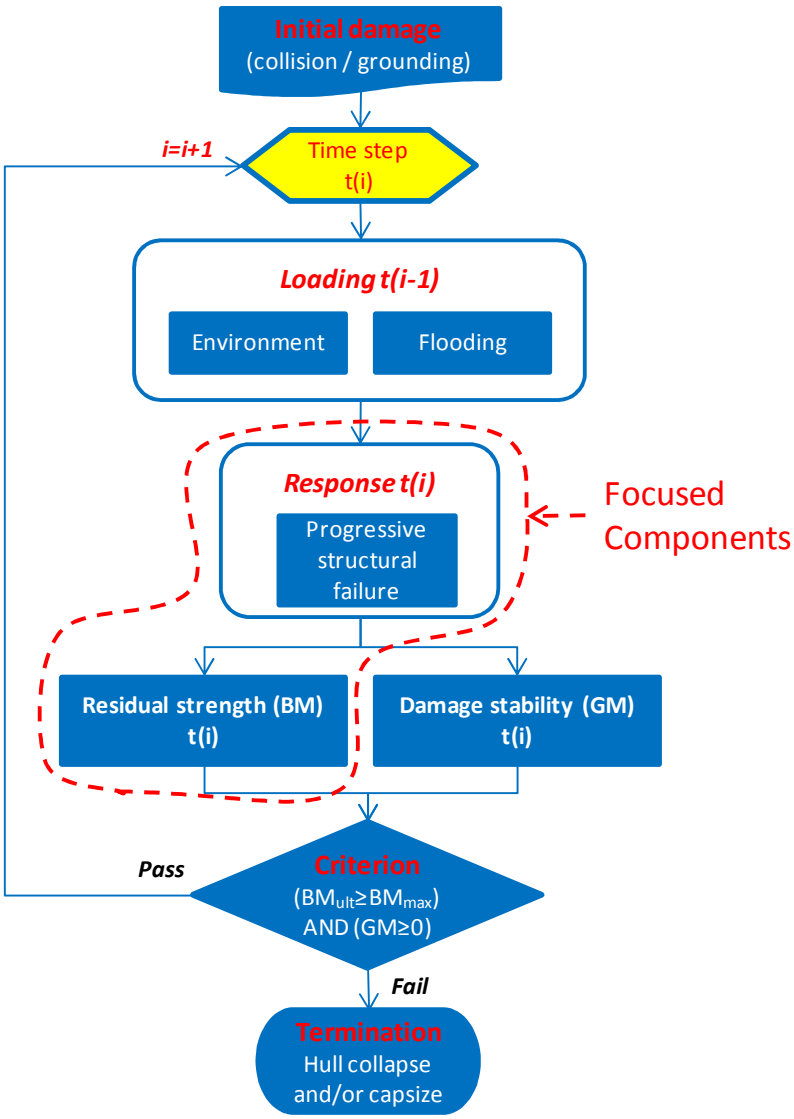

Figure 3-1: High level process of the proposed methodology

The key feature of this approach is the modelling of damage evolution in the time domain. For a damage to propagate (in the form of plate tearing and stiffener severing), a source of loading should be identified and defined properly. The progressive structural failure in a damaged ship is achieved by crack propagation analysis under the wave loading action. Furthermore, when the damaged ship is

flooded the water that ingresses and egresses from the damaged compartment (due to the ship motion and the waves) constitutes another source of loading that deteriorates the damaged area further and induces crack propagation. In turn, the damage extension results to further structural degradation and the cycle repeats until either damage stability is totally lost or residual strength becomes insufficient to sustain the applied loads.

Due to the time domain feature of the process, for every time step of the calculation the crack propagation is analysed and the effect of damage evolution on the survivability of the damaged ship needs to be assessed in terms of criteria pertaining to residual strength and damage stability. In principle, such criteria can be expressed as the bending moment capacity (*BM*) and the metacentric height (*GM*) respectively, and they should account for the dynamics of the situation by focusing on the stress variation and the time to capsize respectively as addressed in Vassalos (2009). The calculation process will be repeated for varying loading input, until either the strength or the stability criterion fails.

The following sections elaborate on a brief description of each component that constitutes the proposed assessment process. The damage stability is shortly explained in Appendix A.

3.3 Environmental loading

The load induced by the waves is the primary source for crack propagation and it is calculated by an in-house 3D panel code with Green's function implementation, Xie (2011) and Kwon, Xie, Calvez and Hodgson (2011). This code offers the capability of calculating ship motions and wave loads both in time domain and frequency domain with inclusion of non-linear wave effects adopting instantaneous wetted hull surface for the calculations of Froud-Kriloff and hydrostatic forces whereas inertia, radiation and diffraction forces are calculated at the mean wetted hull surface. The required data for wave loading analysis and the output are listed below and the flowchart is depicted in Figure 3-2.

Input

- Ship geometry
- Loading condition of the intact ship
- Location and size of the flooded compartment(s)
- Wave condition (Hs, Tz)
- Draft and trim at the damaged condition

Output

- Wave and still water bending moments
- Ship motions

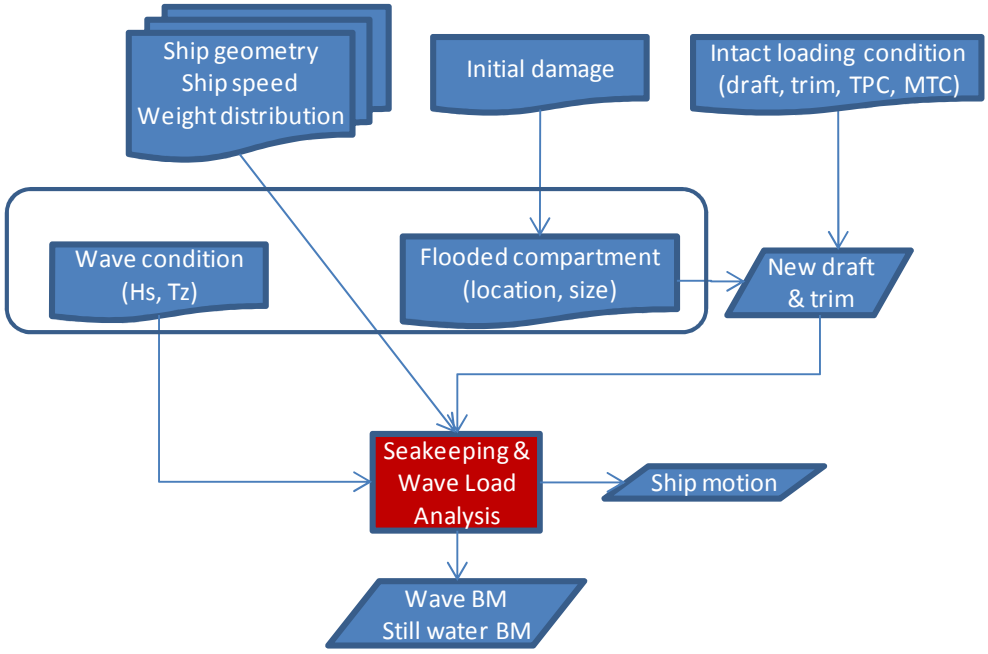

Figure 3-2: Diagram of determining environmental loadings

The obtained wave and still water bending moments form direct input to the progressive structural failure analysis so that they can be used as driving forces for crack propagation. Also, the total bending moment is compared to the residual strength of the damaged ship for every time step of the calculation process. The ship motions are used in the flooding simulation. Figure 3-3 shows an example of output, where wave bending moment in the frequency domain is presented. The difference between hogging and sagging is contributed to the inclusion of the non-linear wave effects especially at the bow and stern part.

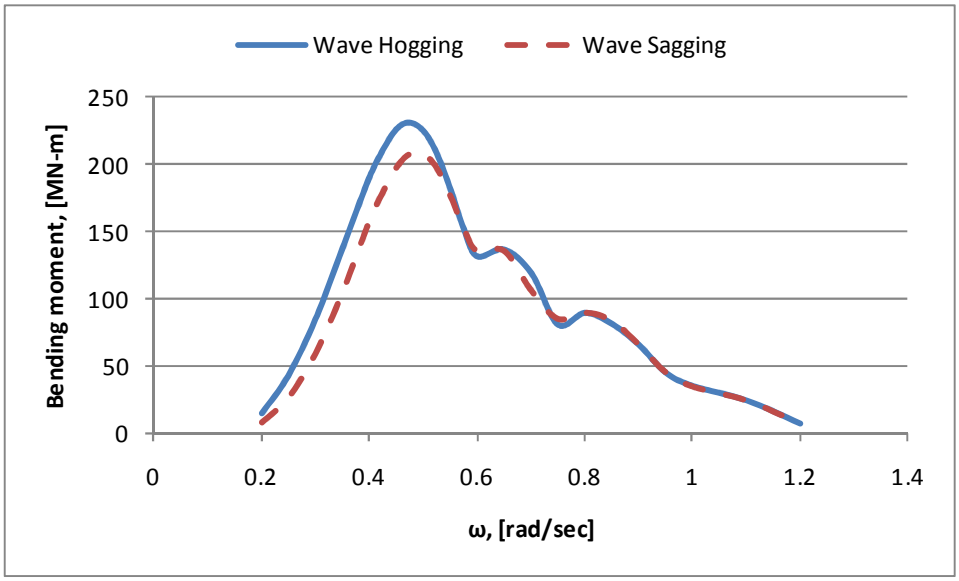

Figure 3-3: An example of wave bending moment response amplitude operators

3.4 Flooding loading

The second component addresses flooding loadings. If the damaged compartment is flooded and water ingress and egress occur continuously due to ship motions and favourable wave heights, the dynamic pressure variation on the interface of the hull surface and the sea will affect the crack propagation. Depending on the size and location of the damage opening, the size of flooded compartment, the amount of the flooded water and the hull motions the induced flooding pressure and its extent is defined. This calculation is currently based on CFD simulations and in particular the solution of the Navier-Stokes equations with the free surface capturing scheme, the so called volume of fluid (VOF) method. The finite volume method is used to discretise the governing equations as explained in Gao, Vassalos and Gao (2010). The required input data and output of the analysis are listed below and the flowchart of the process is summarised in Figure 3-4.

Input

- Damage size and location
- Geometry of the flooded compartment
- Wave condition(s) (Hs, Tz)
- Draft and trim at the damaged condition
- Ship motions

Output

- Inflow / outflow velocity
- Water height in the flooded compartment
- Flooding pressure differential
- Sloshing pressure

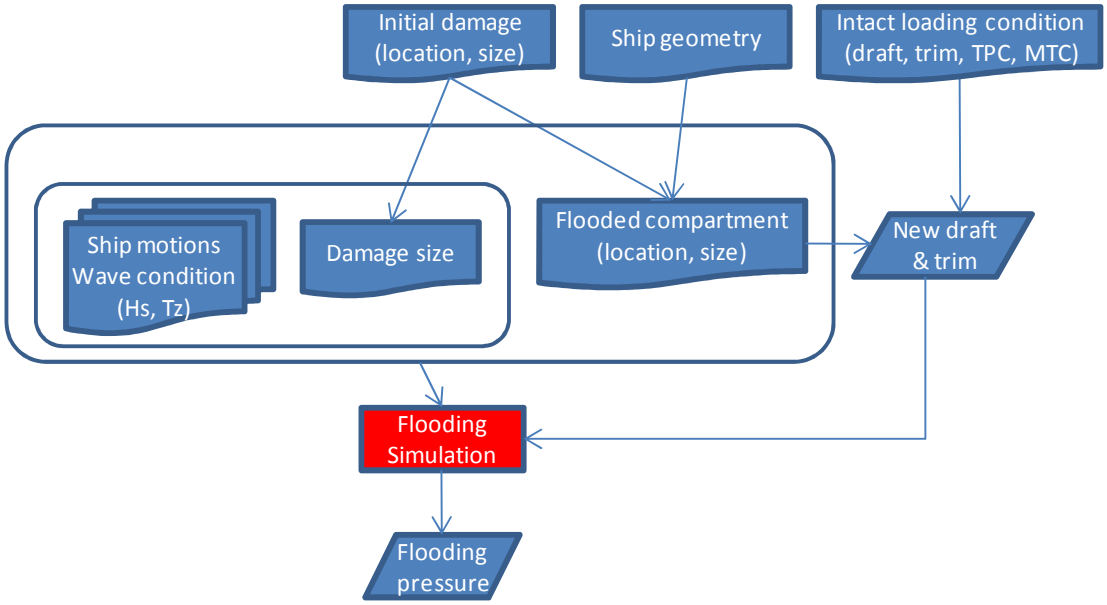

Figure 3-4: Diagram of determining flooding loadings

Time dependant data such as damage size, wave condition and ship motions need to be updated at every time step of the simulation. Figure 3-5 shows a snapshot of dynamic pressure distribution around the damage opening of a box model.

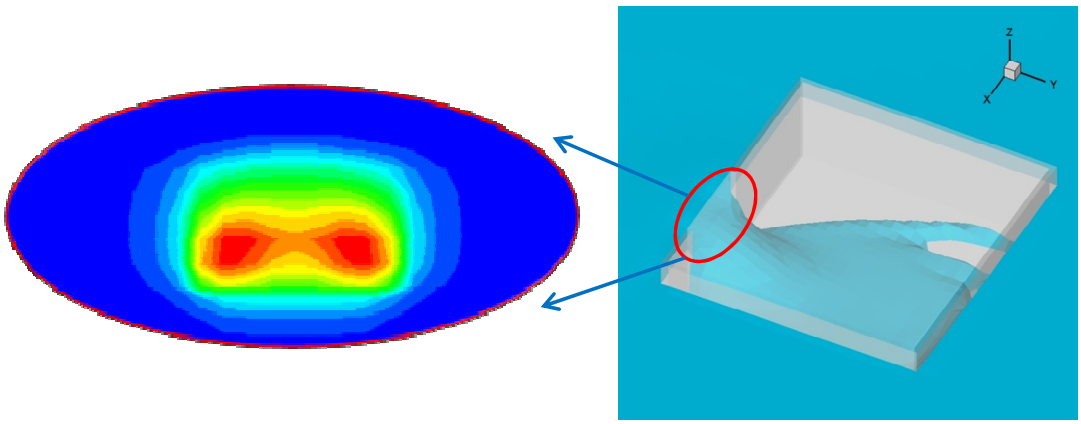

Figure 3-5: An example of dynamic pressure distribution near the opening of a box model, Gao, Vassalos and Gao (2010)

Such appealing results have only been achieved very recently although the whole approach is still at its infancy due to its computational- and modelling-intensive nature. Nonetheless, it signifies a turning point in the way flooding simulations will be treated in the future and constitutes the foundation for its integration in the methodology that is developed in this thesis. However, because these results are based on time-consuming CFD simulations their meaningful utilisation in rapid survivability assessments is hindered. That is, the calculation time for a few seconds of simulation spans several days. Further maturing of the approach will deem the development of parametric models feasible and will enable a true integration with the progressive structural failure analysis. For these reasons, flooding loading will be ignored in the remaining of this thesis.

3.5 Progressive structural failure

Once the loadings are obtained, they are transferred to the progressive structural failure analysis, where the growth of cracks emanating from or near the damaged parts in time domain based on the LEFM and a proper crack growth model such as *Paris Law* in which '*time*' is included implicitly in the number of cycles, *N*, where '*N=time/period*'. Although the LEFM is applicable to brittle materials according to Irwin (1957), it can also be applied to ductile materials, where the plastic zone size around the crack tip is small compared with the crack size. Considering Irwin's estimation on the plastic zone size, r_p, as expressed in Equation (3-1), the plastic zone size becomes 56.5 mm when the SIF (K) is equal to 140 MPa$\sqrt{\text{m}}$ (plane strain fracture toughness, K_{IC}, of mild steels[2]) and the yield stress of 235 MPa is used for mild steels. Such size can be safely assumed small in comparison to the overall crack size which is in the order of metres when including the damage opening size in case collision or grounding. Hence, LEFM is deemed suitable for the purposes of this project.

$$r_p = \frac{1}{2\pi}\left(\frac{K}{\sigma_y}\right)^2 \tag{3-1}$$

where, r_p is the plastic zone size in metre

[2] http://www.efunda.com/formulae/solid_mechanics/fracture_mechanics/fm_lefm_Kc_Matl.cfm

K is the SIF in MPa$\sqrt{\text{m}}$

σ_y is the yield stress of the material in MPa

It should be noted that on top of the above arguments, LEFM for ductile materials has been adopted in other research projects not only in the shipbuilding industry, e.g. Dexter and Pilarski (2000), Dexter and Mahmoud (2004), where crack propagation in a stiffened panel has been studied, but in the aviation industry as well, e.g. Farahmand, Saff, Xie and Abdi (2007).

The empirical expression of *Paris Law*, the basic crack growth model, shows that the rates of crack growth are proportional to the range of SIF, ΔK, when plotted on a log-log scale as expressed in Equation (3-2).

$$\frac{da}{dN} = C \times \Delta K^m \quad \textbf{(3-2)}$$

where, $\frac{da}{dN}$ is crack propagation rate with units of [metres/cycle]

ΔK is range of the SIF with units of [MPa$\sqrt{\text{m}}$], $\Delta K = K_{max} - K_{min}$

C and m are material constants for crack propagation

The above relationship is valid as long as the calculated ranges of SIF, ΔK, are above the threshold values, ΔK_{th}, and the values of the applied maximum SIF, K_{max}, are smaller than the material toughness, K_C. The details of the crack growth rate model which includes the range of threshold SIF, the material fracture toughness limit and the effective range of SIF is presented in Chapter 4.

Based on Equation (3-2), the final crack length, a_f, is estimated with the given initial crack size, a_0, and the number of cycles, N, as follows:

$$a_f = a_0 + \int_0^N C \times \Delta K^m dN \quad \textbf{(3-3)}$$

Also, the required number or cycles, N_r, for an initial crack of size a_0 to grow to size, a_f, is obtained as:

$$N_r = \int_{a_0}^{a_f} \frac{1}{C \times \Delta K^m} da \quad \textbf{(3-4)}$$

In *Paris Law*, when the range of SIF is constant, the corresponding crack growth rate, *da/dN*, becomes constant. However, the range of SIF of a crack tip is subjected to change as the range of the applied external load on the structures, where the crack tip exists, varies over time. In addition, even under a constant range of external loading the range of SIF of the growing crack tip cannot remain constant.

Hence, it is of paramount importance to obtain SIFs of the crack tip accurately for each time step by taking into account both time-varying external loads and geometry surrounding the crack tip. An FE method is deployed to calculate exact SIFs in various conditions of external loads and structural configurations, the results of which are distilled in knowledge-intensive models.

Finally, the procedure for evaluating progressive structural failure using crack growth models e.g. *Paris Law* and LEFM is formulated as shown in Figure 3-6.

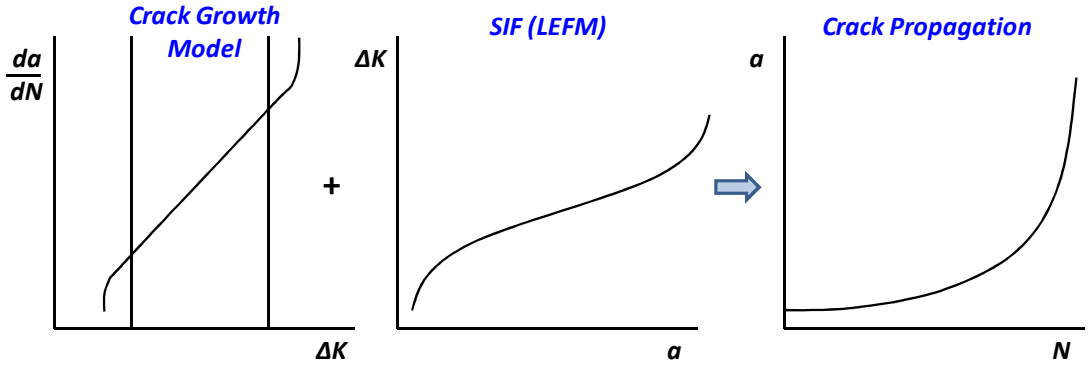

Figure 3-6: Procedure of progressive structural failure

The required data of input and output of the progressive structural failure analysis are summarised below and its process is presented in Figure 3-7. In this process, the time dependant data, such as loading, damage and crack size, are updated for each time step. The extended crack size shall be used (i) in the residual strength assessment, and (ii) to update the opening of the flooded compartment and any adjacent ones if its boundaries are breached.

Input

- Ship geometry
- Initial damage location and size
- Wave bending moment
- Flooding pressure
- Material constants for the crack growth model

Output

- Damage (crack) size growth in the time domain

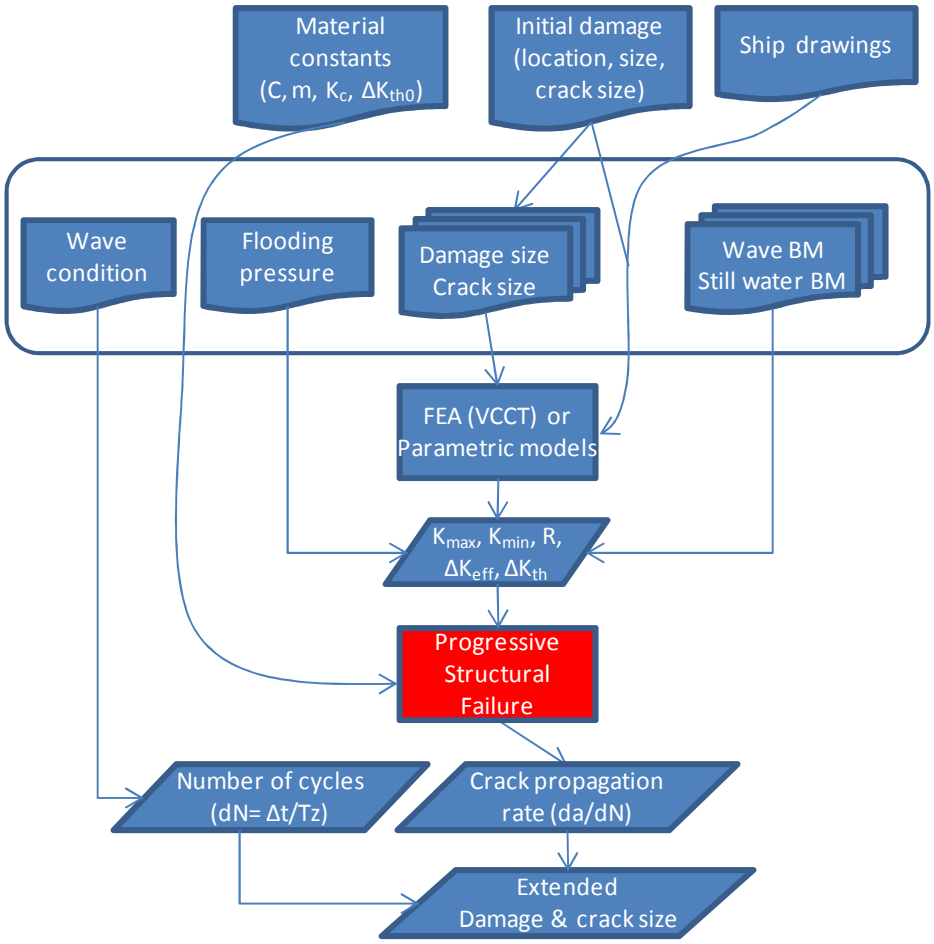

Figure 3-7: Diagram of progressive structural failure analysis

The progressive structural failure analysis is the component that is making difference to the current survivability assessment method from the conventional approaches, where its effect has been ignored. This is also the reason why the progressive structural failure is the focus in this thesis. The details of defining an appropriate

crack growth model and material constants, the determination of SIFs with FE analysis and the developing knowledge-intensive models for SIFs will be elaborated in Chapter 4.

3.6 Residual strength capacity

The effect of the progressive structural failure on the deterioration of the structural strength of the hull girder is determined by the calculation of the residual strength capacity, which is enabled by a method based on an incremental iterative approach which uses the moment-curvature relationship for stiffened panels. Examples of this method can be found in Smith (1977), Gordo, Soares and Faulkner (1996), and CSR rules by IACS (2008).

The moment-curvature result is obtained by imposing a *curvature* from sagging to hogging on the hull girder, which is assumed to consist of several beam-column elements. For each curvature, the average strain of each element is calculated and the stress imposed on each element is obtained from the corresponding load end shortening curve. The moment sustained by the whole section is obtained by summing up the moments of each element induced by axial force and the distance of each element from the neutral position of the section. The ultimate bending strength of the section is the maximum bending moment in the moment-curvature curve in hogging and sagging conditions.

The load-end shortening curve of each element is based on the elastic-perfectly plastic behaviour of the material of each element. The definition of each curve includes the effect of plate-induced failure, flexural bucking failure of column, tripping failure of stiffener and web local buckling failure. The effect of residual stress is also taken into consideration.

The summarised input and output of the residual strength analysis and its flowchart are outlined in Figure 3-8. As damage evolves the effective width of plate as well as loss of stiffeners of the damaged section will be updated for each effective time step so that the ultimate residual bending strength at the given time can be estimated appropriately. This can only be achieved by interaction of this process with the progressive structural failure analysis.

Input

- Load end shortening curve of each element, which is composed of a stiffener and associated plate
- Neutral axis of the respective cross section for the damaged condition
- Range of curvature from sagging to hogging

Output

- Ultimate residual bending moment capacity of the damaged section in hogging and sagging

The details of the load-end shortening curves for various failure modes, the development of a tool for residual strength assessment and the validation of the models are presented in Chapter 5.

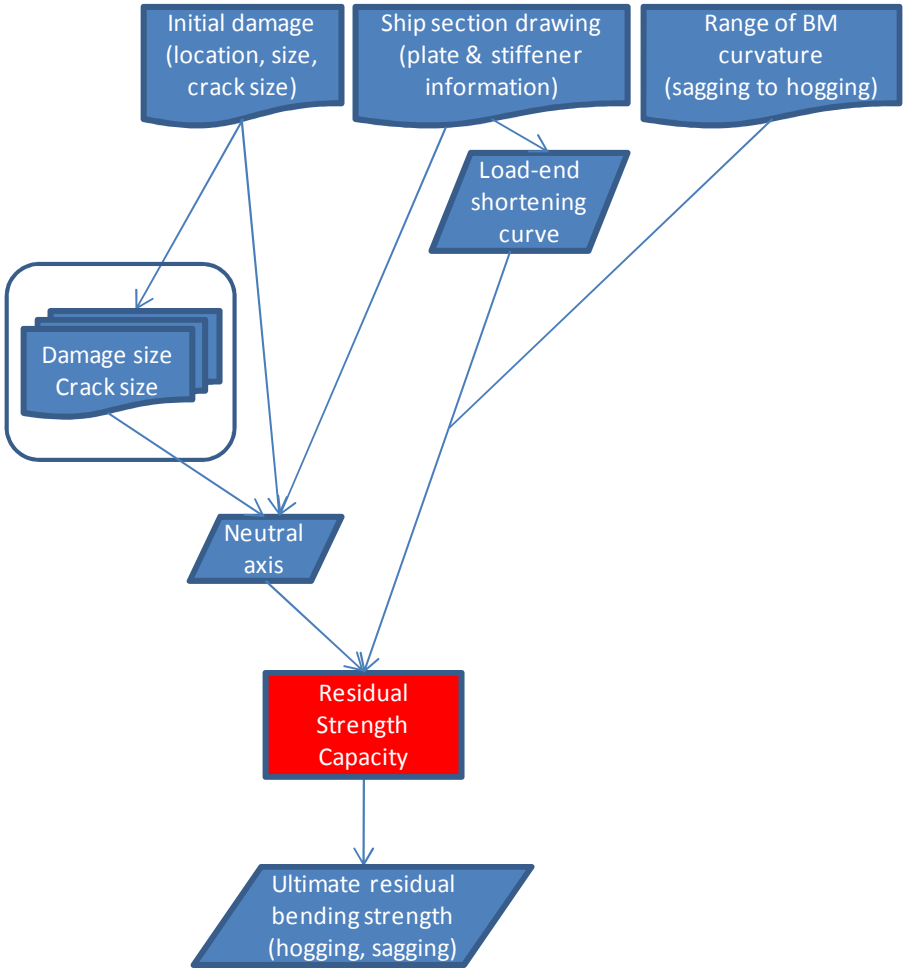

Figure 3-8: Diagram of residual strength analysis

3.7 Interaction between the components

As the current research focuses on the development of the methodology for determining the progressive structural failure and its interrelation with the evaluation of residual strength capacity in *time domain*, a brief explanation of the interacting mechanism between two components is given next.

The interface between the two components is the geometry information of the damaged section. That is, with the initial damage configuration, the section modulus of the damage section is calculated and used for determining the stress level on the crack tips under the given wave conditions. The induced stress will develop damage crack propagation, which will be returned to the geometry model of the residual strength capacity component to update the geometry information of the damaged section and subsequent section modulus as well as stress level. This process (Figure 3-9) will take place in every time step until the collapse of the hull girder or the simulation time reaches its final step.

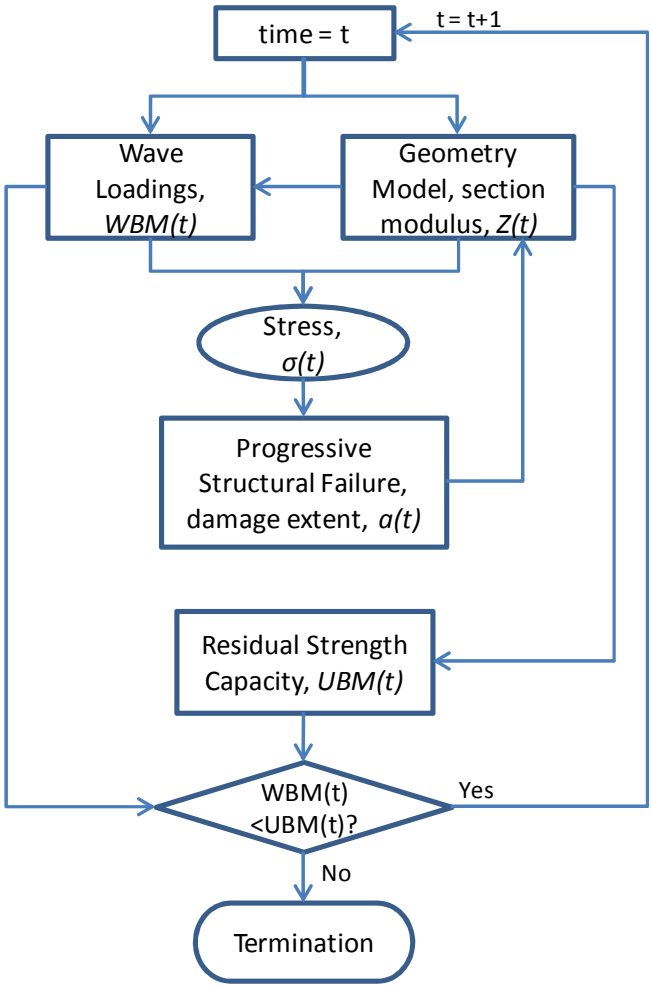

Figure 3-9: Iterative interaction process between two components

3.8 Chapter summary

A methodological approach for evaluating the survivability of a damaged ship is outlined in this chapter. The progressive structural failure analysis, which constitutes the focus point of this research, follows the discussion on the integration with flooding and wave loading, which has detrimental effects at local and global structural level respectively, and it is complemented by ultimate strength assessment. Because of the recent developments in the field it was not possible to integrate all these elements in the current work. Justification for various choices that have been made and more detailed discussion will follow in Chapters 4 and 5.

4 PROGRESSIVE STRUCTURAL FAILURE

4.1 Preamble

This chapter is devoted to the development of a method for progressive structural failure analysis. For this, a crack growth model is founded in a formulation that accounts for material constants, followed by a method of determining the SIFs by the first-principles FE analysis. The chapter closes with the development of knowledge-intensive models for the calculation of SIFs without FE analysis.

4.2 Crack growth model

This section addresses the crack growth model used in the progressive structural failure analysis. Various models are discussed and an equation that covers the whole crack growth region is proposed. Also, the effect of various stress ratios is taken into account in the model, and the material constants are obtained so as the linear region of the proposed formulation is compatible with *Paris Law*.

4.2.1 Equations of crack growth

The basic model of crack growth rate is known as *Paris Law* which expresses that the crack growth rates are proportional to the range of SIF when plotted on a log-log scale. The basic equation of Paris Law is recalled below.

$$\frac{da}{dN} = C \times \Delta K^m \quad \textbf{(4-1)}$$

where, $\frac{da}{dN}$ is crack propagation rate, [metres/cycle]

ΔK is range of the SIF, [MPa$\sqrt{\text{m}}$],

$\Delta K = K_{max} - K_{min}$

C and m are material constants for crack propagation

But based on experimental data, a sigmoid shape rather than a straight line is shown on a log-log scale, which means that crack retardations occur near the range of the threshold SIF and accelerated crack propagations appear when the maximum SIF reaches the material fracture toughness, K_C.

As long as crack propagation occurs for a range of SIF between the threshold and the maximum values, after which unstable growth is observed, the linear Paris Law with properly selected material constants will be sufficient.

However, as this research addresses damaged ship in waves, the range of SIF is expected to vary widely and in accordance with the wave conditions. That is, the crack will be retarded when the dynamic loads are small and the size of the damage is not sufficient for the further development, whilst an accelerated propagation will be expected when the dynamic loads are large enough to increase the SIF beyond the material fracture toughness.

A range of crack growth models have been proposed in the literature, which can be categorized as follows:

- Models with the effective range of SIF
- Models with the threshold range of SIF
- Models with unstable growth
- Models including threshold and unstable regions

A brief explanation of each model is presented in Appendix B with comparison among them. The material constants of C and m are assumed to be 9.5×10^{-12} and 3.0 according to BS PD6493 (1993).

4.2.2 Fracture toughness of materials

Fracture toughness (K_C) is a material property that describes the ability of a material containing a crack to resist brittle fracture and is defined in terms of the SIF at a critical stress state of the crack tip. The most common test specimen configurations for performing a fracture toughness test are the single edge notch bending specimen and the compact tension specimen. It has been shown from test results that the fracture toughness changes with the specimen thickness until the thickness exceeds some critical dimension, after which it becomes relatively constant. This is another material property which is called the plane strain fracture toughness, K_{IC} (Figure 4-1).

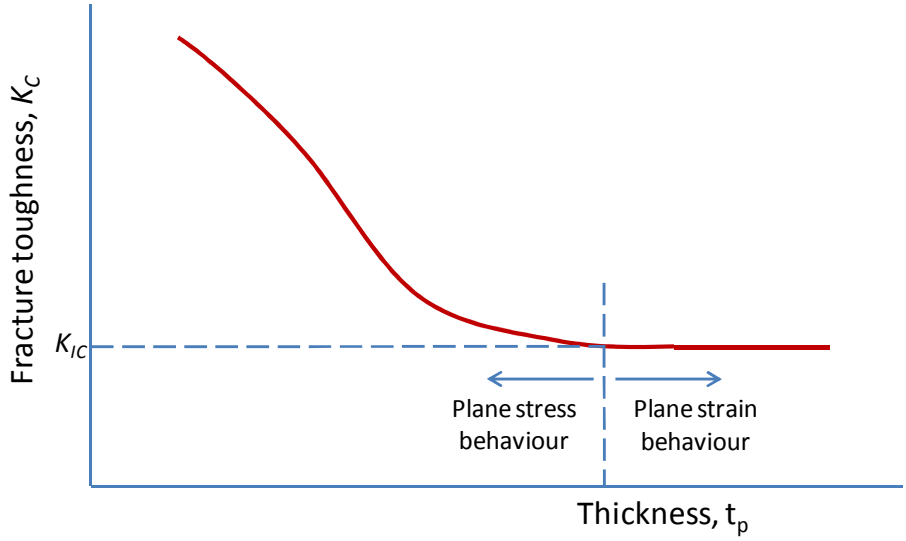

Figure 4-1: Schematic representation showing the effect of plate thickness on fracture toughness

An empirical expression of the fracture toughness proposed by Kanninen and Popelar (1985) who had taken into account the plate thickness and the yield strength of the material as shown in Equation (4-2) and plotted in Figure 4-2. It is assumed that K_{IC} = 140 MPa$\sqrt{\text{m}}$ and the yield stress, σ_y = 235 MPa.

$$K_C = K_{IC} \times \left(1 + \frac{1.4}{t_p} \cdot \left(\frac{K_{IC}}{\sigma_y}\right)^2\right) \quad \textbf{(4-2)}$$

where, t_p is plate thickness in mm

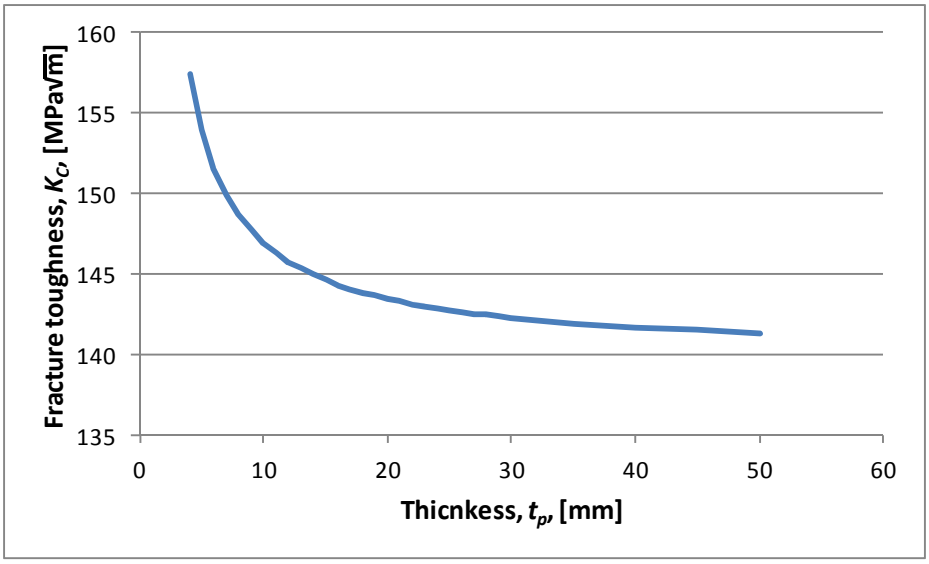

Figure 4-2: Fracture toughness against plate thickness according to Equation (4-2) with K_{IC} = 140 MPa$\sqrt{\text{m}}$ and σ_y = 235 MPa

4.2.3 Material constants

The best way to obtain material constants is to conduct experimental crack growth tests of the concerned materials and carry out regression analysis with the data obtained from tests. If experimental data is not available, published data and information is a good alternative.

Material constants for various grades of steel for *Paris Law*, which have been evaluated in literature through experimental tests as well as recommended by British Standards, are summarised in Table 4-1.

Table 4-1: Material constants of steels for *Paris Law* in literature (with units of MPa and metre)

References	***C***	***m***	**Materials tested**
Barsom (1971)	6.86×10^{-12}	3.0	Ferrite-pearlite steels
Hirt and Fisher (1973)	3.93×10^{-12}	3.0	ASTM A36, A441 and A514
Klingerman (1973)	1.86×10^{-12}	3.1	ASTM A36
Barsom and Rolfe (1987)	6.80×10^{-12}	3.0	Ferrite steels
Yazdani and Albrecht (1989)	1.54×10^{-12}	3.34	Mild and HSLA steels
Fisher et al. (1993)	9.00×10^{-12}	3.0	HSLA-80 steels
BS PD6493 (1993)	9.50×10^{-12}	3.0	British Standards for steels in air
BS 7910 (1999)	1.65×10^{-11}	3.0	British Standards for steels in air

Among the above material constants, the followings should be noted:

- Material constants of Barsom (1971) are based on the low bound line of data tested in mid-range of SIF
- Material constants of Hirt and Fisher (1973) are based on the low bound line of data tested in mid- and high-ranges of SIF
- Material constants of Klingerman (1973) are based on the mean line of data tested in low- and mid-ranges of SIF
- Material constants of Yazdani and Albrecht (1989) are based on the mean line of data in mid-range of SIF and an effective range of the SIF was taken into account
- Material constants of Fisher et al. (1993) are based on the upper bound line of data tested in mid-range of SIF

The guidance of British Standards, BS 7910 (1999), recommends an upper bound line of 1.65 x 10^{-11} for *C* and 3.0 for *m*. However, considering other experimental evaluations this recommendation seems to be excessively conservative. Hence the recommended value of *C* and *m* of the previous version of British Standards, BS PD6493 (1993), is selected as a guidance line of *Paris Law* for this research.

4.2.4 The proposed model of crack growth

As the necessity of using the full range of the SIF in the current research is discussed previously, the model suggested by McEvily and Groeger (1977) seems to be the most suitable one. Although this model has an advantage of nonlinear modelling of crack growth covering below the threshold, the linear and the unstable region, it has two pitfalls: i) The power in the equation is fixed to 2.0 hindering the most suitable value from being selected through regression analysis, and ii) The effect of stress ratio is not properly taken into account in the middle region of the SIF (*Paris* region), although the low and high regions of the SIF are affected.

The former weakness can be addressed by applying a general *m* as other models do. The latter one is treated by substituting the normal range of SIF, ΔK, with the effective range of SIF, ΔK_{eff}. Hence the modified equation of McEvily's model is expressed as follows:

$$\frac{da}{dN} = C \times \left(\Delta K_{eff} - \Delta K_{th}\right)^m \times \left[1 + \frac{\Delta K_{eff}}{K_C - K_{max}}\right] \quad \textbf{(4-3)}$$

where, *C* and *m* are material constants

ΔK_{eff} is the effective range of the SIF, $\Delta K_{eff} = \frac{\Delta K}{1-R_\sigma/Q}$

ΔK_{th} is the threshold range of the SIF, $\Delta K_{th} \approx \Delta K_{th0} \cdot \sqrt[3]{(1 - R_\sigma)}$

K_C is the fracture toughness of the material

K_{max} is the maximum SIF due to the maximum loading

R_σ is the stress ratio, $R_\sigma = \sigma_{min} / \sigma_{max}$

Q is a parameter related with the yield strength of the material, 4.0 for A36 steels, 4.6 for A588 steels and 9.1 for A514 steels are recommended by Yazdani and Albrecht (1989)

ΔK_{th0} is the threshold range of the SIF at $R_\sigma = 0$

In the above equation, the effective range of the SIF, ΔK_{eff}, is obtained according to Yazdani and Albrecht (1989) and the threshold range of the SIF, ΔK_{th}, is approximated according to Davenport and Brook (1979). The fracture toughness of the material is obtained by Equation (4-2).

Figure 4-3 shows the crack growth curves with various R_σ ratio according to Equation (4-3) with $K_C = 140$ MPa$\sqrt{\text{m}}$. One noticeable thing in the graph is that linear region of each curve is steeper than the guidance line (line of *Paris Law*). This means that appropriate selection of the material constants C and m is necessary.

With the defined guidance line of *Paris Law*, the material constants for the proposed crack growth model are obtained so that the linear region of the proposed equation with $R_\sigma = 0.0$ coincides with the defined guide line (*Paris Law* with BS PD6493 recommendation).

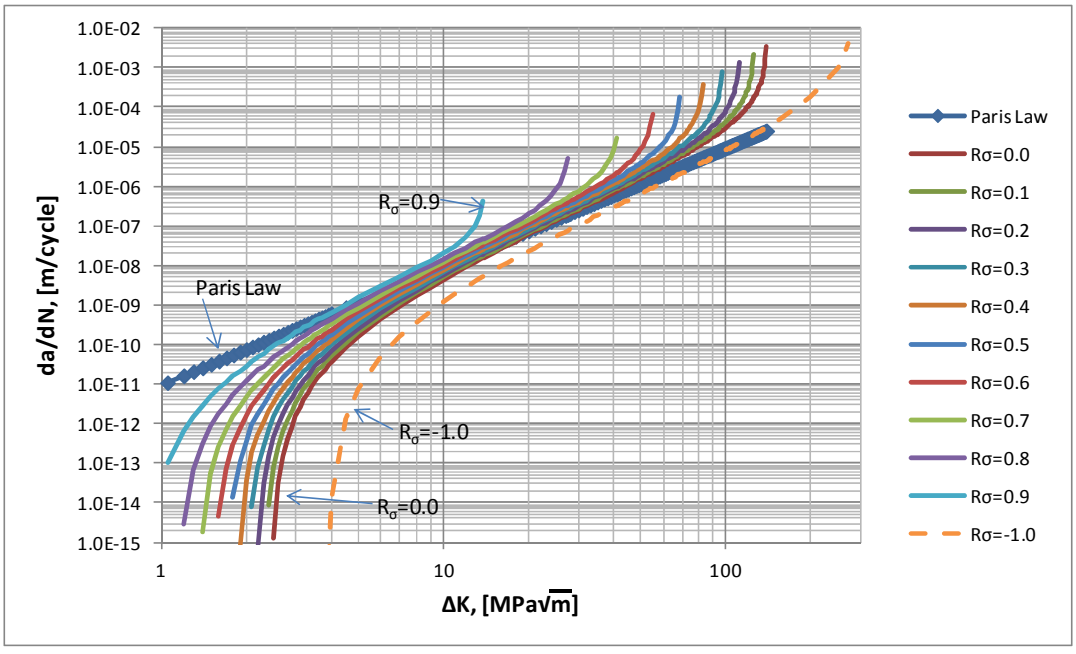

Figure 4-3: Crack growth model according to Equation (4-3)

Recalling the curve of the proposed crack growth model with R_σ = 0.0 and the curve of *Paris Law* (C = 9.5 x 10^{-12} and m = 3.0), the proposed model has a linear region between (at least) 20 MPa$\sqrt{m}$ and 40 MPa$\sqrt{m}$ of ΔK as shown in Figure 4-4.

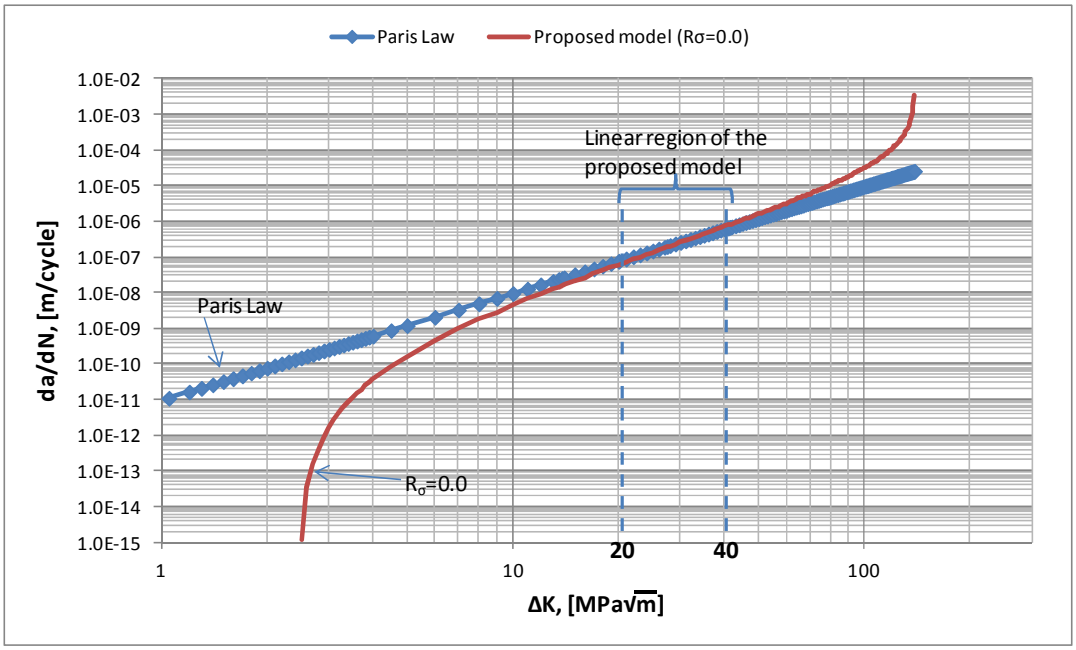

Figure 4-4: Lines of Paris Law and the proposed model of crack growth with R_σ = 0.0 (both lines are based on material constants of C and m of 9.5 x 10^{-12} and 3.0 respectively)

Hence, a set of simultaneous equations is developed to obtain a new set of material constants (C and m) for the proposed crack growth model by setting the crack growth rates of two curves at 20 MPa$\sqrt{m}$ and 40 MPa$\sqrt{m}$ of the same ΔK. These are:

$$\begin{cases} \dfrac{da}{dN} = 9.5 \times 10^{-12} \cdot 20^{3.0} = C \times (20 - \Delta K_{th0})^m \times \dfrac{20}{K_C - 20} \\ \dfrac{da}{dN} = 9.5 \times 10^{-12} \cdot 40^{3.0} = C \times (40 - \Delta K_{th0})^m \times \dfrac{40}{K_C - 40} \end{cases} \quad \textbf{(4-4)}$$

Adopting ΔK_{th0} = 2.45 MPa$\sqrt{m}$ and $K_C = K_{IC}$ = 140 MPa$\sqrt{m}$ for an example, the solution of the simultaneous equations gives the material constants of C and m for the proposed crack growth model as 5.134 x 10^{-11} and 2.494 respectively. The proposed model of crack growth is expressed as Equation (4-5), of which terms are defined in Equation (4-3), and shown in Figure 4-5.

$$\frac{da}{dN} = 5.134 \times 10^{-11} \times \left(\Delta K_{eff} - \Delta K_{th}\right)^{2.494} \times \left[1 + \frac{\Delta K_{eff}}{K_C - K_{max}}\right] \quad \textbf{(4-5)}$$

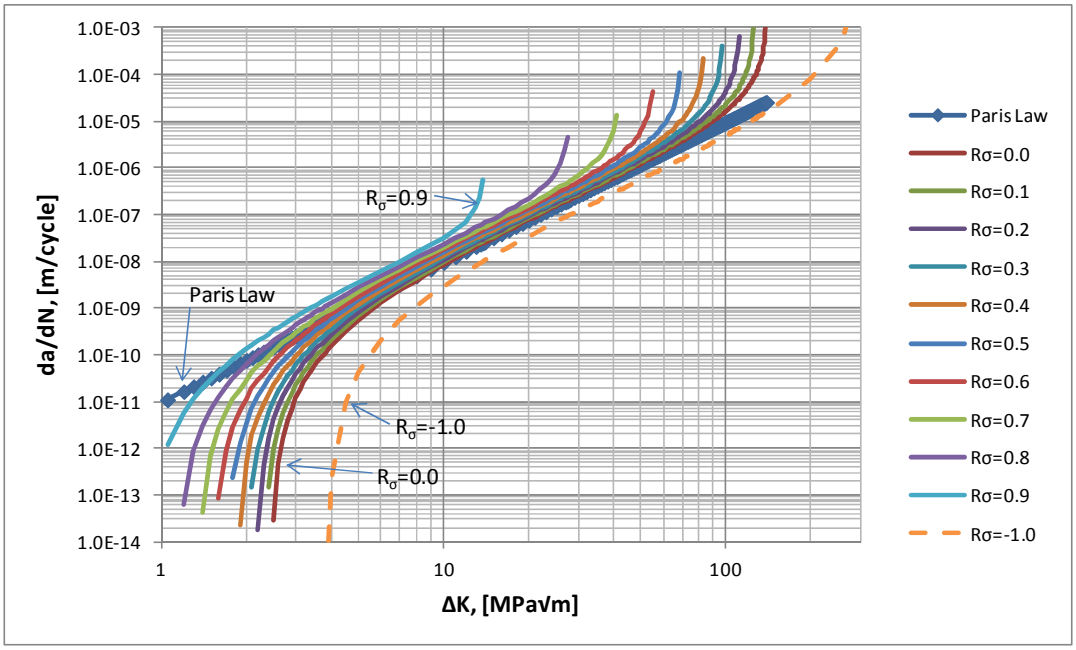

Figure 4-5: Crack growth model proposed with modified material constants

From a mathematical point of view Equation (4-5) may result in negative crack propagation rate when the effective range of SIF, ΔK_{eff}, is smaller than the range of threshold SIF, ΔK_{th}. This would mean that the crack does not propagate any further, i.e. zero propagation rate occurs.

On the other hand, the proposed model gives no crack propagation rate when the maximum SIF, K_{max}, exceeds the fracture toughness, K_C. This does not mean that the damaged hull girder would collapse immediately (i.e. by the next load cycle) but implies that very fast crack propagation is expected. The crack propagation can slow down again in the next cycle depending on the applied load (for example, if weather conditions subside). Therefore, it is more realistic to allow a constant value of crack propagation when such situation arises. In this analysis, 1.0 mm/cycle and 2.0 mm/cycle of crack propagation rates are applied to allow the crack to propagate until the hull girder collapses and to identify the difference in the results. Further elaboration on this topic is recommended to take place in the future work especially for the latter stages of damage evolution (see Section 8.3).

4.3 First-principles method for SIFs

A calculation method of the SIFs is presented in this chapter using a first-principles methodology which adopts a finite element analysis based on the LEFM. The FE analysis is carried out using commercial software, ABAQUS, which enables modelling of quasi-static crack propagation in three dimensions using the VCCT. This chapter elaborates on applications of VCCT on structures to calculate the SIFs of crack tips at each time step during damage propagation. A validation study of using the VCCT in calculation of SIFs is also conducted.

4.3.1 VCCT: The first-principles methodology

The VCCT is a well-known public domain post-processing and re-meshing technique that provides progressive crack growth between bonded surfaces based on the fracture toughness of the bond and the strain energy release rate at the crack tip. Since the idea of VCCT has first proposed in 1977 by Rybicki and Kanninen (1977), VCCT has been a very attractive technique to extract SIFs because its algorithm of application is relatively easy and the results are in a good accuracy with experimental observations.

The original technique has been elaborated and extended to three-dimensional bodies which can be found in as the work of Shivakumar, Tan and Newman (1988), Chang, Choi, Kim and Yagawa (2004) and Leski (2007). Despite the obvious benefits of VCCT its implementation into commercial and general purpose finite element codes has been reported only recently. Xie and Biggers (2006) have developed an interface element of which implementation has been carried out into ABAQUS using the user defined element subroutine. Implementation of VCCT into MSC/Patran, also has been conducted by Leski (2007) through a user subroutine developed in the Patran Command Language. These techniques have been applied as a post processing routine using the FE analysis results.

The analysis technique of VCCT for ABAQUS (Simulia, 2008), which has been an intrinsic feature since version 6.8, offers the capability to analyse brittle interfacial crack propagation due to delamination or debonding. Because VCCT in ABAQUS is allowed to be calculated at runtime rather than at post-processing, no re-meshing or

re-analysis is required, and this shortens the analysis time that is required in the general VCCT approach.

Determination of SIFs using VCCT involves an indirect method which calculates strain energy release rate, G, by determining the changes in energies for crack growth during a given crack extension. The strain energy release rate is divided into three components depending on the modes of fracture as shown in Figure 4-6; the mode I component due to tension (opening) fracture, G_I, the mode II component due to in-plane shear (sliding) fracture, G_{II}, the mode III component due to out-of-plane shear (tearing) fracture, G_{III}.

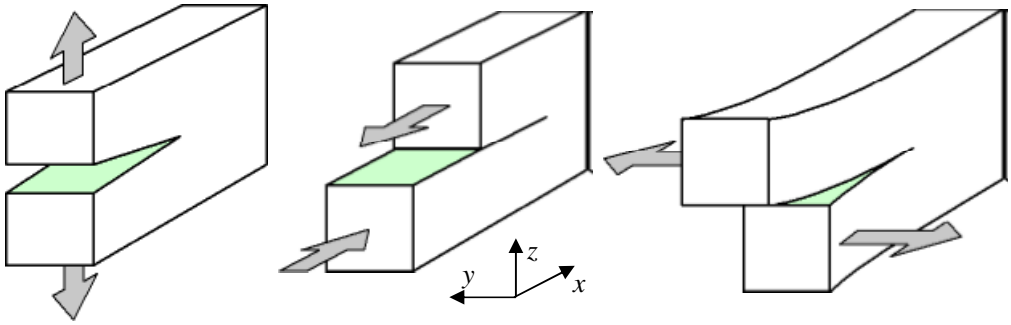

(a) Tension mode (opening) (b) In-plane mode (sliding) (c) Out-of-plane mode (tearing)

Figure 4-6: Three modes of fracture, eFunda (www.efunda.com)

In the tension mode the body is loaded by tensile forces, such that the crack surfaces are pulled apart in the z direction. The deformations are then symmetric with respect to the planes perpendicular to the y- and z-axis. In the in-plane mode of fracture the body is loaded by shear forces parallel to the crack surfaces, which slide over each other in the x direction. The deformations are symmetric with respect to the plane perpendicular to the y axis and skew symmetric with respect to the plane perpendicular to the z axis. Finally, in the out-of-plane mode the body is loaded by shear forces parallel to the crack front, and the crack surfaces slide over each other in the y-direction. The deformations are then skew-symmetric with respect to the plane perpendicular to the y- and z-axis.

In a finite element model made of three-dimensional solid elements as shown in Figure 4-7, the mode I, II, and III components of the strain energy release rate, i.e. G_I,

G_{II} and G_{III} respectively, are calculated as shown in Equation (4-6) according to Shivakumar, Tan and Newman (1988):

$$G_I = \frac{1}{2\Delta A} \cdot Z_{Li} \cdot (w_{Ll} - w_{Ll^*})$$
$$G_{II} = \frac{1}{2\Delta A} \cdot X_{Li} \cdot (u_{Ll} - u_{Ll^*}) \quad \textbf{(4-6)}$$
$$G_{III} = \frac{1}{2\Delta A} \cdot Y_{Li} \cdot (v_{Ll} - v_{Ll^*})$$

where, ΔA is the area virtually closed and calculated as $\Delta A = \Delta a \times \Delta b$

Δa is the length of the elements at the crack front

Δb is the width of the elements

X_{Li}, Y_{Li} and Z_{Li} denote the forces in X, Y and Z directions at the crack front in column L and row i

u_{Ll}, v_{Ll} and w_{Ll} denote the corresponding displacements behind the crack at the top face node row l

u_{Ll^*}, v_{Ll^*} and w_{Ll^*} denote the corresponding displacements behind the crack at the lower face node row l^*

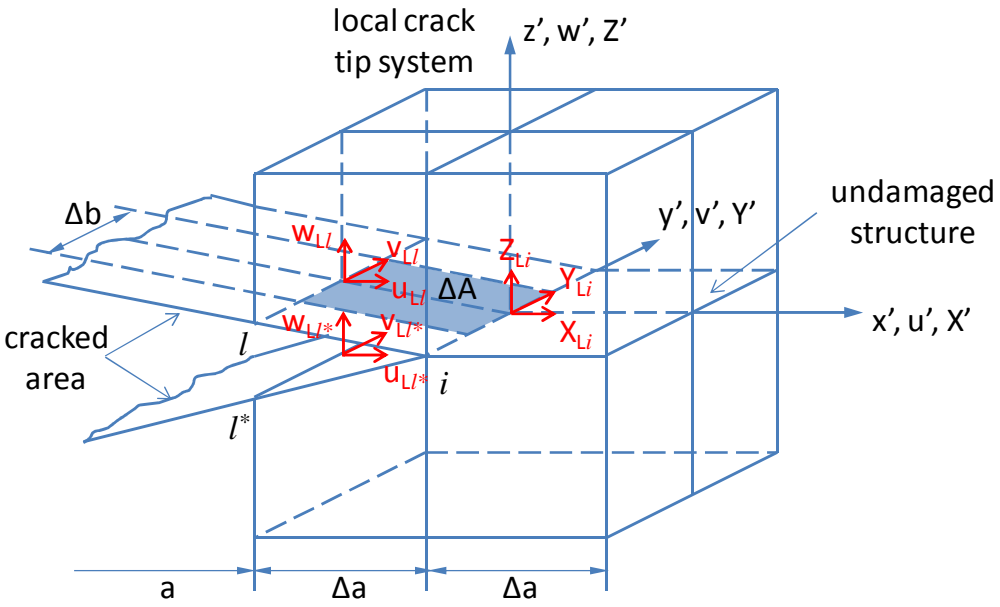

Figure 4-7: VCCT for 8-nodes solid elements, Shivakumar, Tan and Newman (1988)

In a general 3D FE analysis of hull structures, it is custom to use 4-node shell elements and 2-node beam or bar elements for modelling. In this case and according to ABAQUS manual (Simulia, 2008), VCCT implementation requires 3D solid meshes between the two surfaces. Hence, the hull structure around the defined damage has been modelled with 8-node solid elements as shown in Figure 4-9.

Connection of shell elements to solid elements at the boundary of solid meshes is achieved through a surface-based *shell-to-solid* coupling constraint, which is an intrinsic technique in ABAQUS for a transition from shell element modelling to solid element modelling in a 3D FE analysis. The shell-to-solid coupling is enforced by the automatic creation of an internal set of distributing coupling constraints between nodes on the shell edge and nodes on the solid surface. For each shell node involved in the coupling, a distinct internal distributing coupling constraint is created with the shell node acting as the reference node and the associated solid nodes acting as the coupling nodes by forcing initially straight lines through the thickness of solid nodes to remain straight despite rotation and displacement (Figure 4-8):

- The translation of the shell node at the interface must be equal to the translation of the corresponding point on a line of nodes through the thickness of the solid.
- The rotation of the shell node at the interface must be compatible with the rotation of the corresponding line of nodes through the thickness.

Each internal constraint distributes the forces and moments acting at its shell node as forces acting on the related set of coupling surface nodes in a self-equilibrating manner. The resulting line of constraints enforces the shell-to-solid coupling. More details on the shell-to solid coupling are found in ABAQUS manual, Simulia (2008).

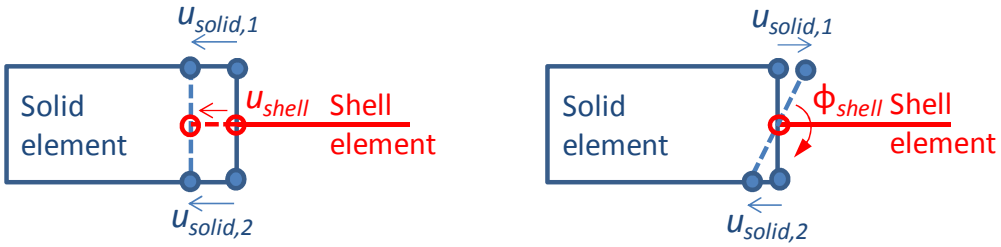

Figure 4-8: Shell-to-Solid coupling constraint of translation and rotation

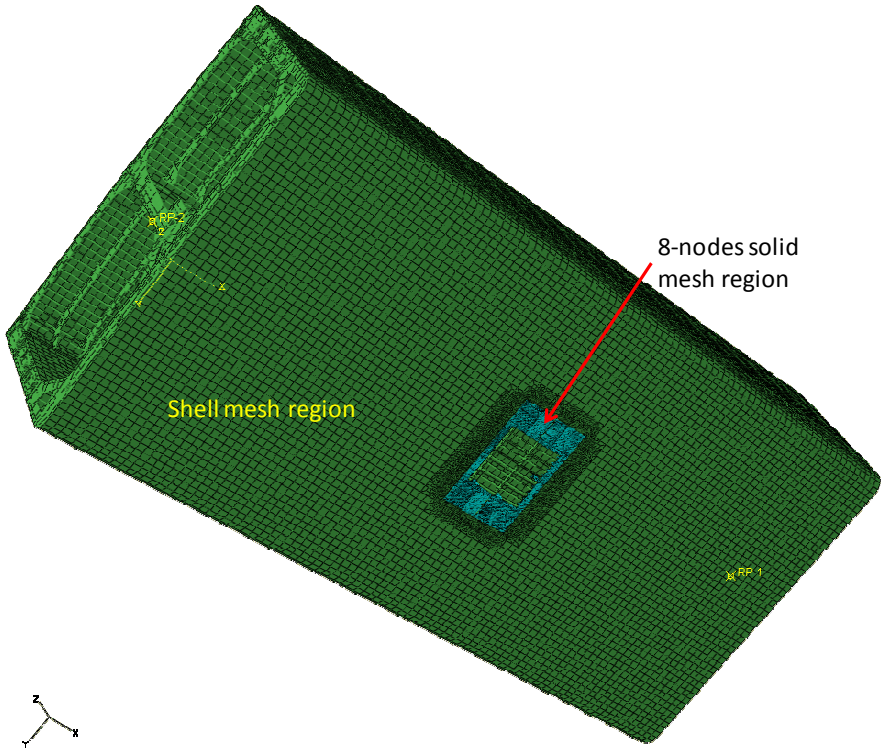

Figure 4-9: An example of FE model with solid elements inserted in shell elements

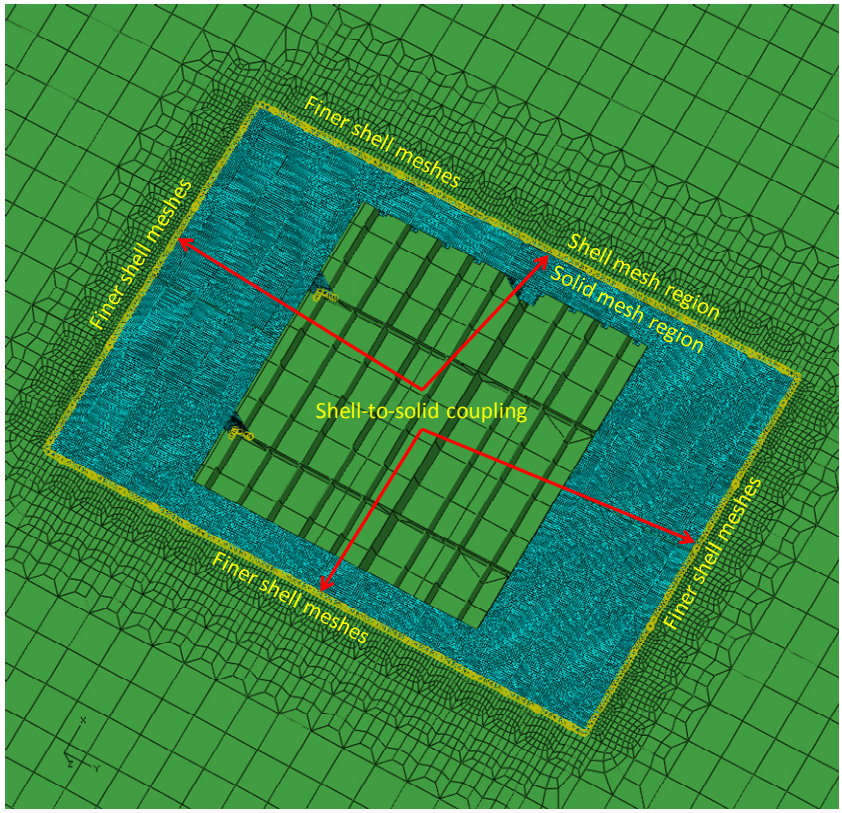

Figure 4-10: An example of shell-to-solid coupling

Application of the shell-to-solid coupling is made in the FE model as shown in Figure 4-10, where an increased mesh density of shell elements near the boundary of solid element region is applied to enhance accuracy of interaction between nodes on shell edges and nodes on solid surfaces.

Simulations of fracture mechanics using VCCT for ABAQUS require surfaces on which cracks would propagate. For this, two surfaces, *master and slave*, are defined as a set of reference and dependent surface to form a contact pair which allows separation of the surfaces in tensions and prevents mutual intrusion in compressions. Also a set of *slave nodes* on the slave surface is assigned in order to constrain the two surfaces to act as one (a bonded condition). With an initial contact condition between master and slave surfaces, the exclusive nodes of the slave nodes' set represent the initial crack of each analysis (Figure 4-11). More details on master and slave surface as well as slave nodes are found in ABAQUS manual, Simulia (2008).

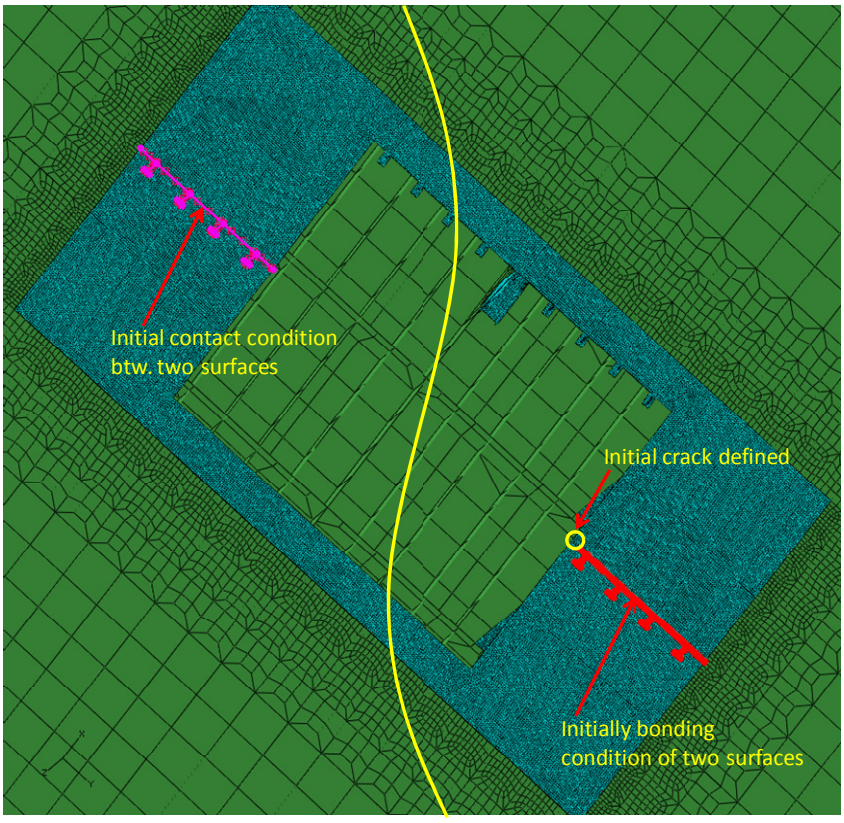

Figure 4-11: An example of defining contact surfaces, initial bonding region and initial crack

In the application of VCCT for ABAQUS, the following commands need to be keyed in manually to activate its implementation as they are not supported by the graphic

user interface of ABAQUS/CAE yet. An example of key editing for implementation of VCCT in ABAQUS is presented in Appendix C.

Once the strain energy release rate, G, is determined the SIF (K) is obtained as a function of G:

$$G = \begin{cases} \frac{K^2}{E} \\ \frac{K^2}{E}(1-\nu^2) \end{cases} \rightarrow K = \begin{cases} \sqrt{GE} & \text{for plane stress} \\ \sqrt{\frac{GE}{1-\nu^2}} & \text{for plane strain} \end{cases} \quad \textbf{(4-7)}$$

where, E is Young's modulus

ν is Poisson's ratio

4.3.2 Validation

As the analysis technique of VCCT was originally developed to analyse delaminating and debonding of surfaces, its validity in calculating the SIFs needs to be checked and proved in order to use this technique in the crack propagation analysis for the progressive structural failure.

Validation of the results is carried out for the following configurations of crack of which solutions are well established either in analytical or empirical approaches.

- Centre cracks in an infinite stripe of plate
- Cracks emanating from a circular opening in an infinite and in a finite plate
- Centre cracks in a finite plate subjected to a linear distribution of stresses
- Centre cracks in a finite stiffened plate

Centre cracks in an infinitely long plate

Since Irwin (1957) has shown that the local stress and displacement near the crack tip has a general closed-form solution that could be described by a constant, SIF in this case, it is proportional to the normal stress σ which is applied perpendicular to the crack surface.

The solution of centre cracks in an infinite stripe of plate is known as one of the classical solutions that can be easily obtained from literature such as the handbook of Tada, Paris and Irwin (2000).

Among the various empirical solutions of the handbook, the following expression proposed by Tada and shown in Equation (4-8) has the best accuracy.

$$K_I = \sigma\sqrt{\pi a} \times \left(1 - 0.025\left(\frac{a}{B}\right)^2 + 0.06\left(\frac{a}{B}\right)^4\right)\sqrt{sec\frac{\pi a}{2B}} \quad \textbf{(4-8)}$$

where, σ is the applied stress

a is the half crack size

B is the half breadth of the plate

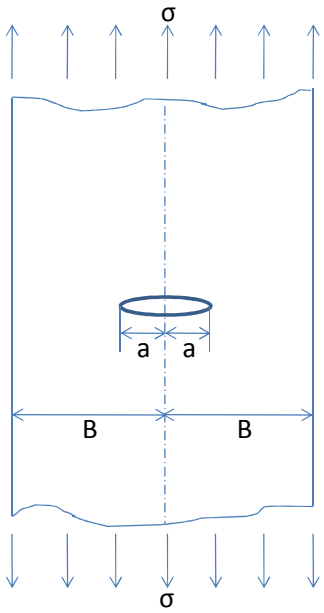

Figure 4-12: Configuration of centre crack in an infinite stripe of plate

Comparison between the results of VCCT and the empirical solution is made for the case of centre cracks in an infinitely long plate and the graphs shown in Figure 4-13 prove that VCCT for ABAQUS is suitable for the determination of SIFs in this case.

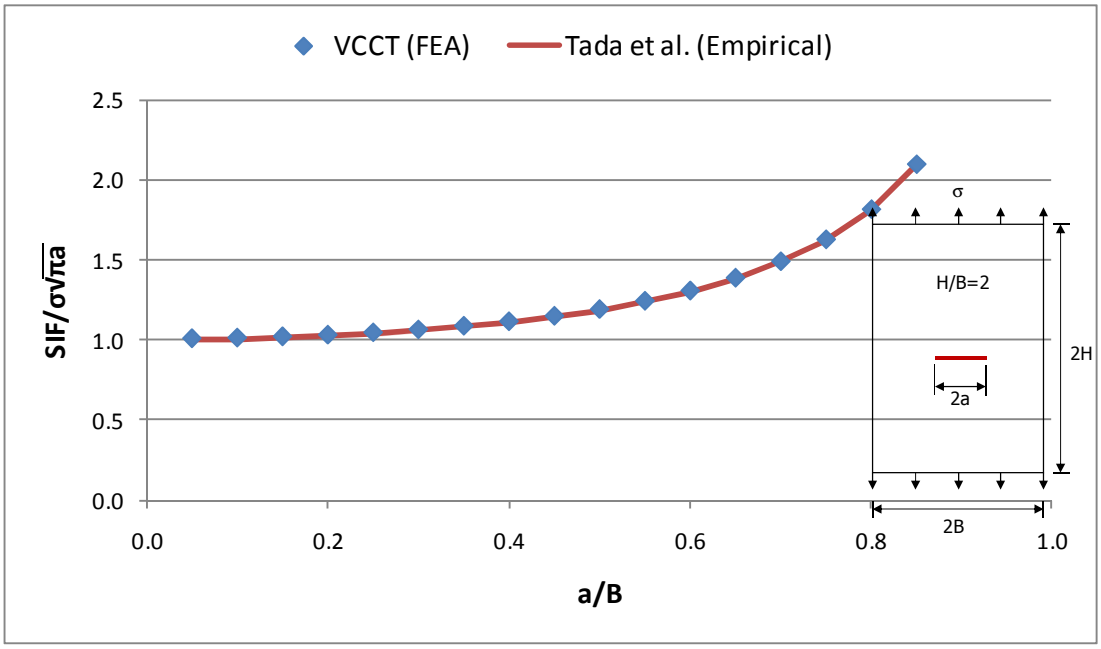

Figure 4-13: SIF ratio from VCCT in an infinitely long plate, compared with Tada, Paris and Irwin (2000)

Cracks emanating from a circular opening in an infinite and a finite plate

Because damage can be attributed to collision/grounding accidents, cracks emanating from an opening are important. Substantial investigation has been carried out on cracks from rivet holes in aircraft structures. The single and double cracks at the circular hole-edge have been studied by Bowie (1956), Newman (1971), and Tweed and Rooke (1973) on infinite and finite plates.

Validation of VCCT for taking into account the effect of a circular hole is performed by comparing its results with those from Newman (1971). Figure 4-14 shows the normalised SIF values from VCCT in a finite plate with a circular opening of radius *R*. It can be said from the comparison result that VCCT captures the effect of the circular opening in a satisfactory manner.

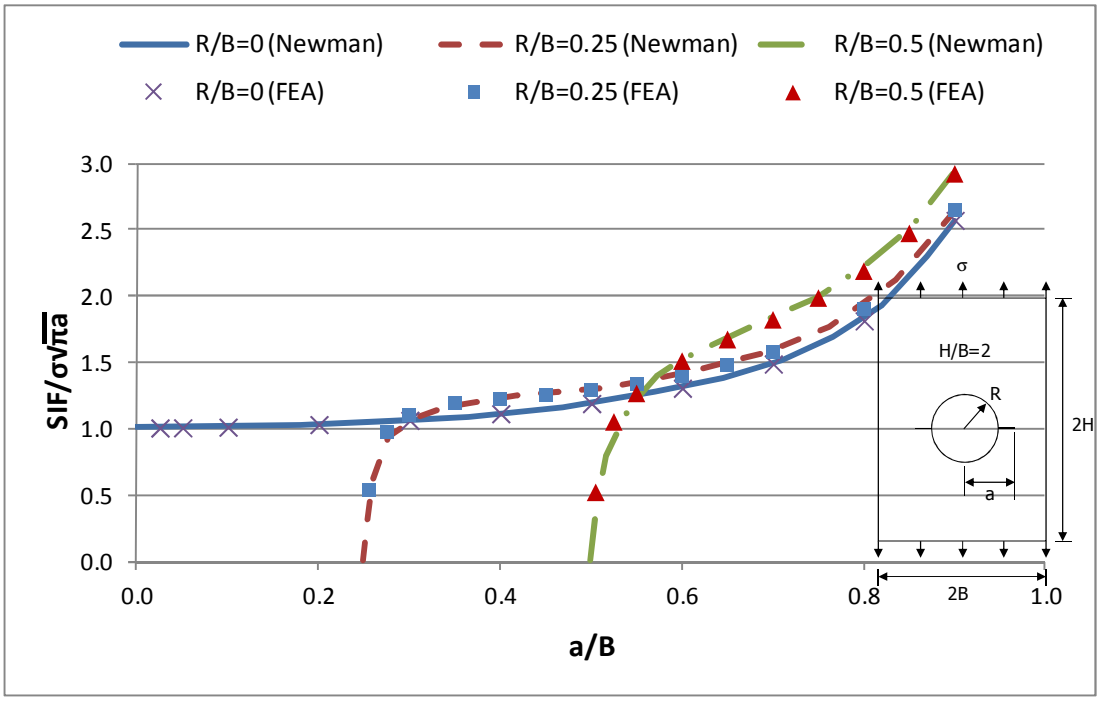

Figure 4-14: SIF ratio in a finite plate with a circular opening, compared with Newman (1971)

The effect of a circular opening determined by VCCT is also compared with the result of Newman for an infinite plate case. In this comparison, x-axis is the non-dimensional value of half crack length, a, over the opening radius, R, as introduced in the reference. It is found that small value of ratio of the opening radius to the half plate width, R/B, follows Newman's result very well (Figure 4-15).

As the ratio of the opening radius to the half plate width, R/B, increases, larger difference between the result of VCCT and Newman's result is found. The difference also becomes large as the ratio of the half crack length to the opening radius, a/R, increases. This difference can be explained by the effect of finite width of the plate used in FE analysis. That is, increase in either R/B ratio or a/R ratio causes SIF ratio to become sensitive to the finite width's effect. This is demonstrated in Figure 4-16, where all the curves merge into the one of Newman's infinite plate case when the effect of the finite width is removed from the calculated SIFs. The correction factor for the finite width of plate is considered in Equation (4-9) based on the empirical solution for the case of the infinite stripe of plate shown in Equation (4-8).

$$Y_{finite\ width} = \left(1 - 0.025\left(\frac{a}{B}\right)^2 + 0.06\left(\frac{a}{B}\right)^4\right)\sqrt{sec\frac{\pi a}{2B}} \quad \textbf{(4-9)}$$

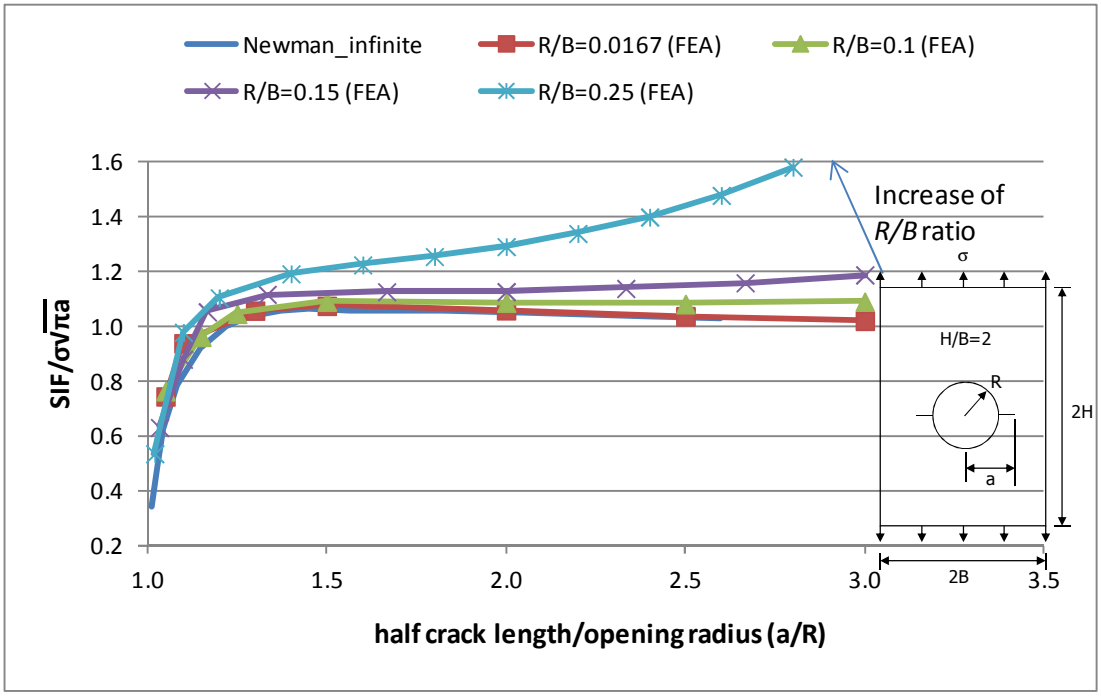

Figure 4-15: SIF ratio in a finite plate with a circular opening, compared with the infinite plate result of Newman (1971)

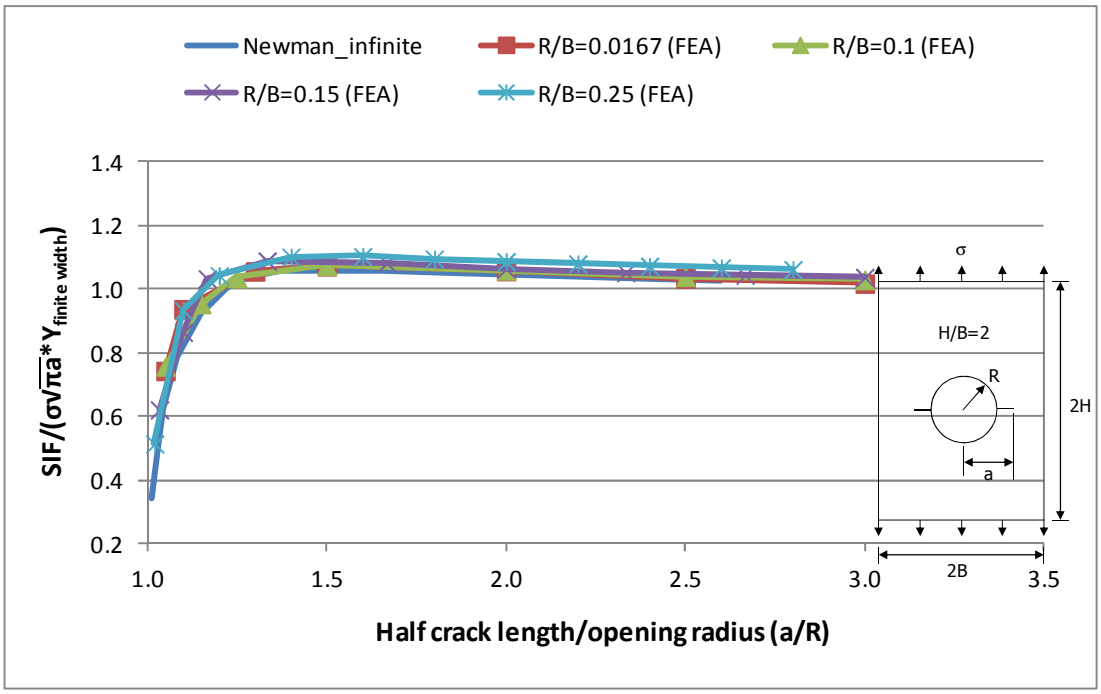

Figure 4-16: SIF ratio in a finite plate with a circular opening, compared with the infinite plate result of Newman (1971) – the effect of finite width is removed from FE results

Centre cracks in a finite plate subjected to a linear distribution of stresses

Basic analytical solutions assume that the stress on the edges of cracked plate is uniformly distributed. In reality normal stresses on the side shell of a ship hull structure vary linearly under vertical wave bending moment. In hogging condition, tensile stresses are induced on the side shell near the deck plate while the side shell plate near the bottom is under compressive stresses and vice versa in a sagging condition. To investigate the effect of this, a load model is tested and results are compared with the empirical solution from Chell (1976). As can be seen in Figure 4-17, the SIF results from VCCT are in excellent agreement with Chell's results, which proves that VCCT for ABAQUS can be used in analysis of crack propagation in a side shell plate of a ship hull.

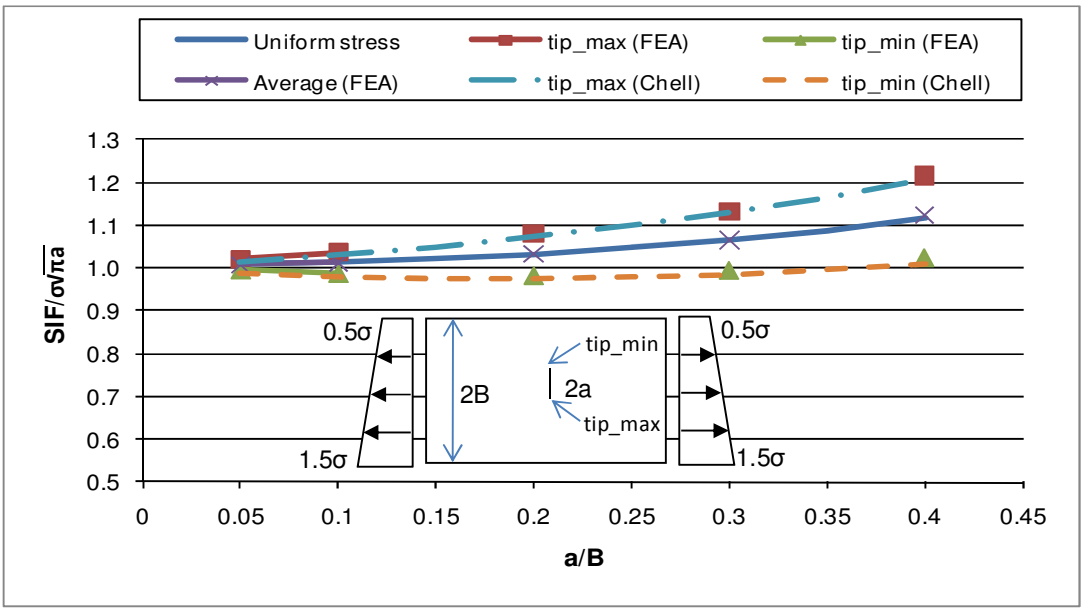

Figure 4-17: SIF due to linearly varying stresses, compared with Chell (1976)

Centre cracks in a finite stiffened plate

The topic of crack propagation in stiffened panel has not received much attention in the literature. The few available references include Poe (1971), Dexter and Pilarski (2000) and Dexter and Mahmoud (2004). A stiffener is considered to restrain the propagation of crack because its presence in front of the crack tip serves as an increased net section of the member. Figure 4-18 shows the proposed stiffeners' effect based on tests conducted by Poe (1971).

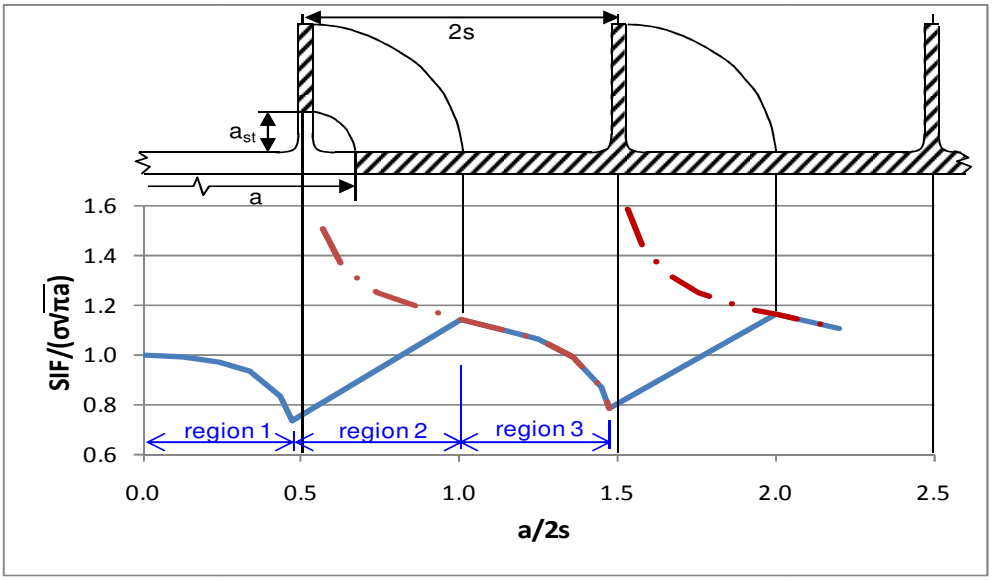

Figure 4-18: Stiffener effect, reproduced from Poe (1971)

FE analysis using VCCT has been carried out stiffened panels (Figure 4-19) with different size of stiffeners and the similar tendency of SIF ratio in stiffened panels can be established(Figure 4-20) for different stiffener depths. Although the result of VCCT is not in full agreement with Poe's proposal (Figure 4-18), it captures the effect of stiffener consistently. Hence the use of VCCT for the analysis of crack propagation in stiffened panels is justified.

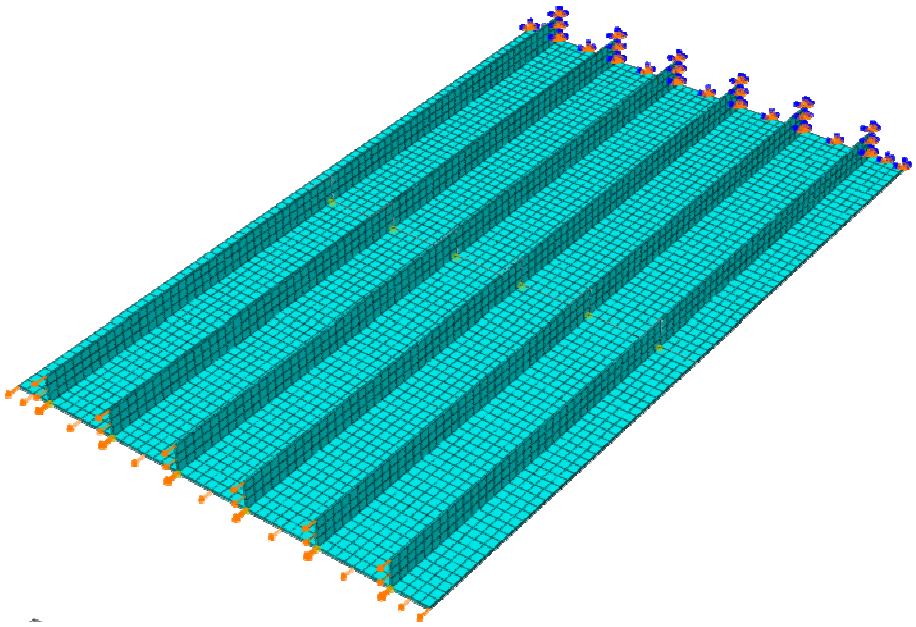

Figure 4-19: An FE model of a stiffened panel with stiffeners of 0.15m depth

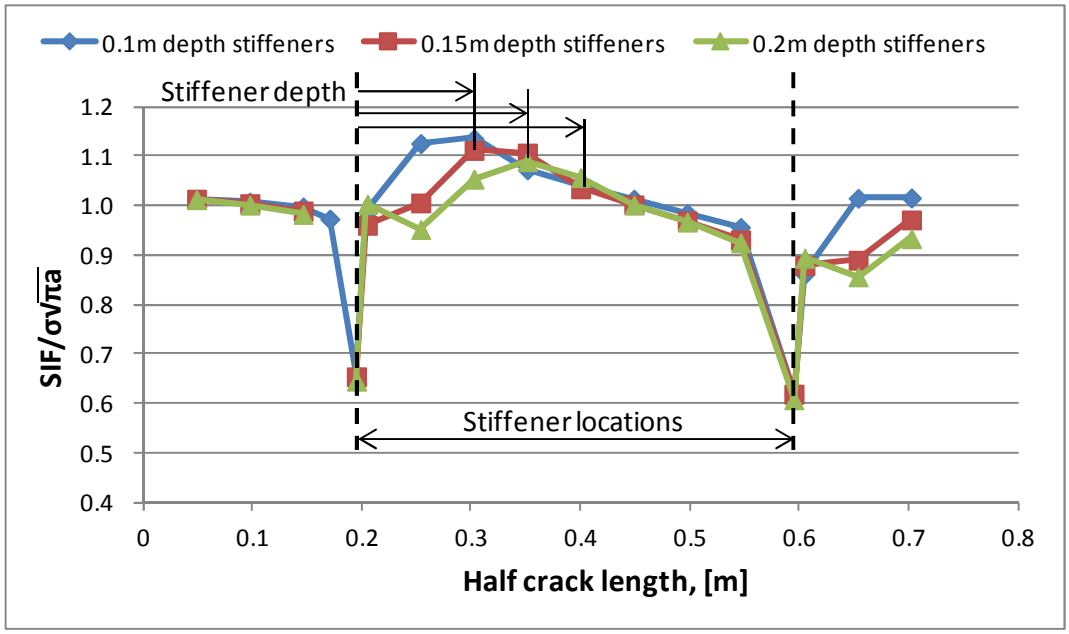

Figure 4-20: SIF ratios calculated by VCCT, for different stiffener depths

4.4 Knowledge-intensive models for SIFs

The SIFs of cracks for various geometries and loading conditions are proved to be obtained by VCCT for ABAQUS. Being different from other FE analyses, this approach is easy to use, accurate and requires less time for calculation. However as an FE method, it requires effort and time to prepare models and run the analyses. As a result, this characteristic of the method limits its use i) in an accidental emergency situation, where a fast and accurate response is crucial for the assessment and management of the situation, and ii) for supporting design-decision making by providing safety-related information that allows trade-off between other design parameters in the early design stage for the maximum flexibility of design change at the minimum cost.

Hence, a fast but reliable method is necessary to determine the SIFs by substituting the FE analysis in such emergency operations and design developments. For this purpose, a set of knowledge-intensive models made of analytical and empirical solutions for the SIFs are proposed.

4.4.1 Knowledge-intensive models

The knowledge-intensive model is a superposition method for determining approximate SIFs of a crack configuration by superposing the separated configurations of which solutions are known in analytical or empirical ways. The method of superposition in determining the SIFs has been proposed and used in the literature by Cartwright and Rooke (1974), Aamodt and Bergan, (1976), Grandt and Kullgren (1983), Ritchie (1986), Dexter and Pilarski (2000) and others. It should be noted that the approaches of superposition in determining the SIFs varies for different between combination of loading conditions and geometries.

Combination of loadings

Because the concept of the SIF is based on the LEFM, the effects of more than one type of loading on the crack tip can be obtained by linearly adding the SIF due to each type of loading with a condition that each SIF should be associated with the same structural geometry.

One example of this type of superposition is experienced in deriving solutions for loading conditions that are not readily available. The process of deriving the stress-intensity factor for a centre crack geometry in an infinite plate, which is uniformly loaded with a pressure (p) illustrates this feature (Figure 4-21).

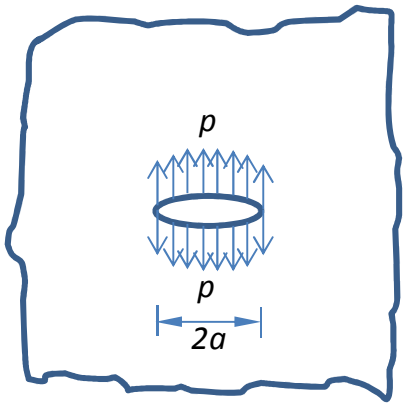

Figure 4-21: Centre crack with uniformly loaded with a internal pressure

Figure 4-22 describes the process where the centre crack geometry with remotely loaded stresses is decomposed into a set of two centre crack geometries which have loading conditions, that when added, result in the cancelling of the crack line internal loadings.

$$SIF_{total} = SIF_1 + SIF_2 \quad \textbf{(4-10)}$$

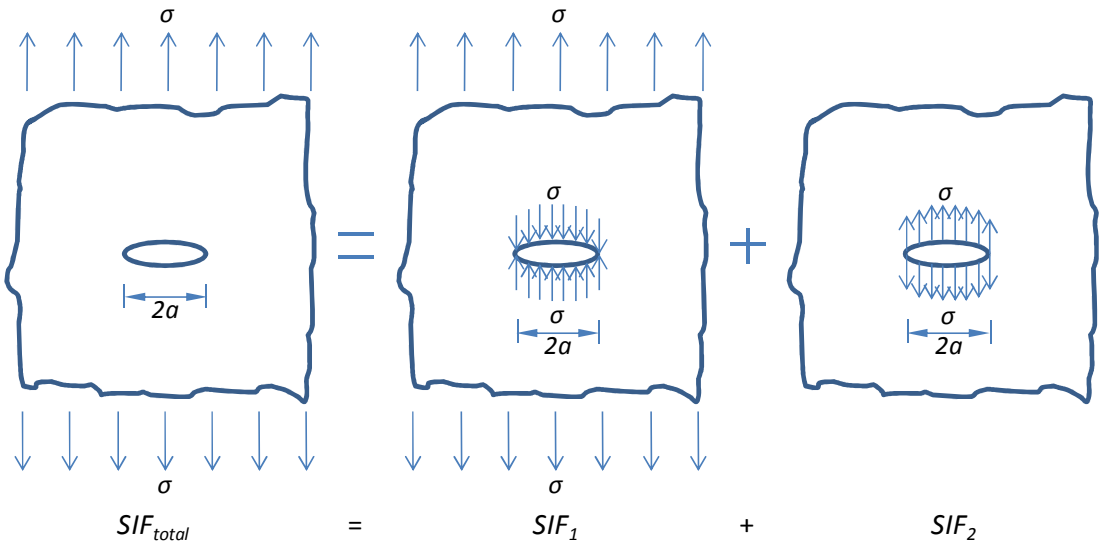

Figure 4-22: Superposition of the SIF for centre cracked geometry

The SIF for the plate loaded with the remote stress condition (σ) and the crack closing stresses (also equal to σ) is zero, i.e. $SIF_1 = 0$, because the crack is clamped closed under such conditions. Thus, the SIF for a pressurized centre crack with pressure (p) equals σ is the same as that associated with the remotely loading stress.

$$SIF_2 = SIF_{total} = \sigma\sqrt{\pi a} \quad \textbf{(4-11)}$$

Combination of geometries

The effect of geometry other than the centre cracked infinite plate, of which the SIF is denoted as SIF_0 (Equation (4-12)), is normally expressed by a dimensionless correction factor, $Y_{geometry}$, and the SIF, $SIF_{geometry}$, is expressed as Equation (4-13).

$$SIF_0 = \sigma\sqrt{\pi a} \quad \textbf{(4-12)}$$

$$SIF_{geometry} = Y_{geometry} \cdot SIF_0 = Y_{geometry} \cdot \sigma\sqrt{\pi a} \quad \textbf{(4-13)}$$

where, σ is remotely applied stress and a is half of the total damage size

There has been much research on the definition of the corrections factors for various geometries including finite plate, circular opening, etc. The summarised efforts on

the correction factors can be obtained from handbooks on the topic such as Tada, Paris and Irwin (2000) and Murakami (2005).

The concept of combining multiple effects of geometry is based on a series of multiplication of correction factors representing the related geometry effects. In this case, the applied loadings should remain the same.

One example of combining effects of geometries is obtaining the SIF of centre cracks emanating from a circular opening in a plate finite width. The process of deriving the solution is illustrated in Figure 4-23, where the combined effects of geometries are divided into (i) the effect of the finite width plate, and (ii) the effect of circular opening.

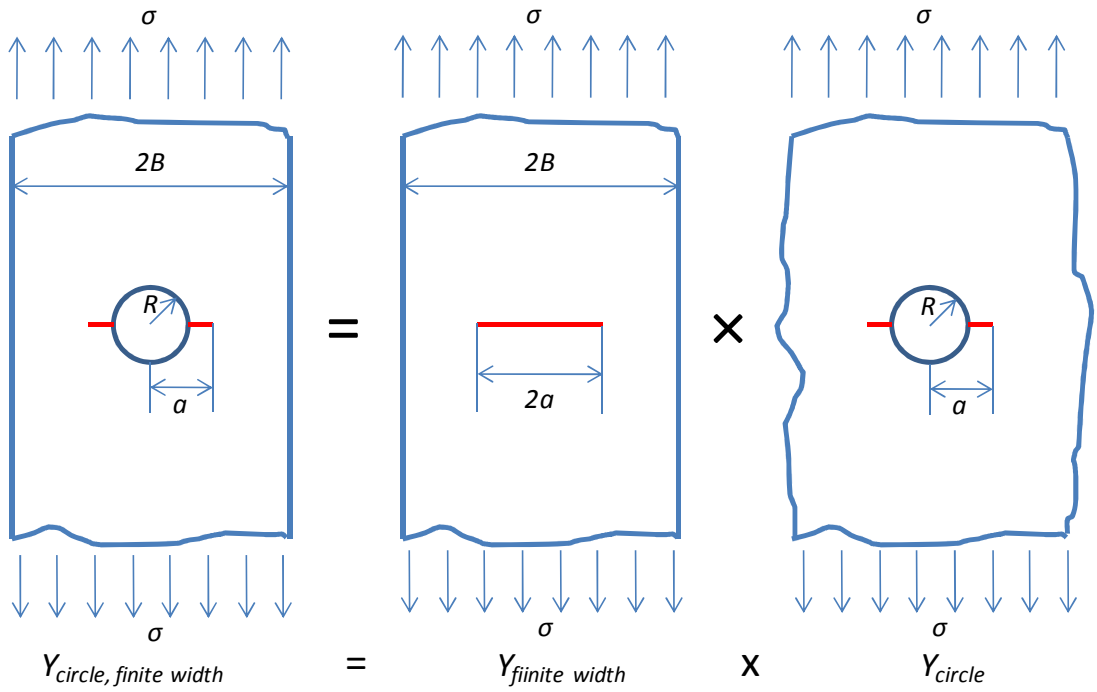

Figure 4-23: Combining correction factors for cracks in finite width plate with circular opening

As the SIF of each case can expressed by SIF_0 multiplied by the corresponding correction factor of geometry, shown in Equations (4-14) to (4-16), the combined effects of geometries is obtained in terms of correction factors as follows:

$$SIF_{circle,finite\ width} = Y_{circle,finite\ width} \times SIF_0 \quad \textbf{(4-14)}$$

$$SIF_{finite\ width} = Y_{finite\ width} \times SIF_0 \quad \textbf{(4-15)}$$

$$SIF_{circle} = Y_{circle} \times SIF_0 \quad \textbf{(4-16)}$$

$$Y_{circle,finite\ width} = Y_{finite\ width} \times Y_{circle} \quad \textbf{(4-17)}$$

Hence, the SIF of centre cracks emanating from circular opening in a finite width plate is expressed as Equation (4-18):

$$SIF_{circle,finite\ width} = Y_{finite\ width} \times Y_{circle} \times SIF_0 \quad \textbf{(4-18)}$$

In the next section, some correction factors are analysed so that their combinations can be successfully applied to the ship hull geometries and predict the SIFs of cracks in complex ship structures.

4.4.2 Correction factors

Finite plate

The effect of finite plate on the SIF is considered in two ways. One is the finite width's effect and the other is finite length's effect. The correction factor for each case is explained below and combining two correction factors would be used to estimate the SIF for cracks in a finite plate in terms of both width and length.

a) Finite width plate

A number of researches have been carried out to calculate the SIF for this case in empirical ways. SIF of a centre crack in a finite width plate shown in Figure 4-24 can be expressed as Equation (4-19).

$$SIF_{finite\ width} = Y_{finite\ width} \times SIF_0 \quad \textbf{(4-19)}$$

where, $SIF_{finite\ width}$ is the SIF of a centre crack in a finite width plate

SIF_0 is the SIF of a centre crack in an infinite plate, $SIF_0 = \sigma\sqrt{\pi a}$

$Y_{finite\ width}$ is the correction factor for the effect of the finite width plate

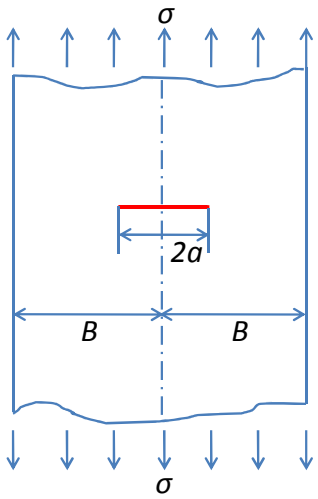

Figure 4-24: A centre crack in a finite width plate

Empirical solutions for this case are shown in Table 4-2 from the handbook of Tada, Paris and Irwin (2000).

Table 4-2: Empirical solutions of correction factor for a finite width plate case

$Y_{finite\ width}\ (a/B)$	Reference	Accuracy
$\sqrt{\frac{2B}{\pi a} tan \frac{\pi a}{2B}}$	Irwin	Better than 0.5% for $a/B \leq 0.5$
$1 + 0.128\left(\frac{a}{B}\right) - 0.288\left(\frac{a}{B}\right)^2 + 1.525\left(\frac{a}{B}\right)^3$	Brown	0.5% for $a/B \leq 0.7$
$\sqrt{sec \frac{\pi a}{2B}}$	Feddersen	0.3% for $a/B \leq 0.7$, 1% at $a/B = 0.8$
$\frac{1 - 0.5\left(\frac{a}{B}\right) + 0.326\left(\frac{a}{B}\right)^2}{\sqrt{1 - \frac{a}{B}}}$	Koiter	1% for any a/B
$\frac{1 - 0.5\left(\frac{a}{B}\right) + 0.370\left(\frac{a}{B}\right)^2 - 0.044\left(\frac{a}{B}\right)^3}{\sqrt{1 - \frac{a}{B}}}$	Tada	0.3% for any a/B
$\left\{1 - 0.025\left(\frac{a}{B}\right)^2 + 0.06\left(\frac{a}{B}\right)^4\right\}\sqrt{sec \frac{\pi a}{2B}}$	Tada	0.1% for any a/B

Among the various solutions above, the last solution proposed by Tada is selected to be used in this research due to the highest accuracy among them. So the correction factor of the finite width plate is as Equation (4-20).

$$Y_{finite\ width} = \left\{1 - 0.025\left(\frac{a}{B}\right)^2 + 0.06\left(\frac{a}{B}\right)^4\right\}\sqrt{sec\frac{\pi a}{2B}} \quad \textbf{(4-20)}$$

where, a is half of the centre crack sizes and B is half width of the finite width plate

b) Finite length plate

Unfortunately, no reference containing correction factors for the finite length plate case is found hence the finite element analysis is introduced in the calculation of SIF in this case. SIF of a centre crack in a finite length plate can be expressed as Equation (4-21).

$$SIF_{finite\ length} = Y_{finite\ length} \times SIF_0 \quad \textbf{(4-21)}$$

where, $SIF_{finite\ length}$ is the SIF of a centre crack in a finite length plate

SIF_0 is the SIF of a centre crack in an infinite plate, $SIF_0 = \sigma\sqrt{\pi a}$

$Y_{finite\ length}$ is the correction factor for the effect of the finite length plate

Due to the difficulty arising from using an infinite width plate in FE model, obtaining of the SIF for the finite length plate is attempted by removing the effect of finite width plate from the result of the SIF for a finite plate case both in width and length. This concept is explained below as in Equation (4-22).

$$SIF_{finite\ plate} = Y_{finite\ width} \times SIF_{finite\ length} \quad \textbf{(4-22)}$$

where, $SIF_{finite\ plate}$ is the SIF of a centre crack in a finite plate

$SIF_{finite\ length}$ is the SIF of a centre crack in a finite length plate

$Y_{finite\ width}$ is the correction factor for the finite width plate as in Equation (4-20)

So, FE analyses are carried out with a series of finite plates of which geometric information is shown in Figure 4-25.

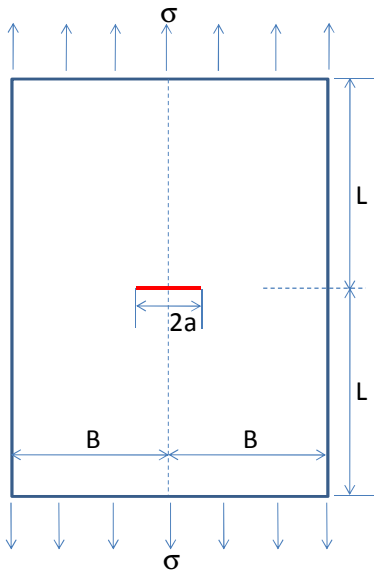

Parameters		Unit
a	0.05	m
B	1.0	m
L	0.1~45	m
E	210	GPa
σ	1.0	MPa

Figure 4-25: Configuration of a finite plate and its dimensions for FE analyses

The SIFs calculated by ABAQUS are shown in Figure 4-26 and it can be noted that the SIF converges as the length/width ratio, *L/B*, increases; in this analysis it converges to 0.397 MPa$\sqrt{m}$.

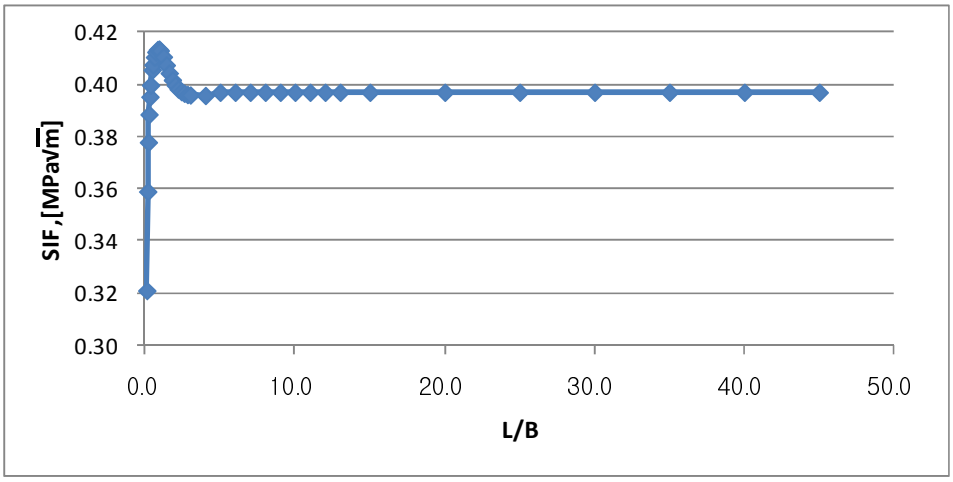

Figure 4-26: SIFs calculated by FE analysis for different finite plates ($SIF_{finite\ plate}$)

Now the correction factor due to the effect of the finite length plate can be obtained as Equation (4-23), which is extracted according to Equations (4-21) and (4-22).

$$Y_{finite\ length} = SIF_{finite\ plate} \div SIF_0 \div Y_{finite\ width} \quad \textbf{(4-23)}$$

The correction factor obtained due to the pure effect of finite length is shown in Figure 4-27 and Figure 4-28, where the values are plotted against *L/B* ratio and a

variable s_L defined as $s_L=L/(L+B)$, respectively. By introducing the variable s_L, the correction factor for finite length can be expressed by the variable confined between 0.0 and 1.0.

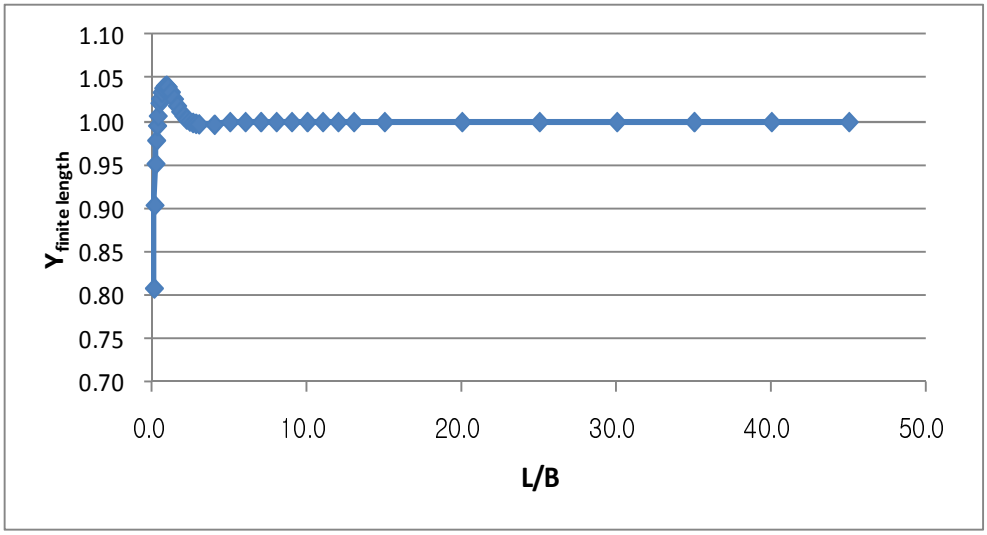

Figure 4-27: Correction factor for the finite length against *L/B*

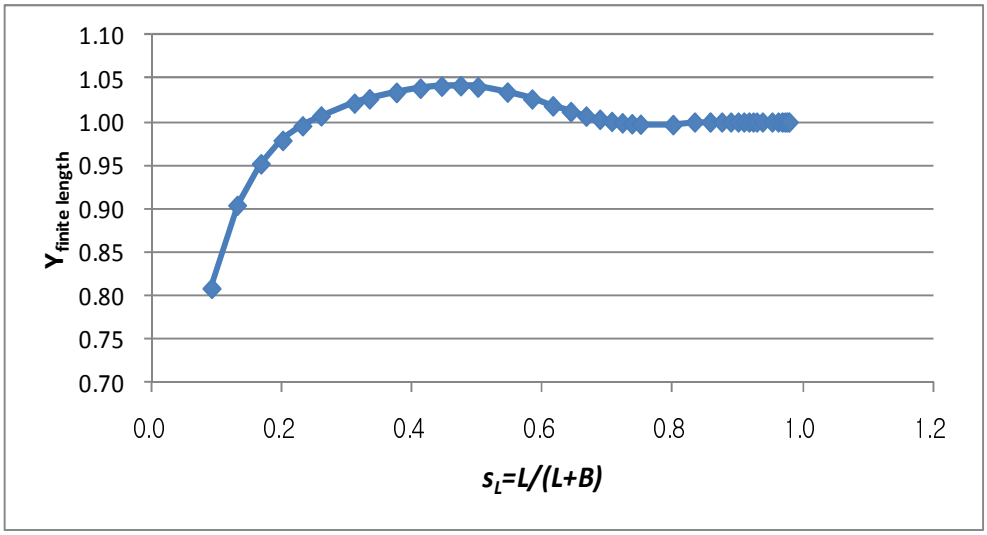

Figure 4-28: Correction factor for the finite length against s_L

Further processing was carried out in order to obtain a proper expression of the correction factor distribution; firstly, the correction factor in Figure 4-28 is divided by the square root of s_L, which enables easy achievement of the trend line with a high accuracy as shown in Figure 4-29. So the final expression of the correction factor for the effect of the finite length plate is obtained as Equation (4-24).

$$Y_{finite\ length} = \sqrt{s_L} \times (-6.0784{s_L}^5 + 19.918{s_L}^4 - 26.087{s_L}^3 + 18.512{s_L}^2 - 8.6119s_L + 3.3462) \quad \textbf{(4-24)}$$

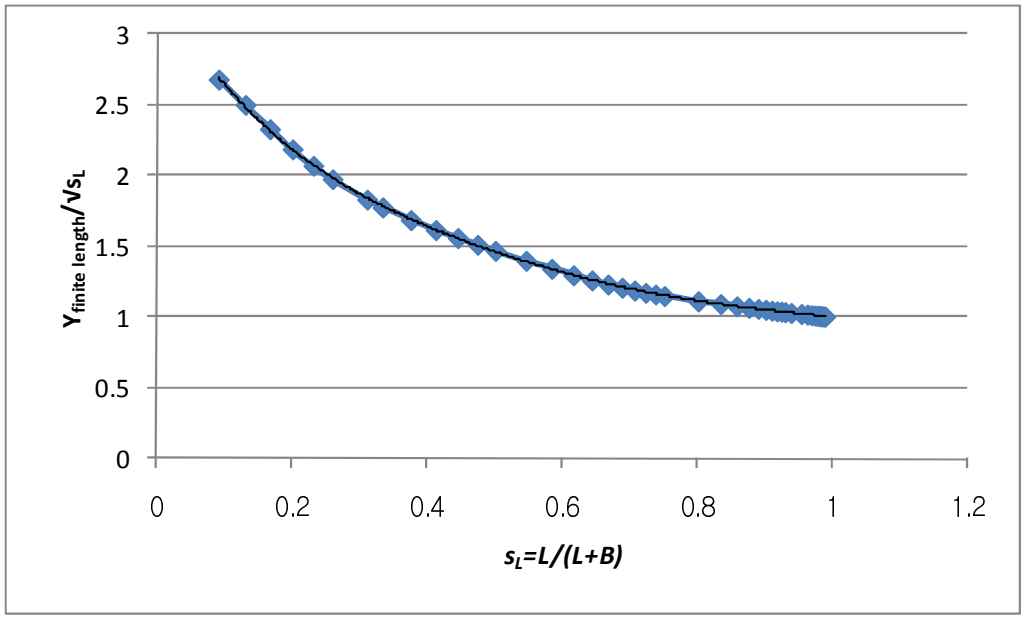

Figure 4-29: A trend line for the modified correction factor

Comparison between the original results calculated by FE analysis and the estimated data according to Equation (4-24) is shown in Figure 4-30 and Figure 4-31, where the agreement between them is presented.

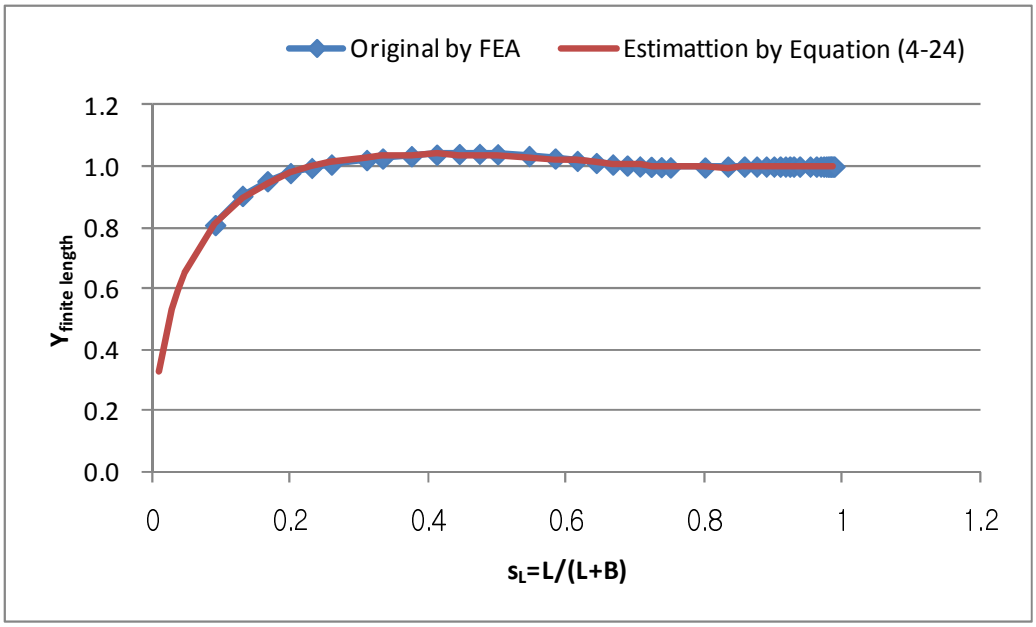

Figure 4-30: Comparison of correction factor for the effect of finite length

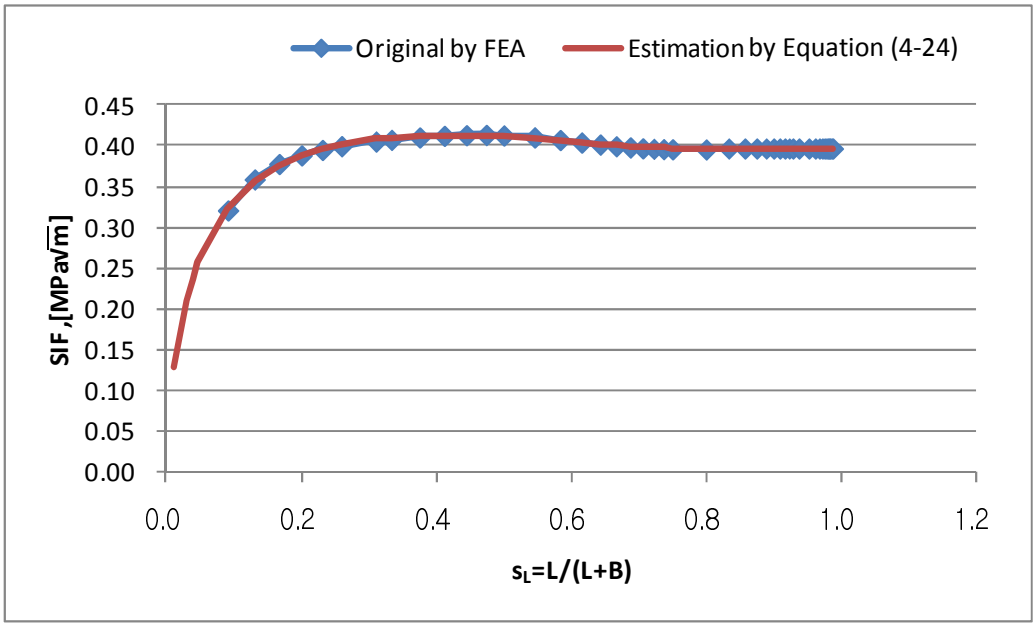

Figure 4-31: Comparison of SIFs in a finite length plate

Circular opening

Research on the effect of the existence of openings on the SIFs of cracks has been carried out focusing on rivet holes in aircraft structures. The basic condition of crack deployments at the circular opening is that a pair of symmetric cracks is initiated around the opening. The effect of the opening on the SIFs of symmetric cracks has been revealed by a number of publications such as Bowie (1956), Newman (1971), Tweed & Rooke (1973), Grandt and Kullgren (1983) and others.

The correction factor accounting for the effect of circular openings can easily be obtained by the virtue of the work from of Tada, Paris and Irwin (2000), whose handbook contains an empirical solution for this problem according to the numerical results from Bowie (1956) and Newman (1971).

The SIF on the symmetric crack tips emanating from a circular opening in an infinite plate subjected to a uniform tension loads (Figure 4-32) can be expressed as Equation (4-25). The correction factor due to the effect of a circular opening is obtained as Equation (4-26) and shown in Figure 4-33.

$$SIF_{circle} = Y_{circle} \times SIF_0 \quad \textbf{(4-25)}$$

where, SIF_{circle} is the SIF of symmetric cracks emanating from a circular opening in an infinite plate

SIF_0 is the SIF of a centre crack in an infinite plate, $SIF_0 = \sigma\sqrt{\pi a}$

Y_{circle} is the correction factor for the effect of the circular opening in an infinite plate

$$Y_{circle} = 0.5(3 - s_c)\{1 + 1.243(1 - s_c)^3\} \times \sqrt{s_c} \quad \textbf{(4-26)}$$

where, s_c is a ratio of a_0 to half of the total damage size, $s_c = \frac{a_0}{a} = \frac{a_0}{R+a_0}$

a_0 is the size of crack emanating from opening

a is half of the total damage size including opening

R is the radius of opening

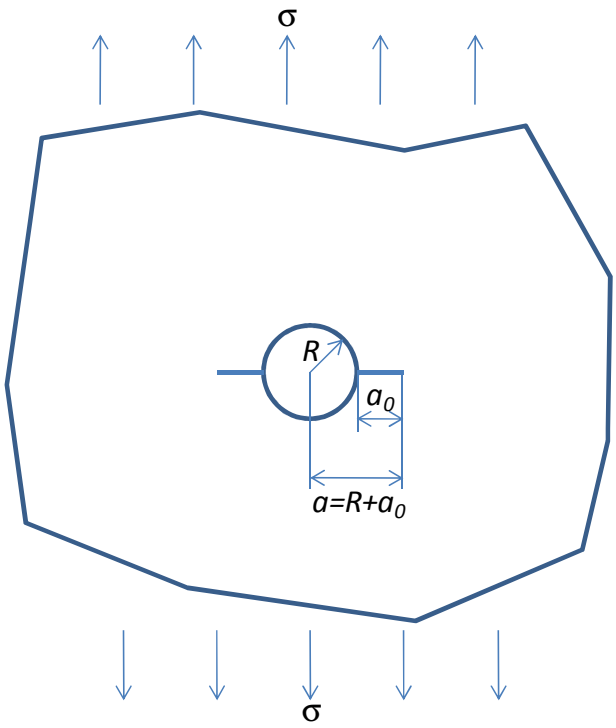

Figure 4-32: Configuration of symmetric cracks emanating from a circular opening in an infinite plate

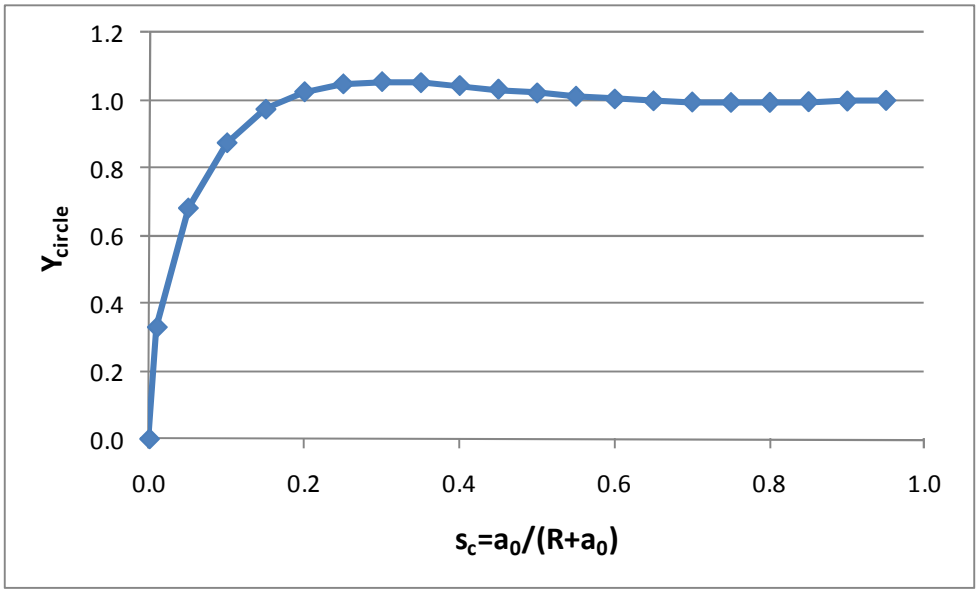

Figure 4-33: Correction factor for the effect of circular openings by Equation (4-26)

When a circular opening and symmetric cracks are located in a finite plate, the SIF can be estimated from the Equation (4-25) multiplied by both correction factors of $Y_{finite\ width}$ and $Y_{finite\ length}$ expressed in Equations (4-20) and (4-24) respectively.

Asymmetric cracks

Cracks initiated from a circular opening-edge considered in the previous section are based on the assumption of symmetry at the moment of the initial damage. In real situations, such cracks are hardly expected as the initial sizes of them are not always the same. Also, different crack propagation rates are expected for different cracks due to the difference in either geometric configurations around cracks or loadings applied to crack tips even though the crack sizes are the same at the initial damage condition.

In spite of the reality in which two opening-edge cracks exist in different lengths, this issue seems to be addressed by some researchers. Tweed and Rooke (1973) have approached this problem in a numerical way by using the principle of superposition. Lai, Zhang and Schijve (1991) also investigated this problem by using a combined complex variable and least square method. Recently Stefanescu, Edwards and Fitzpatrick (2003) tried to extract the correction factor due to the asymmetric cracks at openings according to experimental data.

In this research, a pair of correction factors for asymmetric cracks emanating from a circular opening in an infinite plate under uniaxial tension load (Figure 4-34) is proposed and compared with the results from Lai, Zhang and Schijve (1991) and Stefanescu, Edwards and Fitzpatrick (2003).

SIF at the Primary crack tip 'P' in the Figure 4-34 is estimated from SIF of symmetric cracks, with length of $a_{0,P}$, emanating from a circular opening with radius R. On top of this, a correction factor should be applied due to the different (short) crack length in the Secondary crack tip 'S'. This relationship can be expressed as Equation (4-27).

$$SIF_P = SIF_{circle}(a_{0,P}, R) \times Y_{asym,P}(a_P, a_S) \quad \textbf{(4-27)}$$

where, SIF_P is the SIF at crack tip 'P' in asymmetric cracks illustrated in Figure 4-34

$SIF_{circle}(a_{0,P},R)$ is the SIF of symmetric cracks with length of $a_{0,P}$ emanating from a circular opening with radius of R

$Y_{asym,P}(a_P,a_S)$ is the correction factor at crack tip 'P' due to the different crack length between a_P and a_S

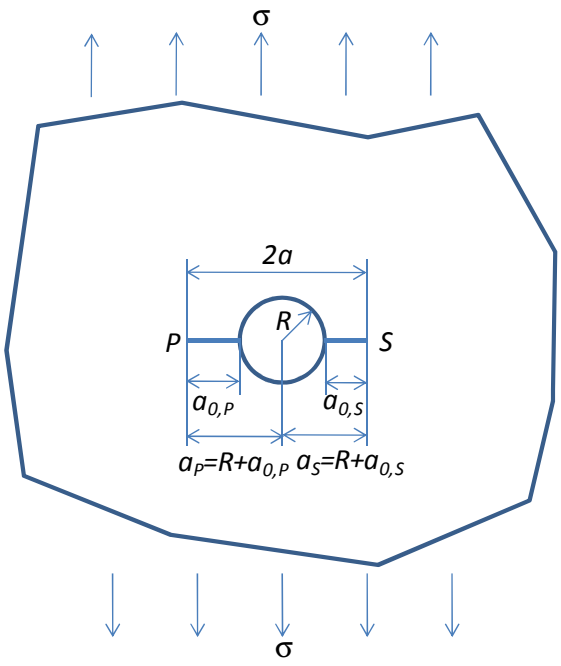

Figure 4-34: Configuration of asymmetric cracks emanating from a circular opening in an infinite plate

In this case, the correction factor is selected to reduce the SIF for the symmetric cracks case and proposed as Equation (4-28).

$$Y_{asym,P}(a_P, a_S) = \sqrt{a/a_P} = \sqrt{(\alpha + 1)/2} \quad \textbf{(4-28)}$$

where, a is the half of the damage length, $2a = a_P + a_S$

α is a ratio of the secondary cack, a_S, to the primary crack, a_P, $\alpha = a_S/a_P$

The same approach can be applied in estimating SIF at crack tip 'S' so that SIF at crack tip 'S' and the corresponding correction factor are expressed in Equation (4-29) and (4-30) respectively with similar definition of variables as in Equation (4-27) and (4-28).

$$SIF_S = SIF_{circle}(a_{0,S}, R) \times Y_{asym,S}(a_P, a_S) \quad \textbf{(4-29)}$$

$$Y_{asym,S}(a_P, a_S) = \sqrt{a/a_S} = \sqrt{(\alpha + 1)/2\alpha} \quad \textbf{(4-30)}$$

It should be noted in Equations (4-27) and (4-29) that different SIF_{circle} is used according to different crack tips. Hence, an additional work is carried out to express the SIFs of asymmetric cracks with the solution of the centre crack in an infinite plate, SIF_0, as shown next:

$$SIF_P = SIF_0 \times Y_{asym,P} = SIF_0 \times Y_{circle}(a_{0,P}, R) \quad \textbf{(4-31)}$$

$$SIF_S = SIF_0 \times Y_{asym,S} = SIF_0 \times Y_{circle}(a_{0,S}, R) \quad \textbf{(4-32)}$$

where, SIF_0 is the SIF of a centre crack in an infinite plate, $SIF_0 = \sigma\sqrt{\pi a}$

$Y_{circle}(a_{0,P}, R)$ is the correction factor for the effect of the circular opening in an infinite plate with opening radius of R and initial crack size of $a_{0,P}$

$Y_{circle}(a_{0,S}, R)$ is the correction factor for the effect of the circular opening in an infinite plate with opening radius of R and initial crack size of $a_{0,S}$

Finally, the pure effect of asymmetric cracks in an infinite plate with a circular opening is obtained as Equation (4-33) and (4-34) for primary and secondary crack tips respectively.

$$Y_{asym,P} = \frac{SIF_P}{SIF_0 \times Y_{circle}(a_0, R)} = \frac{Y_{circle}(a_{0,P}, R)}{Y_{circle}(a_0, R)} \quad \textbf{(4-33)}$$

$$Y_{asym,S} = \frac{SIF_S}{SIF_0 \times Y_{circle}(a_0, R)} = \frac{Y_{circle}(a_{0,S}, R)}{Y_{circle}(a_0, R)} \quad \textbf{(4-34)}$$

where, $Y_{circle}(a_0, R)$ is the correction factor for the effect of the circular opening in an infinite plate with opening radius of R and initial crack size of a_0 and is expressed in Equation (4-26)

a_0 is the averaged crack size, $2a_0 = a_{0,P} + a_{0,S}$

SIFs obtained by this approach are compared to the results from Lai, Zhang and Schijve (1991) and Stefanescu, Edwards and Fitzpatrick (2003) (Figure 4-35). To meet the condition from Stefanescu, Edwards and Fitzpatrick (2003), a_S/R = 1.02 ~ 4.0, α = 0.4 ~ 1.0 is adopted for comparison. Also, for the calculation of the SIF values the radius of the opening is R = 1.0 m and the uniaxial tension load, σ = 10 MPa is applied.

From the comparison in Figure 4-35, the results obtained by current approach and the results from Lai, Zhang and Schijve (1991) show good agreement. The results from Stefanescu, Edwards and Fitzpatrick (2003) show some differences in comparison to other results. Considering the case of symmetric cracks, α = 1.0, where the correction factor for asymmetric cracks of current approach is unity so the calculated SIFs are the same as those of symmetric cracks emanating from a circular opening (Equation (4-26)), the result from Stefanescu, Edwards and Fitzpatrick (2003) is less accurate than others. In addition, their results on the secondary crack do not converge to zero as the crack size reduces, which is not the correct case.

Hence, it can be said that the proposed approach for taking into account the effect of asymmetric cracks emanating from a circular opening is simple and gives reasonable accuracy.

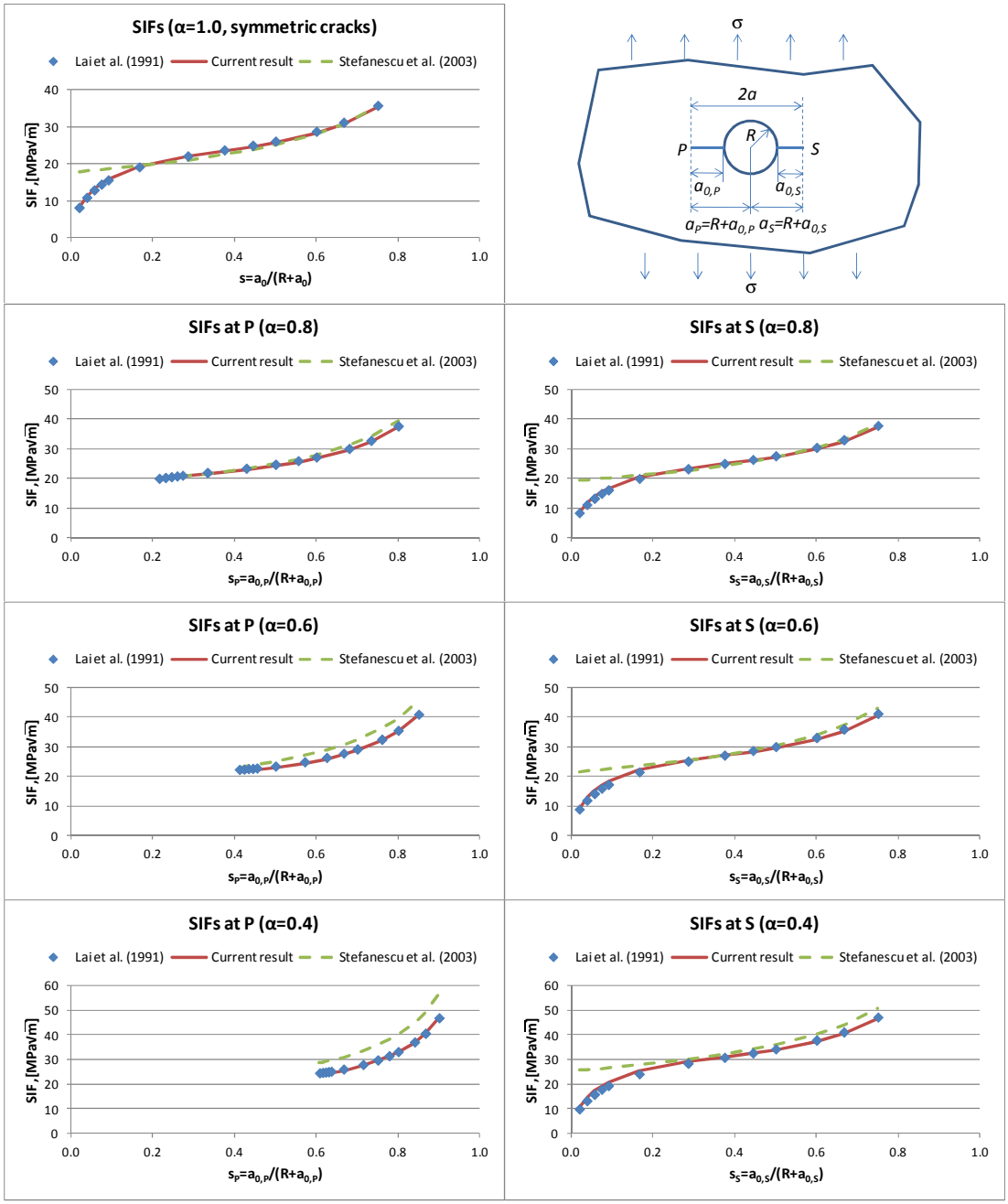

Figure 4-35: SIFs obtained by Equations (4-27) and (4-29) and comparison with two references

Stiffener

The effect of stiffeners in a stiffened panel has been researched by few literature such as Poe (1971), Isida (1973) and Dexter and Pilarski (2000), in which analytical solutions on the effect of stiffeners have been attempted.

In this research, the correction factor for the effect of stiffeners is obtained according to the approach by Dexter and Pilarski (2000), who superposed the effect of stiffener

restraint and the effect of stiffener separation to obtain the full effect of stiffeners in a stiffened panel. This superposition is presented in Figure 4-36 which allows estimation of SIF for cracks in a stiffened panel captured by Equation (4-35).

$$SIF_{stiffener} = Y_{stiffener} \times SIF_0 \quad \textbf{(4-35)}$$

where, $SIF_{stiffener}$ is SIF of centre crack in a stiffened panel

SIF_0 is the SIF of a centre crack in an infinite plate, $SIF_0 = \sigma\sqrt{\pi a}$

$Y_{stiffener}$ is the correction factor for the effect of stiffeners,

$Y_{stiffener} = Y_{stif\_constraint} + Y_{stif\_separation}$

$Y_{stif\_constraint}$ is correction factor due to stiffener constraint

$Y_{stif\_separation}$ is correction factor due to stiffener separation

The effects of constraint and separation of stiffeners are considered separately as shown in Figure 4-36.

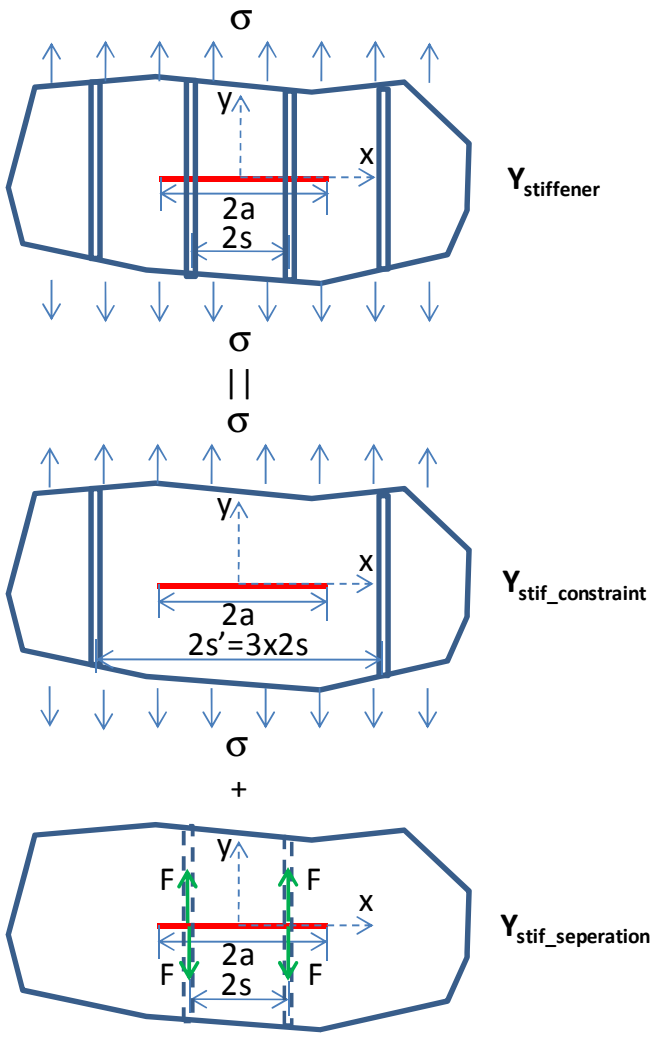

Figure 4-36: The overview of superposition of different factors in a stiffened panel

a) Stiffener constraint

The effect of stiffener constraint was first addressed numerically by Isida (1973), where a Fourier series solution was developed for a centrally cracked strip with stiffened edges. According to Dexter and Pilarski (2000), the correction factor due to the constraint effect of stiffeners can be expressed as Equation (4-36), which is valid for $\chi_i \leq 0.95$.

$$Y_{stif\_constraint,i} = \left(1 - \frac{1}{f_{k,i}}\right)\left(\frac{1}{1+\beta_i}\right)^{\alpha_1} + \frac{1}{f_{k,i}} + \frac{0.3{\chi_i}^2}{f_{k,i}}\left(\frac{4}{{\beta_i}^2 - 2\beta_i + 4} - 1\right) - \alpha_2\left(\frac{{\chi_i}^{10} + {\chi_i}^{30} + {\chi_i}^{50}}{f_{k,i}}\right)\left(\frac{4}{{\beta_i}^2 - 2\beta_i + 4} + 1\right) \quad \textbf{(4-36)}$$

where, i denotes i-th pair of stiffeners

f_k is Koiter's finite width correction, $f_k = \frac{1-0.5\chi+0.326\chi^2}{\sqrt{1-\chi}}$

β_i is axial stiffness ratio of i-th stiffener to relevant plate, $\beta_i = \frac{E_{st,i} \times A_{st,i}}{E_{pl,i} \times t_{pl,i} \times s_i}$

$E_{st,i}$ and $E_{pl,i}$ denote Young's modulus of stiffener and plate respectively

$A_{st,i}$ and s_i are the sectional area and half stiffener space of i-th stiffener respectively

$t_{pl,i}$ is the plate thickness relevant to i-th stiffener

χ_i is the crack distance normalised by i-th stiffener, $\chi_i = \frac{a}{x_i}$

a is half crack length

x_i denotes distance to i-th stiffener from centre of crack, $x_i = 2\sum_{j=1}^{i} s_j - s_1$

α_1 and α_2 are constants characterizing the magnitude of the edge stiffener's restraint

Calibrating the result of Equation (4-36) to fit with the result from FE analysis gives $\alpha_1 = 0.1$ and $\alpha_2 = 0.5$ in this research. The obtained correction factor for the effect of stiffener constraint is shown in Figure 4-37.

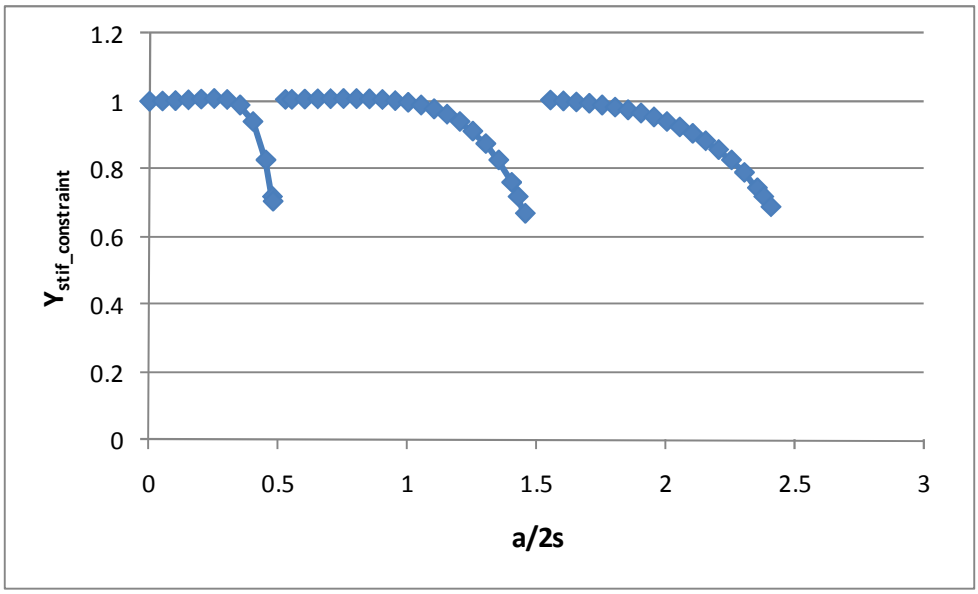

Figure 4-37: Correction factor for stiffener constraint effect, $Y_{stif\_constraint}$

b) Stiffener separation

The effect of severed stiffeners in a stiffened panel is also explained in Dexter and Pilarski (2000). The severed stiffeners are considered to induce additional point force to the crack face as shown in the bottom of Figure 4-36.

The correction factor proposed for the stiffener separation is expressed as Equation (4-37), which is valid only for $\chi_i' > 1.0$.

$$Y_{stif\_separation,i} = \frac{4\mu_i}{\pi(1-\mu_i)\sqrt{\chi_i'^2 - 1}} \quad \textbf{(4-37)}$$

where, i denotes i-th pair of stiffeners

$$\mu_i = \frac{A_{st,i}}{A_{st,i}+2x_i' \times t_{pl,i}}$$

$A_{st,i}$ and s_i are the sectional area and half stiffener space of i-th stiffener respectively

$t_{pl,i}$ is the plate thickness relevant to i-th stiffener

χ_i' is the crack distance normalised by i-th severed stiffener, $\chi_i' = \frac{a}{x_i'}$

a is half crack length

x_i' denotes distance to i-th severed stiffener from centre of crack,

$$x_i' = 2\sum_{j=1}^{i} s_j - s_1$$

The obtained correction factor for the effect of stiffener separation is shown in Figure 4-38.

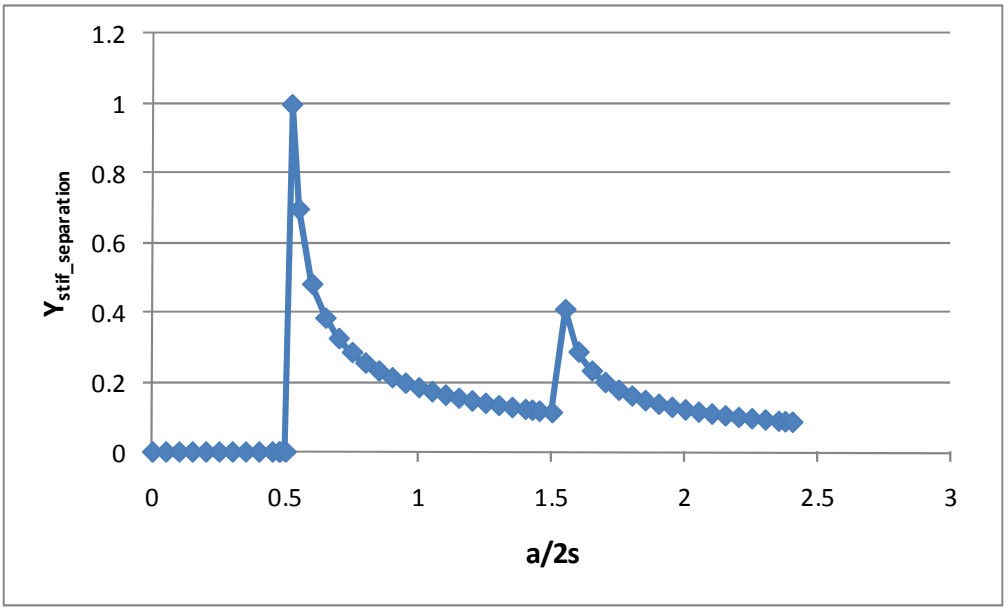

Figure 4-38: Correction factor for stiffener separation effect, $Y_{stif\_separation}$

c) Combined correction factor

The total correction factor due to stiffeners in a stiffened panel can be obtained by summing up the above two correction factors obtained. According to Poe (1971), linear interpolation is adopted in the region which is equal to the depth of stiffener from the centre of each stiffener location. The resultant correction factor for the stiffener effect including the linear interpolation is shown in Figure 4-39 .

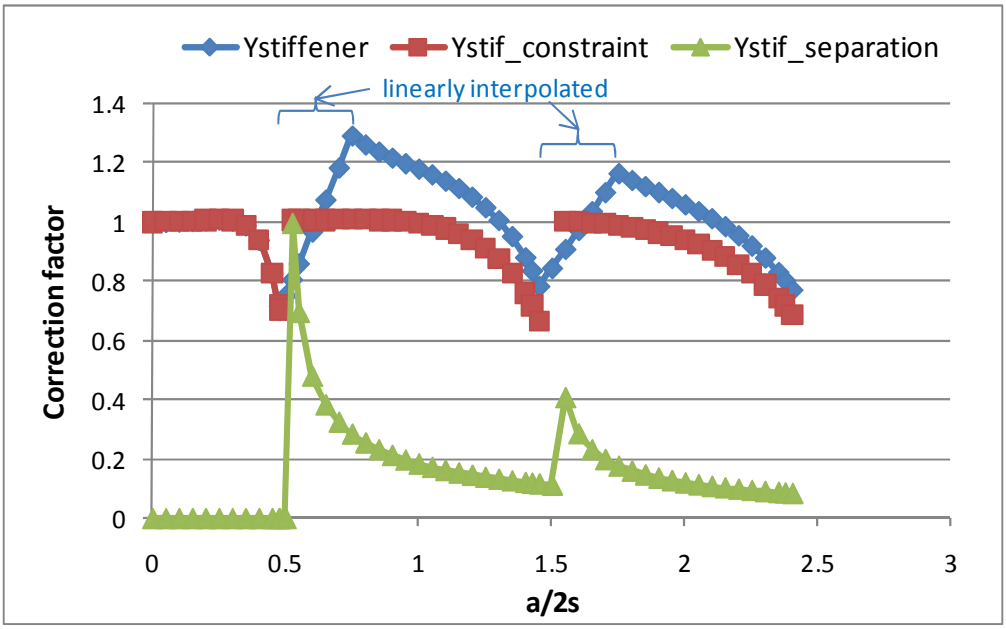

Figure 4-39: Correction factor due to stiffeners in a stiffened panel

Linearly distributed stresses

It is usual to have solutions of SIFs in plates subjected to uniformly distributed stresses. However, when making application to a real ship structure, this is only valid to deck and bottom plating even with an assumption that the ship is only subjected to vertical bending stress in an upright condition. Stresses in the side shell are subjected to variation according to the distance from the neutral axis in the same upright condition. The same situation applies to decks and bottom plates when ships are in heeling condition or subjected to a combination of vertical and horizontal bending moments.

Therefore, the response of cracks in a plate against linearly distributed stresses should be dealt with in this research. The solution of the SIF for this case is based on the work of Chell (1976), who has obtained empirical solutions in the form of polynomials on the numerical solutions for arbitrary distributions of stresses.

The empirical solution of the SIF by Chell (1976) for the case of linearly distributed stresses in a finite width plate, as shown in Figure 4-40, is captured by Equation (4-38).

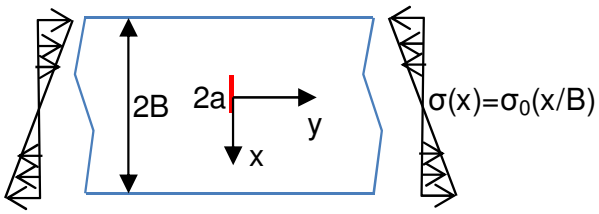

Figure 4-40: Configuration of linearly distributed stresses in a finite width plate

$$SIF_{Chell} = \sigma_0\sqrt{\pi a} \times Y_{finite\ width} \times \left(\frac{a}{B}\right)\left\{0.5 - 0.132\left(\frac{a}{B}\right) - 0.0267\left(\frac{a}{B}\right)^2\right\} \quad \textbf{(4-38)}$$

Expanding this solution to a more practical stress distribution case was attempted. In Figure 4-41, the original distribution of stresses can be divided into uniformly distributed stress of $\sigma_1(x) = \sigma$ and linearly distributed stress of $\sigma_2(x) = \sigma_0(x/b)$ and the SIF can be obtained by summing up the two individual SIFs of SIF_1 and SIF_2, which resulted by loading of $\sigma_1(x)$ and $\sigma_2(x)$ respectively. SIF_1 is obtained by Equation (4-39) with the correction factor for finite width, $Y_{finite\ width}$, of Equation (4-20), as this is the case of finite width plate subjected to a uniform tensile stress of σ.

$$SIF_1 = \sigma\sqrt{\pi a} \times Y_{finite\ width} \quad \textbf{(4-39)}$$

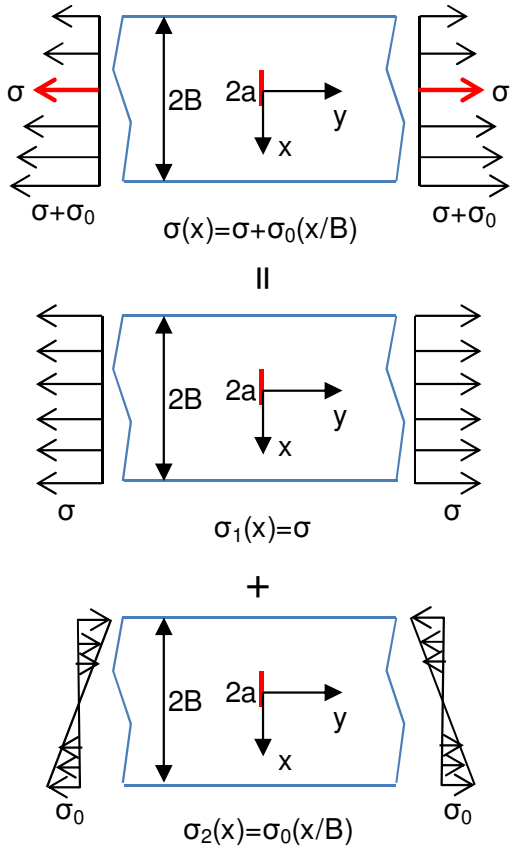

Figure 4-41: A practical stress distribution comprising a uniform and a linearly varying stress

Because the SIF_2 due to linear stress of $\sigma_2(x)$ is the same with the solution of Chell (1976), Equation (4-38), the total SIF for the linearly distributed stresses in a finite width plate can be obtained as follows:

$$SIF_{linear\ stress} = SIF_1 + SIF_2$$
$$= \sqrt{\pi a} \times Y_{finite\ width} \times \left[\sigma + \sigma_0 \left(\frac{a}{B}\right)\left\{0.5 - 0.132\left(\frac{a}{B}\right) - 0.0267\left(\frac{a}{B}\right)^2\right\}\right] \quad \textbf{(4-40)}$$

By defining SIF_0 with stress at centre of crack, σ, the $SIF_{lienar\ stress}$ can be expressed with the correction factor for the linear stress distribution, $Y_{linear\ stress}$, as Equation (4-41). Finally, the correction factor for linearly distributed stresses, $Y_{linear\ stress}$, is obtained by Equation (4-42) considering the locations of the crack tips.

$$SIF_{linear\ stress} = SIF_0 \times Y_{finite\ width} \times Y_{linear\ stress} \quad \textbf{(4-41)}$$

where, $SIF_0 = \sigma\sqrt{\pi a}$

$$Y_{linear\ stress} = 1 + \left(\frac{\sigma_0}{\sigma}\right)\left(\frac{\pm a}{B}\right)\left\{0.5 - 0.132\left(\frac{a}{B}\right) - 0.0267\left(\frac{a}{B}\right)^2\right\} \quad \textbf{(4-42)}$$

where, $+a$ means crack tip locates at positive x-axis as shown in Figure 4-41

$-a$ means crack tip locates at negative x-axis as shown in Figure 4-41

Elliptical opening

The effect of openings on SIFs is further investigated by accounting for an elliptical opening as the damage shape. Considering that damages from grounding accidents happen while the vessel is moving forward or drifting and that damage openings from collision accidents depend on the shape of bow of the striking vessel, it is not only more realistic but also general approach to consider elliptical rather than circular shapes as damage openings.

Reference on this can be found in Newman (1971) who has solved the problem using the boundary collocation method in an infinite plate subjected to uniaxial stress. The result of SIF correction factors for cracks emanating from an elliptical opening obtained by Newman (1971) is reproduced in Figure 4-42.

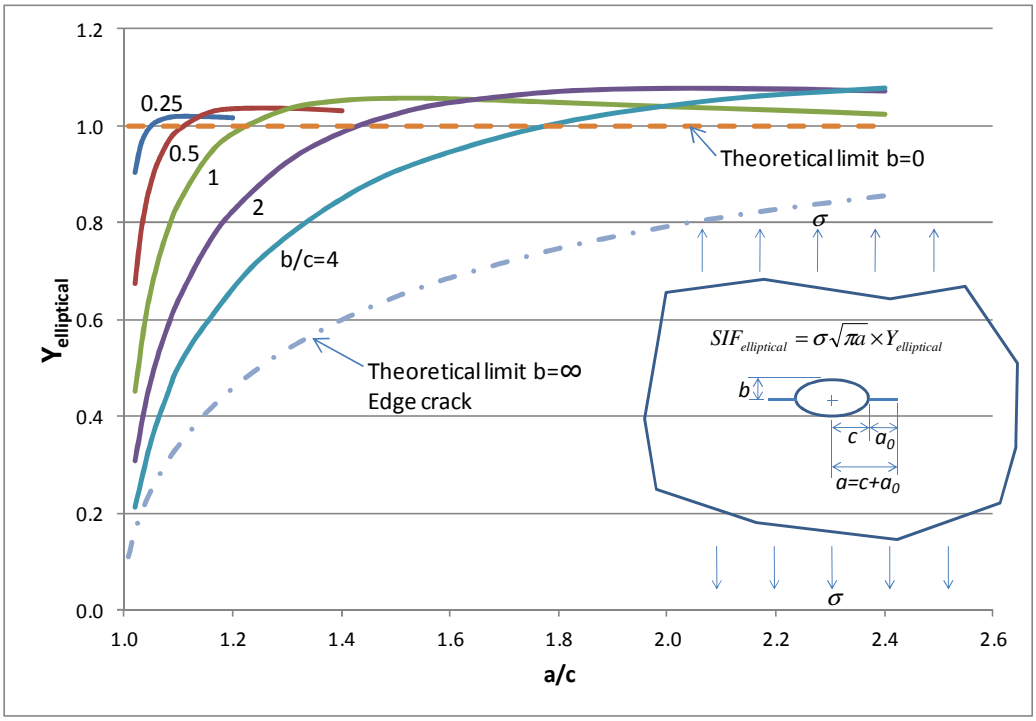

Figure 4-42: Correction factors for the elliptical openings in an infinite plate, Newman (1971)

No analytical or empirical expression is available and data from Newman (1971) is not enough to extract a proper empirical equation. For this reason, a set of FE analysis is deployed using a finite plate with various elliptical openings to produce sufficient data for the required analysis. The configuration of a finite plate with various elliptical openings is shown in Figure 4-43.

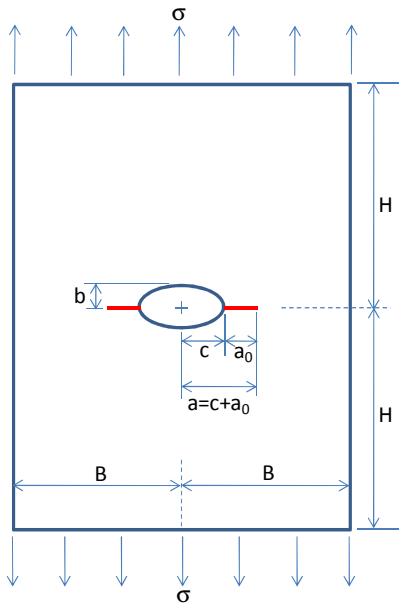

Parameters		Unit
B	2.0	m
H	3.0	m
b	0.125~0.75	m
c	0.25	m
a_0	0.005~1.4	m
E	210	GPa
σ	1.0	MPa

Figure 4-43: Configuration of a finite plate with elliptical openings for FE analysis

SIFs of symmetric crack tips in a finite plate with various elliptical openings are calculated and the correction factors for elliptical openings are obtained by dividing the calculated SIFs from FE analysis by SIFs of centre cracks in a finite plate as expressed in Equation (4-43).

$$Y_{elliptical,FEA} = SIF_{elliptical,FEA} \div SIF_{finite\ plate} \quad \textbf{(4-43)}$$

where, $SIF_{finite\ plate} = SIF_0 \times Y_{finite\ plate} = SIF_0 \times Y_{finite\ width} \times Y_{finite\ height}$

$$SIF_0 = \sigma\sqrt{\pi a}$$

The obtained correction factors are plotted in Figure 4-44 with the non-dimensional horizontal axis of $s_e = a_0/a = a_0/(c+a_0)$ and they are in good agreement with Newman's solution as can be seen in Figure 4-45.

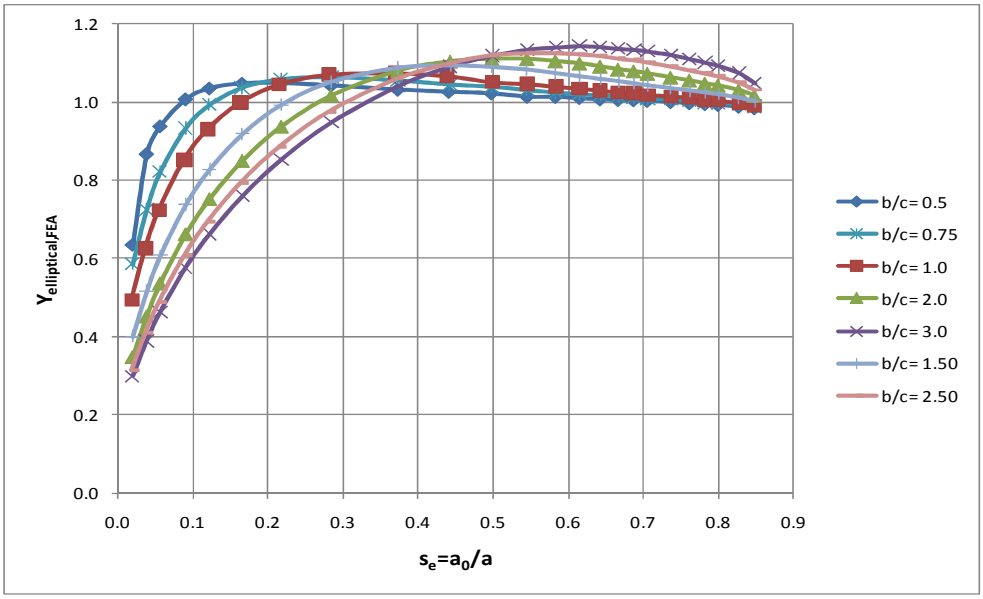

Figure 4-44: Correction factors for elliptical openings from FE analysis

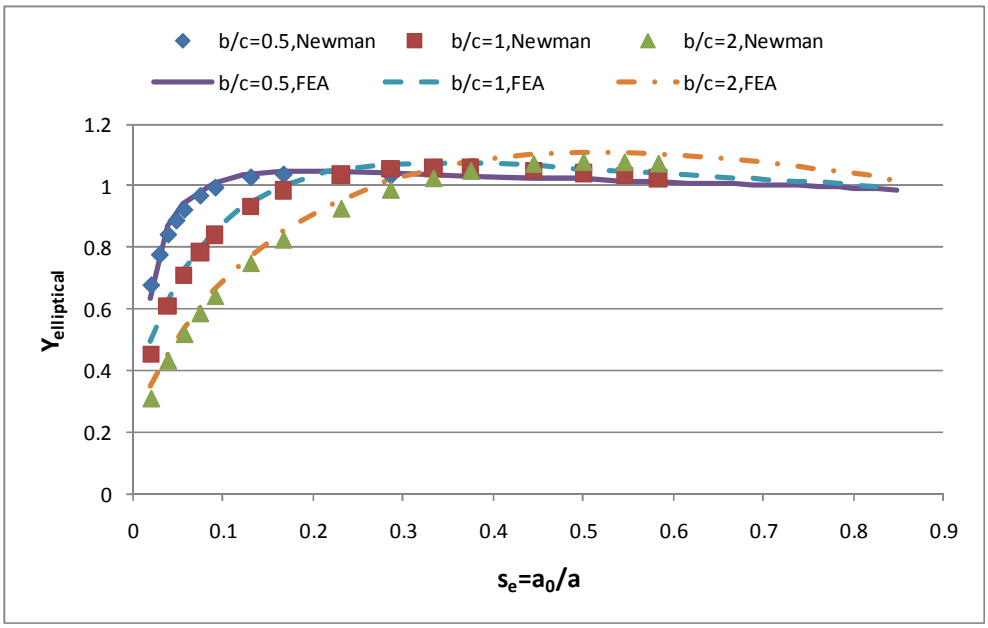

Figure 4-45: Comparison of correction factors for elliptical openings between FE analysis and Newman (1971)

Taking into account that the correction factor for elliptical opening should be expressed as a function of both *b/c* and s_e, its empirical equation is concluded as Equation (4-44) with the help of regression analyses.

$$Y_{elliptical} = {Y_{e,1}}\Big/{S_e\left(\frac{b}{c}\right)} \qquad \textbf{(4-44)}$$

where, $Y_{e,1} = 1 - exp[-exp\{A_0 + A_1X + A_2X^2 + A_3X^3\}]$

$$X = ln\,(s_e)$$

$$s_e = a_0/a = a_0/(c + a_0)$$

$$A_0 = 0.8239 \times \left(\frac{b}{c}\right)^{-0.331}$$

$$A_1 = -0.0268\left(\frac{b}{c}\right)^3 + 0.229\left(\frac{b}{c}\right)^2 + 0.3856\left(\frac{b}{c}\right) + 1.0969$$

$$A_2 = 0.1858 \times \left(\frac{b}{c}\right)^{-0.843}$$

$$A_3 = 0.0293 \times \left(\frac{b}{c}\right)^{-0.914}$$

b and c are radii of elliptical opening in the directions of perpendicular and parallel to crack respectively

a_0 is the initial crack size

Comparison of correction factors between estimation from Equation (4-44) and Newman's result is shown in Figure 4-46. It should be noted that the above equation is valid only for $0.5 \leq b/c \leq 4.0$ as the FE analysis results are provided in the conditions.

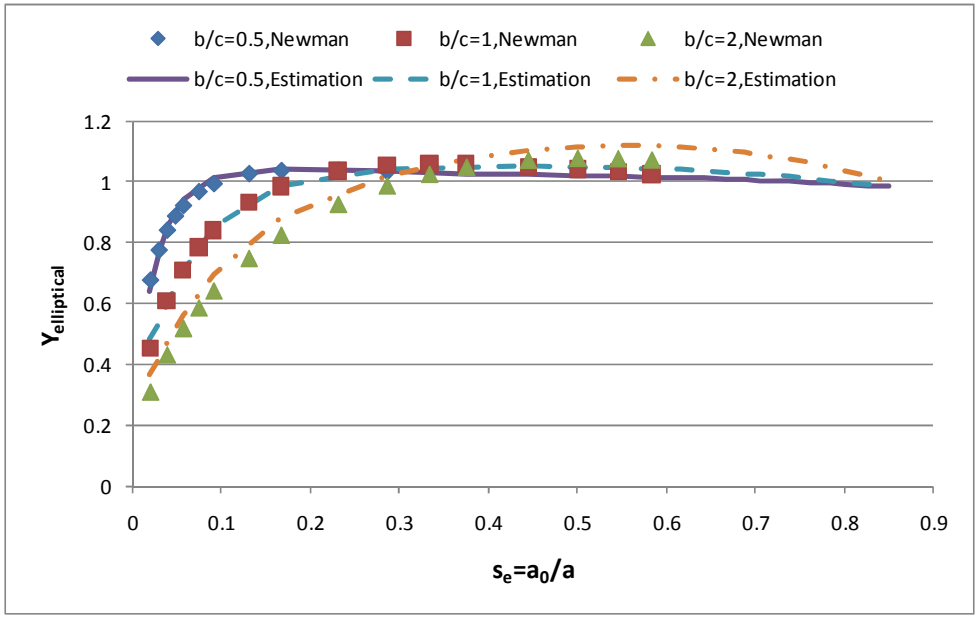

Figure 4-46: Comparison of correction factors for elliptical openings with Newman (1971)

L-shaped plate

When a collision accident results in damages over the waterline and includes the side shell and deck structure, the consequence in terms of residual strength degradation would be the severest among other damages from collision accidents. This is why the collision damage is assumed to be located at the upper part of the side shell, down from the strength deck in ABS guidelines (1995) for residual strength assessment.

As the concerned region is not a simple flat plate but an L-shaped joint plate and no reference has been found in the literature, in order to investigate the effect of the special geometry on the SIFs of crack tips, a set of FE analysis is deployed.

The responses of cracks in an L-shaped plate are analysed for a) cracks emanating from the corner without openings, and b) cracks emanating from the elliptical opening edges of an L-shaped plate.

a) Cracks without openings

Identification of the pure effects of geometry is obtained by a set of FE analyses with the geometric information shown in Figure 4-47.

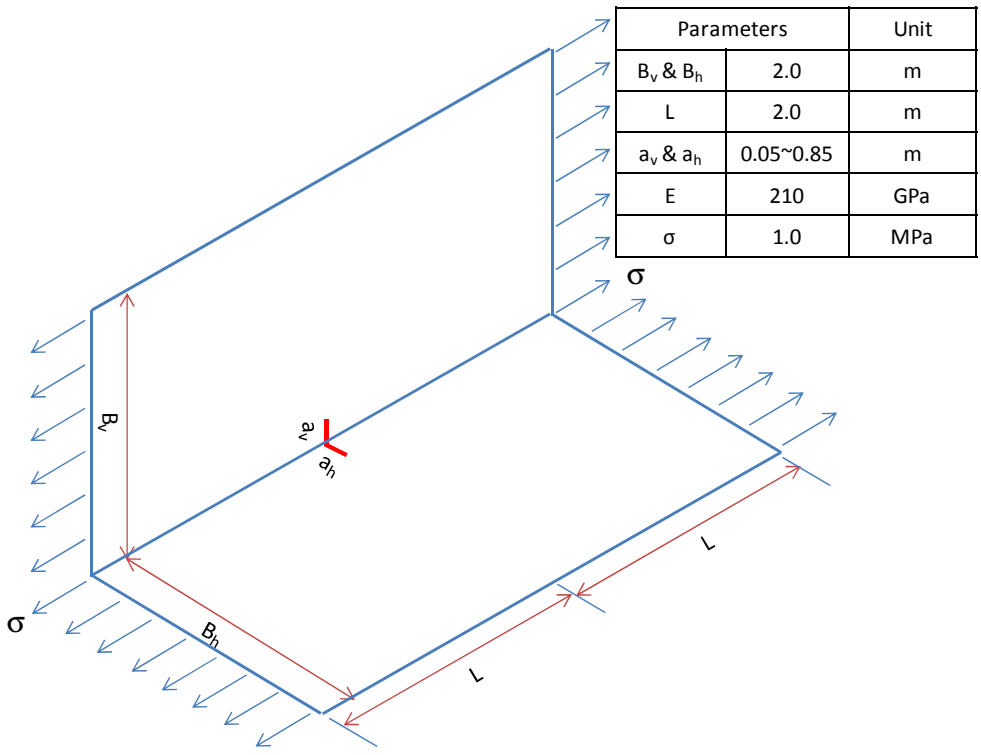

Figure 4-47: An L-shaped finite plate for FE analysis

When the cracks are symmetric, the calculated SIFs are compared with some empirical solutions for flat plate cases with different configurations from Tada, Paris and Irwin (2000). The empirical solutions include a centre crack in an infinite plate, SIF_0, a centre crack in a finite width plate, $SIF_{finite\ width}$ and an edge crack in a finite width plate, $SIF_{edge,\ finite\ width}$.

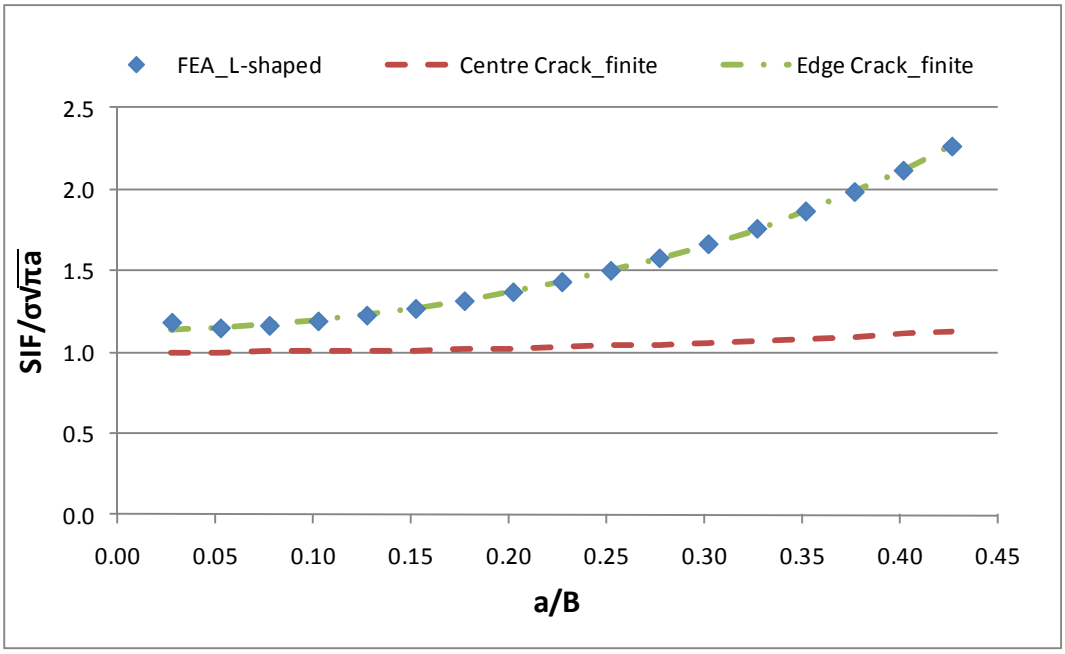

Figure 4-48: SIFs for an L-shaped plate with symmetric cracks compared with empirical solutions of flat plate configurations

As can be seen in Figure 4-48, the normalised SIF values of an L-shaped plate with symmetric cracks calculated by FE analysis are exactly the same with those of the single edge crack in a finite width plate. As such, the correction factor for a single edge crack in a finite width plate is regarded as adequate to be used as a basis for inducing the correction factor for an L-shaped plate. Hence, using the empirical formula of the correction factor for a single edge crack in a finite width plate from the handbook of Tada, Paris and Irwin (2000), the correction factor for cracks in an L-shaped finite width plate (Figure 4-47) is assumed to be expressed by Equation (4-45).

$$Y_{L-shape,finite\ width} = Y_{edge,finite\ width} \times Y_{L-shape,asymmetry} \quad \textbf{(4-45)}$$

where, $Y_{edge,finite\ width} = \sqrt{\frac{2B}{\pi a} tan \frac{\pi a}{2B}} \cdot \frac{0.752+2.02\left(\frac{a}{B}\right)+0.37\left(1-sin\frac{\pi a}{2B}\right)^3}{cos\frac{\pi a}{2B}}$

a and B are crack and width of plate where the SIF is calculated

$Y_{L\text{-}shape,\ asymmetry}$ is a correction factor for the asymmetric cracks in an L-shaped panel

With a simple calculation, the effect of $Y_{L\text{-}shape,\ asymmetry}$ is obtained as illustrated in Figure 4-49 and Figure 4-50 for the shorter and longer cracks respectively. Their analytical expressions are obtained in the polynomial forms of Equations (4-46) and (4-47) for the shorter and longer cracks respectively.

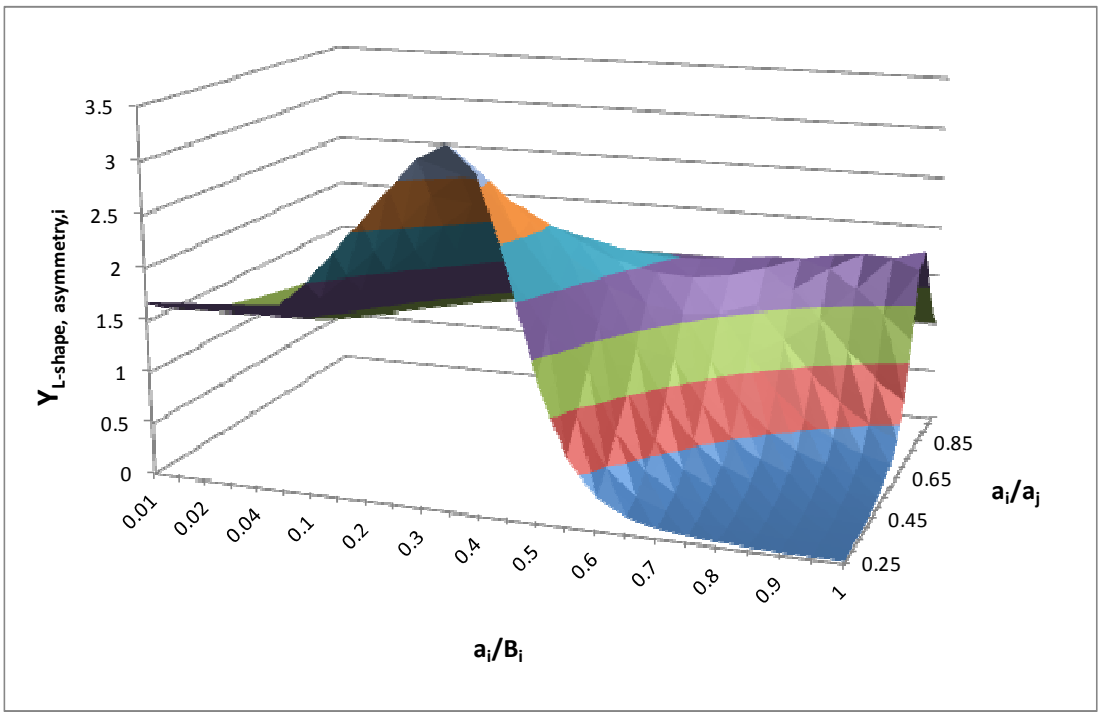

Figure 4-49: $Y_{L\text{-}shape,\ asymmetry}$ for the shorter crack, i

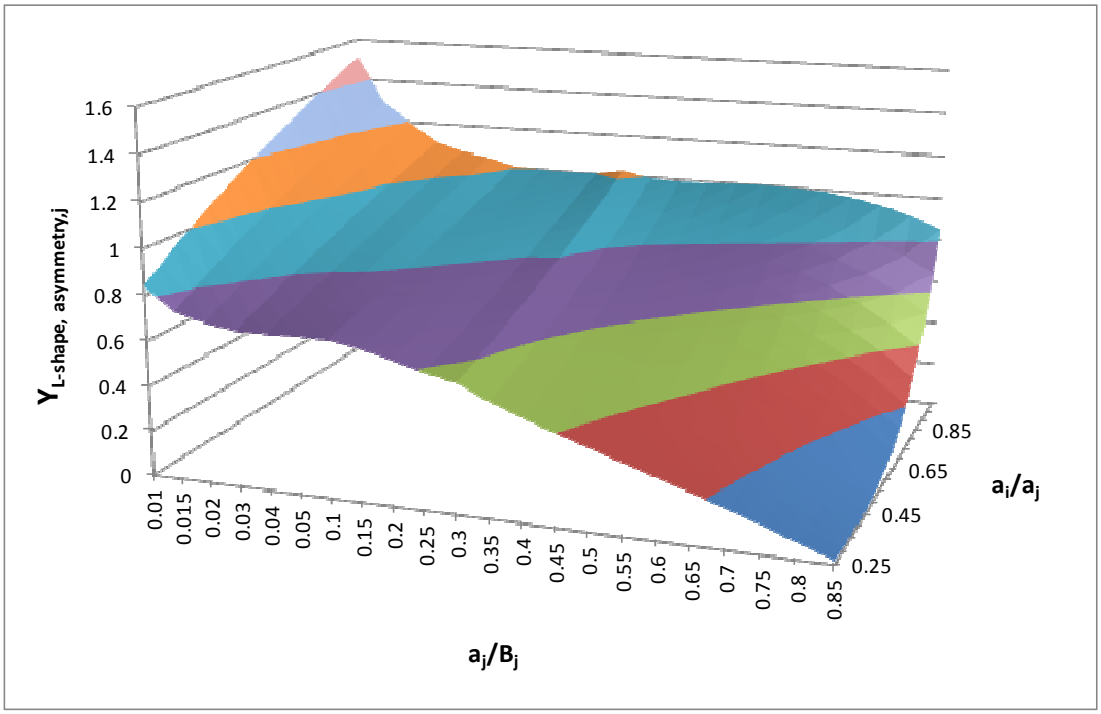

Figure 4-50: $Y_{L\text{-shape, asymmetry}}$ for the longer crack, j

$$Y_{L-shape,asymmetry}\left(\frac{a_i}{a_j},\frac{a_i}{B_i}\right)=\left[B_{0,i}+B_{1,i}X_i+B_{2,i}{X_i}^2+B_{3,i}{X_i}^3\right]^{(-B_i/a_i)} \quad \textbf{(4-46)}$$

where, $X_i=\left(\frac{a_i}{a_j}\right)^{a_i/B_i}$

$$\begin{cases} B_{0,i}=0 \\ B_{1,i}=9104.5\left(\frac{a_i}{B_i}\right)^3-1878.2\left(\frac{a_i}{B_i}\right)^2+121.75\left(\frac{a_i}{B_i}\right)-1.566 \\ B_{2,i}=-18380\left(\frac{a_i}{B_i}\right)^3+3779.2\left(\frac{a_i}{B_i}\right)^2-244.57\left(\frac{a_i}{B_i}\right)+5.8217 \\ B_{3,i}=9276\left(\frac{a_i}{B_i}\right)^3-1900.9\left(\frac{a_i}{B_i}\right)^2+122.81\left(\frac{a_i}{B_i}\right)-3.2558 \end{cases} for\ \frac{a_i}{B_i}<0.1$$

$$\begin{cases} B_{0,i}=229.89\left(\frac{a_i}{B_i}\right)^3-163.81\left(\frac{a_i}{B_i}\right)^2+38.353\left(\frac{a_i}{B_i}\right)-1.3478 \\ B_{1,i}=-746.48\left(\frac{a_i}{B_i}\right)^3+529.54\left(\frac{a_i}{B_i}\right)^2-125.25\left(\frac{a_i}{B_i}\right)+5.3884 \\ B_{2,i}=808.25\left(\frac{a_i}{B_i}\right)^3-574.95\left(\frac{a_i}{B_i}\right)^2+135.88\left(\frac{a_i}{B_i}\right)-4.0465 \\ B_{3,i}=-291.68\left(\frac{a_i}{B_i}\right)^3+209.24\left(\frac{a_i}{B_i}\right)^2-48.992\left(\frac{a_i}{B_i}\right)+1.0063 \end{cases} for\ \frac{a_i}{B_i}\geq 0.1$$

a_i and a_j are the sizes of the shorter and longer cracks respectively

B_i is width of plate where the shorter crack is embedded

$$Y_{L-shape,asymmetry}\left(\frac{a_i}{a_j},\frac{a_j}{B_j}\right)=\left[B_{0,j}+B_{1,j}X_j+B_{2,j}{X_j}^2+B_{3,j}{X_j}^3\right]^{(B_j/a_j)} \quad \textbf{(4-47)}$$

where, $X_j=\left(\frac{a_i}{a_j}\right)^{a_j/B_j}$

$$\begin{cases} B_{0,j}=355.17\left(\frac{a_j}{B_j}\right)^3-272.22\left(\frac{a_j}{B_j}\right)^2+67.581\left(\frac{a_j}{B_j}\right)-4.5513 \\ B_{1,j}=-1201.1\left(\frac{a_j}{B_j}\right)^3+925.17\left(\frac{a_j}{B_j}\right)^2-235.05\left(\frac{a_j}{B_j}\right)+19.623 \\ B_{2,j}=1338.3\left(\frac{a_j}{B_j}\right)^3-1039.6\left(\frac{a_j}{B_j}\right)^2+268.08\left(\frac{a_j}{B_j}\right)-23.062 \\ B_{3,j}=-492.8\left(\frac{a_j}{B_j}\right)^3+386.96\left(\frac{a_j}{B_j}\right)^2-100.68\left(\frac{a_j}{B_j}\right)+8.9951 \end{cases} for\ \frac{a_j}{B_j}<0.3$$

$$\begin{cases} B_{0,j}=-1.5482\left(\frac{a_j}{B_j}\right)+1.2866 \\ B_{1,j}=1.72\left(\frac{a_j}{B_j}\right)^2-0.3642\left(\frac{a_j}{B_j}\right)-0.1123 \\ B_{2,j}=-13.546\left(\frac{a_j}{B_j}\right)^3+9.812\left(\frac{a_j}{B_j}\right)^2-2.0921\left(\frac{a_j}{B_j}\right)+0.0542 \\ B_{3,j}=10.501\left(\frac{a_j}{B_j}\right)^3-7.0809\left(\frac{a_j}{B_j}\right)^2+1.8924\left(\frac{a_j}{B_j}\right)+0.0941 \end{cases} for\ 0.3\le\frac{a_j}{B_j}\le 0.85$$

a_i and a_j are the sizes of the shorter and longer cracks respectively

B_j is width of plate where the longer crack is embedded

b) Cracks with an elliptical opening

As the responses of the symmetric corner crack tips in an L-shaped plate are expressed by those of single edge crack tips in a finite width plate, the effect of elliptical opening in an L-shaped plate with symmetric cracks is compared with that of the same elliptical opening in a flat plate through a set of FE analyses.

The geometry information of two models is shown in Figure 4-51 and the comparison is made in Figure 4-52 in terms of correction factor for an elliptical opening, which is calculated by dividing the calculated SIF values from FE analysis by the SIF values of a single edge crack case. As in the case of the L-shaped plate without openings, the response of the symmetric cracks emanating from the edge of an elliptical opening in an L-shaped plate is identified to be same as that of a finite flat plate case.

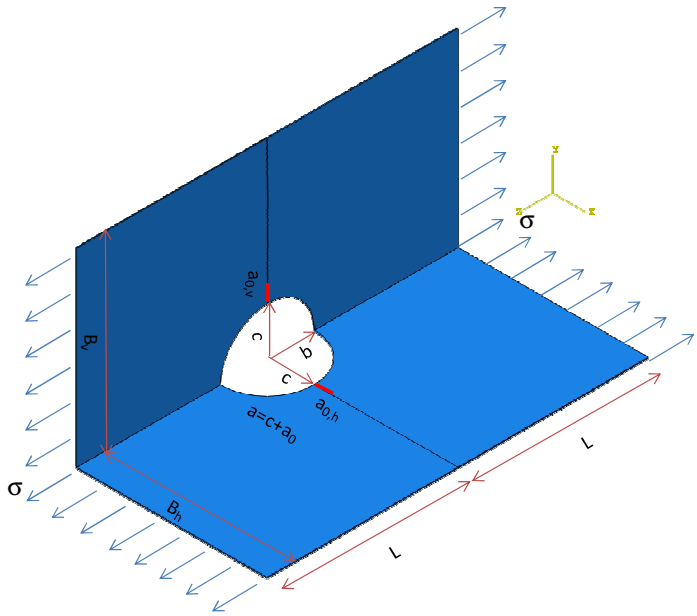

Parameters		Unit
B_v & B_h	2.0	m
L	2.0	m
b	0.25, 0.5, 1.0	m
c	0.5	m
$a_{0,v}$ & $a_{0,h}$*	0.05~0.7	m
E	210	GPa
σ	1.0	MPa

* flat plate case includes a_0 = 0.025 m

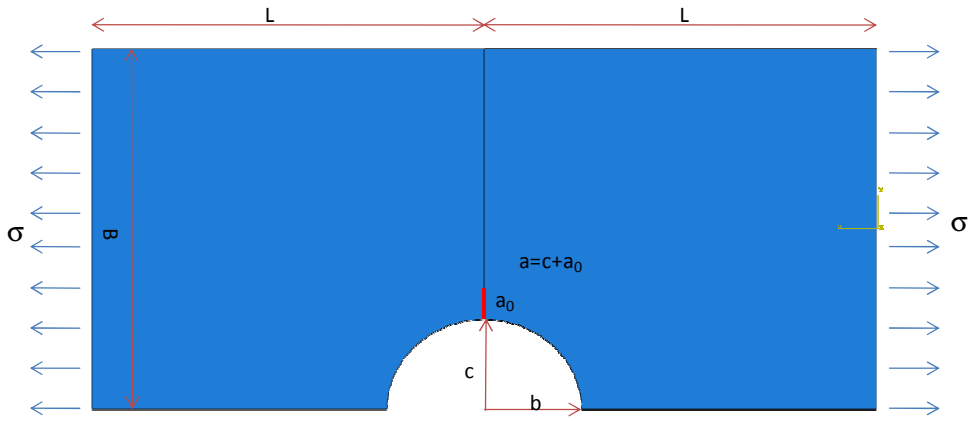

Figure 4-51: Configurations of elliptical openings in an L-shaped plate and in a finite flat plate

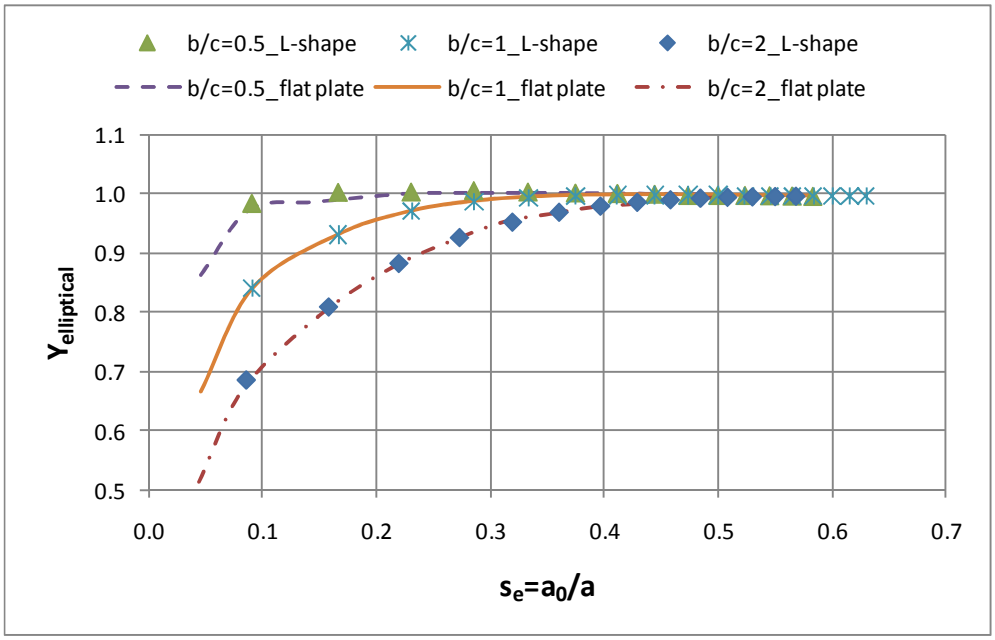

Figure 4-52: Comparison of correction factors for elliptical opening between in an L-shaped plate with symmetric cracks and in a flat plate

Therefore, it is reasonable to use a finite flat plate with a single edge crack emanating from an elliptical opening for analysing the response of symmetric cracks due to an elliptical opening in an L-shaped plate. To obtain an empirical formula, the same approach which is used in investigating the correction factor for elliptical openings in a finite plate is adopted.

The SIF of the single edge crack emanating from an elliptical opening in a finite width plate is expressed with the corresponding correction factor of Equation (4-48), which is written again as Equation (4-49) by decomposing the correction factor into two correction factors.

$$SIF_{elliptical,edge,finite\ width} = \sigma\sqrt{\pi a} \times Y_{elliptical,edge,finite\ width} \quad \textbf{(4-48)}$$

$$SIF_{elliptical,edge,finite\ width} = \sigma\sqrt{\pi a} \times Y_{edge,finite\ width} \times Y_{elliptical\ |\ edge,finite\ width} \quad \textbf{(4-49)}$$

where, $Y_{edge,\ finite\ width}$ is the correction factor for edge crack in a finite width plate as expressed in Equation (4-45)

From a series of FE analyses that take into account various configurations of elliptical openings and crack sizes (Figure 4-53), a set of correction factors for

elliptical openings in a finite width plate with a single edge crack are obtained as shown in Figure 4-54.

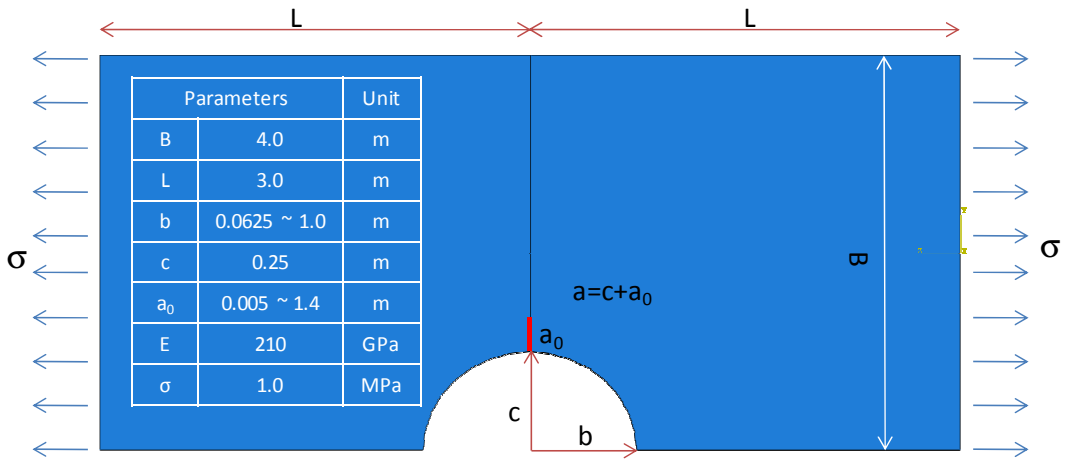

Figure 4-53: Configuration of an elliptical opening in a finite plate with an edge crack for FE analysis

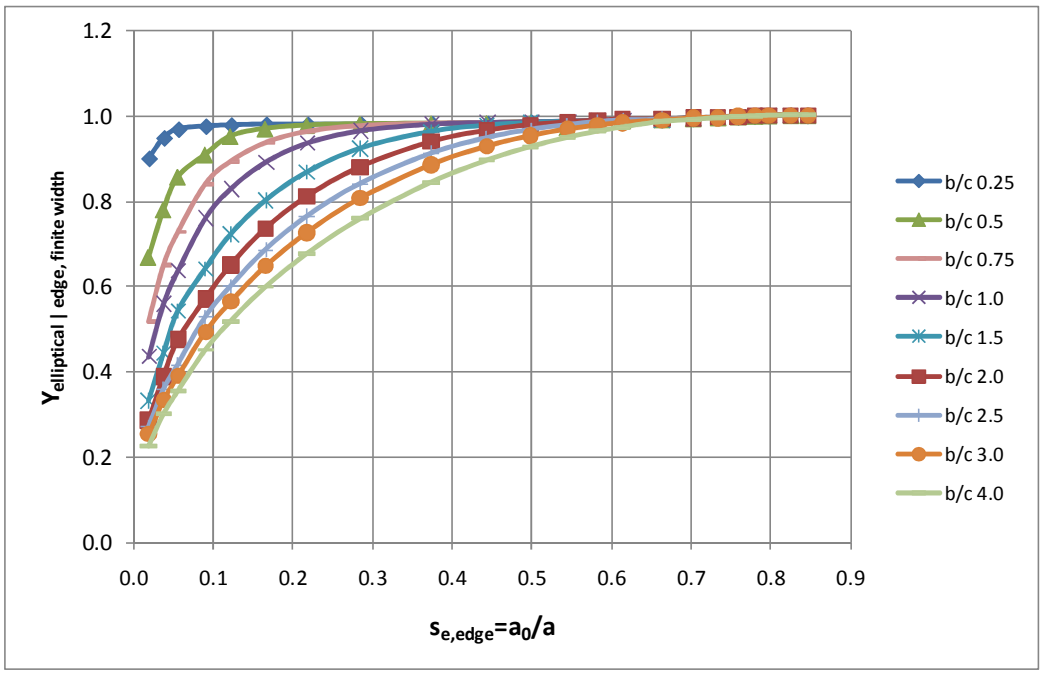

Figure 4-54: Correction factors for elliptical openings in a finite flat plate with an edge crack, results of FE analysis

Based on the expression of the correction factor for symmetric cracks emanating from an elliptical opening in a finite plate, the empirical formula for the current correction factor is obtained by Equation (4-50):

$$Y_{elliptical\,|\,edge,finite\,width} = \begin{cases} {Y_{e,edge,1}}\Big/{s_{e,edge}{}^{\left(\frac{b}{c}\right)}}, for\ s_{e,edge} < 0.8 \\ 1.0 \qquad\qquad\qquad\quad , for\ s_{e,edge} \geq 0.8 \end{cases} \tag{4-50}$$

where, $Y_{e,edge,1} = 1 - exp[-exp\{C_0 + C_1 X' + C_2 X'^2 + C_3 X'^3\}]$

$$X' = ln\,(s_{e,edge})$$

$$s_{e,edge} = a_0/a = a_0/(c + a_0)$$

$$\begin{cases} C_0 = -0.0026\left(\frac{b}{c}\right)^3 + 0.0326\left(\frac{b}{c}\right)^2 - 0.2053\left(\frac{b}{c}\right) + 0.7585 \\ C_1 = 1.349 \times \left(\frac{b}{c}\right)^{0.8574} \\ C_2 = C_3 = 0 \end{cases} \quad for\ s_{e,edge}{}^{\left(\frac{b}{c}\right)} < 1 - exp\,(-1)$$

$$\begin{cases} C_0 = -0.1688\left(\frac{b}{c}\right)^3 + 0.4396\left(\frac{b}{c}\right)^2 - 0.6476\left(\frac{b}{c}\right) + 1.5942 \\ C_1 = -0.6173\left(\frac{b}{c}\right)^3 - 0.701\left(\frac{b}{c}\right)^2 + 4.6115\left(\frac{b}{c}\right) + 0.857 \\ C_2 = -6.1284\left(\frac{b}{c}\right)^3 + 9.4447\left(\frac{b}{c}\right)^2 + 0.5573\left(\frac{b}{c}\right) + 0.497 \\ C_3 = -9.5623\left(\frac{b}{c}\right)^3 + 17.929\left(\frac{b}{c}\right)^2 - 6.8161\left(\frac{b}{c}\right) + 1.0128 \end{cases} \quad for\ s_{e,edge}{}^{\left(\frac{b}{c}\right)} \geq 1 - exp\,(-1)$$

b is radius of elliptical opening in the direction perpendicular to crack

c is radius of elliptical opening in the direction parallel to crack

a_0 is the initial crack size

It should be noted that the above equation is valid only for $0.25 \leq b/c \leq 4.0$ as the FE analysis results are provided within these bounds.

The effect of the asymmetric cracks can be included in the estimation of SIFs of cracks emanating from the edges of an elliptical opening by adopting the correction factor expressed in Equation (4-46) and (4-47).

4.5 Chapter summary

This chapter adds details on the development of the model of crack growth. Unlike general cracks from welds, crack propagation from accidental damages could experience slow, medium and accelerated crack growth rates depending on the initial

damage size and the environmental conditions. To cover the whole regions of the crack growth rates (i.e. SIFs), the crack growth model proposed by McEvily and Groeger (1977) is modified to take into account the effect of stress ratio.

Also, the establishment of the method to determine the SIFs based on the first-principles methodology using the FE analysis deployed by VCCT for ABAQUS is elaborated in this chapter. Although it is proved as an accurate and relatively fast FE method that supports complex structures such as the ship hull, the need for an alternative approach using parametric models is found necessary. Contributing factor to this are the requirement to provide results in a rapid and accurate way in the course of the decision-making process in an emergency operation and in the early ship design stage, where informed decisions are of critical importance.

In light of these, a set of knowledge-intensive models for determining SIFs have been proposed. The main concept on which they are based is the combination of individual effects of geometries and loadings towards the total effect of a complex configuration of ship hull structure. A couple of dimensionless correction factors are employed by empirical solutions from the literature and determined based on a series of FE analyses. More research is needed in obtaining correction factors for other geometric effects of hull structures so that the knowledge-intensive models can be deployed with an extended coverage.

5 RESIDUAL STRENGTH

5.1 Preamble

This chapter elaborates on the development of the parametric model for determining the residual strength capacity of the damaged hull girder. The method is based on the ultimate bending moment capacity assessment and includes details pertaining to the modelling of the damaged section and the failure modes leading to global collapse. This chapter concludes with the validation of the developed model using experimental data and information from the literature.

5.2 Method adopted

Various methods to determine the ultimate strength and the residual strength of structures have been proposed and developed as discussed in Chapter 2. These methods can be broadly categorized into analytical and numerical. The analytical approaches include methods based on the elastic section modulus, e.g. Vasta (1958), the fully plastic moment, e.g. Caldwell (1965) and its modifications e.g. Paik and Mansour (1995) by use of ultimate stress. Also, the beam-column method that has been proposed by Smith (1977) belongs to this category. The numerical approaches consist of detailed and simplified FEA like the ISUM proposed by Ueda and Rashed (1984). Generally speaking, both of approaches have advantages and disadvantages in terms of accuracy and cost. That is, analytical approaches are easy to use and they can be implemented fast but show relatively less accuracy. On the other hand, numerical approaches give relatively accurate results but require much time to prepare the model and to run the analysis.

Considering that the residual strength assessment should be fast, accurate and easily linked to the crack propagation model, the analytical approach will be pursued. Among the available methods the beam-column is selected for the purposes of this research as it provides more accurate and realistic results in comparison to the rest of the analytical methods by including post-buckling behaviour of individual components as discussed by Wang, X. et al. (2008), Gordo and Soares (2000, 2009), and Ozguc, Das and Barltrop (2005).

The post-damage residual strength assessment of a ship is based on a moment-curvature relationship for stiffened panels. The general approach of calculating the

moment curvature of the hull girder from the contribution of each element is similar to the ones adopted by Smith (1977), Dow, Hugill, Clark and Smith (1981), Rutherford and Caldwell (1990), Gordo, Soares and Faulkner (1996), etc., and proposed by IACS (2008, 2009).

The basic assumptions of the method are listed below:

- The damaged parts, e.g. plates and stiffeners, of the affected cross section are unable to carry any load imposed on them.
- The cross section is comprised of elements, which are composed of longitudinal stiffener and relevant effective breadth of plate, and they are considered to behave independently.
- The ship cross section is plane and remains plane when curvature increases.
- The transverse frames are sufficiently strong to avert overall grillage collapse of the deck and bottom structures.
- The ultimate bending moment capacity is calculated at a cross section between two adjacent web frames.
- The hull material has non-linear elasto-plastic behaviour.
- Each failure mode is independent hence, the lowest stress among the values obtained from each failure mode governs the failure of each element.

The most general case corresponds to accidentally damage events in which the ship heels and experiences curvature in the *y*- and *z*-directions, denoted as $\kappa_{y,i}$ and $\kappa_{z,i}$ respectively; the *i*-th overall combined curvature, κ_i, is related to these two components and their relationship is expressed by Equation (5-1) in a right-hand coordinate system.

$$\kappa_i = \sqrt{{\kappa_{y,i}}^2 + {\kappa_{z,i}}^2} \; or \; \begin{cases} \kappa_{y,i} = \kappa_i \cdot cos\,\theta \\ \kappa_{z,i} = \kappa_i \cdot sin\,\theta \end{cases} \quad \textbf{(5-1)}$$

where, θ is the angle between the neutral axis and the horizontal *y*-axis.

The average strain of the *j*-th element (stiffener and associated effective plate), ε_{ij}, under the *i*-th curvature, κ_i, is obtained by Equation (5-2) with its induced position.

$$\varepsilon_{ij} = z_{g,ij} \cdot \kappa_{y,i} - y_{g,ij} \cdot \kappa_{z,i} = \kappa_i \cdot (z_{g,ij} \cdot cos\,\theta - y_{g,ij} \cdot sin\,\theta) \quad \textbf{(5-2)}$$

where, $y_{g,ij}$ and $z_{g,ij}$ are horizontal and vertical distance from the instantaneous geometrical centre of gravity (CG) of the section under i-th curvature to the centre of the j-th element respectively.

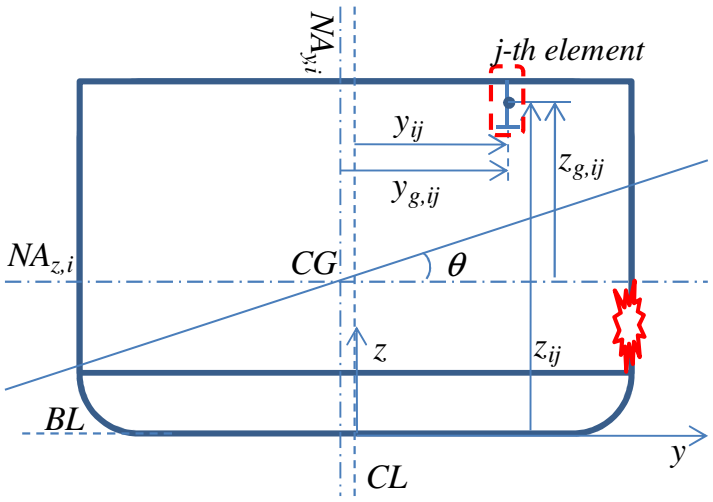

Figure 5-1: Coordinate and definition of variables

When the average strain of each element is determined, the average stress is calculated from the corresponding load-end shortening curve of each element and consequently the bending moment sustained by each element given a curvature are calculated by Equation (5-3).

$$\begin{cases} M_{y,ij} = z_{g,ij} \cdot \Phi(\overline{\varepsilon_{ij}}) \cdot \sigma_y \cdot A_j \\ M_{z,ij} = y_{g,ij} \cdot \Phi(\overline{\varepsilon_{ij}}) \cdot \sigma_y \cdot A_j \end{cases} \quad \textbf{(5-3)}$$

where, $M_{y,ij}$ and $M_{z,ij}$ are vertical and horizontal bending moment on j-th element under i-th curvature

$y_{g,ij}$ and $z_{g,ij}$ are horizontal and vertical distance from the instantaneous centre of gravity (CG) of the section to the centre of the j-th element

$\Phi(\overline{\varepsilon_{ij}})$ is the average normal stress of j-th element under i-th curvature normalised by yield stress, σ_y, at a normalised average strain of $\overline{\varepsilon_{ij}}$

$\overline{\varepsilon_{ij}}$ is the average strain of j-th element under i-th curvature normalised by yield strain, ε_y

A_j is the sectional area of j-th element

The moment components sustained by the whole section are obtained by summing up the moment of each element and the total bending moment is obtained by Equation (5-4) for the given curvature. The ultimate residual hull girder bending moment capacity is the maximum value of the bending moment curve against various curvatures of the damaged cross section.

$$M_i = \sqrt{{M_{y,i}}^2 + {M_{z,i}}^2} \quad \textbf{(5-4)}$$

where, $M_{y,i}$ is the total vertical BM on the whole section under i-th curvature,

$M_{y,i} = \sum_j M_{y,ij}$

$M_{z,i}$ is the total horizontal BM on the whole section under i-th curvature,

$M_{z,i} = \sum_j M_{z,ij}$

During the calculation, it is important to use the instantaneous CG of the cross section because it is necessary to adjust it to achieve axial force equilibrium on it as curvature changes. The force in each structural element is obtained from its area multiplied by the average stress induced on it and the total axial force (Equation (5-5)) on the cross section is derived by summing these forces for each element.

$$F_i = \sum_j \Phi(\overline{\varepsilon_{ij}}) \cdot \sigma_y \cdot A_j \quad \textbf{(5-5)}$$

For each imposed curvature, adjustment of CG should take place in order to reach force equilibrium in the cross section. Rutheford & Caldwell (1990) suggested that the shift of CG, ΔCG, could be taken equal to:

$$\Delta CG_i = \frac{\sum_j (A_j \cdot \sigma_{ij})}{\kappa_i \cdot \sum_j (A_j \cdot E_j)} \quad \textbf{(5-6)}$$

where, σ_{ij} is the average stress of the j-th element under i-th curvature, κ_i

E_j is the Young's modulus of the j-th element

This requires a number of iterations until the required shift of CG is equal or less than a sufficient low value, which is chosen to be 1.0e-5 mm in this analysis.

5.3 Procedure

The method adopted in this work is based on the moment-curvature curves, which is obtained by means of an incremental iterative approach. The detailed steps of the incremental iterative approach required in the procedure are explained below and a flow chart is presented in Figure 5-3.

- Define the damaged part of the concerned transverse section.
- Divide the damaged hull girder transverse section into structural elements, i.e. longitudinal stiffened panels and hard corners (details on these are covered in the Section 5.4).
- Derive the load-end shortening curves (stress-strain curves) for all the structural elements according to failure modes (Section 5.5).
- Estimate the maximum required curvature, κ_{max}, using the maximum yield bending moment. The recommended value from IACS (2008) is:

  $$\kappa_{max} = 3 \times \frac{BM_y}{EI}$$

  where, $BM_y = max\ (Z_{dk} \cdot \sigma_y, Z_{btm} \cdot \sigma_y)$

  Z_{dk}, Z_{btm} are section modulus at deck and bottom respectively

  σ_y is the minimum yield stress of the material

  E is the Young's modulus

  I is the hull girder moment of inertia
- Define the curvature step size $\Delta\kappa$ and set the starting curvature, κ_1 is to be taken as $-\kappa_{max}$ which is the maximum value of the sagging condition.
- Derive the initial centre of gravity CG_i for the first incremental step of curvature, κ_i, with the value of hull girder moment of inertia.
- For each structural element with index j, calculate the axial strain ε_{ij} corresponding to the imposed curvature, κ_i, using the Equation (5-2).
- Calculate the corresponding axial stress σ_{ij} of each element according to the defined load-end shortening curves.
- Calculate the total axial force on the cross section using Equation (5-5) and determine the new position of the centre of gravity by shifting it according to Equation (5-6) until the force equilibrium is satisfied (iteration is required). In

this analysis the equilibrium is satisfied when the change in the centre of gravity is less than 1.0e-5 mm.

- When the force equilibrium is satisfied, calculate the total bending moment of the cross section by summing up the bending moment contributions of all elements using the Equations of (5-3) and (5-4).
- Increase the curvature by $\Delta\kappa$ and use the current centre of gravity position as the initial value for the next curvature increment. Then repeat from the calculation of the strain, ε_{ij}, corresponding to the current curvature until the maximum required curvature, κ_{max}, is reached.
- When the curve of moment-curvature is completed, the ultimate bending moment capacity of the damaged section in sagging and hogging is the peak value of the curve in sagging and hogging condition respectively (Figure 5-2).
- If the peak does not occur in the moment-curvature curve, increase the maximum required curvature κ_{max} until the peak is reached in both of sagging and hogging conditions.

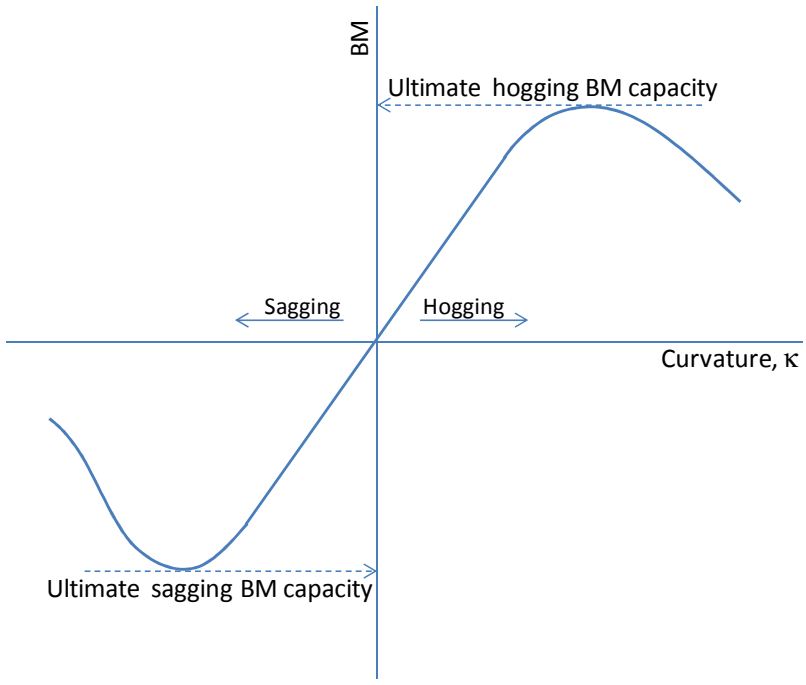

Figure 5-2: An example of moment-curvature curve and ultimate bending moment capacity

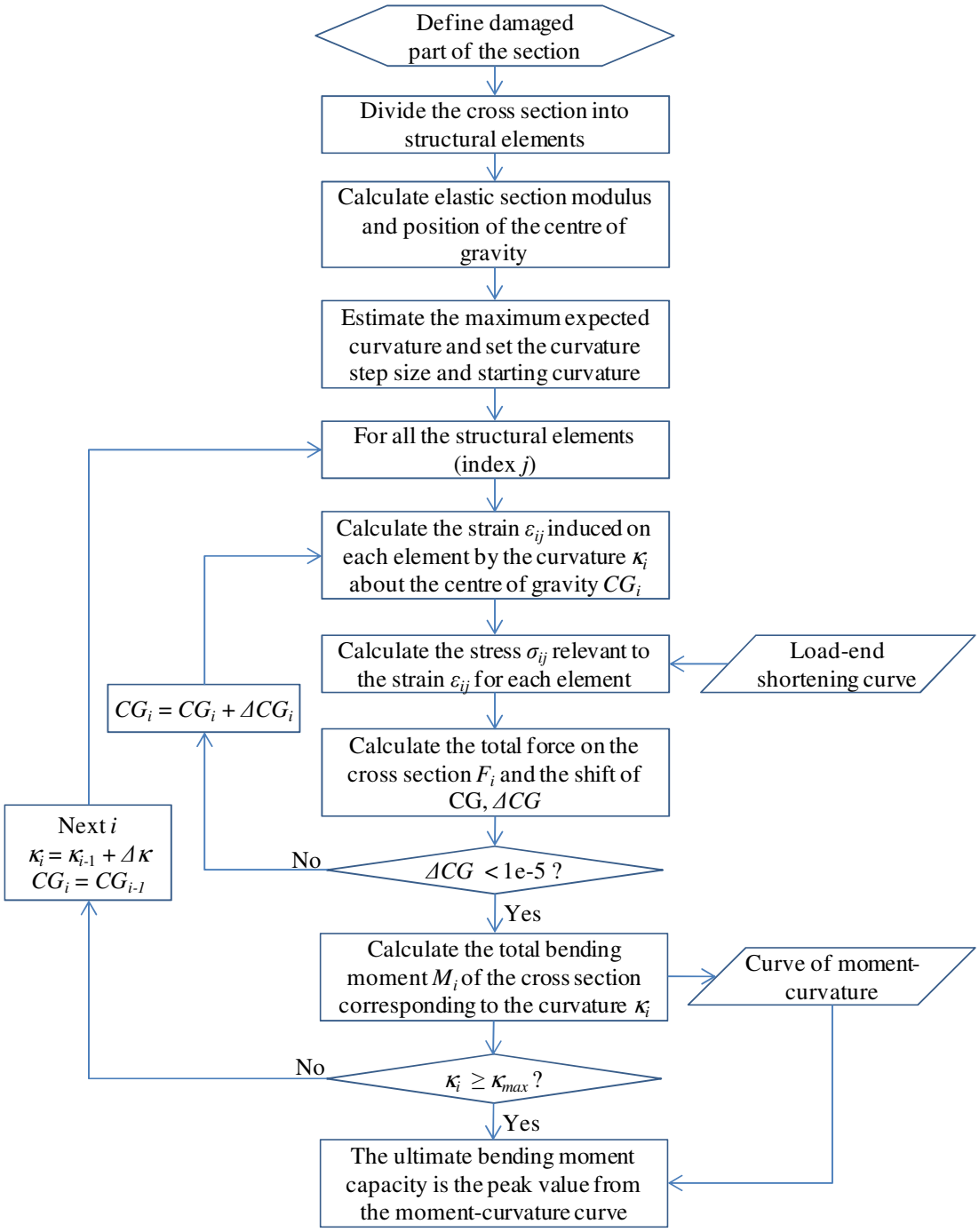

Figure 5-3: Flow chart of the procedure for determining the ultimate BM capacity

5.4 Modelling of the hull girder damaged section

In applying the procedure explained above, the damaged hull girder cross section needs to be divided into structural elements, the types of which are listed and explained next.

Longitudinal stiffener element

In the longitudinally stiffened system, the stiffener constitutes a longitudinal stiffener element together with the attached plate. The attached plate width is defined as i) equal to the mean spacing of the longitudinal stiffeners, when the panels on both sides of the stiffener are longitudinally stiffened, or ii) equal to the width of the longitudinally stiffened panel, when the panel on one side of the stiffener is longitudinally stiffened and the other panel is of the transversely stiffened.

Stiffened plate element

The transversely stiffened panel, the plate between longitudinal stiffener elements, between a longitudinal stiffener element and a hard corner element or between hard corner elements is to be treated as a stiffened plate element.

Hard corner element

In the transverse section, the hard corner element is defined in the areas of the plating adjacent to intersecting plates, the plate area adjacent to knuckles in the plating with an angle greater than 30 degrees, and the plating comprising rounded gunwales. The extent of a hard corner element is considered to be half of the stiffener spacing from the intersection for longitudinally stiffened plates and equal to 20 times of the plate thickness from the plate intersection for transversely stiffened plates, IACS (2008).

Some examples of modelling hull cross sections are illustrated in Figure 5-4 and Figure 5-5 for typical double hull tankers and typical bulk carriers respectively. The former mostly consists of longitudinal stiffener elements and hard corner elements. The latter is made up of both types of elements as well as stiffened plate elements.

In case that the attached plating is made of steels having different thicknesses and/or yield stresses, average values based on each portion are used for the calculation.

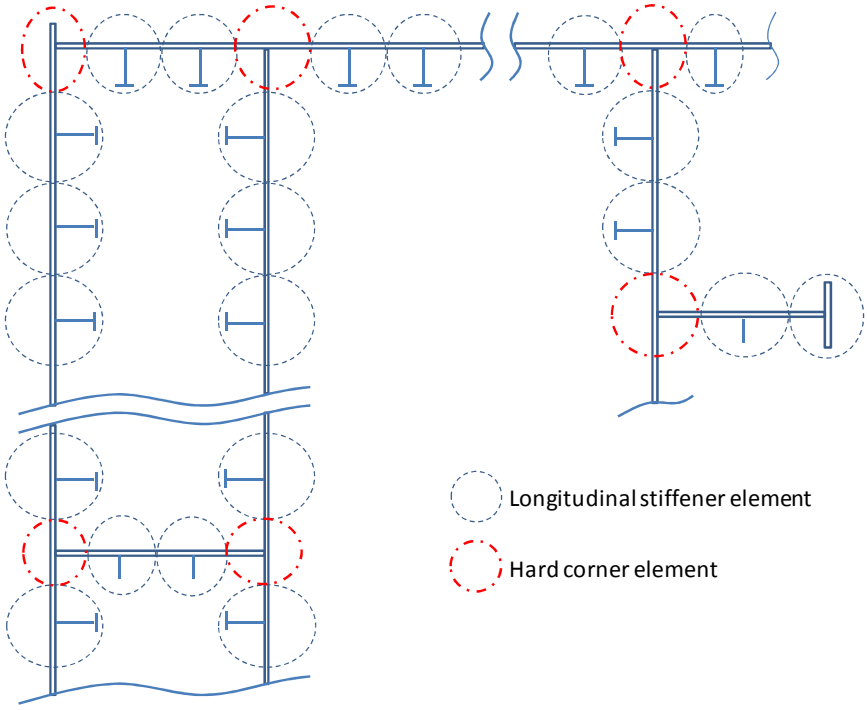

Figure 5-4: Example of defining structural elements for a typical double hull tanker section

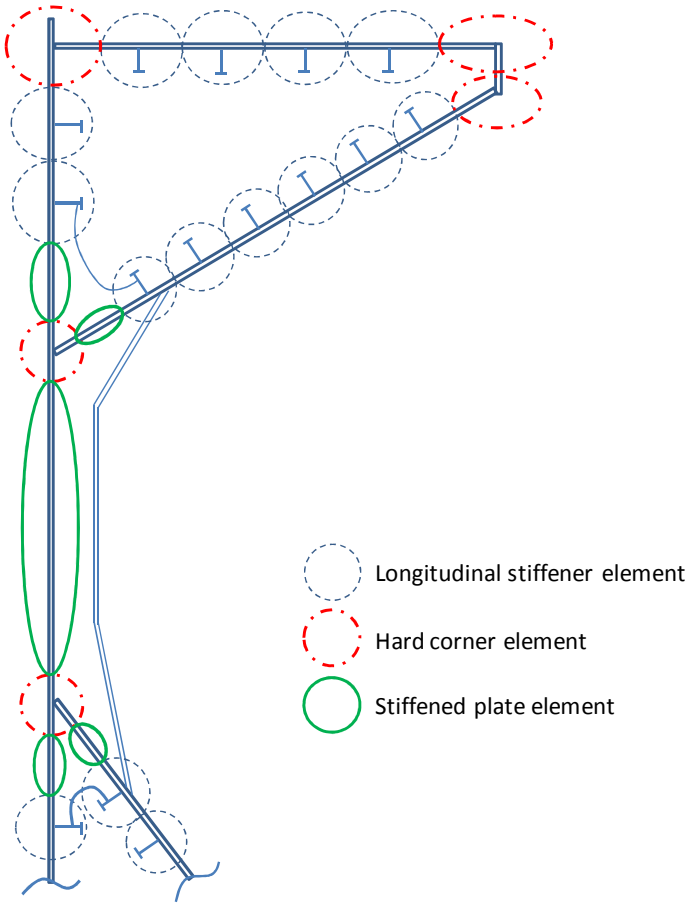

Figure 5-5: Example of defining structural elements for a typical bulk carrier section

5.5 Failure modes and load-end shortening curves

The structural elements described in the previous section will fail according to one of the failure modes tabulated in Table 5-1 depending on the type of loading, the type of element, and the geometry and mechanical properties of the element. Some typical failure modes of stiffened panels are illustrated in Figure 5-6.

Table 5-1: Failure modes of structural elements

Element type	Loading direction	Failure modes
Longitudinal stiffener element	Tension	Elastic-perfectly plastic failure
	Compression	Beam column buckling Torsional buckling (Tripping of stiffener) Web local buckling of stiffener
Hard corner element	Tension	Elastic-perfectly plastic failure
	Compression	Elastic-perfectly plastic failure
Stiffened plate element	Tension	Elastic-perfectly plastic failure
	Compression	Plate buckling

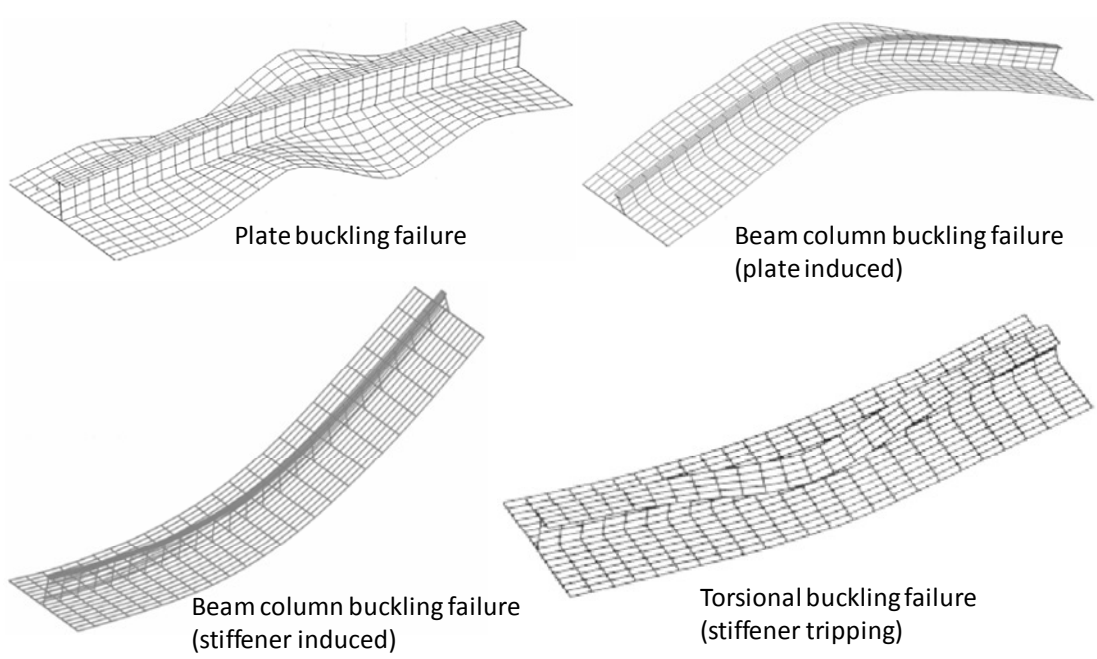

Figure 5-6: Typical failure modes of stiffened panels, Wang, Grondin and Elwi (2006)

Each of the failure modes is defined by a load-end shortening curve that relates the (normalised) stress of an element with the (normalised) strain of it. In this analysis, the load-end shortening curves of elements are obtained from direct formulation that has been adopted in the common structural rules for oil tankers and bulk carriers based on elasto-plastic behaviour of materials, IACS (2008, 2009).

In the following sections the load-end shortening curve of each failure mode is described. It should be noted that the positive value of strain means compression of the elements.

5.5.1 Elastic-perfectly plastic failure

This mode of failure involves material yielding and is applied to tensile strain of all types of elements as well as compressive strain of hard corner element type. As the load-end shortening curve follows an elastic, perfectly plastic material behaviour, the equation of the stress-strain curve is obtained as the edge stress ratio, Φ_e, with the normalised forms of both stress and strain.

$$\Phi_e = \begin{cases} -1\,, & for\ \bar{\varepsilon} < -1 \\ \bar{\varepsilon}\,, & for\ -1 \le \bar{\varepsilon} \le 1 \\ 1\,, & for\ \bar{\varepsilon} > 1 \end{cases} \quad \textbf{(5-7)}$$

where, $\bar{\varepsilon}$ is the average strain ratio, $\bar{\varepsilon} = \varepsilon/\varepsilon_y$

ε and ε_y are element strain and yield strain, respectively, $\varepsilon_y = \frac{\sigma_y}{E}$

σ_y and E are yield stress of the element and the Young's modulus of the material

5.5.2 Beam column buckling

The overall buckling failure of beam column entails simultaneous buckling of the stiffener and the attached plate and it is attributed mainly to the excessive slenderness of the beam column. According to the initial shape of deformation and the type of loading, this failure mechanism is divided into the plate induced- and the stiffener induced- beam column buckling (Figure 5-6). However, in a continuous panel, it is usual that the buckling failure is towards the plate in one span and towards the stiffeners in the adjacent span.

The buckling of beam column in this research follows the proposal of Faulkner, Adamchak, Snyder and Vetter (1973), which is based on the Johnson-Ostenfeld formulation, where inelastic effects of beam column buckling are accounted for. The maximum edge stress that a beam column can sustain is related to the yield stress defined by the Johnson-Ostenfeld approach but the reduction of the tangent modulus in a bending situation should be considered in calculation of the flexural buckling rigidity of the beam column. The load-end shortening curve for the beam column buckling, $\Phi_{cb}(\bar{\varepsilon})$, is expressed in Equation (5-8) including buckling inelastic effect:

$$\Phi_{cb}(\bar{\varepsilon}) = \Phi_{JO}(\bar{\varepsilon}) \cdot \frac{A_s + \Phi_w \cdot b_p \cdot t_p}{A_s + b_p \cdot t_p} \quad \textbf{(5-8)}$$

where, $\Phi_{JO}(\bar{\varepsilon})$ is the Johnson-Ostenfeld stress ratio

$$\Phi_{JO}(\bar{\varepsilon}) = \begin{cases} \left(1 - \frac{1}{4 \cdot \Phi_{EC}(\bar{\varepsilon})}\right) \cdot \Phi_e \,, & for\ \Phi_{EC}(\bar{\varepsilon}) \geq 0.5 \\ \Phi_{EC}(\bar{\varepsilon}) \cdot \Phi_e \,, & for\ \Phi_{EC}(\bar{\varepsilon}) < 0.5 \end{cases}$$

$\Phi_{EC}(\bar{\varepsilon})$ is the Euler column buckling stress ratio, $\Phi_{EC}(\bar{\varepsilon}) = \frac{\left(\frac{\pi}{\lambda}\right)^2}{\bar{\varepsilon}}$

λ is the slenderness of the column, $\lambda = (l/r_{ce}) \cdot \sqrt{\varepsilon_y}$

l is the span of the element

r_{ce} is the equivalent radius of inertia, $r_{ce} = \sqrt{I_{ce}/\left(A_s + b_e{}' \cdot t_p\right)}$

I_{ce} is the moment of inertia of the element

A_s is the area of stiffener

b_e' is the tangent effective width of the plate, $b_e{}' = \frac{b_p}{\beta_p} \cdot \sqrt{\frac{\sigma_y}{\sigma_e}} = \frac{b_p}{\beta_p} \cdot \sqrt{\Phi_e{}^{-1}}$

b_p and t_p are width and thickness of the plate, respectively

β_p is the plate slenderness, $\beta_p = \begin{cases} \frac{b_p}{t_p} \cdot \sqrt{\varepsilon} \,, & for\ \varepsilon \geq 0 \\ NA \,, & otherwise \end{cases}$

Φ_e is the edge stress ratio shown in Equation (5-7)

Φ_w is the ratio of the effective plate width

$$\Phi_w = \begin{cases} \frac{2}{\beta_p} - \frac{1}{{\beta_p}^2} & ,for\ \beta_p > 1.0 \\ 1 & ,for\ \beta_p \leq 1.0 \end{cases} \quad \textbf{(5-9)}$$

The load-end shortening curve for the beam column buckling failure, Φ_{cb}, is shown in Figure 5-7 with edge stress ratio, Φ_e and the Johnson-Ostenfeld stress ratio, Φ_{JO}.

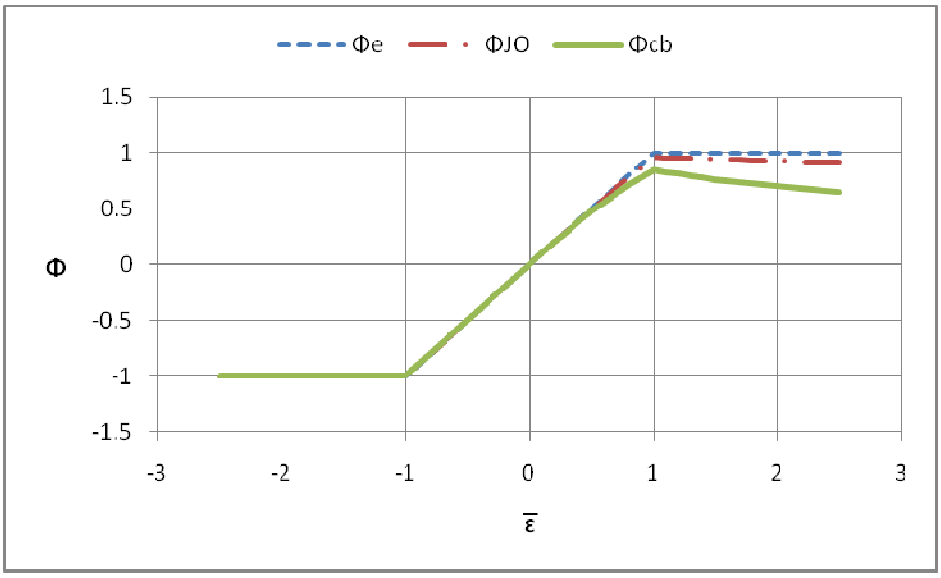

Figure 5-7: An example of load-end shortening curve for the beam column buckling failure and other stress ratios, positive Φ means compression

5.5.3 Torsional buckling

The torsional buckling or tripping failure of stiffeners is the rotation of the stiffener about the stiffener-to-plate joint. Usually, it is attributed to the lack of torsional rigidity of the stiffener. This is known to be the most dangerous failure of stiffened panels as it results in a rapid decrease of load carrying capacity of an element, Gordo and Soares (1993). In this research, the load-end shortening curve of the stiffened panel with different types of profile is obtained by Equation (5-10).

$$\Phi_{tc}(\bar{\varepsilon}) = \Phi_e \cdot \frac{\Phi_{cr} \cdot A_s + \Phi_w \cdot b_p \cdot t_p}{A_s + b_p \cdot t_p} \quad \textbf{(5-10)}$$

where, Φ_e is the edge stress ratio shown in Equation (5-7)

Φ_w is the ratio of the effective plate width shown in Equation (5-9)

Φ_{cr} is the critical stress ratio of stiffener, $\Phi_{cr} = \begin{cases} 1 - \frac{1}{4\Phi_{ET}} & ,for\ \Phi_{ET} \geq 0.5 \\ \Phi_{ET} & ,for\ 0 < \Phi_{ET} < 0.5 \\ 1.0 & ,for\ \Phi_{ET} \leq 0 \end{cases}$

Φ_{ET} is the Euler torsional buckling stress ratio, $\Phi_{ET} = \frac{\sigma_{ET}}{E \cdot \varepsilon} = \frac{\sigma_{ET}}{\sigma_o \cdot \bar{\varepsilon}}$

σ_{ET} is Euler torsional buckling stress, $\sigma_{ET} = \frac{E}{I_P} \cdot \left(\frac{\epsilon_{dof} \cdot \pi^2 \cdot I_\omega}{a^2} + 0.385 \cdot I_T \right)$

ϵ_{dof} is degree of fixation, $\epsilon_{dof} = 1 + \sqrt{\frac{l^4}{\frac{3}{4} \cdot \pi^4 \cdot I_\omega \left(\frac{b_p}{{t_p}^3} + \frac{4 d_w}{3 {t_w}^3} \right)}}$

I_P is polar moment of inertia of the stiffener

$$I_P = \begin{cases} \frac{{d_w}^3 \cdot t_w}{3} & ,for\ flat\ bar \\ \frac{{d_w}^3 \cdot t_w}{3} + (b_f \cdot t_f) \left(d_w + \frac{t_f}{2} \right)^2 & ,for\ angle\ and\ T-section \end{cases}$$

I_T is St. Venant's moment of inertia of the stiffener

$$I_T = \begin{cases} \frac{d_w \cdot {t_w}^3}{3} \left(1 - 0.63 \frac{t_w}{d_w} \right) & ,for\ flat\ bar \\ \frac{d_w \cdot {t_w}^3}{3} \left(1 - 0.63 \frac{t_w}{d_w} \right) + \frac{b_f \cdot {t_f}^3}{3} \left(1 - 0.63 \frac{t_f}{b_f} \right) & ,for\ angle, T-section \end{cases}$$

I_ω is sectorial moment of inertia of the stiffener

$$I_\omega = \begin{cases} \frac{(d_w \cdot t_w)^3}{36} & ,for\ flat\ bar \\ \frac{{b_f}^3 \cdot t_f \cdot \left(d_w + \frac{t_f}{2} \right)^2}{12} \cdot \left(\frac{b_f \cdot t_f + 2.6 d_w \cdot t_w}{A_s} \right) & ,for\ angle \\ \frac{{b_f}^3 \cdot t_f \cdot \left(d_w + \frac{t_f}{2} \right)^2}{12} & ,for\ T-section \end{cases}$$

A_s is the area of stiffener, $A_s = d_w \cdot t_w + b_f \cdot t_f$

b_f and t_f are width and thickness of the flange

d_w and t_w are depth and thickness of web

b_p and t_p are width and thickness of the plate, respectively

$\bar{\varepsilon}$ is the average strain ratio, $\bar{\varepsilon} = \varepsilon/\varepsilon_y$

ε and ε_y are element strain and yield strain, respectively, $\varepsilon_y = \frac{\sigma_y}{E}$

σ_y and E are yield stress of the element and Young's modulus of material

l is the span of the stiffener

The load-end shortening curves for the tripping failure of the T-section stiffener and flat bar are shown in Figure 5-8.

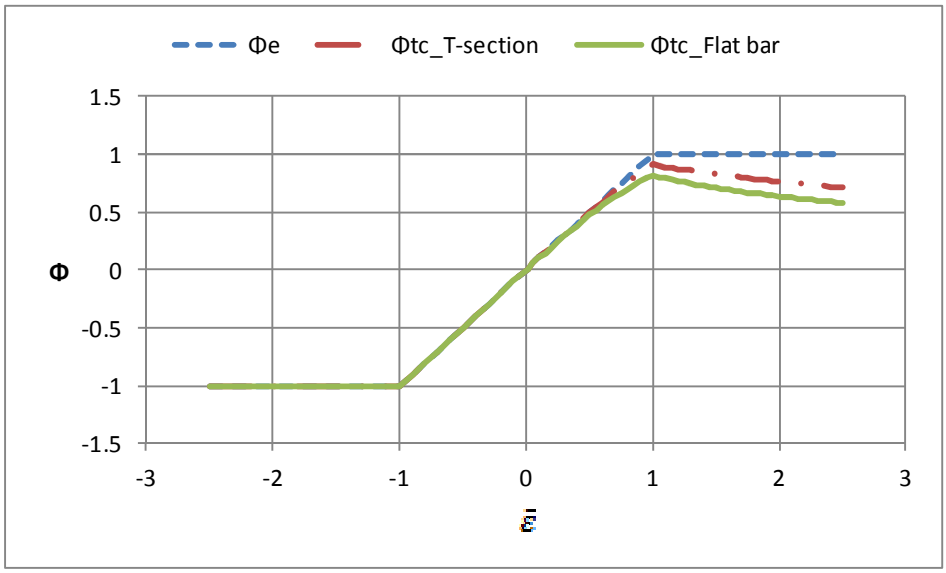

Figure 5-8: An example of load-end shortening curve for torsional buckling of stiffeners, positive *Φ* means compression

5.5.4 Web local buckling

The local buckling of web of stiffeners is determined for different types of stiffeners. The load-end shortening curve of stiffeners with flanged profiles including web local buckling is obtained by Equation (5-11).

$$\Phi_{wb} = \begin{cases} \Phi_e \cdot \dfrac{\Phi_{dw} \cdot d_w \cdot t_w + b_f \cdot t_f + \Phi_w \cdot b_p \cdot t_p}{A_s + b_p \cdot t_p} & ,for\ flanged\ profiles \\ \Phi_e \cdot \dfrac{\Phi_{cw} \cdot A_s + \Phi_w \cdot b_p \cdot t_p}{A_s + b_p \cdot t_p} & ,for\ flat\ bar \end{cases} \quad \textbf{(5-11)}$$

where, Φ_e is the edge stress ratio shown in Equation (5-7)

Φ_{dw} is the ratio of the effective depth of the web

$$\Phi_{dw} = \begin{cases} \left(\frac{2}{\beta_w} - \frac{1}{\beta_w}\right) & ,\ for\ \beta_w > 1.0 \\ 1 & ,\ for\ \beta_w \le 1.0 \end{cases}$$

β_w is the slenderness ratio of web, $\beta_w = \begin{cases} \frac{d_w}{t_w} \cdot \sqrt{\varepsilon}\,, & for\ \varepsilon \ge 0 \\ 0 & ,\ otherwise \end{cases}$

Φ_w is the ratio of the effective plate width as shown in Equation (5-9)

A_s and is the area of the stiffener, $A_s = d_w \cdot t_w + b_f \cdot t_f$

d_w and t_w are depth and thickness of the web

b_f and t_f are width and thickness of the flange

b_p and t_p are width and thickness of the plate

Φ_{cw} is the critical stress ratio of web, $\Phi_{cw} = \begin{cases} 1 - \frac{1}{4\Phi_{EL}} & ,\ for\ \Phi_{EL} > 0.5 \\ \Phi_{EL} & ,\ for\ 0 < \Phi_{EL} \le 0.5 \\ 1.0 & ,\ for\ \Phi_{EL} \le 0 \end{cases}$

Φ_{EL} is the Euler local buckling stress ratio of web, $\Phi_{EL} = \frac{\left(400 \cdot \frac{t_w}{d_w}\right)^2}{\varepsilon \cdot E}$

ε is the element strain

E is Young's modulus

The load-end shortening curves due to web local buckling of the T-section and flat bar are illustrated in Figure 5-9.

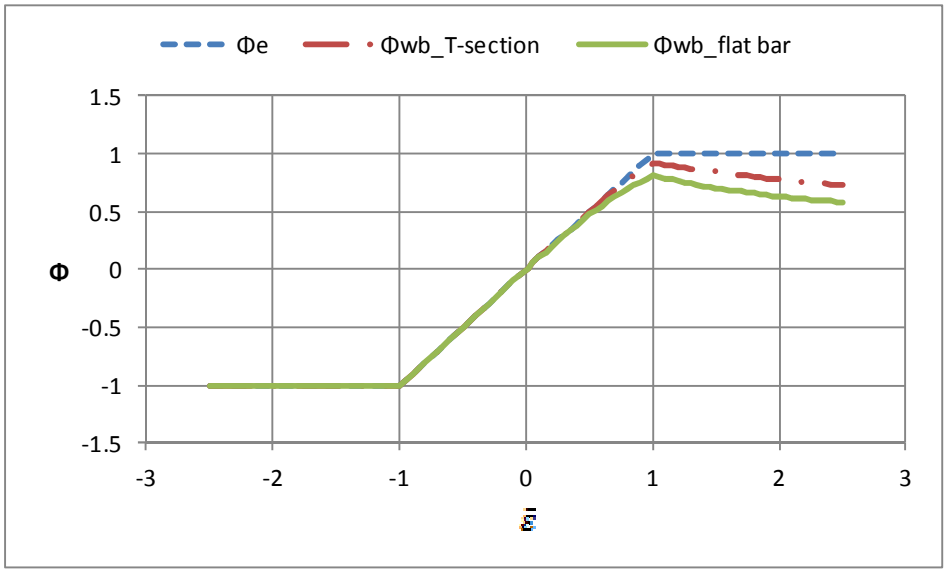

Figure 5-9: An example of load-end shortening curves for web local buckling failure of stiffeners, positive Φ means compression

5.5.5 Plate buckling

The buckling failure of transversely stiffened panels is described by the load-end shortening curve expressed in Equation (5-12).

$$\Phi_{pb} = \begin{cases} \Phi_e \cdot min\left[1, \frac{b_p}{l} \cdot \Phi_w + 0.1\left(1 - \frac{b_p}{l}\right)\left(1 + \frac{1}{\beta_p}\right)^2\right], for\ \varepsilon \geq 0 \\ \Phi_e \qquad\qquad\qquad\qquad\qquad\qquad\qquad\qquad\qquad\qquad\qquad\qquad , for\ \varepsilon < 0 \end{cases} \tag{5-12}$$

where, Φ_e is the edge stress ratio shown in Equation (5-7)

Φ_w is the ratio of the effective plate width as shown in Equation (5-9)

l is the span of the stiffener, equal to spacing of primary supporting members

b_p is width of the plate

β_p is the plate slenderness, $\beta_p = \begin{cases} \frac{b_p}{t_p} \cdot \sqrt{\varepsilon}, & for\ \varepsilon \geq 0 \\ NA, & otherwise \end{cases}$

An example of the stress-strain curve for buckling of plate is illustrated in Figure 5-10.

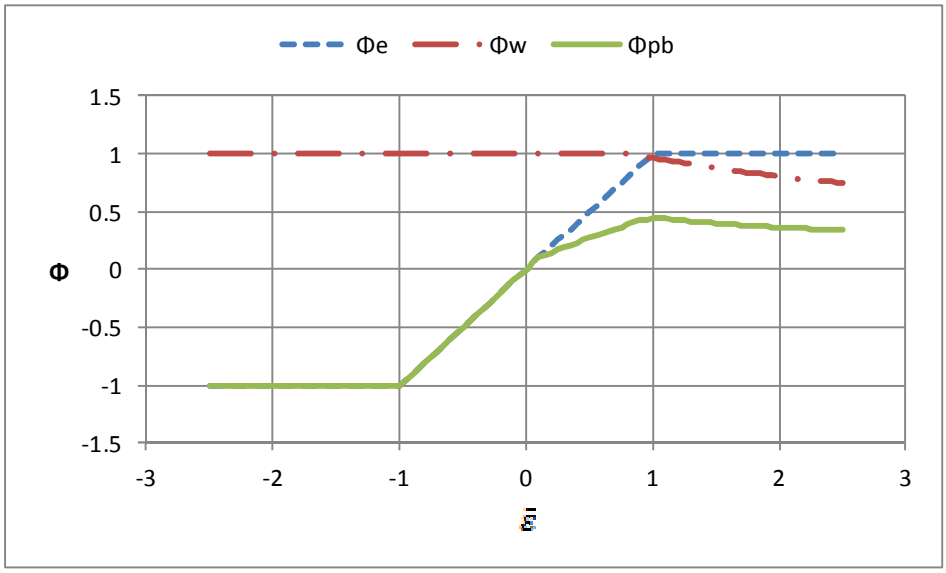

Figure 5-10: An example of load-end shortening curve for plate buckling failure and other stress ratios, positive *Φ* means compression

5.6 Validation

Validation of the approach discussed so far was made through comparison with experimental results together with results from other simplified solutions for ultimate strength of intact structures. Then a comparison with FE analysis results for residual ultimate strength of damaged structures has been carried out.

5.6.1 Ultimate strength of intact structures

For the ultimate strength of intact structures, the following structures are considered.

- Two models from Dowling, Chatterjee, Frieze and Moolani (1973)
- Five models from Nishihara (1984)
- A 1/3-scale frigate model from Dow (1991)

Dowling Tests

Two models from tests of Dowling, Chatterjee, Frieze and Moolani (1973), named *Model 2* and *Model 4* as shown in Figure 5-11, are taken into account. The calculated ultimate bending moments (without residual stress effect) are summarised in Table 5-2, where the results are compared with the results from experiment and from other references. For the *Model 2*, an FE analysis was carried out and found to give larger ultimate strength than other results. One of the reasons for this can be attributed to

the fixed (not moving during analysis) loading points on the sections during FE analysis even though failure of some components occurs in compressive parts and the neutral axis is adjusted. Another reason is due to the effect of residual stresses which was not considered in FE analysis at all. The comparison between results from FE analysis and current analysis for intact condition can be used as a reference in validating the current analysis code for calculating the residual ultimate strength of damaged structures.

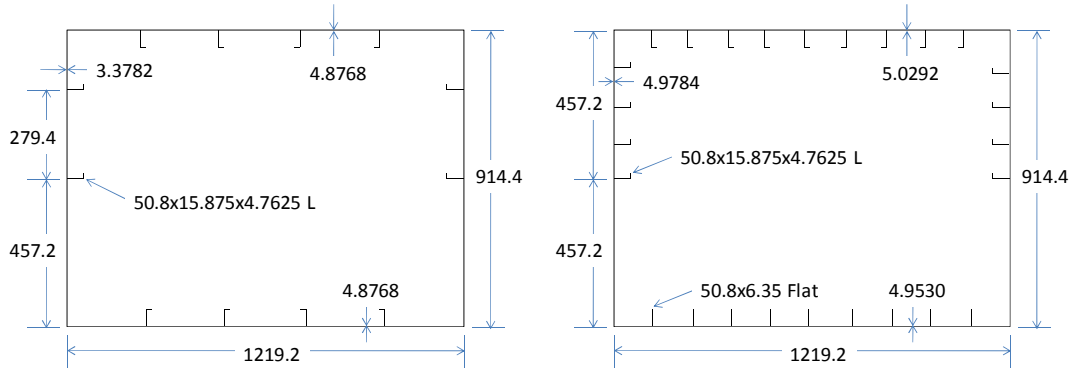

Figure 5-11: Two models of Dowling, Chatterjee, Frieze and Moolani (1973), left: *Model 2*, right: *Model 4* (units in mm), length = 787.4 mm

Table 5-2: Comparison of ultimate hogging bending moment of Dowling's models

Methods	Model 2		Model 4	
	BM (MN-m)	Diff. (%)	BM (MN-m)	Diff. (%)
Experiment	1.567	-	2.127	-
ALPS/ISUM [1)]	1.657	5.7	2.157	1.4
Frieze and Lin [1)]	1.652	5.4	2.303	8.3
Paik and Mansour (1995)	1.654	5.6	2.162	1.7
Gordo and Soares (1996)	1.660	5.9	2.466	15.9
FE analysis	1.868	19.2	-	-
Current method (σ_r=0)	1.739	11.0	2.396	12.6
Current method ($\sigma_r=\alpha_r \cdot \sigma_0$) [2)]	1.616	3.1	2.382	8.4

1) Data are obtained from Paik and Mansour (1995)

2) According to Gordo and Soares (1996), the average levels of residual stress coefficient, α_r, were 0.176 and 0.562 for *Model 2* and *Model 4*, respectively

Nishihara Tests

Among models of Nishihara test (1984), the five models shown in Figure 5-12 were considered for comparison. Each model represents different ship type; MST for single hull tankers, MSD for double bottom tankers, MSB for bulk carriers and MSC for container ships. For MST model, two different thickness plates were adopted and denoted as MST-3 and MST-4. The comparison with experimental results and results from other sources are summarised in Table 5-3.

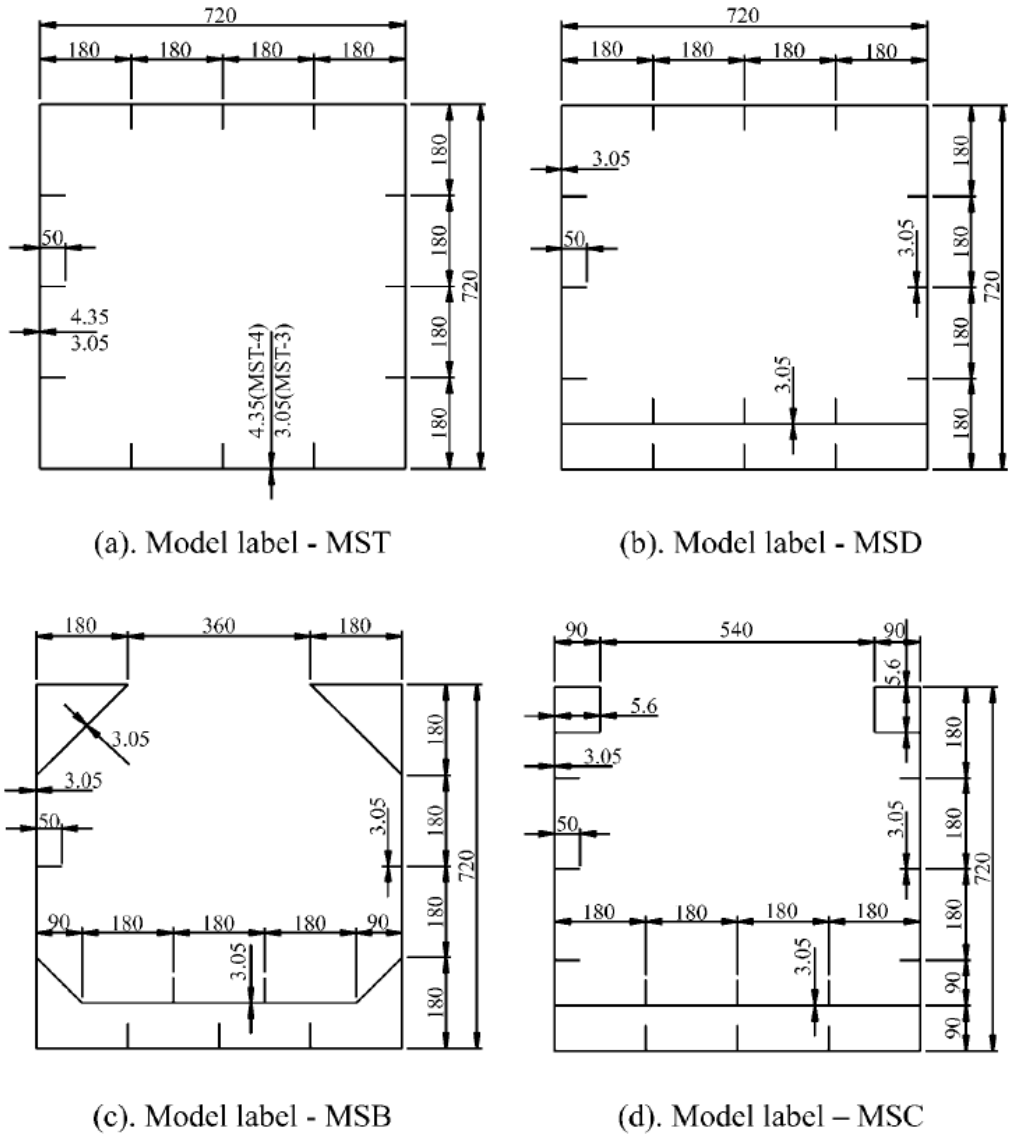

Figure 5-12: Models of Nishihara (1984), length = 540 mm (units in mm)

Table 5-3: Summary of ultimate bending moment of Nishihara's models

Methods		Exp.	Nishihara (1984)	ALPS/ ISUM[1)]	Frieze and Lin[1)]	Paik and Mansour (1995)	Lin[2)]	Paik[2)]	Gordo & Soares (1996)	Current Method
MST-3	Sag (MN-m)	0.589	-	0.569	0.578	0.625	-	-	0.634	0.640
	Diff. (%)	-	-	-3.36	-1.82	6.15	-	-	7.66	8.66
MST-4	Sag (MN-m)	0.868	-	0.806	0.880	0.882	-	-	0.909	0.908
	Diff. (%)		-	-7.20	1.37	1.61	-	-	4.7	4.58
MSD	Hog (MN-m)	0.839	0.793	-	-	-	0.749	0.747	0.861	0.839
	Diff. (%)	-	-5.50	-	-	-	-10.75	-10.99	2.65	0.03
	Sag (MN-m)	0.594	0.600	-	-	-	0.571	0.585	0.672	0.644
	Diff. (%)	-	1.16	-	-	-	-3.77	-1.44	13.23	8.51
MSB	Hog (MN-m)	0.672	0.726	-	-	-	0.451	0.451	-	0.739
	Diff. (%)	-	8.03	-	-	-	-32.93	-32.95	-	10.01
	Sag (MN-m)	0.482	0.516	-	-	-	0.488	0.490	-	0.520
	Diff. (%)	-	7.13	-	-	-	1.38	1.71	-	7.88
MSC	Hog (MN-m)	0.863	0.829	-	-	-	0.686	0.684	0.917	0.881
	Diff. (%)	-	-3.98	-	-	-	-20.59	-20.73	6.22	2.00
	Sag (MN-m)	1.113	0.950	-	-	-	0.881	0.879	0.970	0.912
	Diff. (%)	-	-14.71	-	-	-	-20.85	-21.09	-12.88	-18.10

1) Data are obtained from Paik and Mansour (1995)

2) Data are obtained from Kuo and Chang (2003)

Dow Test

Dow (1991) tested a 1/3-scale model of frigate hull structure subjected to a sagging bending moment. The cross section of the model is shown in Figure 5-13 and the comparison of results is summarised in Table 5-4.

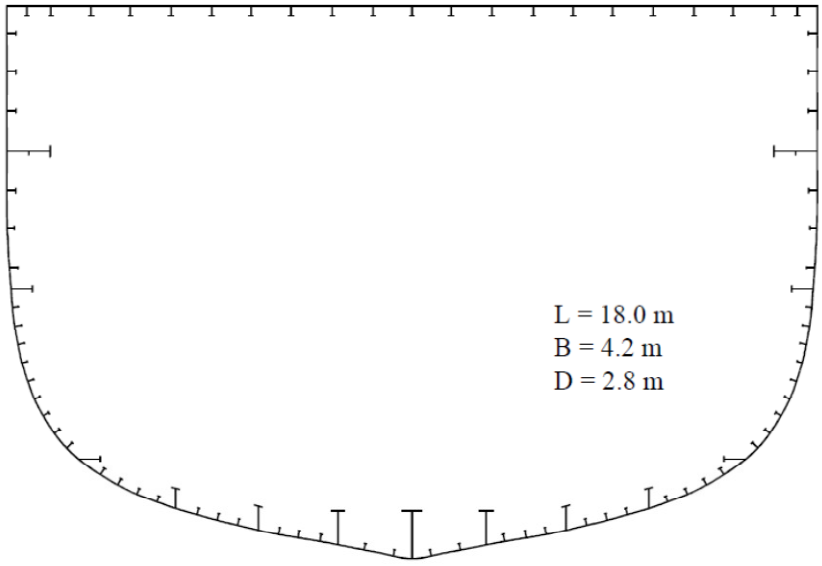

Figure 5-13: 1/3-scale frigate model of Dow (1991)

Table 5-4: Summary of ultimate bending moment of Dow's model

Methods		Exp.	ALPS/ ISUM[1)]	Frieze & Lin[1)]	Paik & Mansour (1995)	Gordo & Soares (1996)	Current Method
1/3-scale frigate	Sag (MN-m)	9.489	9.607	9.312	9.489	9.630	9.680
	Diff. (%)	-	1.24	-1.86	0.00	1.48	2.01

1) Data are obtained from Paik and Mansour (1995)

From the above comparison results, although some deviations exist it can be said that the current analysis gives reasonably good results for estimating ultimate strength of intact structures.

5.6.2 Residual ultimate strength of damaged structures

Validation of the developed code for predicting the residual ultimate strength of damaged structures was made through comparison with FE analysis results. A small box girder (*Model 2*) for tests of Dowling, Chatterjee, Frieze and Moolani (1973) was considered to be damaged in the bottom as shown in Figure 5-14.

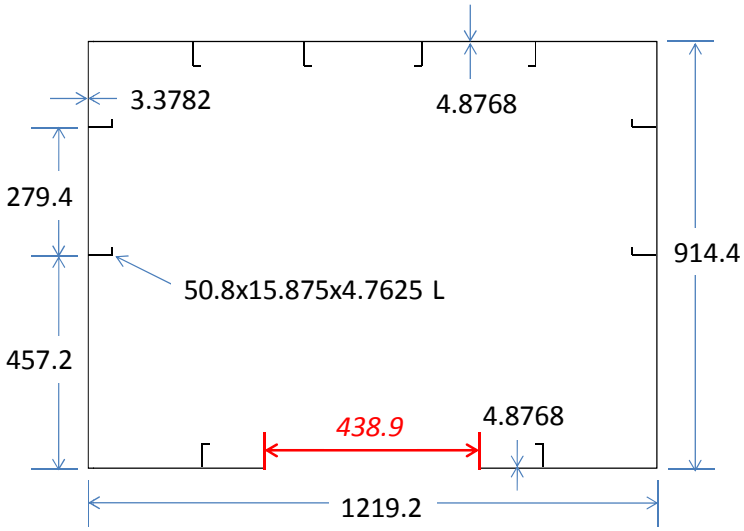

Figure 5-14: Model 2 of Dowling, Chatterjee, Frieze and Moolani (1973) with bottom damage (units in mm)

FE results of the model with damaged bottom at the residual ultimate strength conditions are shown in Figure 5-15 and the moment-curvature curves of the box girder were obtained by the current method for bottom damage condition as well as for intact condition and they are presented in Figure 5-16. Comparison of the residual ultimate strength of the box girder between results obtained by the developed code and results from FE analysis is summarised in Table 5-5.

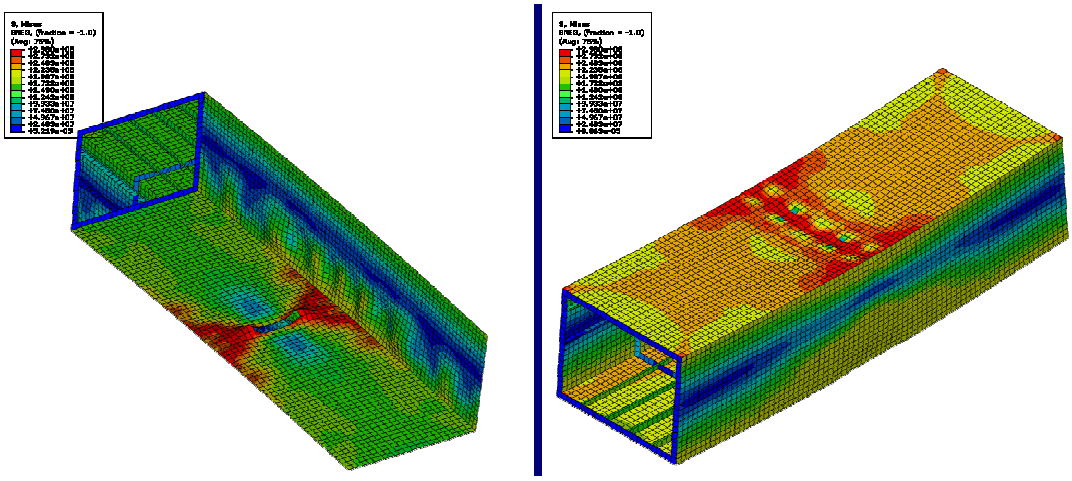

Figure 5-15: The box girder with bottom damage at the ultimate bending conditions (left: hogging, right: sagging)

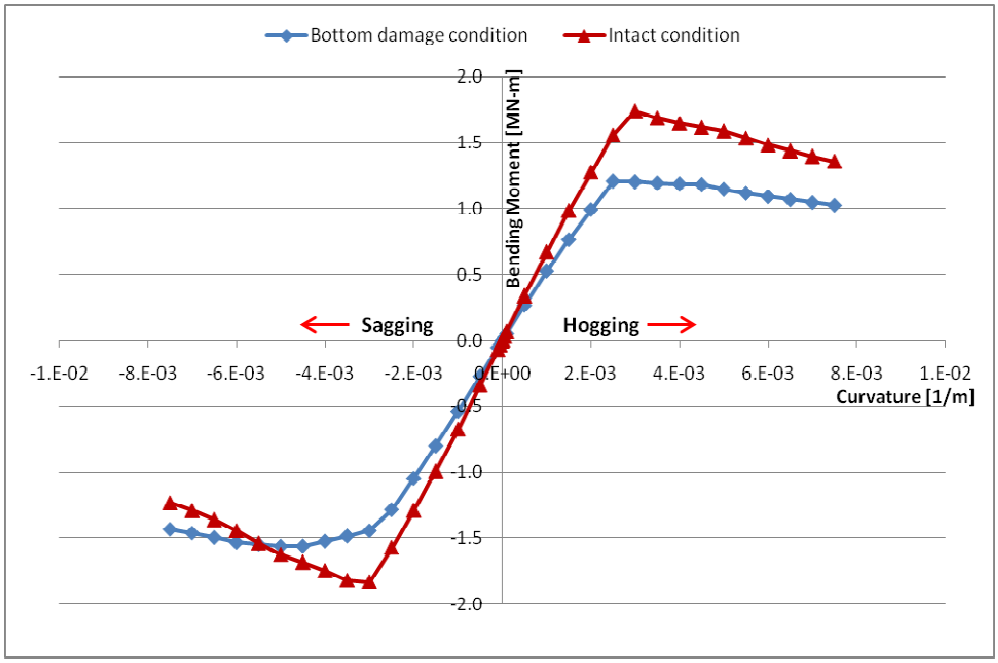

Figure 5-16: Moment-curvature curves of the box girder

Table 5-5: Summary of residual ultimate bending strength

Methods		Exp.	FE analysis	Current method	Diff. (%)[1)]
Intact	Hog (MN-m)	-	1.868	1.739	-6.90
	Hog (MN-m) (σ_r=0.176σ_0)	1.567	-	1.616	3.10[2)]
	Sag (MN-m)	-	2.002	1.834	-8.40
Bottom damage	Hog (MN-m)	-	1.271	1.211	-4.71
	Sag (MN-m)	-	1.662	1.561	-6.04

1) Difference in percentage of results by current method to those of FE analysis

2) Difference between the result by current method and experimental result

In general, the current method gives conservative and consistent results of the residual ultimate strength about 5 ~ 6% less than those from FE analysis. Although, a direct comparison of the residual ultimate strength between predicted by current code and experimentally obtained is not possible, considering that the predicted ultimate strength with average residual stress taken into account is very similar with the experimental result (approximately 3% difference) and that the level of ultimate strength of the box girder predicted by current method is about 7 ~ 8% less than that from FE analysis, it can be said that the current developed code predicts the ultimate residual strength in a reasonable way.

However, it should be noted that the uncertainty from the geometry and the material property of the model needs to be identified and analysed. The geometrical information includes uncertainty related to the damage location, size and hull deformation, and the material mechanical properties. Furthermore, uncertainty also arises from the mathematical assumptions of the failure models employed in the analysis. Considering that the kinds of uncertainty discussed above are inherent in any modelling exercise, it is necessary to identify the dominant contributors to uncertainty and quantify its effects on the results. This requirement will be discussed in greater detail in Chapter 7.

5.7 Chapter summary

The development of the parametric model that enables determination of the ultimate residual strength capacity of damaged structures is developed in this chapter. Once a damage configuration of a hull girder is identified following an accidental event, the developed code will be used to calculate ultimate strength capacity of the intact hull girder as well as of the initial damaged hull section. The propagation of the initial damage will be determined by the progressive structural failure analysis which has been elaborated in Chapter 4 and will be forwarded to the ultimate residual strength capacity assessment for every time step. The applicability of this process will be assessed in the next chapter for a real ship structure.

6 CASE STUDY – AFRAMAX TANKER

6.1 Preamble

This chapter elaborates on the application of the proposed approach to a real ship hull structure. As the validation of the approach is difficult to be achieved due to the lack of accidental damage data of ships, various damage cases are studied with an Aframax tanker in order to prove the applicability of the proposed approach. The application procedure includes the definition of the damage case, the determination of the SIFs, the analysis of the progressive failure of the structure and the calculation of the residual strength of the hull girder in the time domain. Also, a set of wave conditions is taken into account in order to obtain a realistic wave loading. The damage cases include i) a bottom damage, ii) a deck & side damage, and iii) a side shell damage.

6.2 Need for validation

The purpose of the validation is mainly the comparison of the crack propagation results emanating from a damage opening in a real ship structure between the estimated and the recorded by taking into account the recorded time varying wave loads with the recorded loading condition. As it would be extremely difficult to identify the exact size of the damage opening and its location, it is desirable to consider variational change of the damage configuration with a probabilistic approach and the recorded result would be checked along with the confidence for its accuracy. For this to be viable, at least the following information is required:

- Structural drawings of the ship and corrosion status of the structural member especially in the damaged area;
- Loading condition (weight distribution) of the ship at the intact condition;
- A record of sea states in time domain during the ship's movement after damage (significant wave height, zero-crossing wave period and ship's heading angle);
- Ideally, the information of the initial damage configuration and its recorded change in time domain (opening location, size and the initial crack sizes).

The validation of the proposed methodology could be made by applying retrospectively to incidents that have happened and for which good data is available. Also, experimental tests could provide data for validation.

6.3 Ship's particulars

The ship used in the analysis is a crude oil double hull carrier of 112,700 DWT. The ship has twelve cargo tanks; six tanks on each side. The principal dimensions of it are summarised in Table 6-1.

Table 6-1: Principal dimensions of the Aframax tanker

Type	Value	Unit
Length O. A.	250.17	M
Length B. P.	239.00	M
Breadth MLD.	44.00	M
Depth MLD.	21.00	M
Draught MLD. (Design)	14.60	M
Draught MLD. (Scantling)	14.60	M
Frame spacing	3.78	M

Drawings of the general arrangement, the ordinary midship section and the typical web section are provided in Figure 6-1, Figure 6-2 and Figure 6-3 respectively.

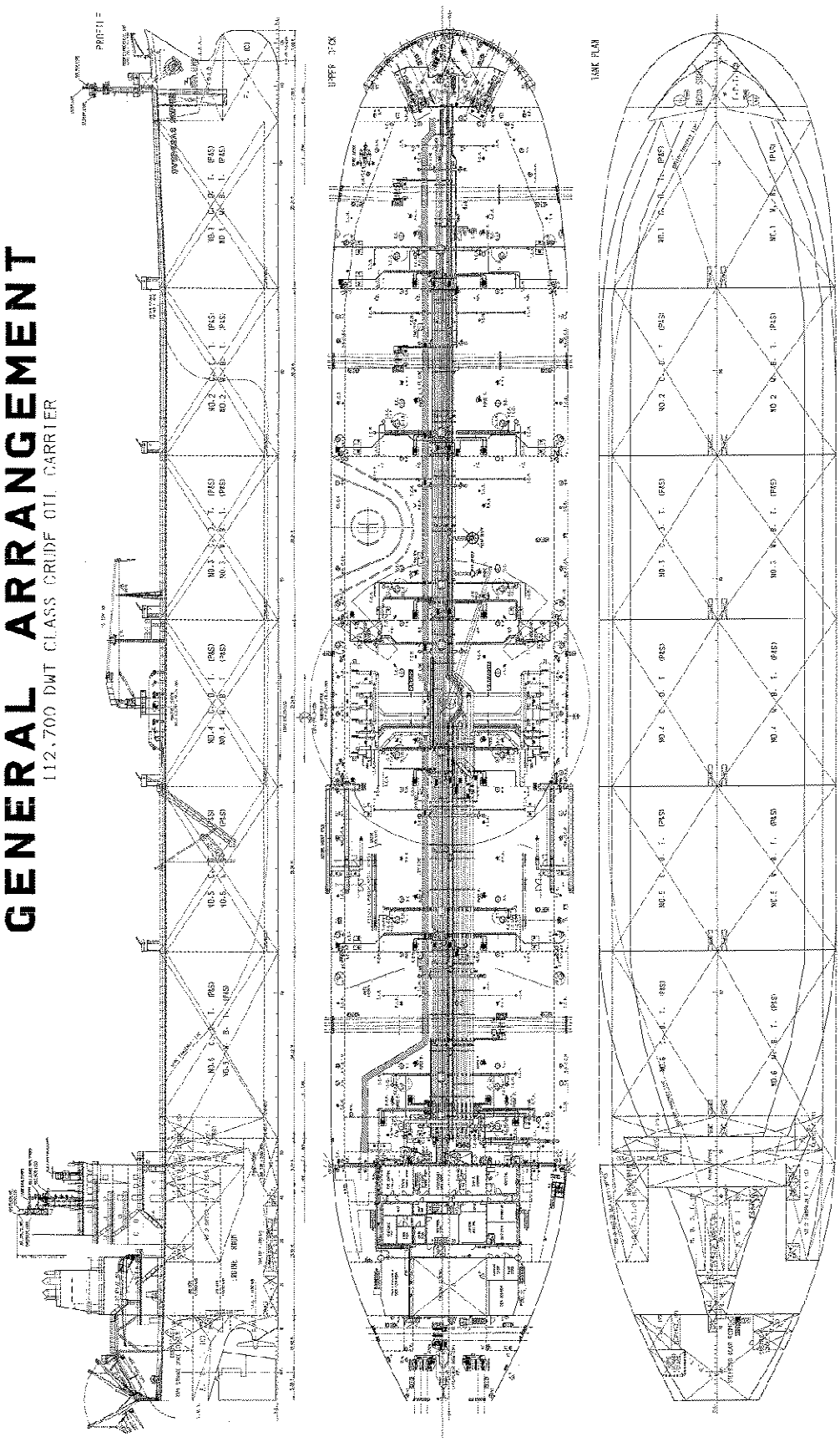

Figure 6-1: Drawing of the general arrangement of an Aframax tanker

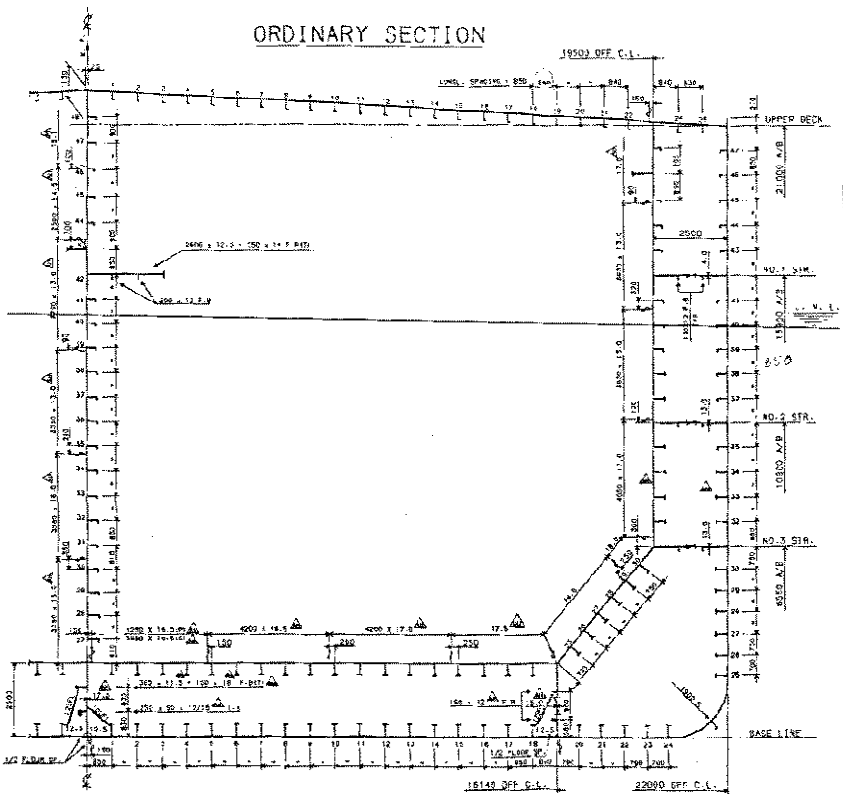

Figure 6-2: Drawing of the ordinary midship section of an Aframax tanker

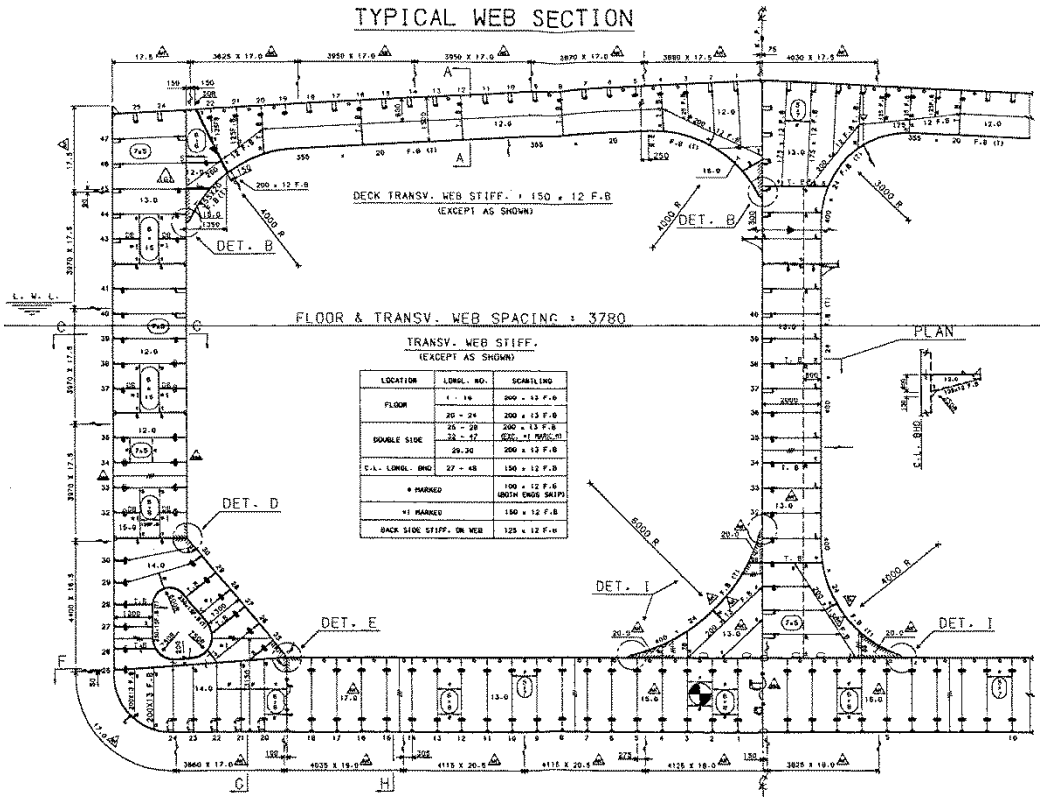

Figure 6-3: Drawing of the typical web section of an Aframax tanker

6.4 Bottom damage

6.4.1 Description of damage

In this part of the analysis the extent and location of a grounding damage are assumed according to the ABS guidelines (1995).This reference has been used to define the damage extents due to collision and grounding accidents, and for calculation of the residual strength of a damaged ship in Paik, Thayamballi and Yang (1998), and SAFEDOR project (2006), in the course of developing probabilistic models for collapse limit state.

According to the guidelines, the location of the damaged bottom structure due to a grounding accident is considered to be in the most unfavourable location anywhere on the flat bottom within the fore part of the hull between 0.5L and 0.2L aft from F.P. Also, it is considered that the bottom structures are damaged over a considerable length and the damaged longitudinal strength members are excluded from the hull girder. The extent of a grounding damage includes bottom girders attached to the damaged bottom shell plate to a certain depth as well as bottom shell plate and attached stiffeners.

According to the ABS guideline, the structural members assumed to be damaged and excluded completely or partially are discussed in Table 6-2 and shown in Figure 6-4. In this analysis, the grounding damage is assumed to be located at the centre of the bottom structure near amidships within No. 4 (port and starboard) cargo tanks. The extent of the initial damage is defined in Table 6-2 and sketched as in Figure 6-5.

A circular damage opening is assumed, from which initial cracks emanate symmetrically towards the side shell so that the vertical bending moment from wave loads allows the cracks to propagate. The initial crack length is assumed to be 1.0% of the radius of the initial damage. That is, 36.65 mm of crack size (a_0) at each side of edge of damage is adopted as the initial condition (Figure 6-5). The effect of the size of the initial damage on the outcome of the analysis is discussed in Chapter 7.

Table 6-2: Guideline on the grounding damage extent and its application in the case study

ABS guideline (1995)	Selected values for damage extent
• Bottom shell plating for a width of 4 m or $B_{hull}/6$, whichever is greater, where B_{hull} is the ship breadth	• Width of damage on the bottom shell plate: 7.33 m (= $B_{hull}/6$)
• Double bottom girders attached to the damaged shell plating are assumed to be damaged and ineffective up to the following percentage of the girders height: - 25% for girders situated within 1 metre marginal zones of the damaged plating - 75% for girders situated between the marginal zones	• Height of damage at the centre girder: 1.875 m (= $0.75h_{DB}$)
• All of the bottom longitudinals within the damaged bottom shell and the longitudinal stiffeners within the damaged parts of girders	• 4 stiffeners on the bottom shell plate at each of port and starboard side and 2 stiffeners on the centre girder

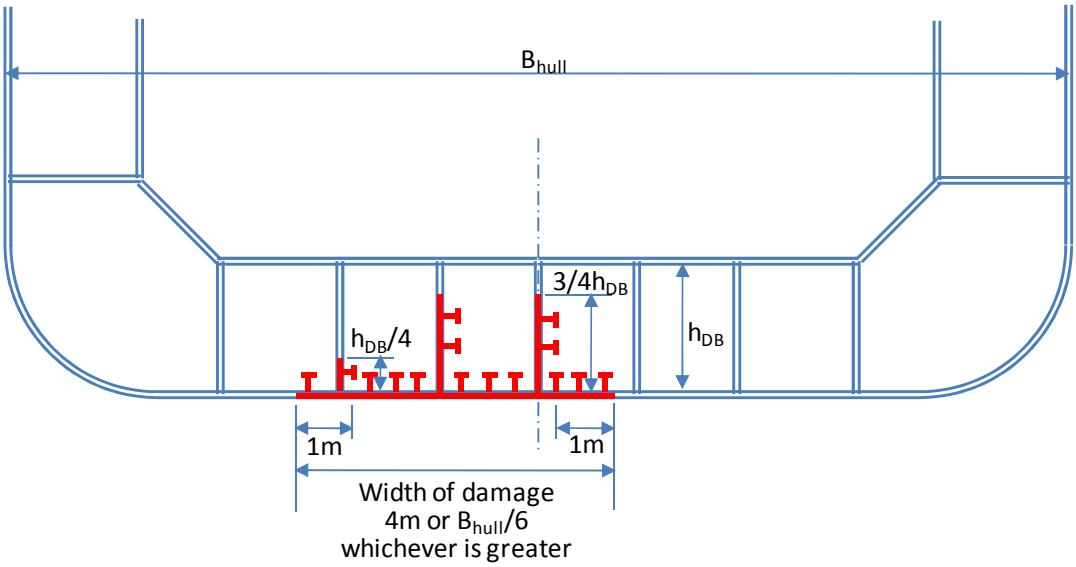

Figure 6-4: Extent of damage due to grounding accident, ABS (1995)

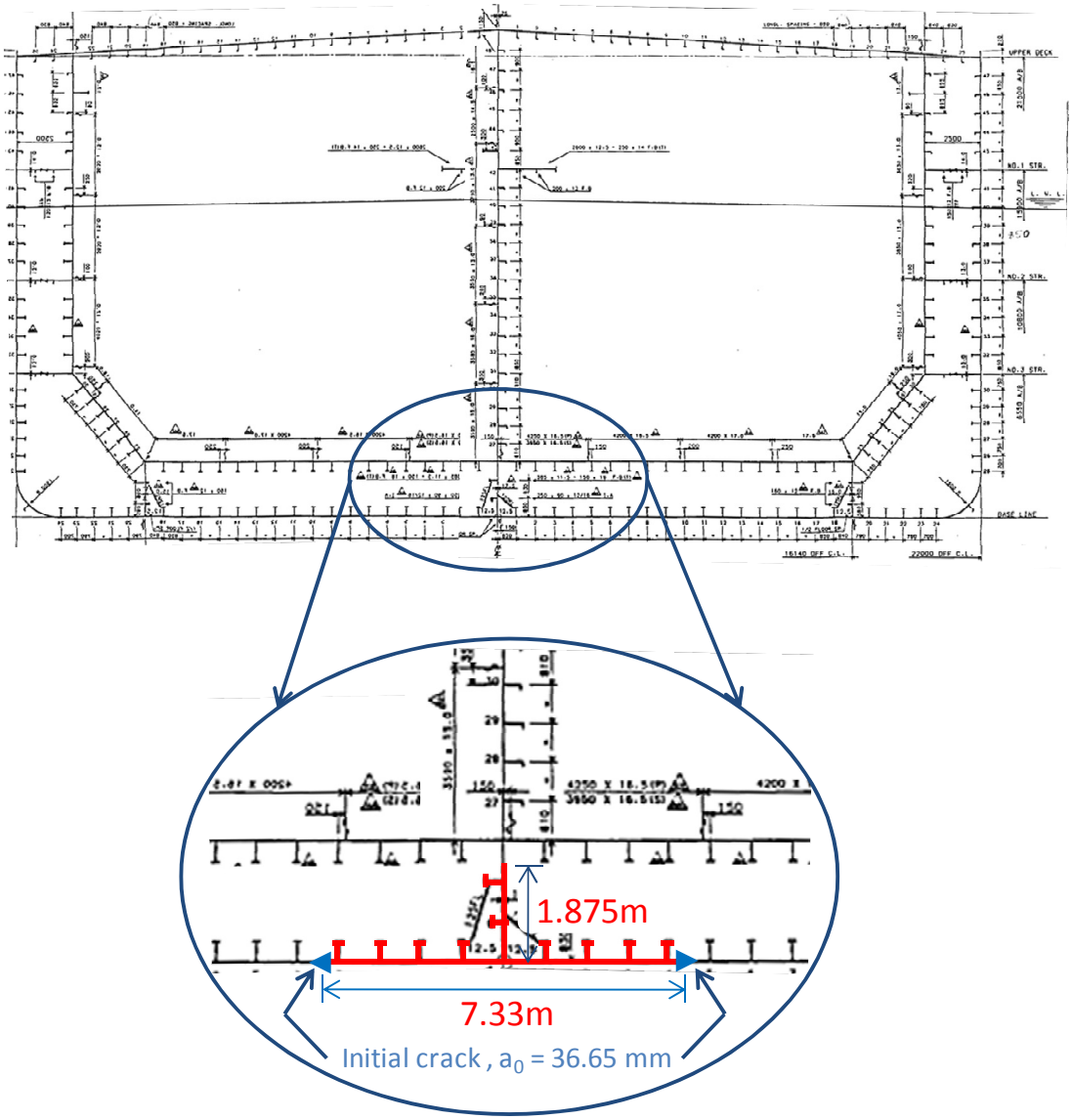

Figure 6-5: Extent and location of grounding damage of the Aframax tanker in cross-section

6.4.2 FE model and SIF calculation

With the grounding damage extent defined above, a finite element model of the tanker is prepared for the calculation of the SIF with VCCT in ABAQUS. The FE model (Figure 6-6) consists of three cargo tanks (No. 3, 4 and 5 C.O.T. tanks) along the length of the ship and includes the full breadth and height of the ship. 4-node shell elements are used primarily to model hull plating and web of longitudinal stiffeners while 2-node beam elements are adopted for modelling of flange of longitudinal stiffeners as well as other stiffeners. In the damaged area, 3D solid elements are deployed and the shell-to-solid coupling as well as the surface contact is applied in the model (Figure 6-7).

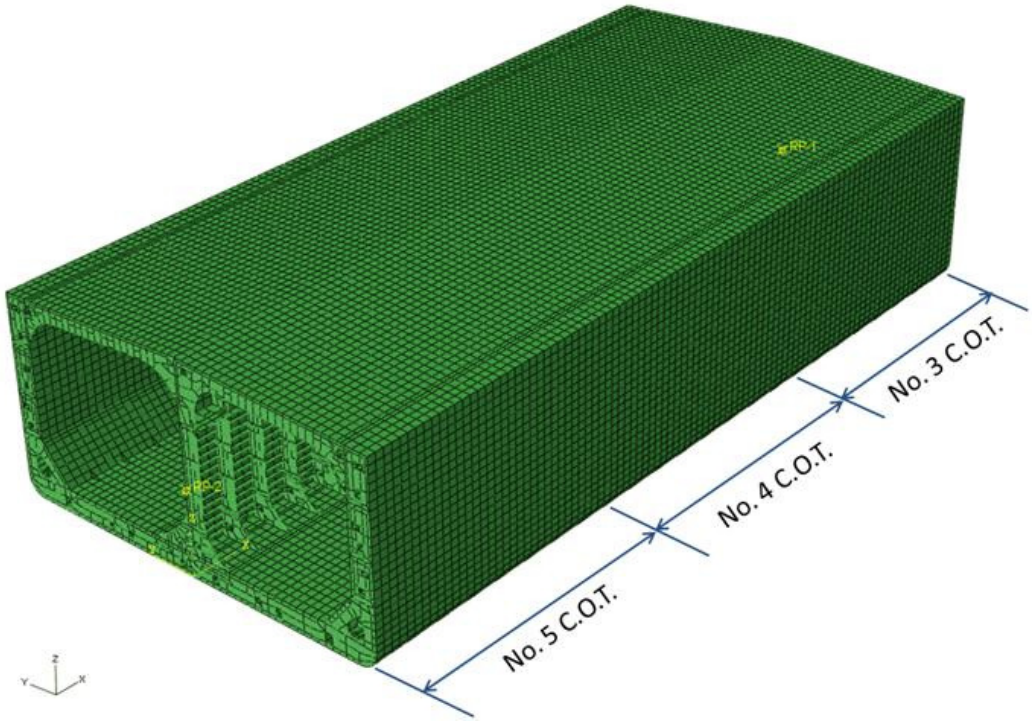

Figure 6-6: 3-hold FE model in an isometric view

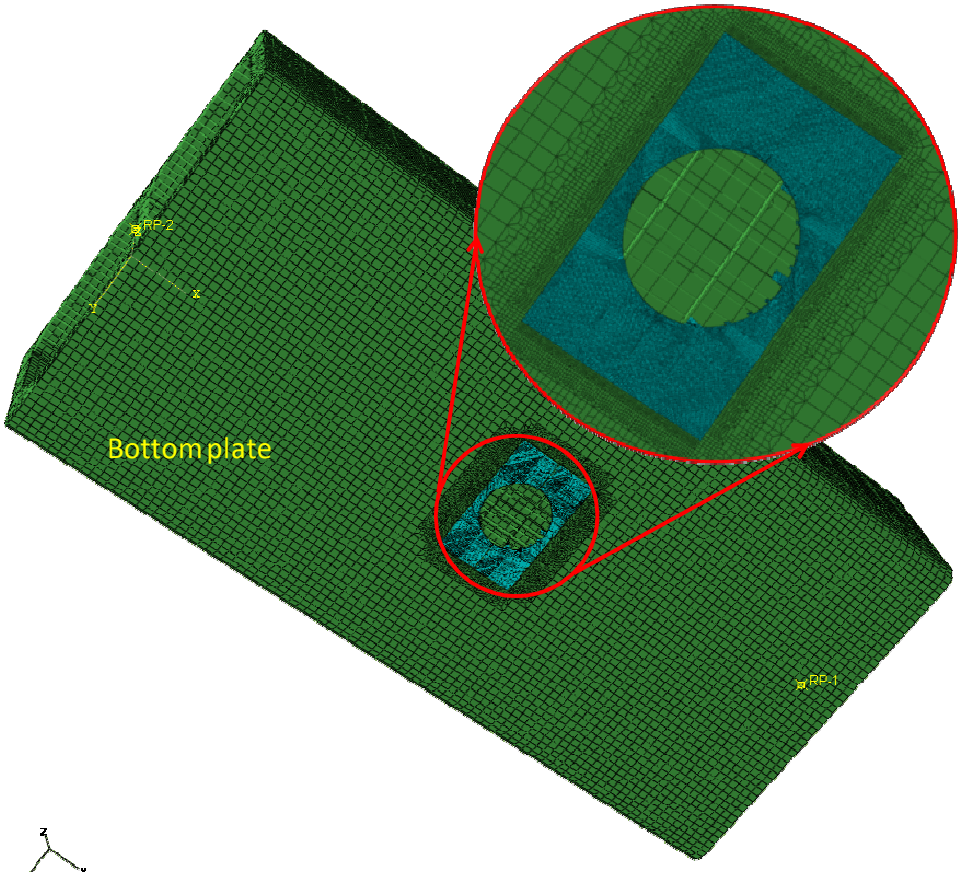

Figure 6-7: FE model with 8-node solid elements around the damage

SIFs are calculated using a *unit* vertical sagging bending moment applied on both ends of the FE model. The load transmission from the reference points where the vertical bending moment is applied to the whole end sections is enabled by using multi-point constraints (MPCs). The reference point is located at the inter section of the neutral axis and the centre line of each end section (Figure 6-8).

A pair of 1.0 MN-m of vertical bending moment is applied to the reference points to induce sagging condition and an appropriate set of boundary conditions is applied (Figure 6-9); one reference point is pinned, the other reference point is restrained to avoid abnormal behaviour of the model, i.e. rigid body motions due to lack of constraints. The detail boundary conditions are summarised in Table 6-3.

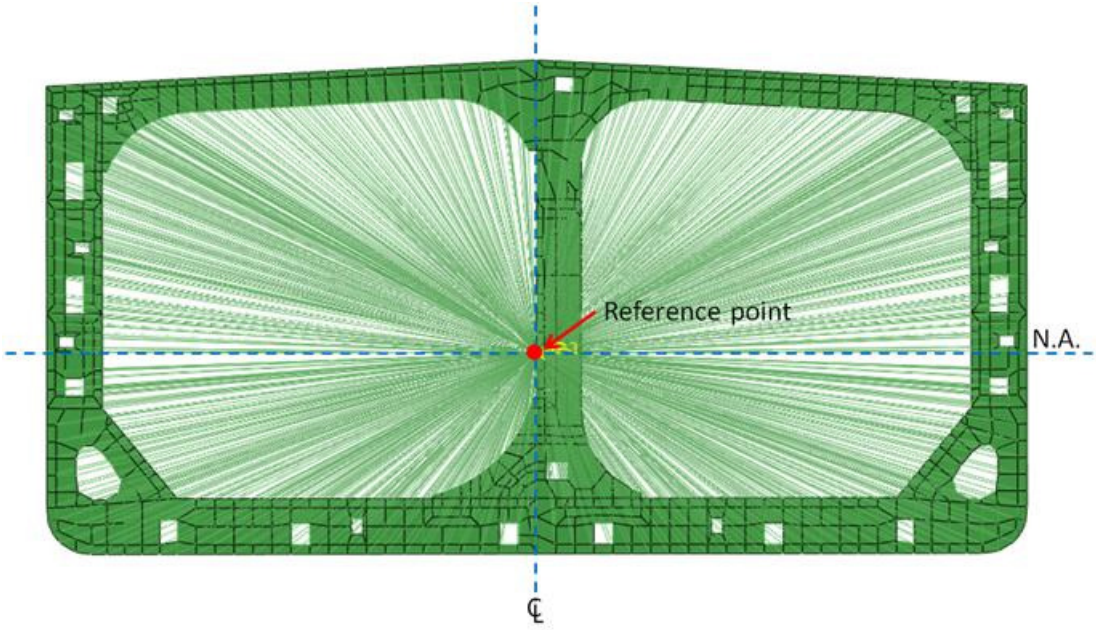

Figure 6-8: Multi-points constraint at end sections

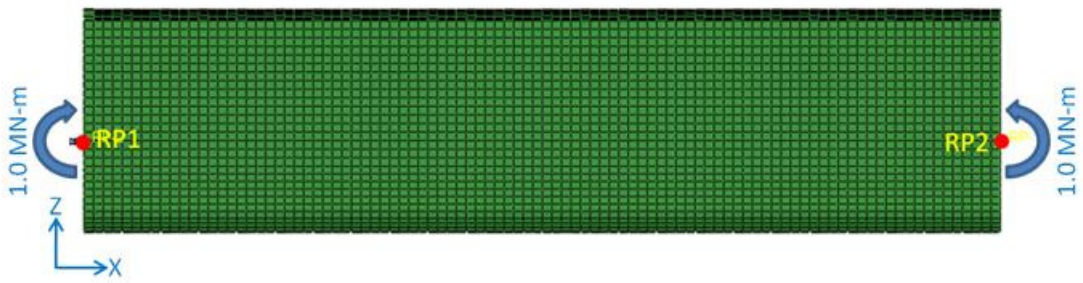

Figure 6-9: Load and boundary conditions applied (side view)

Table 6-3: Boundary conditions ('O' denotes applied constraint)

Locations	UX	UY	UZ	RX	RY	RZ
RP1	O	O	O	-	-	-
RP2	-	O	O	O	-	-

With the boundary conditions and the unit bending moment applied, a series of analyses is carried out to calculate the strain energy release rate for each size of crack. Figure 6-10 is an example of results showing the Von-Mises stress distribution and the strain energy release rate. Finally, a curve of SIF against the half damage size (sum of half initial opening size and crack size) is shown in Figure 6-11 and a combination of this curve with actual wave loads together with the crack growth rate model would result in the prediction of damage propagation for the bottom damage case.

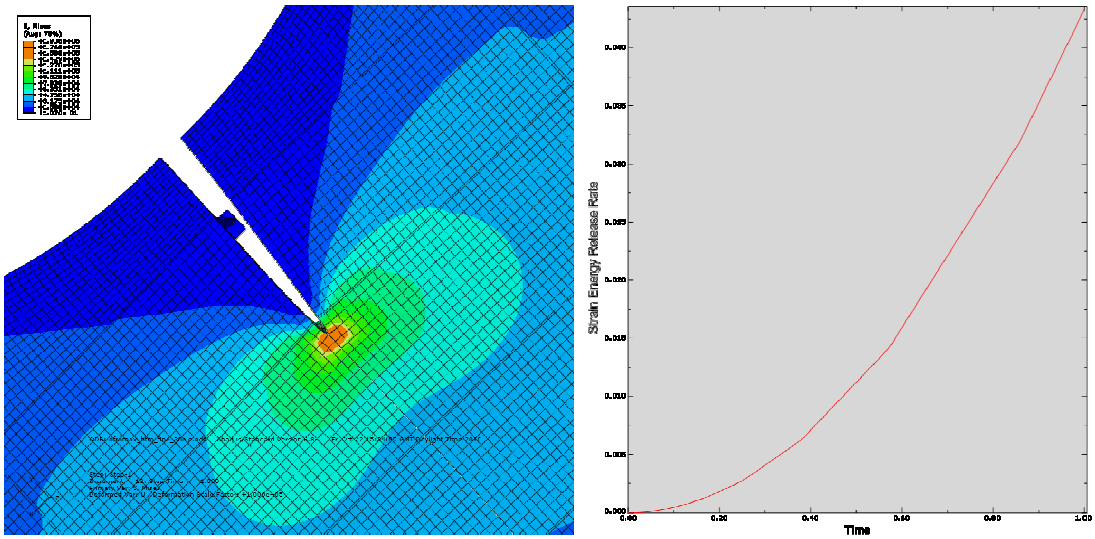

Stress distribution (Von-Mises) Strain energy release rate at the crack tip

Figure 6-10: An example of analysis for calculating the strain energy release rate

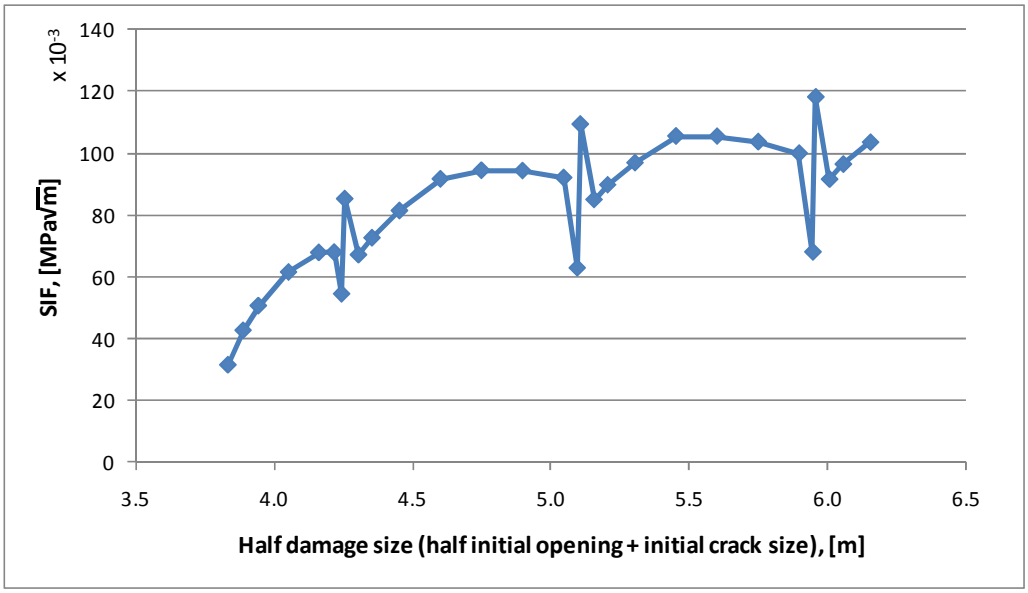

Figure 6-11: SIF curve calculated by VCCT using a unit bending moment pair of 1.0 MN-m

6.4.3 Knowledge-intensive (parametric) model

In the bottom damage case, three correction factors are taken into account in order to capture the response of cracks in the structure and finally to build up a solution for the estimation of SIFs in various instances.

Finite plate

Considering that the bottom plate of the ship hull has limited dimension in length and breadth, the effect of finite plate is applied by considering correction factors for finite width and finite length of the plate. Recalling the correction factors from the handbook of Tada, Paris and Irwin (2000) and from the FE analysis, they are expressed below again.

$$Y_{finite\ width} = \left\{1 - 0.025\left(\frac{a}{B}\right)^2 + 0.06\left(\frac{a}{B}\right)^4\right\}\sqrt{sec\frac{\pi a}{2B}} \quad \textbf{(6-1)}$$

$$Y_{finite\ length} = \sqrt{s_h} \times (-6.0784{s_h}^5 + 19.918{s_h}^4 - 26.087{s_h}^3 + 18.512{s_h}^2 - 8.6119s_h + 3.3462) \quad \textbf{(6-2)}$$

where, a is half of the centre crack sizes

$$s_h = \frac{L}{(L+B)}$$

B and L are half-width and half-length of the finite bottom plate

Hence the correction factor for finite plate of bottom is obtained as Equation (6-3).

$$Y_{finite\ plate} = Y_{finite\ width} \times Y_{finite\ length} \quad \textbf{(6-3)}$$

Damage opening

Another factor to be included in the parametric model is the damage opening, the effect of which is achieved by considering the correction factor for a circular opening, due to the damage opening in bottom plate being a circle, which is expressed in Equation (6-4) from the handbook of Tada, Paris and Irwin (2000).

$$Y_{circle} = 0.5(3 - s_c)\{1 + 1.243(1 - s_c)^3\} \times \sqrt{s_c} \quad \textbf{(6-4)}$$

where, s_c is a ratio of a_0 to half of the total crack size, $s_c = \frac{a_0}{a} = \frac{a_0}{R+a_0}$

a_0 is the size of the crack emanating from the opening

a is half of the total crack size including the opening

R is the radius of the circular opening

Stiffeners

As the bottom plate consists of a continuous stiffened panel, the effect of stiffeners is the third parameter to be included in the model. Recalling that the correction factor for stiffeners is composed of two correction factors, the correction factor for the i-th stiffener is expressed by Equation (6-5).

$$Y_{stiffener,i} = Y_{stif\_constraint,i} + Y_{stif\_separation,i} \quad \textbf{(6-5)}$$

where, $Y_{stif_{constraint},i} = \left(1 - \frac{1}{f_{k,i}}\right)\left(\frac{1}{1+\beta_i}\right)^{\alpha_1} + \frac{1}{f_{k,i}} + \frac{0.3{\chi_i}^2}{f_{k,i}}\left(\frac{4}{{\beta_i}^2 - 2\beta_i + 4} - 1\right) - \alpha_2\left(\frac{{\chi_i}^{10} + {\chi_i}^{30} + {\chi_i}^{50}}{f_{k,i}}\right)\left(\frac{4}{{\beta_i}^2 - 2\beta_i + 4} + 1\right)$

$$Y_{stif\_separation,i} = \frac{4\mu_i}{\pi(1 - \mu_i)\sqrt{{\chi_i}'^2 - 1}}$$

The rest of the variables are discussed in Chapter 4, Section 4.4.2.

On the other hand, an attempt has been made to obtain the correction factor for the stiffeners using FE analysis. This correction factor is expected to be the ratio of the calculated SIF over the estimated SIF including all other effects from the finite plate and the opening. Hence, the correction factor for stiffeners based on FE analysis is obtained from Equation (6-6).

$$Y_{stiffener,BTM,FEA} = \frac{SIF_{FEA}}{SIF_0 \times Y_{finite\ plate} \times Y_{circle}} \quad \textbf{(6-6)}$$

where, $SIF_0 = \sigma\sqrt{\pi a}$

σ is the bending stress on the bottom plate

a is the half damage size including opening, $a = a_0 + R$

Data obtained by the Equation (6-6) is plotted in Figure 6-12 from FE results shown in Figure 6-11 and regression analysis is made in order to obtain the corresponding formulas which are expressed in combinations of power and polynomial forms as shown in Equation (6-7).

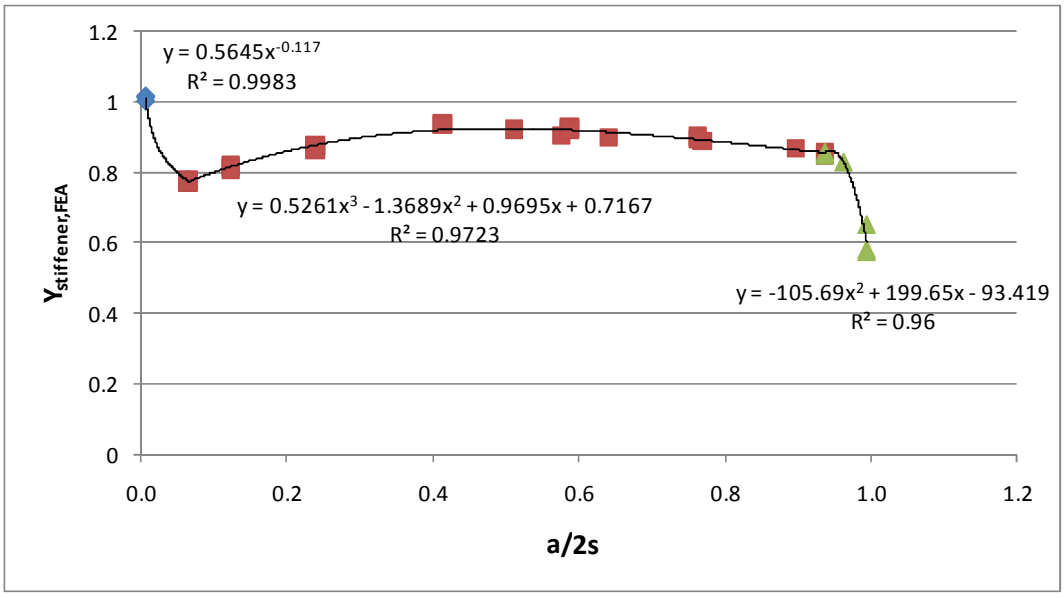

Figure 6-12: Regression analysis for defining $Y_{stifferner,FEA}$ in bottom damage case

$$Y_{stiffener,BTM,FEA} = \begin{cases} 101.65\left(\frac{a}{2s}\right) + 0.541 & ; 0.0 < \left(\frac{a}{2s}\right) \leq 0.005 \\ 0.5645 \times \left(\frac{a}{2s}\right)^{-0.117} & ; 0.005 < \left(\frac{a}{2s}\right) \leq 0.065 \\ 0.5261\left(\frac{a}{2s}\right)^3 - 1.3689\left(\frac{a}{2s}\right)^2 + 0.9695\left(\frac{a}{2s}\right) + 0.7167 & ; 0.065 < \left(\frac{a}{2s}\right) \leq 0.95 \\ -105.69\left(\frac{a}{2s}\right)^2 + 199.65\left(\frac{a}{2s}\right) - 93.419 & ; 0.95 < \left(\frac{a}{2s}\right) \leq 1.0 \end{cases} \quad \textbf{(6-7)}$$

where, a is the half damage size including opening, $a = a_0+R$

$2s$ is the stiffener's spacing

Although the correction factor for stiffeners in the analytical form, Equation (6-5), is generally applicable to stiffened panels, the correction factor obtained from FE analysis, Equation (6-7), has the characteristic that it is specific to the bottom stiffened plates and their surrounding structure . Hence, the correction factor for stiffeners from FE analysis is applicable in the case of this tanker only.

Knowledge-intensive model of SIFs for the bottom damage case

Recreation of the SIF curve of cracks emanating from a circular opening in the bottom plate is carried out using the correction factors obtained previously. Considering all the related correction factors, the SIF is determined by the knowledge-intensive model defined in Equation (6-8). The resulting SIF curve is shown in Figure 6-13. The discontinuities of the curve correspond to the longitudinal stiffener locations (at approx. 850 mm intervals).

$$SIF_{BTM\ damage} = SIF_0 \times Y_{finite\ plate} \times Y_{circle} \times Y_{stiffener,BTM,FEA} \quad \textbf{(6-8)}$$

where, $SIF_0 = \sigma\sqrt{\pi a}$

σ is the bending stress on the bottom plate

a is the half damage size including opening, $a = a_0+R$

$Y_{finite\ plate}$, Y_{circle} and $Y_{stiffener,FEA}$ are defined in Equation (6-3), (6-4) and (6-7) respectively

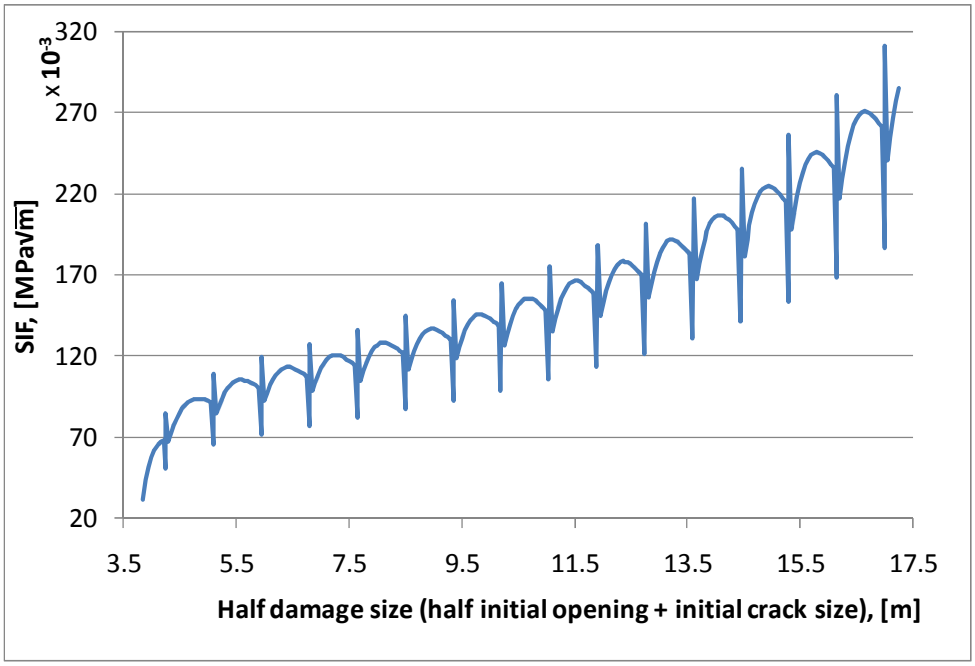

Figure 6-13: SIF curve obtained by the parametric model for the bottom damage case

The validity of the knowledge-intensive model of SIFs in the bottom damage case is proved through comparison with the SIFs calculated by FEA as plotted in Figure 6-14, where a good agreement between the two results is identified.

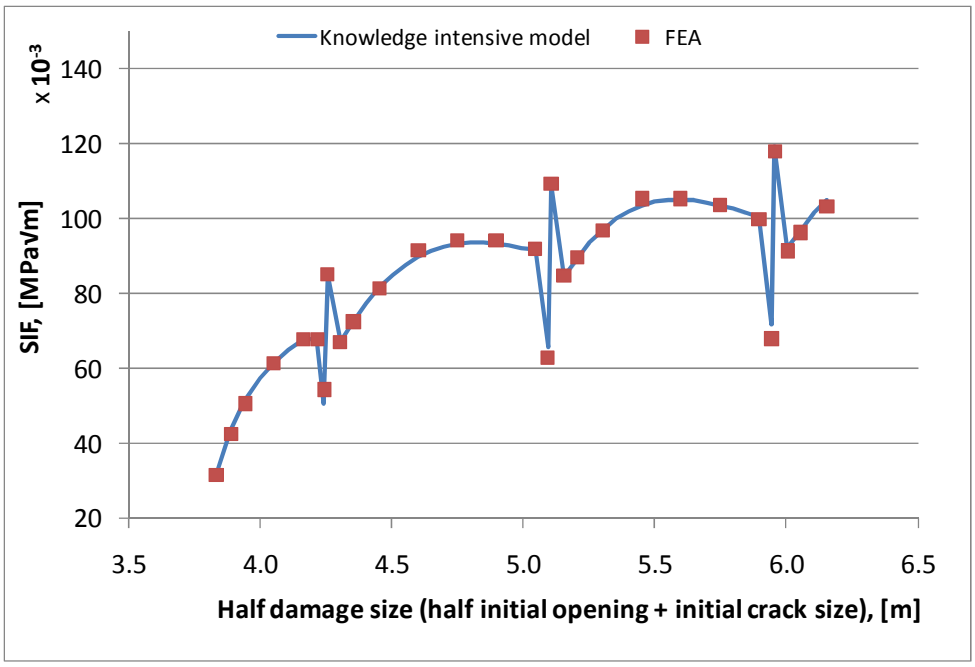

Figure 6-14: Comparison of SIF calculated by FEA and estimated by the model

6.4.4 Wave loads

Wave loads are calculated by a 3D panel code, Xie (2011), for deep water. The fully loaded condition, in which the still water bending moment in sagging at the damaged section is calculated as 1329 MN-m, is considered with some modification of draught and trim taking into account the loss of buoyancy due to the flooded compartments in the double bottom where the damage is initiated. Response amplitude operators (RAOs) of the wave bending moment in hogging and sagging are calculated with linear regular wave condition and their values at the damage section are shown in Figure 6-15. Only the head wave is considered and the zero-forward speed of the ship is taken into account. This corresponds to a ship in distress that is drifting in a seaway.

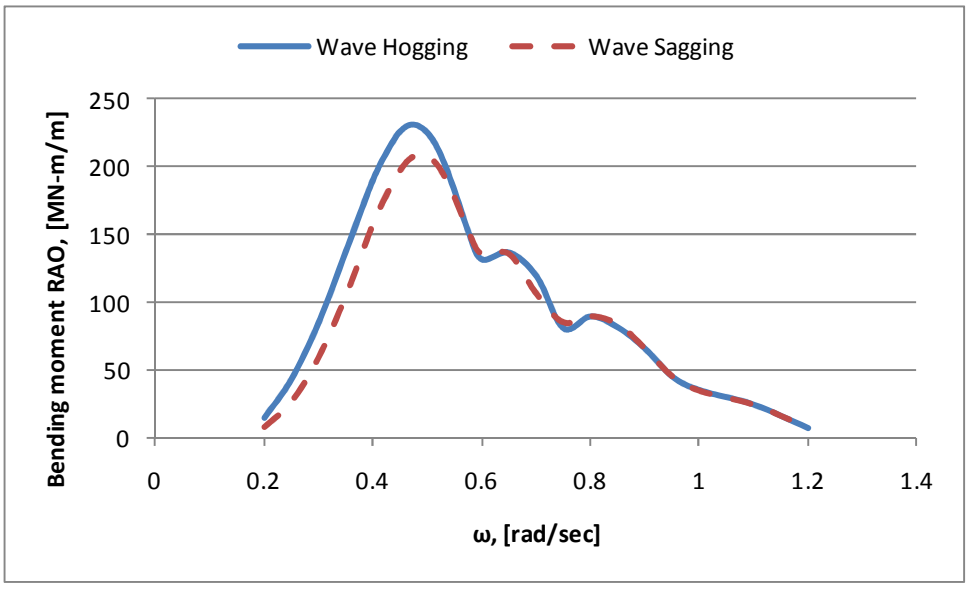

Figure 6-15: Response amplitude operator of wave bending moments in the fully loaded condition

The wave data shown in Figure 6-16 is assumed to be the same as those estimated in the report for the *Prestige* accident prepared by Bahamas Maritime Authority (2004), for 3-hour intervals. For simplicity, linear regular wave is assumed in head seas.

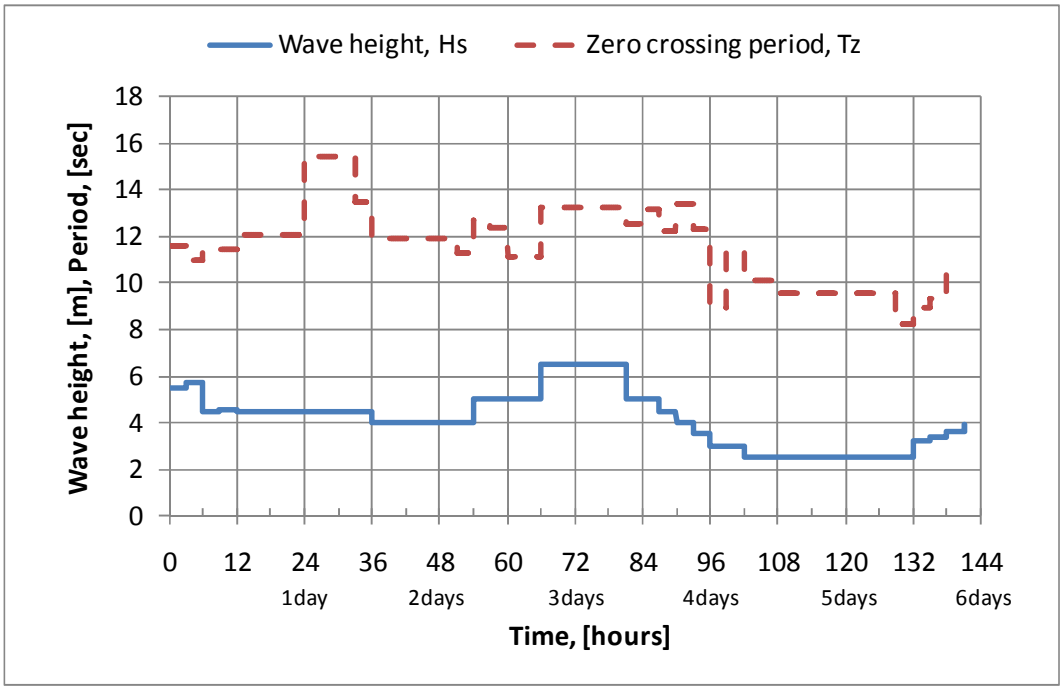

Figure 6-16: Wave data from *Prestige* accident report by Bahamas Maritime Authority (2004)

The dynamic wave bending moments in hogging and sagging under intact and damaged condition are calculated at the damaged section and shown in Figure 6-17 in succession to the given wave data (Figure 6-16).

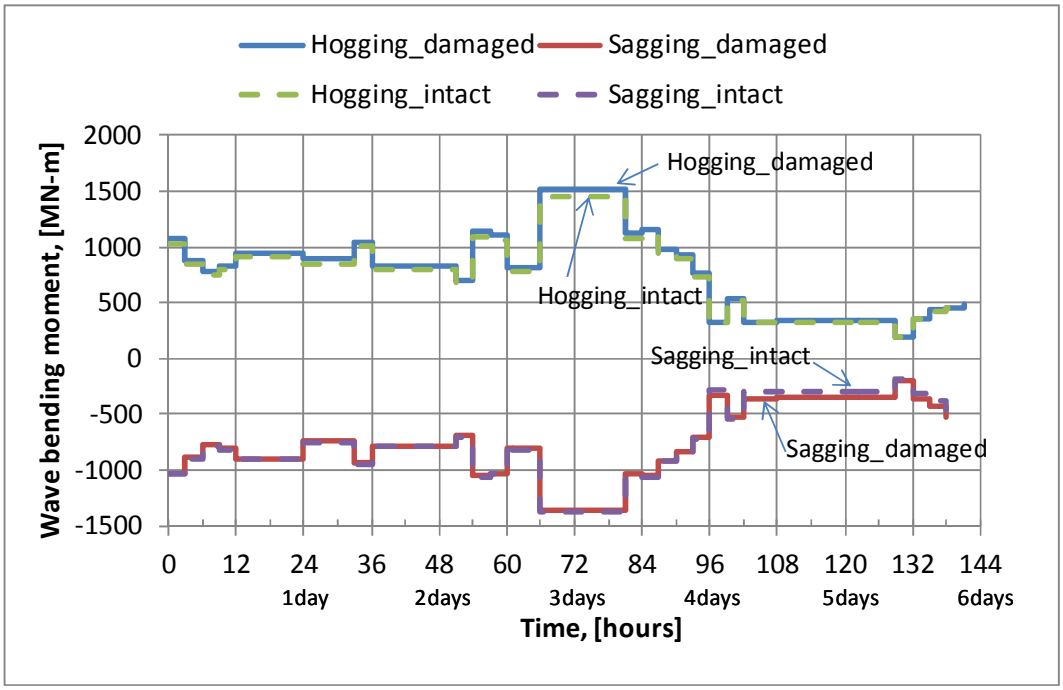

Figure 6-17: Wave induced dynamic bending moments in the fully loaded condition

6.4.5 Damage propagation

With the SIF curve and the variation of the wave bending moment over time, the damage propagation analysis of the bottom damage case is carried out in accordance with the proposed crack growth model that is recalled in Equation (6-9).

$$\frac{da}{dN} = C \times \left(\Delta K_{eff} - \Delta K_{th}\right)^{m} \times \left[1 + \frac{\Delta K_{eff}}{K_C - K_{max}}\right] \quad \textbf{(6-9)}$$

The coefficients of C and m are decided based on the properties of the plate material in which crack tip is located. Adopting the plane strain fracture toughness as K_{IC} = 140 MPa$\sqrt{\text{m}}$ and the threshold range of SIF as ΔK_{th0} = 2.45 MPa$\sqrt{\text{m}}$, the fracture toughness of the corresponding bottom plate is determined and the coefficients for the crack growth model are also obtained as explained in section 4.2.2 and 4.2.4, respectively.

Adopting a zero-crack propagation rate in the region below the threshold range of SIF and 1.0 mm/cycle and 2.0 mm/cycle of crack propagation rates in the region above the material's fracture toughness, the outcome of the damage propagation analysis for the bottom damage case is shown in Figure 6-18. The stable region of the damage followed by an interval of rapid growth and instability has been verified by salvage experts, the advice of which has been sought by the author: the combination of the two phases has been repeatedly observed in salvage situations and indicates that the proposed methodology complies with physical observations.

The uncertainty associated to the characteristics of the material properties e.g. K_{IC}, ΔK_{th0} as well as their effect on the unstable crack propagation rate are further analysed through a sensitivity analysis in Chapter 7.

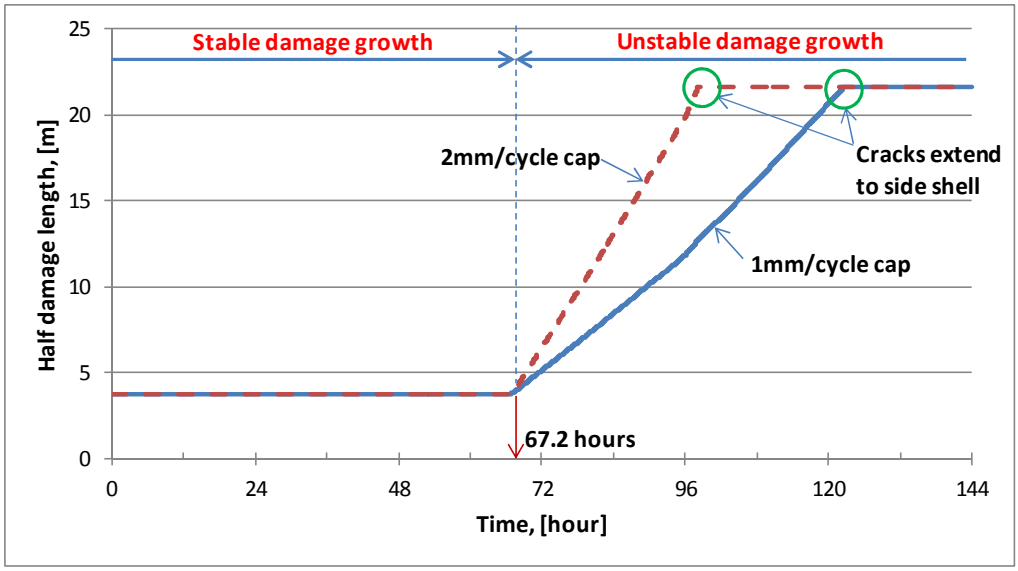

Figure 6-18: Damage propagation against time in the bottom damage case

It is found that the damage propagation starts to increase in an unstable manner just after 67 hours (Figure 6-19) when the maximum SIF, K_{max}, exceeds the material's fracture toughness, K_C = 141.89 MPa$\sqrt{m}$. Although the maximum SIF drops to the material toughness value (circled region) as the crack tip enters the first stiffener's constraint zone, it recovers soon just after the crack passes the stiffener location, after which the maximum SIF stays above the material toughness limit with the given wave data.

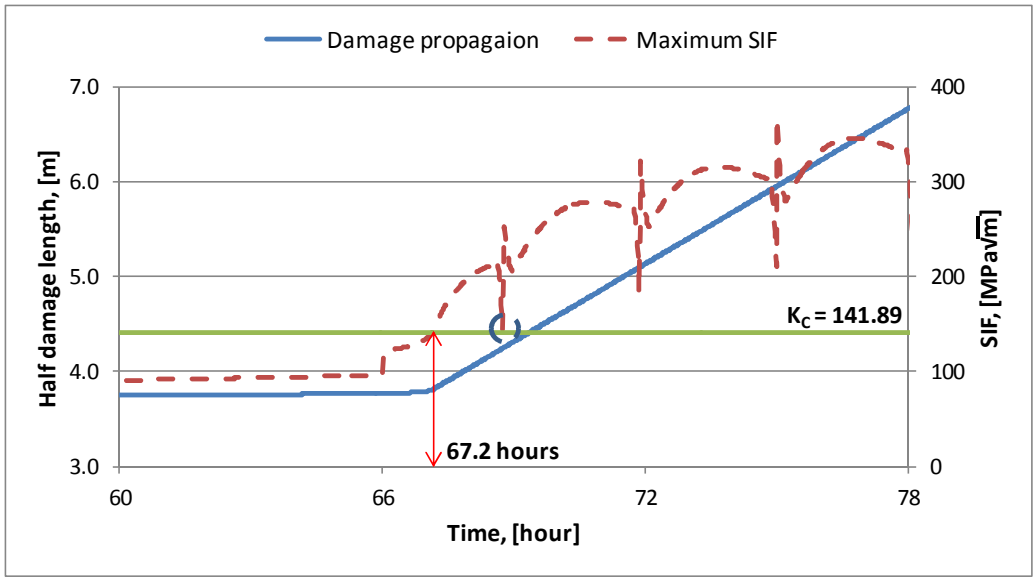

Figure 6-19: Damage propagation and maximum SIF at the moment of unstable damage propagation in bottom damage case

It should be noted in this bottom damage case that the damage propagation in the bottom and side shell plates is considered with the possible initial damage to the bottom girders. Any damage propagation to the centreline bulkhead and to the inner bottom plate is not taken into account at this stage of development.

6.4.6 Residual strength

The residual strength of the damaged ship is calculated by taking into consideration the damage extent for every time step including the initial damage condition. Also, the ultimate strength of the tanker for intact condition is calculated for comparison purposes.

Figure 6-20 shows the damage extent as a function of time from the damage propagation results where 1.0 mm/cycle of crack growth rate is applied in the region above the material's fracture toughness. Based on this, the resultant ultimate residual strength of the damaged section is identified from a series of moment-curvature curves (Figure 6-21) and shown in Figure 6-22, in which rapid strength degradation starts after around the third day from the initial damage. This reflects that the unstable damage propagation triggers structural degradation in the damaged section.

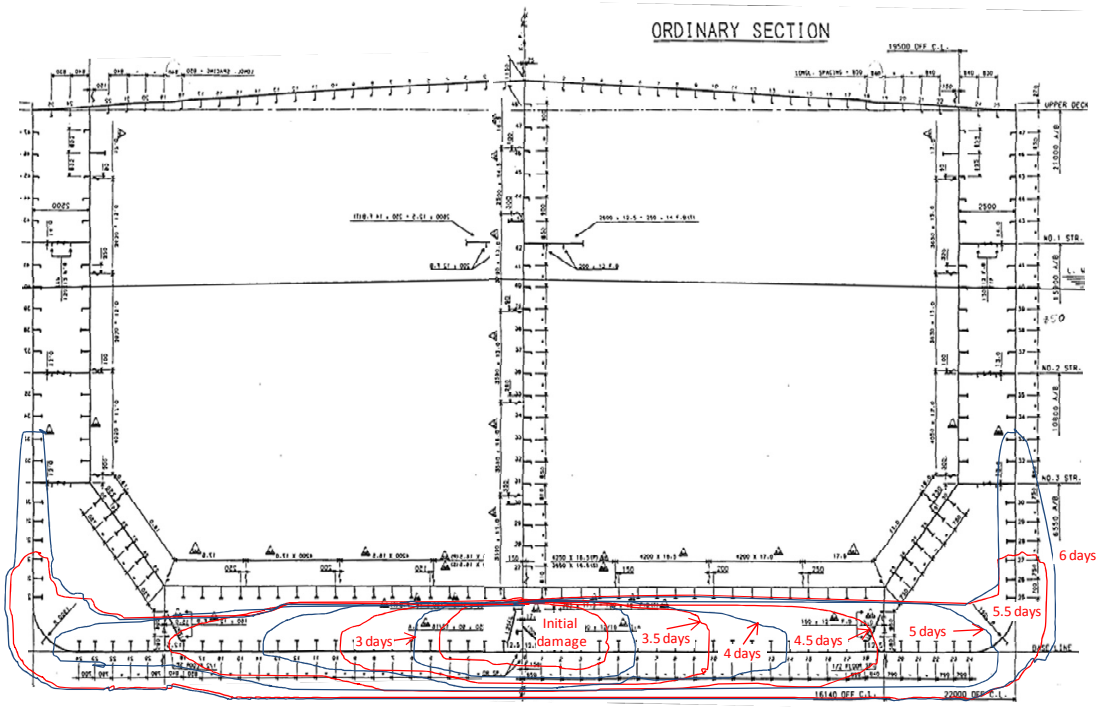

Figure 6-20: Change of damage extents of the bottom damage case (1.0 mm/cycle)

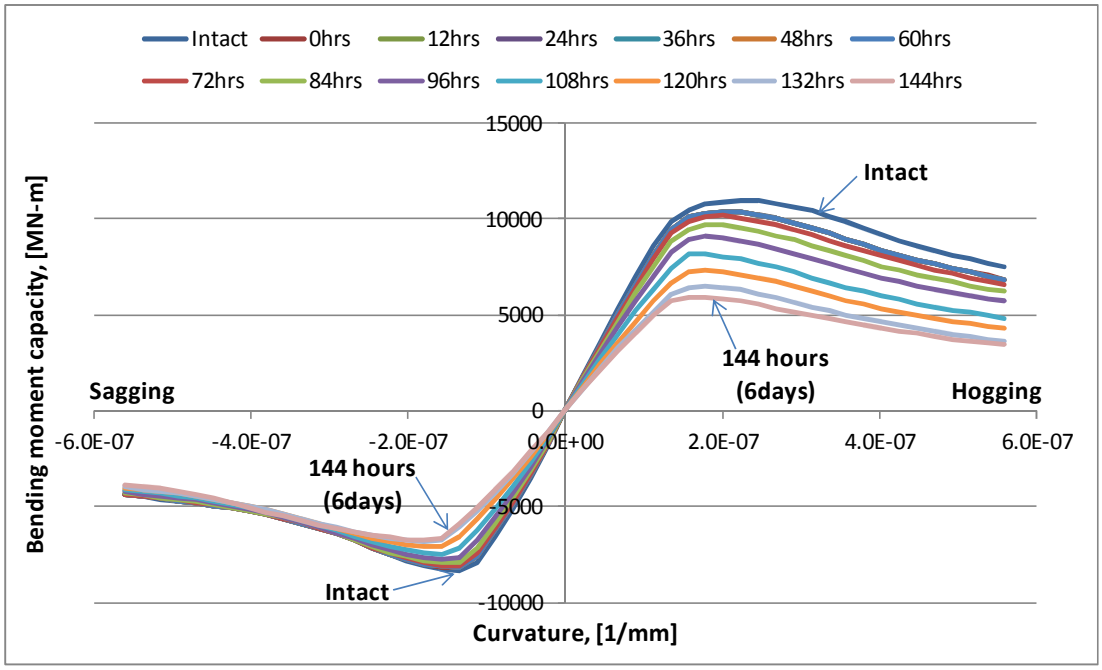

Figure 6-21: Change of moment-curvature curves for the bottom damage case (1.0 mm/cycle)

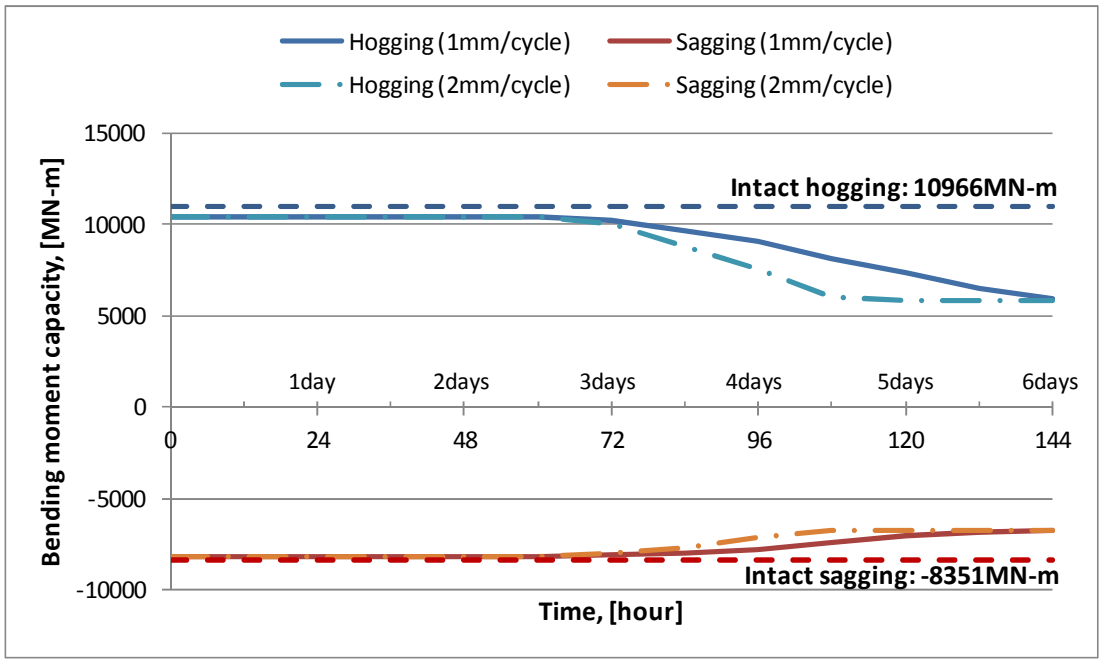

Figure 6-22: Change of the ultimate bending capacity in the bottom damage case

Table 6-4: Summary of ultimate bending capacity in the bottom damage case (1.0 mm/cycle)

Capacity	Hogging		Sagging	
	BM (MN-m)	Diff. (%)	BM (MN-m)	Diff. (%)
Intact condition	10966.1	-	-8350.1	-
Initial damage	10398.9	- 5.17	-8186.8	-1.97
1 day later	10308.5	-5.18	-8186.3	-1.97
2 days later	10398.0	-5.18	-8185.6	-1.98
3 days later	10190.2	-7.08	-8101.8	-2.98
3.5 days later	9687.9	-11.66	-7955.1	-4.74
4 days later	9105.1	-16.97	-7776.4	-6.88
4.5 days later	8147.8	-25.70	-7472.7	-10.52
5 days later	7324.4	-33.21	-7083.1	-15.18
5.5 days later	6465.8	-41.04	-6861.2	-17.84
6 days later	5906.3	-46.14	-6760.2	-19.05

From the summary of the ultimate bending capacity (Table 6-4) of the Aframax tanker having the initial bottom damage, it is found that the hogging bending capacity is reduced by about 46.1% and the sagging bending capacity is degraded by about 19.1% 6 days after the initial damage. It should be noted that the final reduction of the ultimate residual strength is strongly dependent on the extent of damage which, in turn, depends on the rate of crack growth in the region above the material's fracture toughness (Figure 6-18). That is, if the damage propagates with a rate of 2.0 mm/cycle in the region beyond the material's fracture toughness, it would take less than 5 days rather than 6 days for the residual strength of the damaged section to decrease by the same amount in hogging and sagging bending capacity.

Quite evidently, the higher is the damage propagation rate, the faster the strength capacity is reduced. This constitutes yet another element of uncertainty which should be investigated. Nevertheless, in this particular case, it should be noted that the onset of the unstable damage propagation is independent of the maximum crack growth rate triggering the rapid reduction of the residual strength of the damaged ship (Figure 6-22) hence, it should be considered as a critical point for the evaluation of the damage propagation.

6.5 Deck and side damage

6.5.1 Damage description

The extent and location of the collision damage are defined according to ABS (1995). That is, the location of the damaged side structure due to a collision accident is considered to be in the most unfavourable location anywhere on the freeboard between 0.15L aft from F.P. and 0.2L forward from A.P. Also the damage is assumed to be located at the upper part of the side shell, down from (and including) the stringer plate of the strength deck. The extent of the collision damage is considered to include stringers attached to the damaged side shell plating to a certain width as well as side shell plating and the attached stiffeners. The structural members assumed to be damaged and excluded completely or partially according to ABS (1995) are explained in Table 6-5 and sketched in Figure 6-23.

Table 6-5: Guideline on the collision damage extent and its application in the case study

ABS guideline (1995)	Selected values for damage extent
• Side shell plating for the vertical extent of 4 m or $D_{hull}/4$, whichever is greater, down from the upper edge of the shear strake, where D_{hull} is the ship depth	• Height of damage at side shell: 4.98 m
• Strength of deck plating including the stringer plate extending from the side shell to the inner skin • Side stringers and platforms, within the damaged zone extending for 75% of the double side width	• Width of damage at upper deck: 2.38 m
• All deck and side longitudinal and longitudinal stiffeners attached to the damaged plating	• 5 stiffeners on the upper side shell and 2 stiffeners on the upper deck

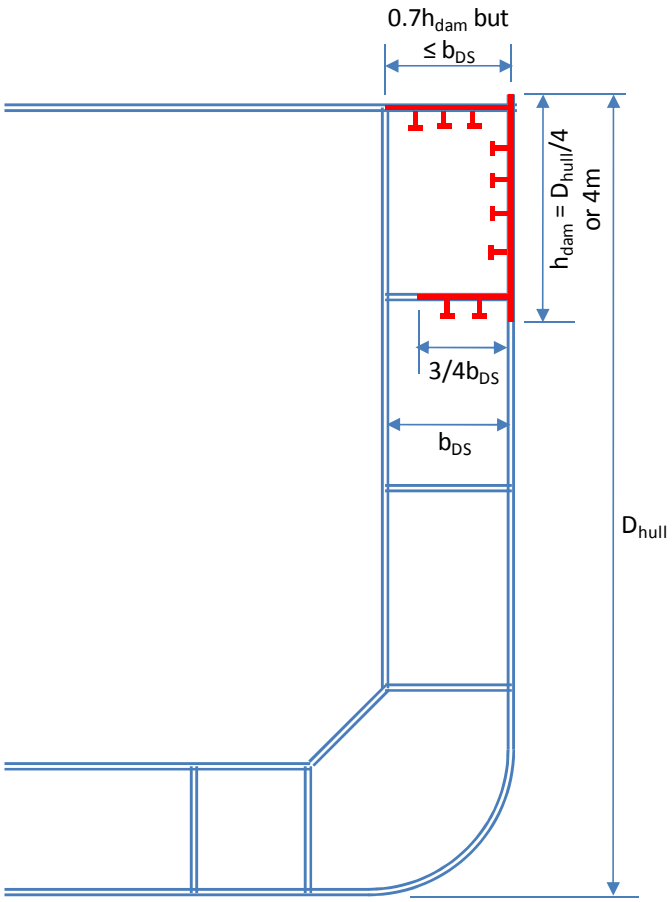

Figure 6-23: Extent of damage due to collision accident, ABS (1995)

In this analysis, the damage due to a collision accident is assumed to be located at the top side shell of the struck ship within No. 4 water ballast tank. The damage extent includes the upper parts of the side shell and edge parts of the deck structure in the double side region. The depth and width of the damage are defined according to the ABS guideline but limited so as the initial cracks do not cross the first barrier of plating: the inner skin and the No.1 stringer (Table 6-5). The length of the damage is assumed to be two frame spaces, 7.56 m, which results in elliptical damage openings at both sides.

Initial cracks are assumed to be emanating from the edges of the opening towards the deck and side shell so that the vertical bending moment from wave loads allows the cracks to propagate. The initial length of crack (a_0) is assumed to be 1.0% of the openings' radii, i.e. 23.8 mm and 49.8 mm at the edge of damage on deck and side shell plate, respectively. The effect of difference in the initial damage condition is

discussed in the next chapter. A 3D sketch of the damage opening is shown in Figure 6-24, where a set of two semi-elliptical openings are considered as damage shapes in deck and side structures.

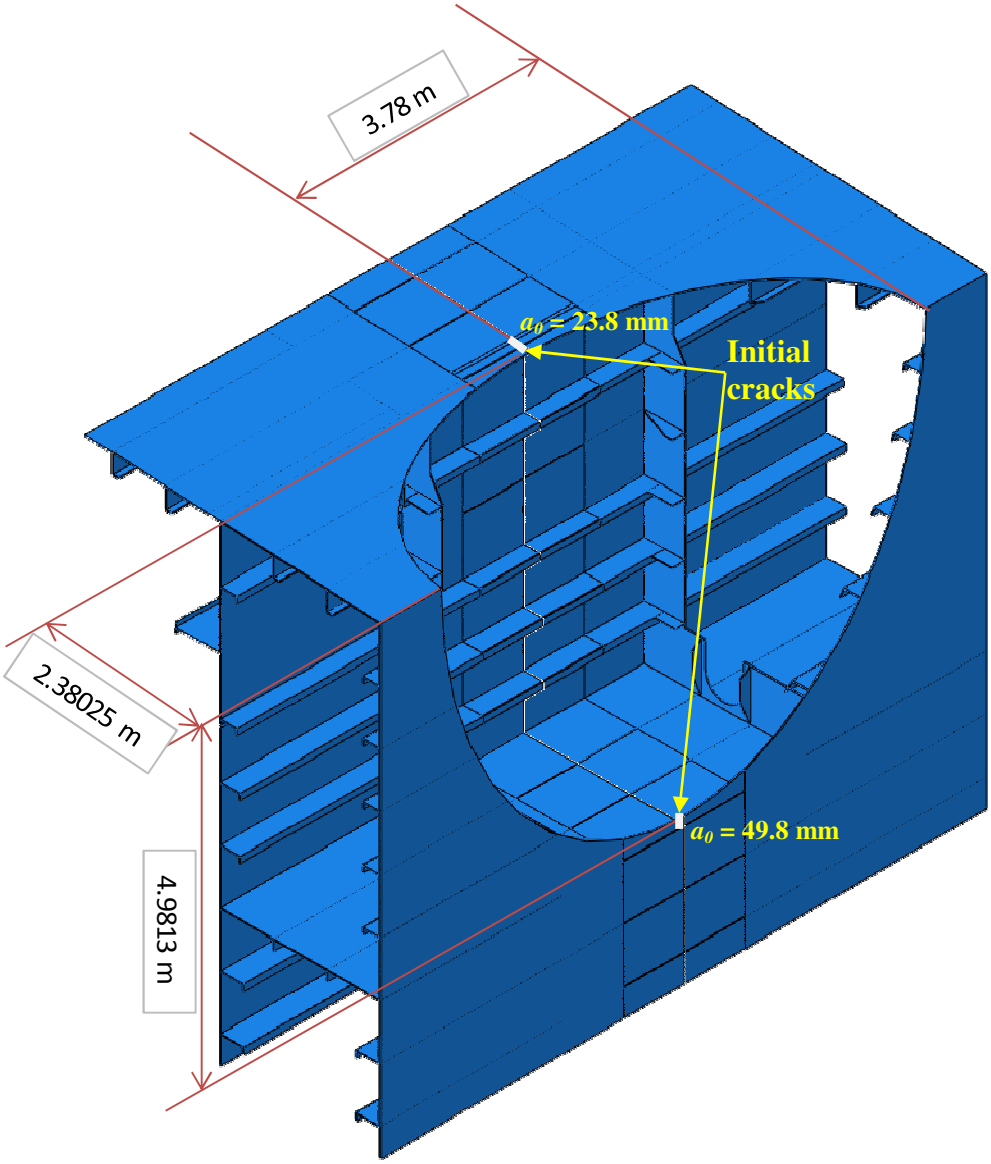

Figure 6-24: Sketch of the damage opening for the deck and side damage case

6.5.2 FE model and SIF calculation

The approach adopted for generating the FE model for this case is the same as for the bottom case. A model of three cargo hold tanks is prepared mainly using shell and beam elements while 3D solid elements are deployed around the damage opening. Also the shell-to-solid coupling as well as the surface contact is applied in the model, which is shown in Figure 6-25.

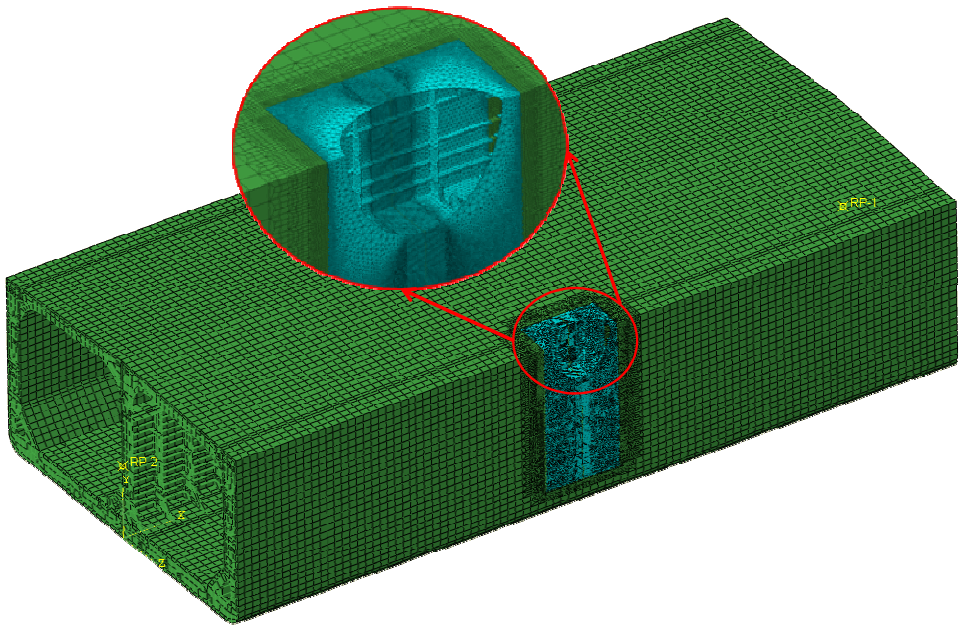

Figure 6-25: FE model for the deck and side shell damage case

A set of reference points are defined at the junction of the neutral axis and the centre line of each end section and multi-points constraints are applied to link the reference point and each end section. Boundary conditions are applied in the same way as for the bottom damage case. A pair of unit vertical bending moments (1.0 MN-m) is applied at the reference points but a hogging moment is induced so that tensile stresses are resulted in the damaged area (Figure 6-26).

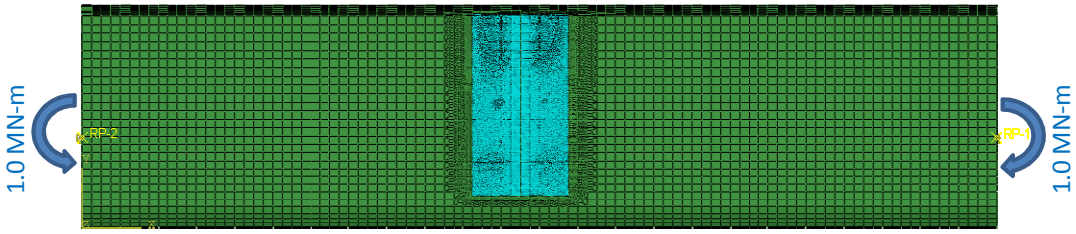

Figure 6-26: Application of vertical hogging unit bending moment

Through a series of FE analysis, a set of SIF curves against the damage size are obtained for cracks on the deck and side shell plating as shown in Figure 6-27. The higher value of the SIF on the deck plating, despite the fact that it is the smaller part of the initial damage, is attributed to the higher level of the bending stress at the crack tip of the deck plating.

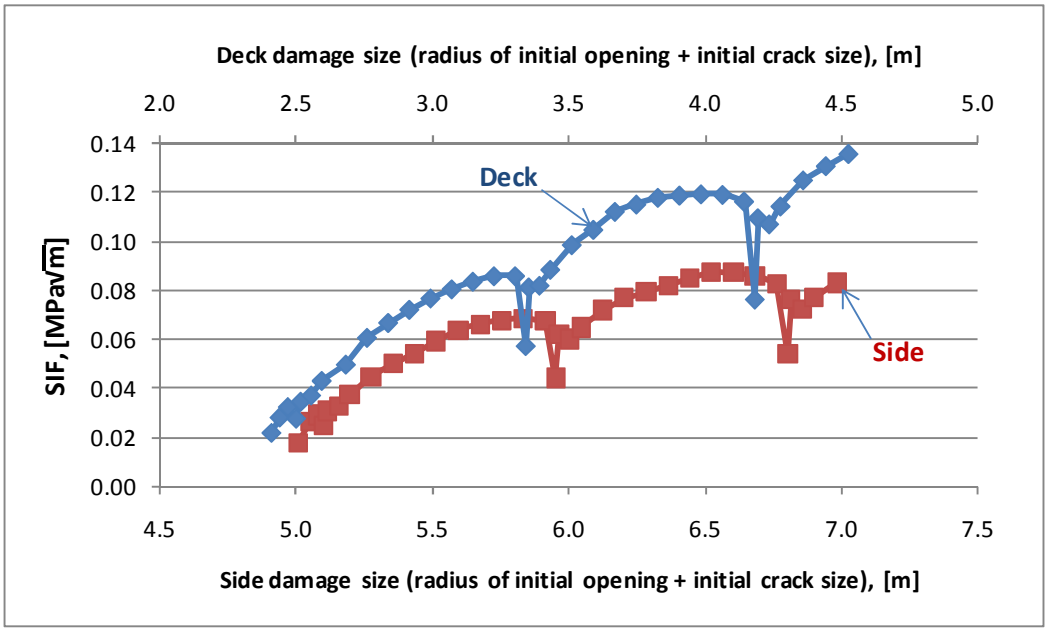

Figure 6-27: SIF curves calculated by VCCT

6.5.3 Knowledge-intensive (parametric) model

In the preparation of a parametric model for the deck and side damage case, three correction factors are taken into account and combined due to the configuration of the damage (Figure 6-24).

L-shaped plate

As the damage has taken place at the joint of the deck plate and the side shell plate, the effect of the joint structure is required to be included. Considering that deck plate and side shell plate are finite in size, the correction factor for the L-shaped finite width plate is determined by Equation (6-10), where the behaviour of cracks is expressed as a single edge crack in a plate of finite width, of which correction factor is available in handbooks e.g. Tada, Paris and Irwin (2000) with an additional correction factor for the asymmetric effect of the crack.

$$Y_{L-shape,finite\ width} = Y_{edge,finite\ width} \times Y_{L-shape,asymmetry} \quad \textbf{(6-10)}$$

where, $Y_{edge,finite\ width} = \sqrt{\frac{2B}{\pi a} tan \frac{\pi a}{2B}} \cdot \frac{0.752+2.02\left(\frac{a}{B}\right)+0.37\left(1-sin\frac{\pi a}{2B}\right)^3}{cos\frac{\pi a}{2B}}$

$$Y_{L-shape,asymmetry}\left(\frac{a_i}{a_j}, \frac{a_i}{B_i}\right) = \left[B_{0,i} + B_{1,i}X_i + B_{2,i}{X_i}^2 + B_{3,i}{X_i}^3\right]^{(-B_i/a_i)}$$

$$Y_{L-shape,asymmetry}\left(\frac{a_i}{a_j},\frac{a_j}{B_j}\right)=\left[B_{0,j}+B_{1,j}X_j+B_{2,j}{X_j}^2+B_{3,j}{X_j}^3\right]^{(B_j/a_j)}$$

$$X_i=\left(\frac{a_i}{a_j}\right)^{a_i/B_i},\ X_j=\left(\frac{a_i}{a_j}\right)^{a_j/B_j}$$

$$\begin{cases}B_{0,i}=0\\ B_{1,i}=9104.5\left(\frac{a_i}{B_i}\right)^3-1878.2\left(\frac{a_i}{B_i}\right)^2+121.75\left(\frac{a_i}{B_i}\right)-1.566\\ B_{2,i}=-18380\left(\frac{a_i}{B_i}\right)^3+3779.2\left(\frac{a_i}{B_i}\right)^2-244.57\left(\frac{a_i}{B_i}\right)+5.8217\\ B_{3,i}=9276\left(\frac{a_i}{B_i}\right)^3-1900.9\left(\frac{a_i}{B_i}\right)^2+122.81\left(\frac{a_i}{B_i}\right)-3.2558\end{cases}\ for\ \frac{a_i}{B_i}<0.1$$

$$\begin{cases}B_{0,i}=229.89\left(\frac{a_i}{B_i}\right)^3-163.81\left(\frac{a_i}{B_i}\right)^2+38.353\left(\frac{a_i}{B_i}\right)-1.3478\\ B_{1,i}=-746.48\left(\frac{a_i}{B_i}\right)^3+529.54\left(\frac{a_i}{B_i}\right)^2-125.25\left(\frac{a_i}{B_i}\right)+5.3884\\ B_{2,i}=808.25\left(\frac{a_i}{B_i}\right)^3-574.95\left(\frac{a_i}{B_i}\right)^2+135.88\left(\frac{a_i}{B_i}\right)-4.0465\\ B_{3,i}=-291.68\left(\frac{a_i}{B_i}\right)^3+209.24\left(\frac{a_i}{B_i}\right)^2-48.992\left(\frac{a_i}{B_i}\right)+1.0063\end{cases}\ for\ \frac{a_i}{B_i}\geq 0.1$$

$$\begin{cases}B_{0,j}=355.17\left(\frac{a_j}{B_j}\right)^3-272.22\left(\frac{a_j}{B_j}\right)^2+67.581\left(\frac{a_j}{B_j}\right)-4.5513\\ B_{1,j}=-1201.1\left(\frac{a_j}{B_j}\right)^3+925.17\left(\frac{a_j}{B_j}\right)^2-235.05\left(\frac{a_j}{B_j}\right)+19.623\\ B_{2,j}=1338.3\left(\frac{a_j}{B_j}\right)^3-1039.6\left(\frac{a_j}{B_j}\right)^2+268.08\left(\frac{a_j}{B_j}\right)-23.062\\ B_{3,j}=-492.8\left(\frac{a_j}{B_j}\right)^3+386.96\left(\frac{a_j}{B_j}\right)^2-100.68\left(\frac{a_j}{B_j}\right)+8.9951\end{cases}\ for\ \frac{a_j}{B_j}<0.3$$

$$\begin{cases}B_{0,j}=-1.5482\left(\frac{a_j}{B_j}\right)+1.2866\\ B_{1,j}=1.72\left(\frac{a_j}{B_j}\right)^2-0.3642\left(\frac{a_j}{B_j}\right)-0.1123\\ B_{2,j}=-13.546\left(\frac{a_j}{B_j}\right)^3+9.812\left(\frac{a_j}{B_j}\right)^2-2.0921\left(\frac{a_j}{B_j}\right)+0.0542\\ B_{3,j}=10.501\left(\frac{a_j}{B_j}\right)^3-7.0809\left(\frac{a_j}{B_j}\right)^2+1.8924\left(\frac{a_j}{B_j}\right)+0.0941\end{cases}\ for\ 0.3\leq\frac{a_j}{B_j}\leq 0.85$$

a_i and a_j are the sizes of the shorter and longer cracks respectively

B_i and B_j are the width of plates correspond to cracks of a_i and a_j respectively

Elliptical opening

As the opening of the damage is not circular but elliptical both in deck and side shell plating and the response of a crack in an L-shaped plate can be substituted by that of edge crack in a plate, the correction factor for elliptical openings in an L-shaped plate is expressed again in Equation (6-11), which is valid in the range $0.25 \leq b/c \leq 4.0$.

$$Y_{elliptical\ |\ edge,finite\ width} = \begin{cases} Y_{e,edge,1} \Big/ s_{e,edge}^{\left(\frac{b}{c}\right)}, for\ s_{e,edge} < 0.8 \\ 1.0 \qquad\qquad\qquad\quad , for\ s_{e,edge} \geq 0.8 \end{cases} \tag{6-11}$$

where, $Y_{e,edge,1} = 1 - exp[-exp\{C_0 + C_1 X' + C_2 X'^2 + C_3 X'^3\}]$

$$X' = ln\ (s_{e,edge})$$

$$s_{e,edge} = a_0/a = a_0/(c + a_0)$$

$$\begin{cases} C_0 = -0.0026\left(\frac{b}{c}\right)^3 + 0.0326\left(\frac{b}{c}\right)^2 - 0.2053\left(\frac{b}{c}\right) + 0.7585 \\ C_1 = 1.349 \times \left(\frac{b}{c}\right)^{0.8574} \\ C_2 = C_3 = 0 \end{cases} for\ s_{e,edge}^{\left(\frac{b}{c}\right)} < 1 - exp\ (-1)$$

$$\begin{cases} C_0 = -0.1688\left(\frac{b}{c}\right)^3 + 0.4396\left(\frac{b}{c}\right)^2 - 0.6476\left(\frac{b}{c}\right) + 1.5942 \\ C_1 = -0.6173\left(\frac{b}{c}\right)^3 - 0.701\left(\frac{b}{c}\right)^2 + 4.6115\left(\frac{b}{c}\right) + 0.857 \\ C_2 = -6.1284\left(\frac{b}{c}\right)^3 + 9.4447\left(\frac{b}{c}\right)^2 + 0.5573\left(\frac{b}{c}\right) + 0.497 \\ C_3 = -9.5623\left(\frac{b}{c}\right)^3 + 17.929\left(\frac{b}{c}\right)^2 - 6.8161\left(\frac{b}{c}\right) + 1.0128 \end{cases} for\ s_{e,edge}^{\left(\frac{b}{c}\right)} \geq 1 - exp\ (-1)$$

b is radius of elliptical opening in the direction perpendicular to crack

c is radius of elliptical opening in the direction parallel to crack

a_0 is the initial crack size

Stiffeners

The correction factor for stiffeners in this damage case is obtained in the same manner as for the bottom damage case. The SIF calculated by FE analyses are divided by other correction factors described above so that the correction factor for stiffeners is obtained as Equation (6-12).

$$Y_{stiffener,FEA} = \frac{SIF_{FEA}}{SIF_0 \times Y_{L-shape,finite\ width} \times Y_{elliptical|edge,finite\ width}} \quad \textbf{(6-12)}$$

where, $SIF_0 = \sigma\sqrt{\pi a}$

σ is the bending stress on the deck and side shell plate, measured at the location of the crack tip for the side shell damage

a is the damage size including opening, $a = a_0 + c$

The results of the above equation are found different between damages in deck and side shell structures. The data extracted from Equation (6-12) are plotted in Figure 6-28 and Figure 6-29 and results of regression analysis are expressed in Equation (6-13) and Equation (6-14) for the deck and side shell stiffeners respectively.

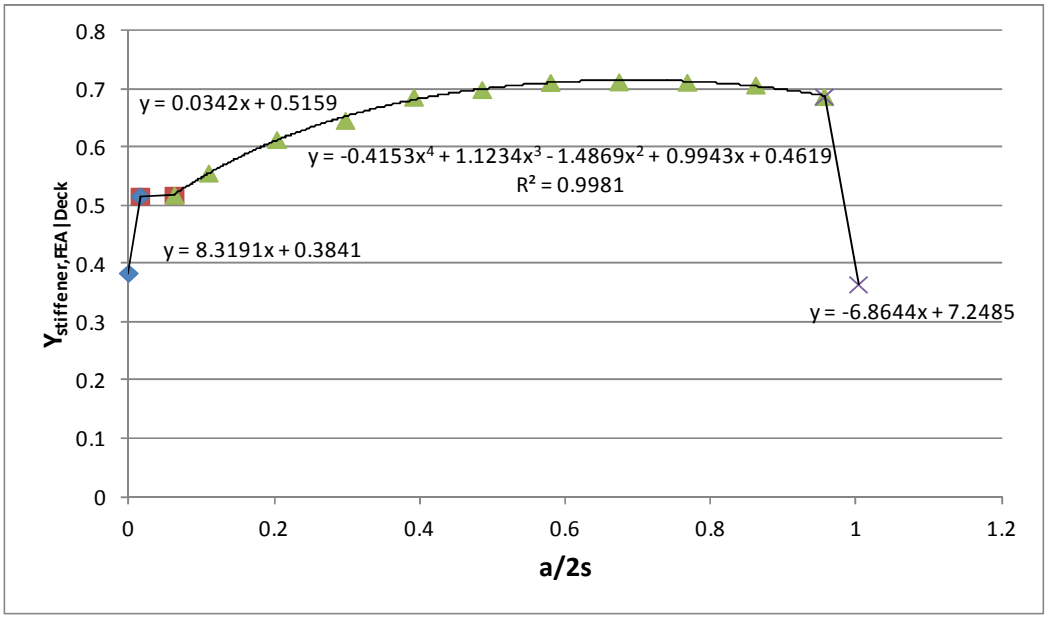

Figure 6-28: Regression analysis for defining $Y_{stifferner,FEA}$ for deck in deck & side damage case

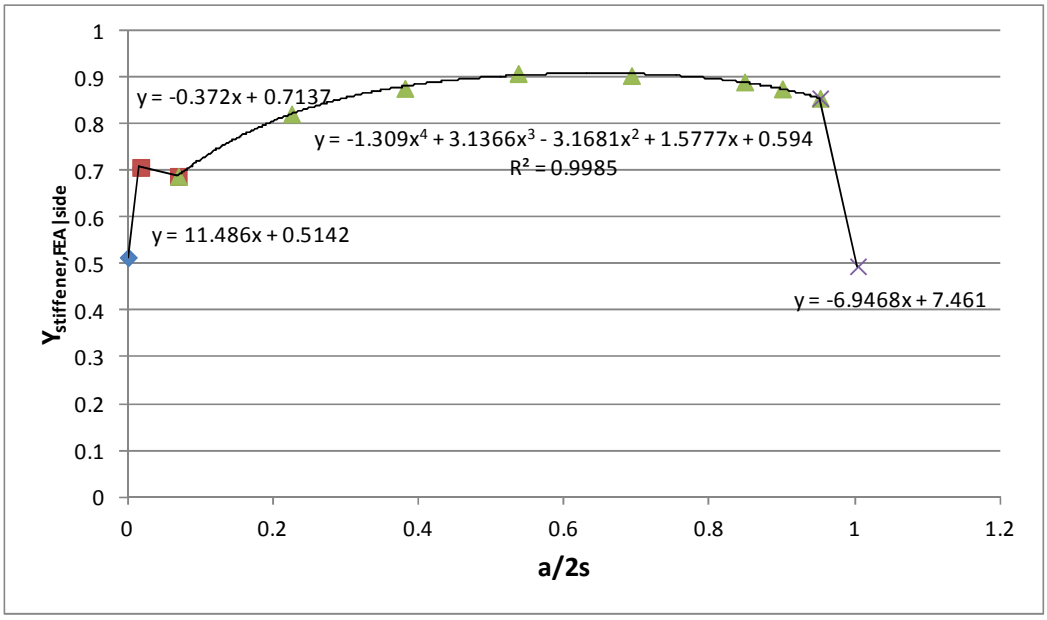

Figure 6-29: Regression analysis for defining $Y_{stifferner,FEA}$ for side in deck & side damage case

$$Y_{stiffener,FEA\,|\,Deck} = \begin{cases} 8.3191\left(\frac{a}{2s}\right) + 0.3841 & ; 0.0 < \frac{a}{2s} \le 0.016 \\ 0.0342\left(\frac{a}{2s}\right) + 0.5159 & ; 0.016 < \frac{a}{2s} \le 0.063 \\ -0.4153\left(\frac{a}{2s}\right)^4 + 1.1234\left(\frac{a}{2s}\right)^3 - 1.4869\left(\frac{a}{2s}\right)^2 + 0.9943\left(\frac{a}{2s}\right) + 0.4619 & ; 0.063 < \frac{a}{2s} \le 0.96 \\ -6.8644\left(\frac{a}{2s}\right) + 7.2485 & ; 0.96 < \frac{a}{2s} \le 1.0 \end{cases} \quad \textbf{(6-13)}$$

$$Y_{stiffener,FEA\,|\,Side} = \begin{cases} 11.486\left(\frac{a}{2s}\right) + 0.5142 & ; 0.0 < \frac{a}{2s} \le 0.017 \\ -0.372\left(\frac{a}{2s}\right) + 0.7137 & ; 0.017 < \frac{a}{2s} \le 0.068 \\ -1.309\left(\frac{a}{2s}\right)^4 + 3.1366\left(\frac{a}{2s}\right)^3 - 3.1681\left(\frac{a}{2s}\right)^2 + 1.5777\left(\frac{a}{2s}\right) + 0.594 & ; 0.068 < \frac{a}{2s} \le 0.95 \\ -6.9468\left(\frac{a}{2s}\right) + 7.461 & ; 0.95 < \frac{a}{2s} \le 1.0 \end{cases} \quad \textbf{(6-14)}$$

where, a is the damage size including opening, $a = a_0 + c$

$2s$ is the stiffener's spacing

Knowledge-intensive (parametric) model of SIFs for deck and side damage case

Reproducing SIF curves of cracks emanating from a damage opening in the deck and side structures is carried out by combining the correction factors obtained above. The parametric models for SIFs are presented in Equation (6-15) and Equation (6-16).

The resultant SIF curves are plotted in Figure 6-30 with discontinuities at the stiffener intervals due to the imposed restraints.

$$SIF_{Deck|\ Deck\ \&\ Side\ dmamge} = SIF_0 \times Y_{L-shape,finite\ width} \times Y_{elliptical|edge,finite\ width} \times Y_{stiffener,FEA|Deck} \quad \textbf{(6-15)}$$

$$SIF_{Side|\ Deck\ \&\ Side\ dmamge} = SIF_0 \times Y_{L-shape,finite\ width} \times Y_{elliptical|edge,finite\ width} \times Y_{stiffener,FEA|Side} \quad \textbf{(6-16)}$$

where, $SIF_0 = \sigma\sqrt{\pi a}$

σ is the bending stress on the deck and side shell plate, measured at the location of the crack tip for the side shell damage

a is the damage size including opening, $a = a_0 + c$

$Y_{L\text{-}shape,\ finite\ width}$, $Y_{elliptical|edge,\ finite\ width}$, $Y_{stiffener,\ FEA|Deck}$ and $Y_{stiffener,\ FEA|Side}$ are defined in Equation (6-10), (6-11), (6-13) and (6-14) respectively

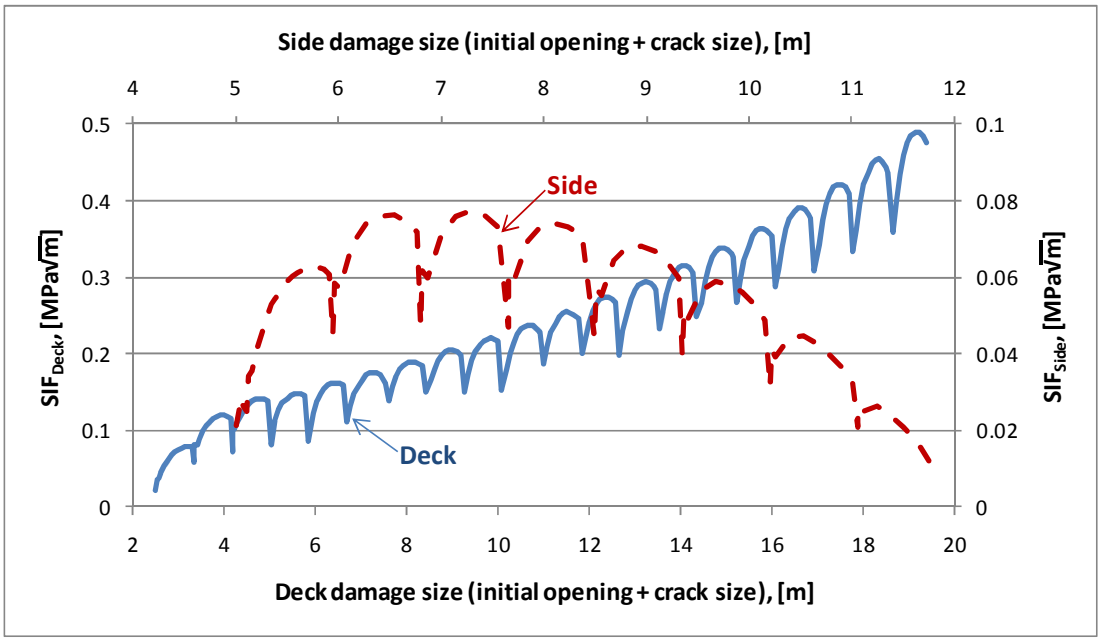

Figure 6-30: SIF curves obtained by the parametric models for side & deck damage case

In the case of side damage, the SIF drops after a short increase from the damage initiation. This can be explained by the decreasing tendency of the bending stress on the side shell plate as the crack tip propagates and approaches the neutral axis of the damaged hull section.

The validity of the parametric models of SIFs in the deck and side damage case is demonstrated through comparison with the SIFs calculated by FEA as plotted in Figure 6-31and Figure 6-32, where a good agreement between two results is identified for each damage crack.

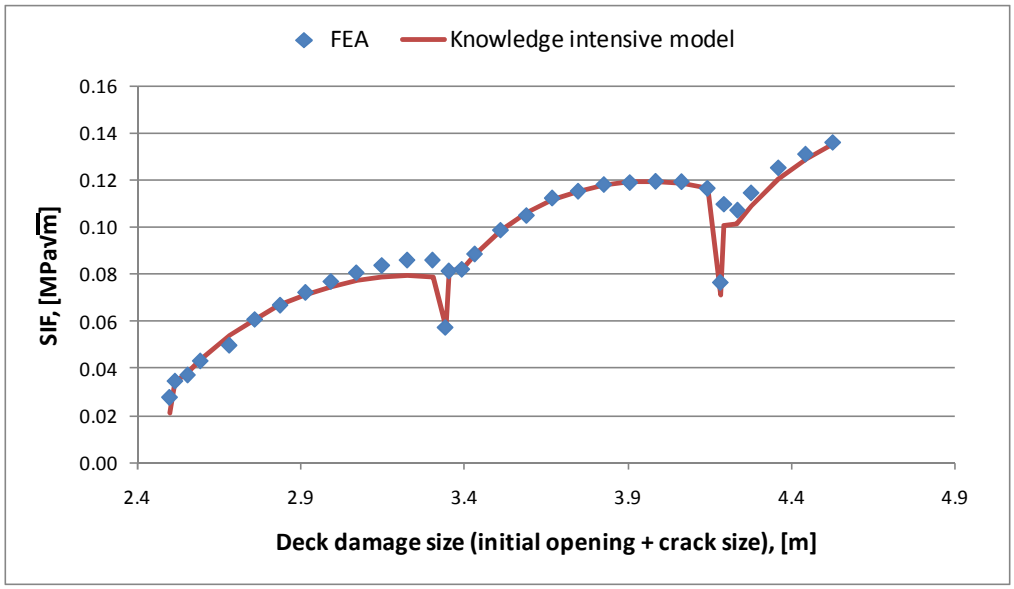

Figure 6-31: Comparison of SIFs between calculated by FEA and estimated by the knowledge-intensive model for deck damage

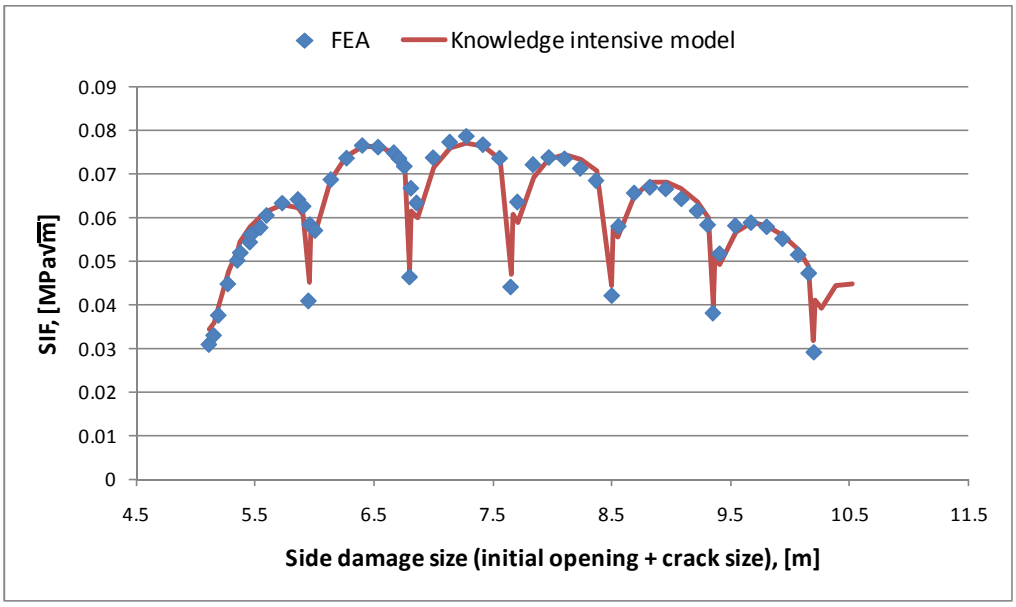

Figure 6-32: Comparison of SIFs between calculated by FEA and estimated by the knowledge-intensive model for side damage

6.5.4 Wave loads

Wave loads are calculated using the same code for the bottom case. A ballast loading condition, in which still water bending moment at the damaged section is 2629 MN-m in hogging is considered. In this damage case, no modification of draft and trim due to initial damage is considered as the damage is initiated above the seawater level. As no flooding is involved, response of the intact condition is used. Response amplitude operators (RAOs) of the wave bending moment in hogging and sagging at the section of damage are calculated under linear regular wave conditions and shown in Figure 6-33.

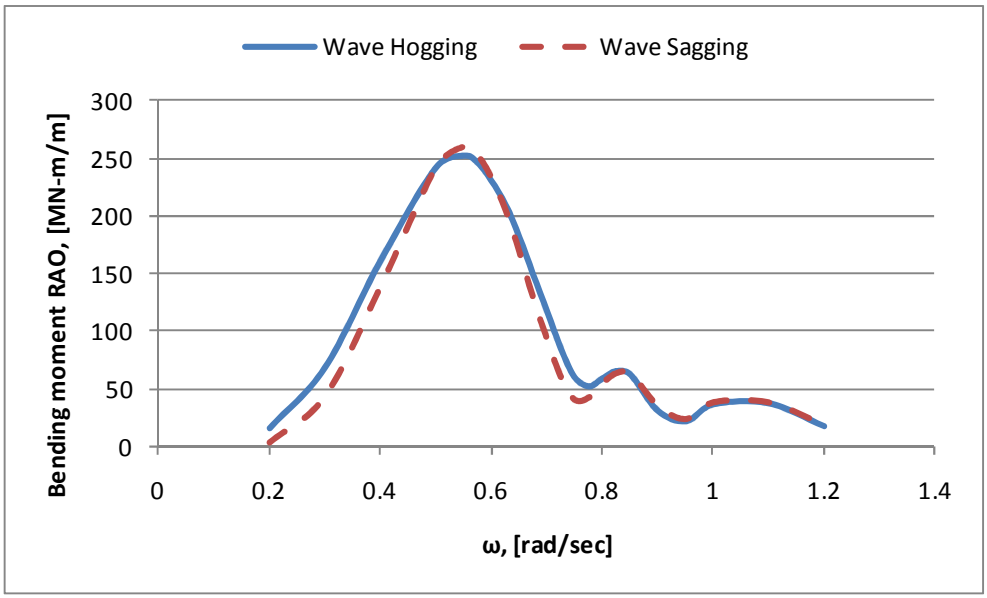

Figure 6-33: Response amplitude operator of wave bending moments in the ballast condition

Applying the same wave data (Figure 6-16) and adopting the same approach used in the bottom damage case, the dynamic wave bending moments are calculated in the time domain and shown in Figure 6-34.

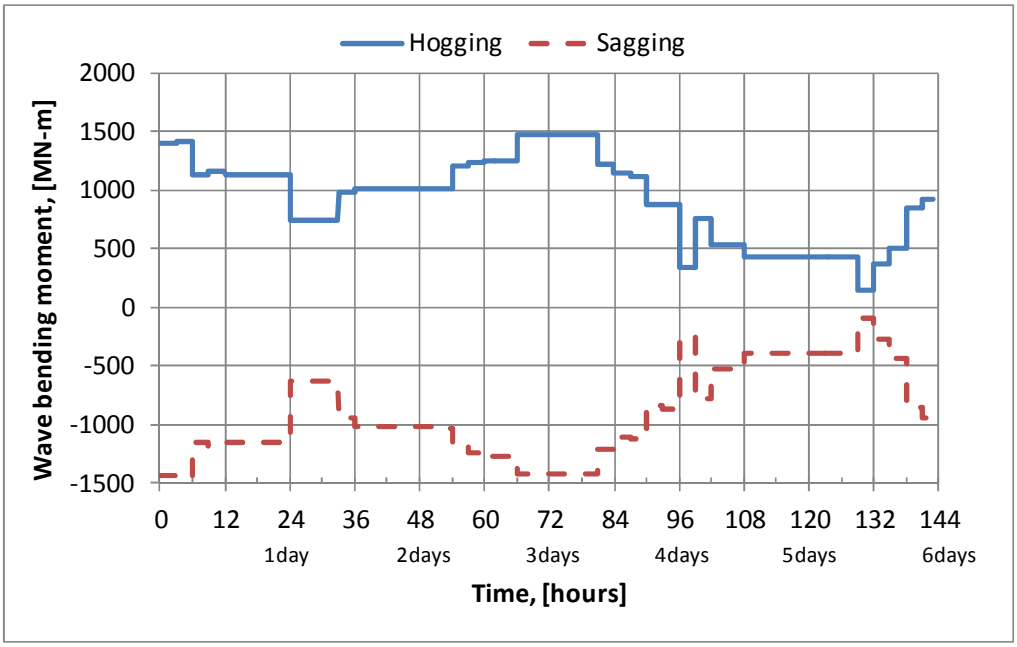

Figure 6-34: Wave induced dynamic bending moments in the ballast condition

6.5.5 Damage propagation

The analysis of the damage propagation of deck and side damage case is carried out using the proposed crack growth model (Equation (6-9)). Also a comparison of damage propagations between crack growth rates of 1.0 mm/cycle and 2.0 mm/cycle in the unstable region is made.

The main difference from the bottom damage case is the asymmetric damage propagations in the deck and the side plate. This comes from the difference in (i) the initial opening and crack sizes, (ii) the different configuration of the adjacent structure, and (iii) the difference of the level of stress on the crack tips induced by the wave loading. Handling of the asymmetric damage propagation in this damage case is based on the correction factor for asymmetric cracks in an L-shaped plate as discussed in the section 4.4.2 and incorporated in the parametric model developed in the section 6.5.3.

Another point of interest that arises during damage propagation in this case is the restraint effects of structural elements other than stiffeners. Damage propagation to the longitudinal bulkhead (LBHD, or inner skin) plate from the initial damage of deck structure and to the stringer plates from the initial damage of side shell structure are such cases.

According to FE result, it is found that the SIF of the newly developed crack in the LBHD plate is very similar with that of the propagating crack in the deck plate when the original crack extends and passes the joint of the two plates. This phenomenon has been observed by Poe (1971) in his fatigue tests of stiffened panels, which has shown that a crack of a stiffener propagates with the same rate of crack propagation as the crack of the plate in a stiffened panel. Then it is observed that each crack behaves similarly but keeps its own propagation rate due to the configuration of the adjacent structure and the stress variation, (Figure 6-35).

A similar behaviour is found in the damage of the side structure. The initiating SIF of the newly developed crack in the stringer No.1 is observed close to that of the crack on the side structure when the joint of two plates is breached by the original crack (Figure 6-36).

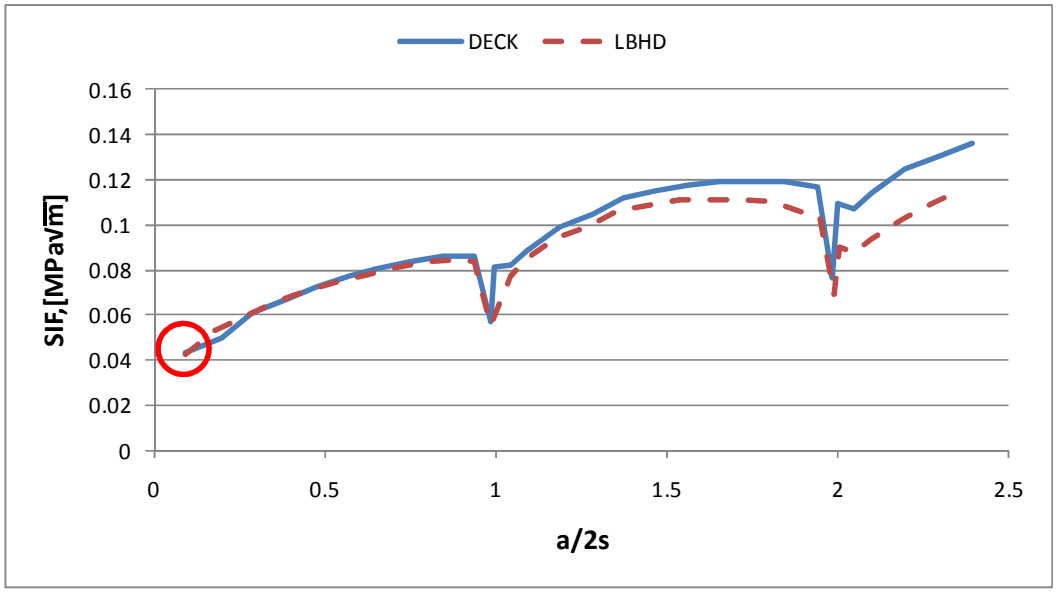

Figure 6-35: Behaviours of cracks after the joint of deck and LBHD is breached

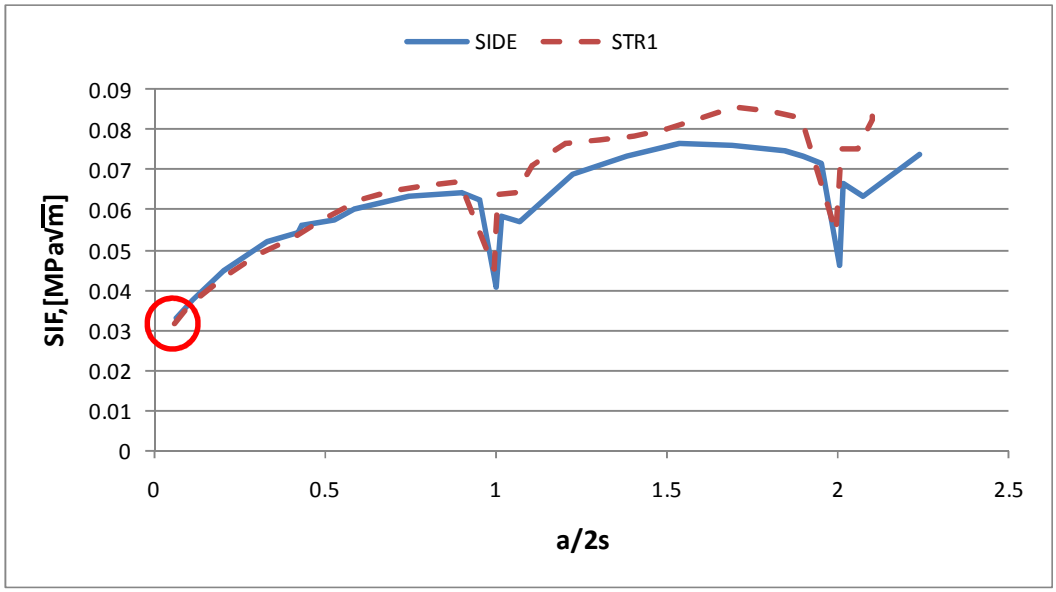

Figure 6-36: Behaviours of cracks after the joint of side shell and stringer No.1 is breached

Hence, the numerical handling of the SIFs of the newly initiated cracks in the LBHD plate and the stringer plate is made to start with the same SIF of cracks in the deck and side shell plates respectively. This is achieved by applying the same configurations of the original damage in the deck and side shell plate to the LBHD and stringer plate respectively. However, the difference in the stiffener arrangement and in the applied stresses induced by the external loading is taken into account for the following development of the SIF of the crack tip in each plate. The same approach is adopted in assessing damage propagations of the centre line bulkhead plate connected to the deck plate and the stringer No.2 plate connected to the side shell plate.

Considering all the major members through which cracks could propagate, the crack growth model of each plate is developed based on the properties of the plate in which the crack tip is located. Using the plane strain fracture toughness and the threshold range of SIF of steel that have been used in the previous damage case, the fracture toughness of each plating member is determined and the coefficients for the corresponding crack growth model are obtained. The results of the damage propagation of all the concerned plates initiated from the deck and side shell damage are shown in Figure 6-37.

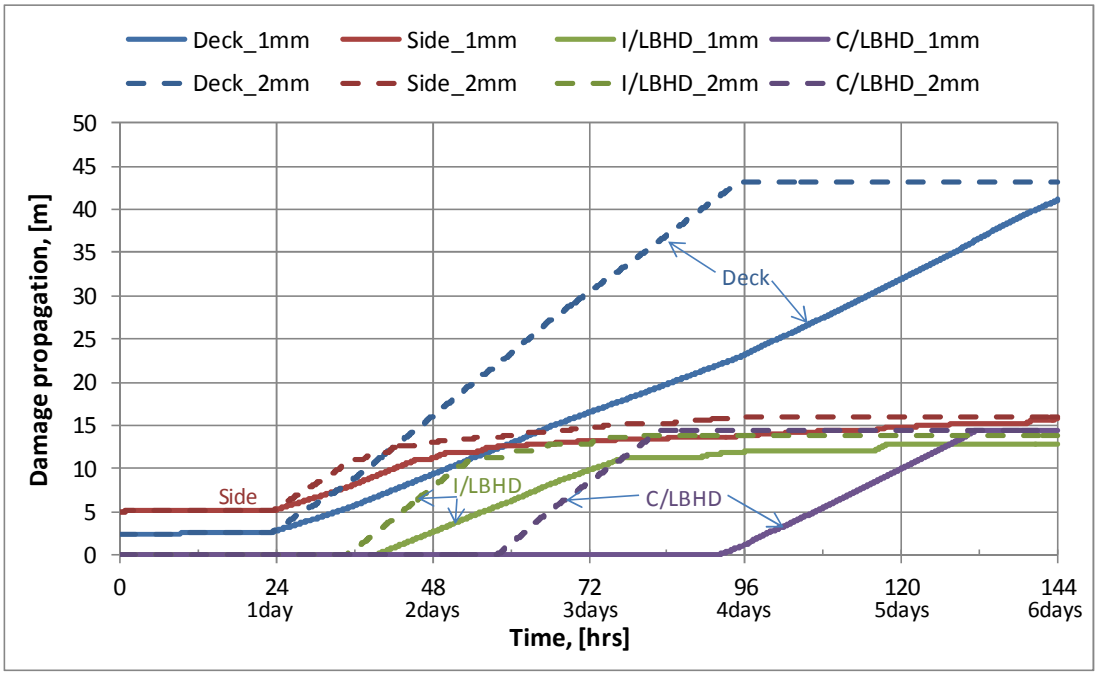

Figure 6-37: Damage propagation against time in the deck &side shell damage case

The variation of the propagation rate results in different required times for each damage to propagate a certain length (or final damage length within a specific time), as opposed to the time required for damage propagation to become unstable. Exception is the inner skin and centre line bulkhead cases, which are strongly dependant on the damage propagation of the deck plate because their damages are not initiated until the deck damage reaches the corresponding joints.

One noticeable point in the damage propagation of this damage case is the behaviour of damage in the side shell, the inner skin and the centre line bulkhead. Their damages start to increase rapidly as their maximum SIFs exceed the material fracture toughness but their damage propagations become more stable later. This phenomenon occurs because the stress levels of the vertical plates decrease as crack tips on them propagate towards the neutral axis of the damaged section, which also descends due to the damage extending in the upper part of the section. This can be identified in Figure 6-38 where the damage propagation, the location of the neutral axis and the crack tip as well as the stress level at the crack tip of the side shell plate are illustrated (1.0 mm/cycle of damage propagation rate is applied). This applies to other vertical plating, e.g. the inner skin and the centre line bulkhead.

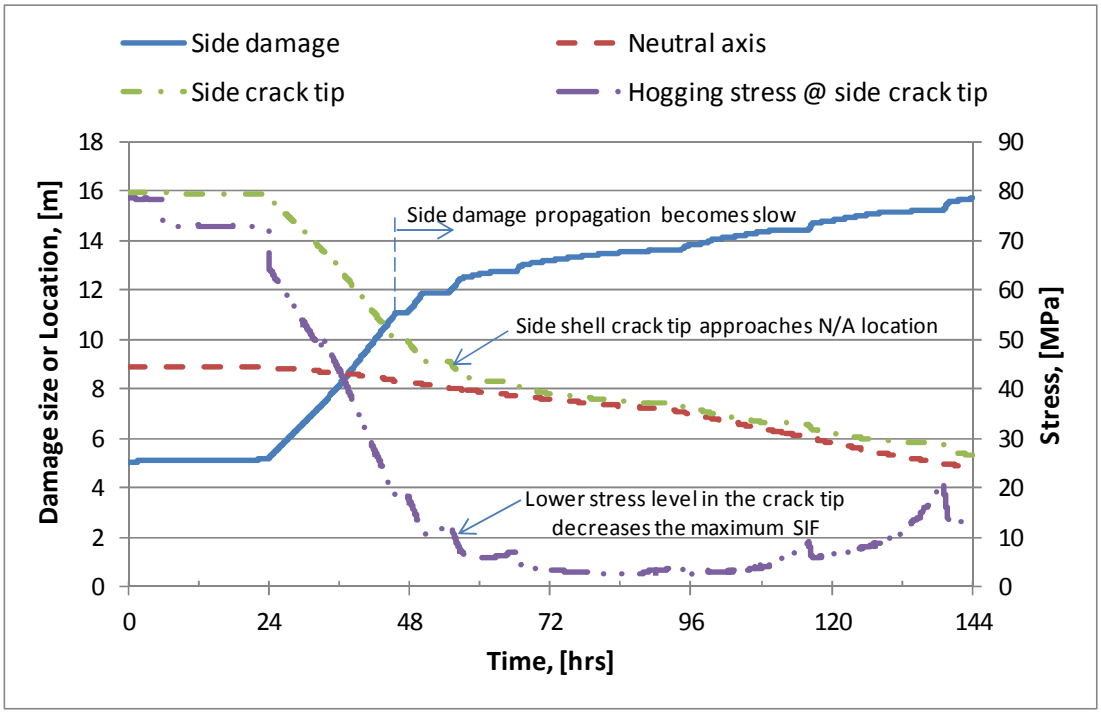

Figure 6-38: Damage propagation of the side shell becomes slow as the crack tip approaches the location of the neutral axis and the bending stress reduces

6.5.6 Residual strength

The residual strength of the damaged ship is calculated by taking into consideration the damage extent at every time step, including the initial damage condition. Also, the ultimate strength of the tanker at the intact condition is obtained for comparison.

Figure 6-39 shows the damage evolution in time base from the damage propagation results where 1.0 mm/cycle of crack growth rate is applied in the region above the material fracture toughness. The resultant ultimate residual strength of the damaged section is identified from a series of moment-curvature curves (Figure 6-40) and shown in Figure 6-41, in which rapid strength degradation starts after the first day of the initial damage.

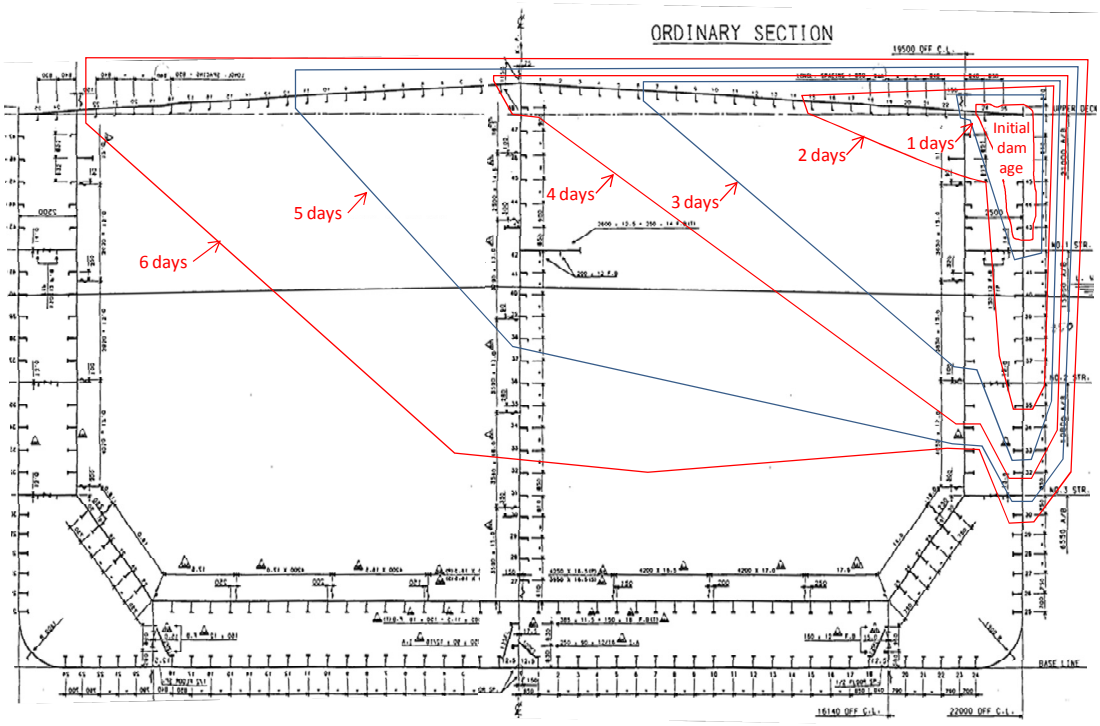

Figure 6-39: Change of damage extents of the deck and side damage case (1.0 mm/cycle)

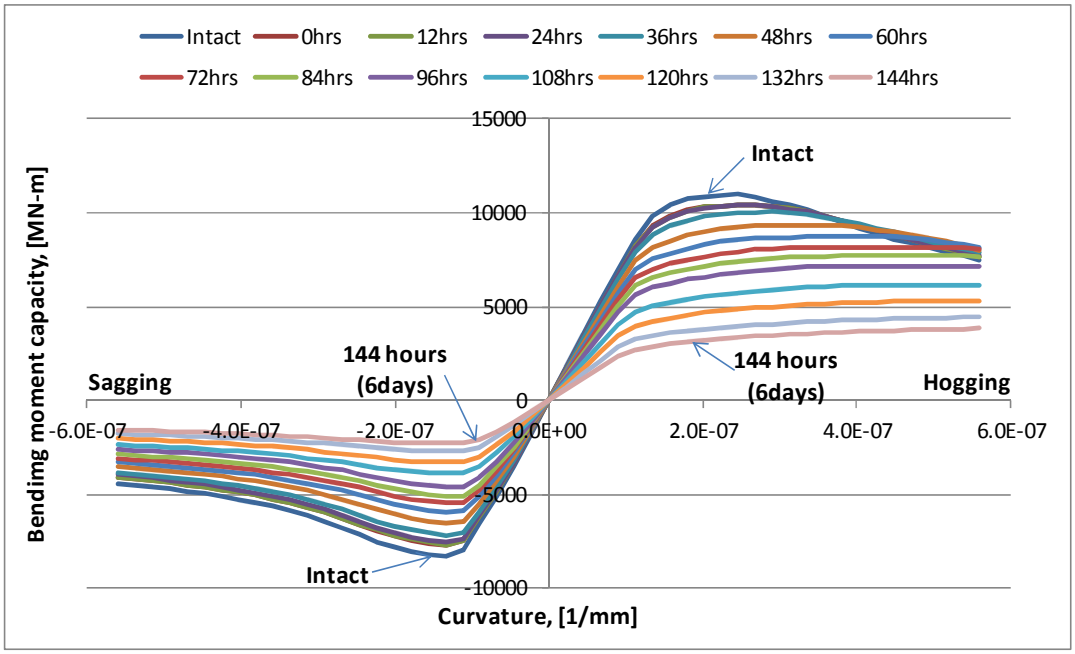

Figure 6-40: Change of moment-curvature curves in the deck and side damage case (1.0 mm/cycle)

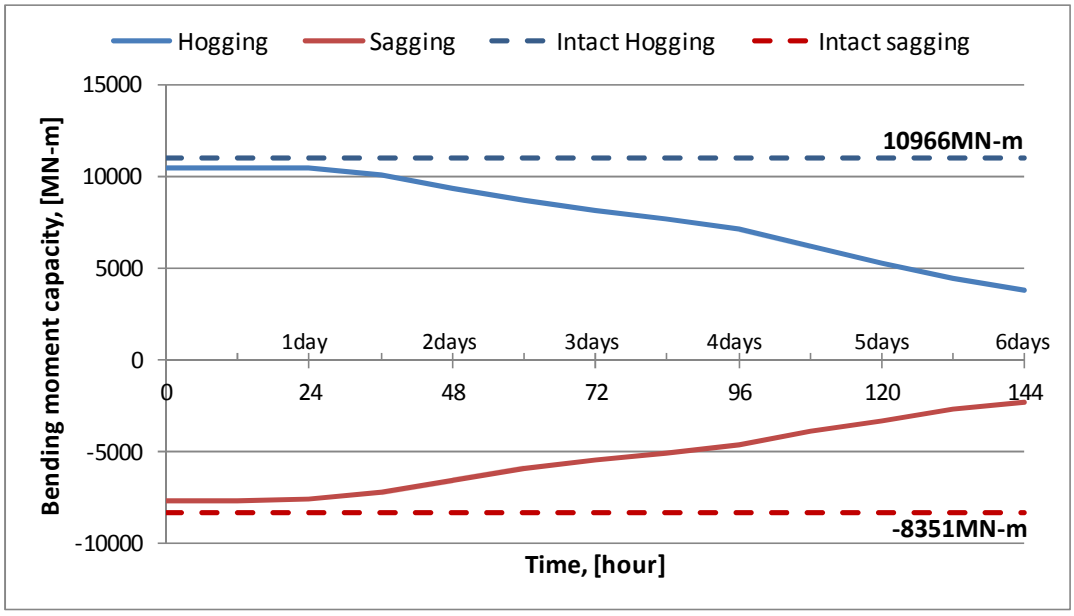

Figure 6-41: Change of the ultimate bending capacity in the deck and side damage case (1.0 mm/cycle)

According to the summary of the ultimate bending capacity (Table 6-6) of the Aframax tanker having damage in the deck and side shell structures, it is found that the hogging bending capacity is reduced by 65.1% and the sagging bending capacity is degraded by 72.4% in six days after the initial damage. It should be noted that the final reduction of the ultimate residual strength is strongly dependent on the extent of damage which depends highly on the rate of crack growth in the region above the material's fracture toughness. In this particular case where complex damage propagations occur due to spreading of the initial damage to the adjacent structures, the importance of the accurate growth rate of crack in the unstable region is emphasized. A sensitivity analysis is carried out in order to investigate the effect of the unstable crack growth rate as well as other parameters on the reduction of the ultimate residual strength in Chapter 7.

Table 6-6: Summary of ultimate bending capacity in the deck and side damage case

Capacity	Hogging		Sagging	
	BM (MN-m)	Diff. (%)	BM (MN-m)	Diff. (%)
Intact condition	10966.1	-	-8350.9	-
Initial damage	10458.6	-4.63	-7696.6	-7.84
1 day later	10410.5	-5.07	-7569.6	-9.36
1.5 days later	10043.4	-8.41	-7185.9	-13.95
2 days later	9348.4	-14.75	-6529.4	-21.81
2.5 days later	8722.9	-20.46	-5942.9	-28.84
3 days later	8155.2	-25.63	-5480.1	-34.38
3.5 days later	7697.9	-29.80	-5106.7	-38.85
4 days later	7138.2	-34.91	-4629.3	-44.56
4.5 days later	6153.7	-43.88	-3901.4	-53.28
5 days later	5298.9	-51.68	-3305.0	-60.42
5.5 days later	4429.5	-59.61	-2691.4	-67.77
6 days later	3825.1	-65.12	-2306.7	-72.38

6.6 Side shell damage

6.6.1 Damage description

The damage is assumed to be located near the neutral axis (above No. 3 stringer) on the side shell within the No. 4 ballast tank while its extent and size are defined according to ABS guidelines (1995). The extent includes side shell plate, No. 2 stringer plate and the attached stiffeners of the damaged plate (Figure 6-42). A circular damage opening on the side shell plate is assumed.

- Diameter of damage at side shell: 5.25 m
- Width of damage at No. 2 stringer: 1.875 m

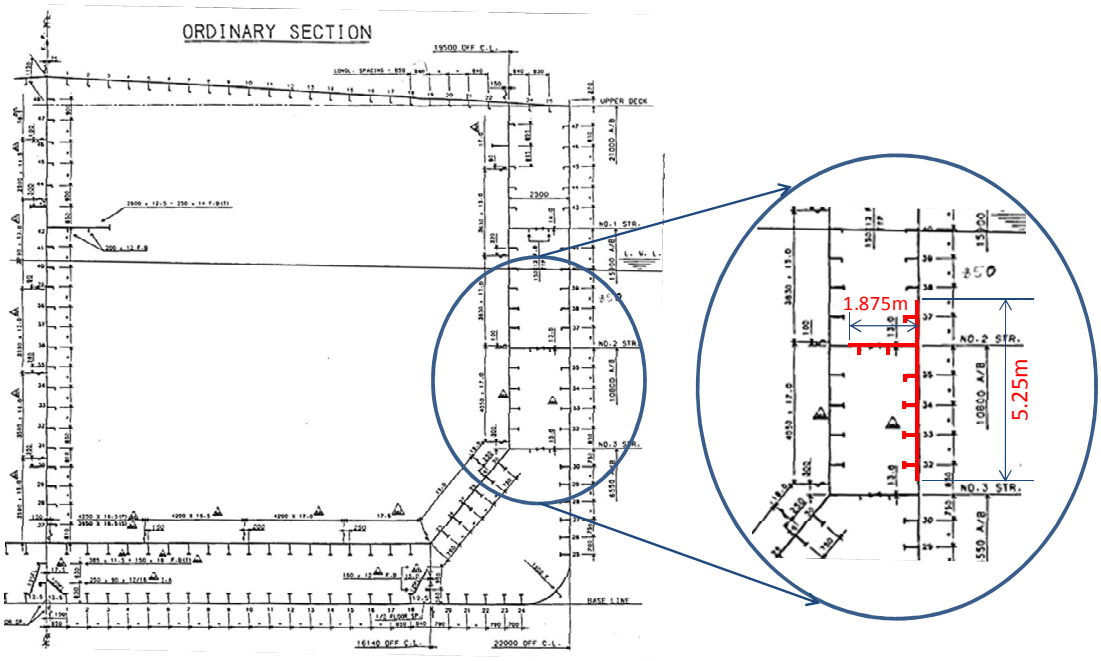

Figure 6-42: Extent and location of side shell damage

Initial cracks are assumed to emanate from the opening edges upwards and downwards on the side plating so that the vertical bending moment from wave loads induces crack propagation further. The initial length of crack (a_0) is assumed to be 1.0% of the opening radius. The effect of difference in the initial damage condition is discussed in the following chapter. A 3D sketch of the damage opening is shown in Figure 6-43, where a circular damage opening is considered on the side shell plate.

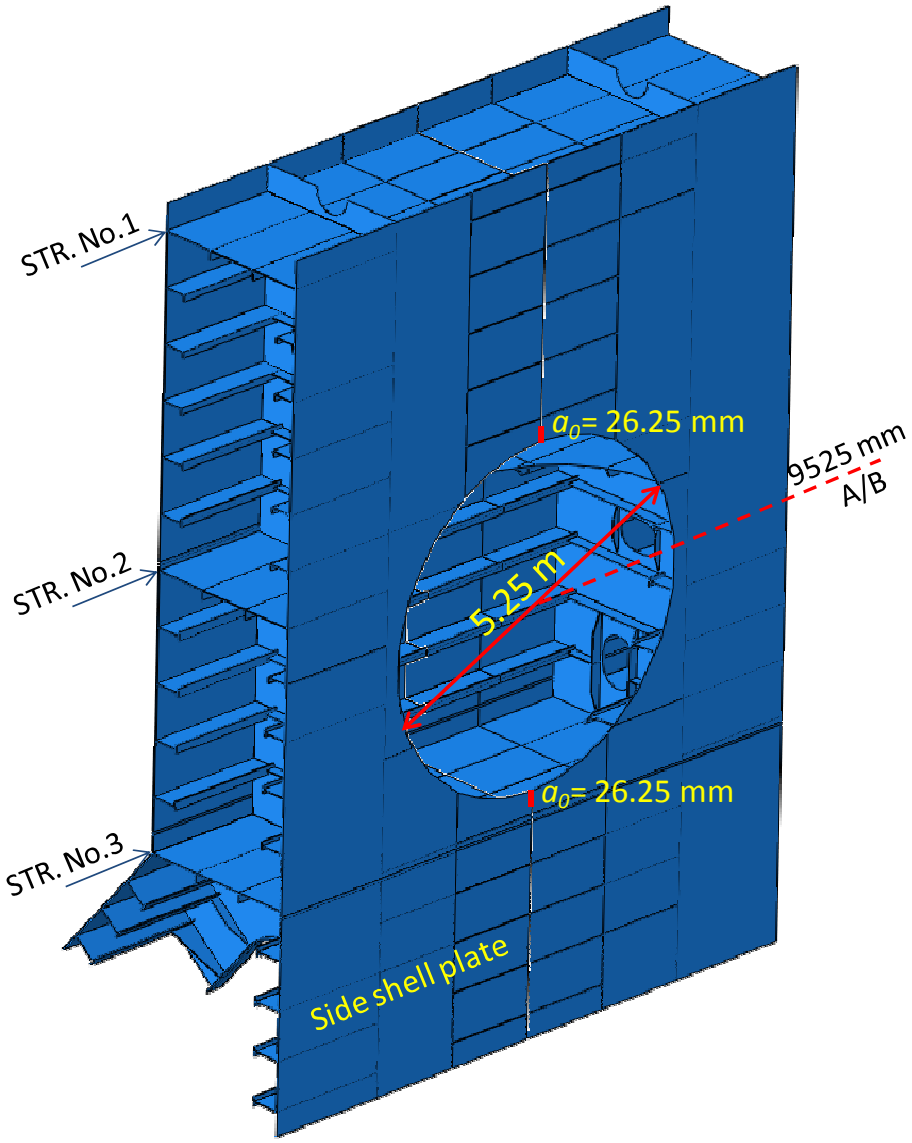

Figure 6-43: Sketch of the damage opening of the side shell damage case

6.6.2 FE model and SIF calculation

An FE model of three cargo hold tanks is prepared using shell and beam elements while the damage opening area is modelled with 3D solid elements (Figure 6-44). Interactions, multi point constraints and boundary conditions are properly defined similarly to the previous cases.

A pair of unit (1.0 MN-m) vertical bending moments is loaded at the reference points. Hogging as well as sagging moment is induced as the initial crack tips are located opposite with the neutral axis of the damaged section located between them.

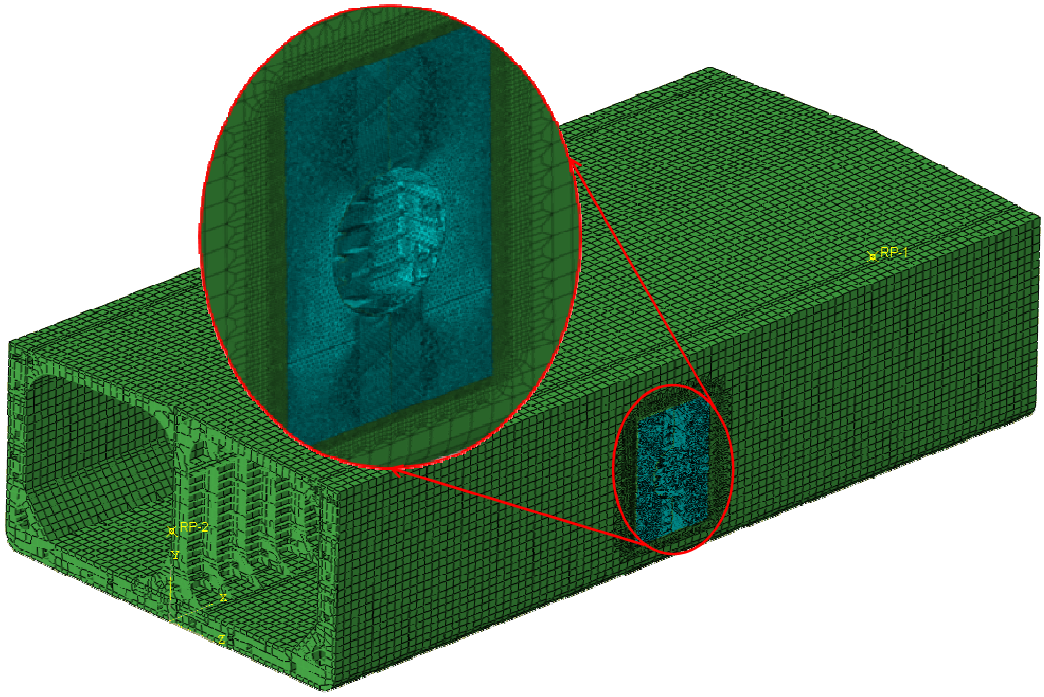

Figure 6-44: FE model for the side shell damage case

Through a series of FE analysis, a set of SIF curves against the crack size is obtained for cracks in the side shell plate as shown in Figure 6-45. The higher value of the SIF in the upper crack is attributed to the higher level of the bending stress at the crack tip, from which relative distance to the neural axis is greater than from the lower crack.

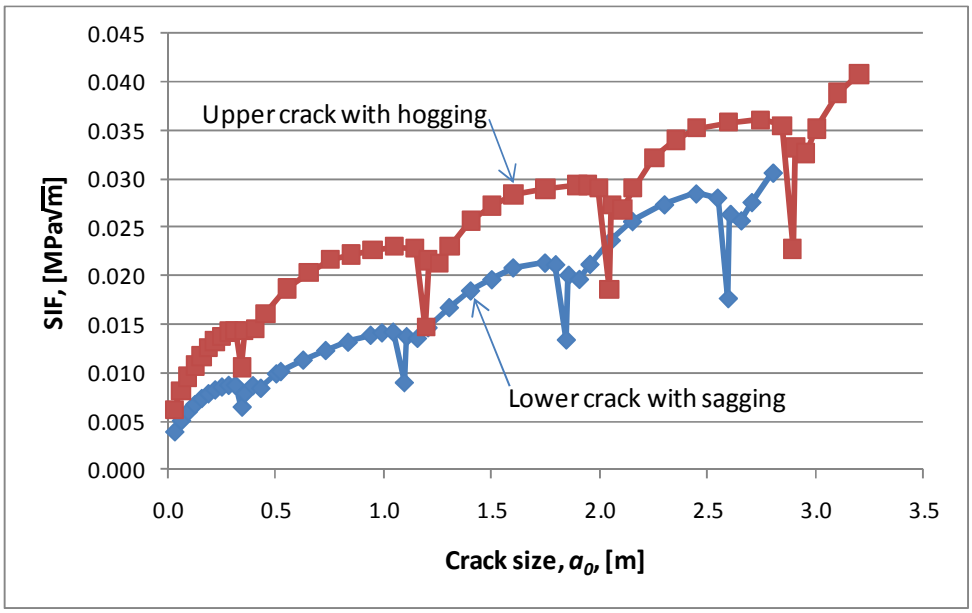

Figure 6-45: SIF curves calculated by VCCT using a unit bending moment pair of 1.0 MN-m

6.6.3 Knowledge-intensive (parametric) model

A knowledge-intensive model for the damage case in the middle of side shell plate is prepared by combining the relevant correction factors. From the geometric configuration of the damage and the surrounding structure, the correction factors for a finite plate, a damage opening and stiffeners need to be included. Also, the effects from the linearly distributed stresses and from the asymmetric crack propagation need to be incorporated.

Finite plate

Considering the finite dimensions of the side shell plate, the correction factor for the finite plate is required to be included in the knowledge-intensive model. Details of this correction factor are explained for the bottom damage case in Equation (6-1) – Equation (6-3). In this case, the half breadth of the plate, *B*, is defined as the half-depth of the side shell plate.

Damage opening

The correction factor for a circular opening is also established for the bottom damage case by Equation (6-4).

Linearly distributed stresses

In a ship subjected to vertical wave bending moments, the induced stresses on its side shell plate are not uniform but linearly distributed from compression to tension according to the direction of the bending moment applied and the location of the neutral axis of the section considered. In this case, the behaviour of cracks under the linearly distributed bending stresses is determined by adopting the expression proposed by Chell (1976).

The bending stresses in the side shell plate are decomposed into two components as shown in Figure 6-46: (i) a uniformly distributed stress, $\sigma_1(x) = \sigma$, and (ii) the remaining linearly distributed stresses, $\sigma_2(x) = \sigma_0(x/B)$. The uniform stress, σ, is the initially induced bending stress at the centre of crack and the empirical equation of Chell is applied to the remaining stress, $\sigma_2(x)$. As such, the correction factor for the effect of the linearly distributed stresses on the side shell plate of a ship is obtained by the Equation (6-17).

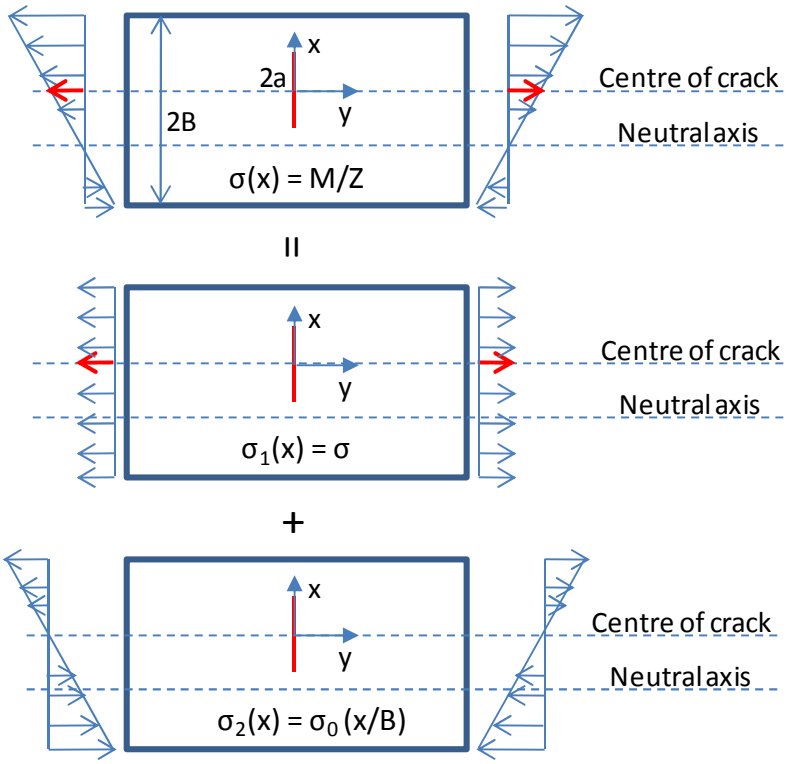

Figure 6-46: Bending stresses decomposed into two stress components

$$Y_{linear\ stress} = 1 + \left(\frac{\sigma_0}{\sigma}\right)\left(\frac{\pm a}{B}\right)\left\{0.5 - 0.132\left(\frac{a}{B}\right) - 0.0267\left(\frac{a}{B}\right)^2\right\} \quad \textbf{(6-17)}$$

where, σ is the bending stress at the centre of crack

σ_0 is the slope of the linearly distributed stress

$+a$ means that the crack tip is located at the positive x-axis (Figure 6-46)

$-a$ means that the crack tip is located at the negative x-axis (Figure 6-46)

Asymmetric cracks

Although the initial damage condition is symmetric, the difference in geometry as well as the variation of the stress distribution around crack tips prevents the crack propagation from being symmetric in the later stage.

Recalling the effect of the asymmetric cracks propagating from the edge of a circular opening in an infinite plate (Figure 6-47), the correction factor for each crack tip is expressed as Equation (6-18) and Equation (6-19).

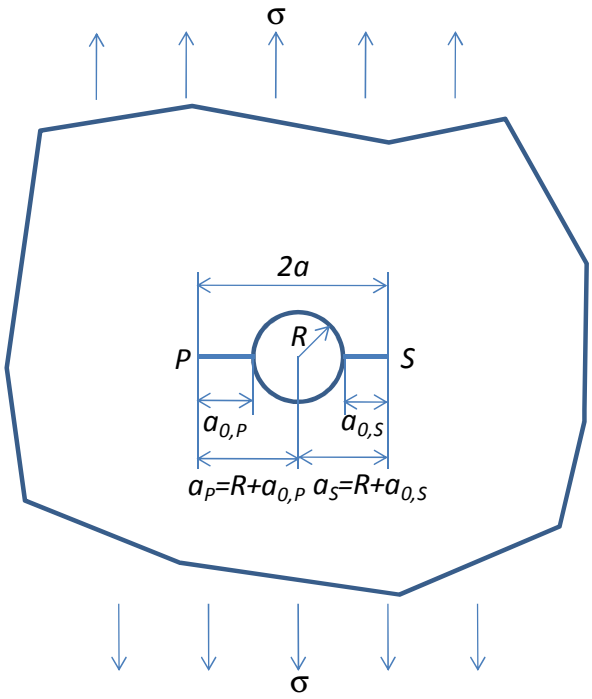

Figure 6-47: Configuration of asymmetric cracks emanating from a circular opening in an infinite plate

$$Y_{asym,Primary} = \frac{Y_{circle}(a_{0,P}, R)}{Y_{circle}(a_0, R)} \quad \textbf{(6-18)}$$

$$Y_{asym,Secondary} = \frac{Y_{circle}(a_{0,S}, R)}{Y_{circle}(a_0, R)} \quad \textbf{(6-19)}$$

where, $Y_{circle}(a_0, R)$ is the correction factor for the effect of the circular opening in an infinite plate with opening radius of R and initial crack size of a_0

$Y_{circle}(a_0, R) = 0.5(3 - s_c)\{1 + 1.243(1 - s_c)^3\} \times \sqrt{s_c}$

s_c is a ratio of a_0 to half of the total damage size, $s_c = \frac{a_0}{R+a_0}$

a_0 is the average crack size, $2a_0 = a_{0,P} + a_{0,S}$

$a_{0,P}$ and $a_{0,S}$ are crack sizes at the primary and secondary crack respectively

R is the radius of a circular damage opening

Stiffeners

The effect of stiffeners on the crack propagation in a side shell damage case is obtained using a series of FE analyses. The correction factor for stiffeners is expected to be the ratio of the calculated SIF over the SIF determined including for all other effects discussed above except the stiffeners' effect and is expressed in Equation (6-20).

$$Y_{stiffener,Side,FEA} = \frac{SIF_{FEA}}{SIF_0 \times Y_{finite\ plate} \times Y_{circle} \times Y_{linear\ stress} \times Y_{asym}} \quad \textbf{(6-20)}$$

where, $SIF_0 = \sigma\sqrt{\pi a}$

σ is the bending stress at the centre of the damage opening

a is the half of the damage size including opening

Data obtained by FE simulations are plotted in Figure 6-48 and their regression analysis is carried out as shown in Figure 6-49, from which the correction factor for stiffeners in the side shell damage is obtained in polynomial form as Equation (6-21).

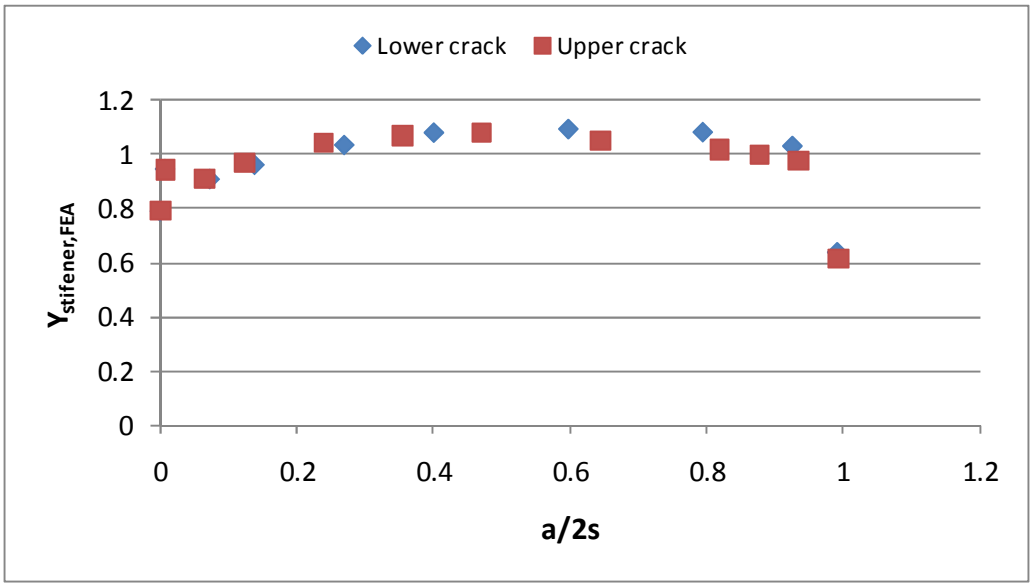

Figure 6-48: Data obtained by Equation (6-20) from both upper and lower cracks

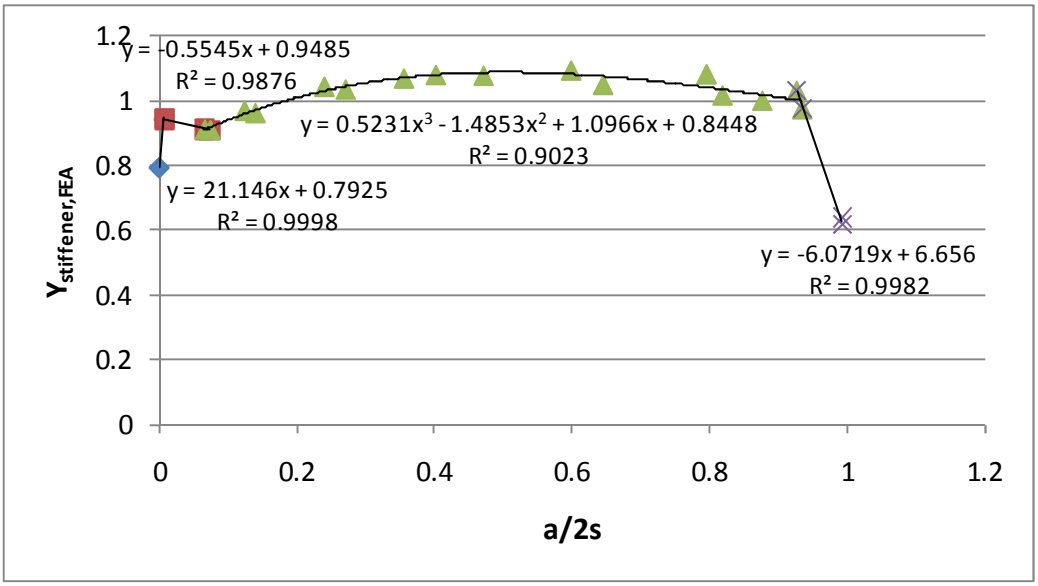

Figure 6-49: Regression analysis for defining $Y_{stifferner,FEA}$ for the side damage case

$$Y_{stiffener,Side,FEA} = \begin{cases} 21.146\left(\frac{a_j}{2s}\right) + 0.7925 & ; 0.0 < \left(\frac{a_j}{2s}\right) \leq 0.0072 \\ -0.5545\left(\frac{a_j}{2s}\right) + 0.9485 & ; 0.0072 < \left(\frac{a_j}{2s}\right) \leq 0.067 \\ 0.5231\left(\frac{a_j}{2s}\right)^3 - 1.4853\left(\frac{a_j}{2s}\right)^2 + 1.0966\left(\frac{a_j}{2s}\right) + 0.8448 & ; 0.067 < \left(\frac{a_j}{2s}\right) \leq 0.9315 \\ -6.0719\left(\frac{a_j}{2s}\right) + 6.656 & ; 0.9315 < \left(\frac{a_j}{2s}\right) \leq 1.0 \end{cases} \quad \textbf{(6-21)}$$

where, a_j is the damage size at crack j including radius of the opening, $a_j = a_{0,j}+R$

$a_{0,j}$ is the crack size at crack j

R is the radius of the circular damage opening

j denotes crack locations, j = P, S for primary and secondary crack locations

$2s$ is the stiffener's spacing

Knowledge-intensive (parametric) model of SIFs for the side damage case

Using the correction factors obtained above, a set of SIF curves of cracks emanating from a circular opening on the side shell plate is recreated. Considering all the related correction factors, the SIFs of cracks on the side shell damage can be determined by Equations (6-22) and (6-23). The resulting SIF curves are shown in Figure 6-50 and

Figure 6-51 for the lower crack and the upper crack under the vertical bending moment of 1.0 MN-m in sagging and hogging respectively.

$$SIF_{Lower\ |\ Side\ dmamge} = SIF_0 \times Y_{finite\ plate} \times Y_{circle} \times Y_{linear\ stress} \times Y_{asym,lower} \times Y_{stiffener,Side,FEA} \quad \textbf{(6-22)}$$

$$SIF_{Upper\ |\ Side\ dmamge} = SIF_0 \times Y_{finite\ plate} \times Y_{circle} \times Y_{linear\ stress} \times Y_{asym,upper} \times Y_{stiffener,Side,FEA} \quad \textbf{(6-23)}$$

where, $SIF_0 = \sigma\sqrt{\pi a}$

σ is the bending stress at the centre of damage opening in the side shell plate

a is the half of the damage size including opening

$Y_{finite\ plate}$, Y_{circle}, $Y_{linear\ stress}$, Y_{asym} and $Y_{stiffener,Side,FEA}$ are defined in Equation (6-3), (6-4), (6-17), (6-18) (or Equation (6-19)) and (6-21) respectively

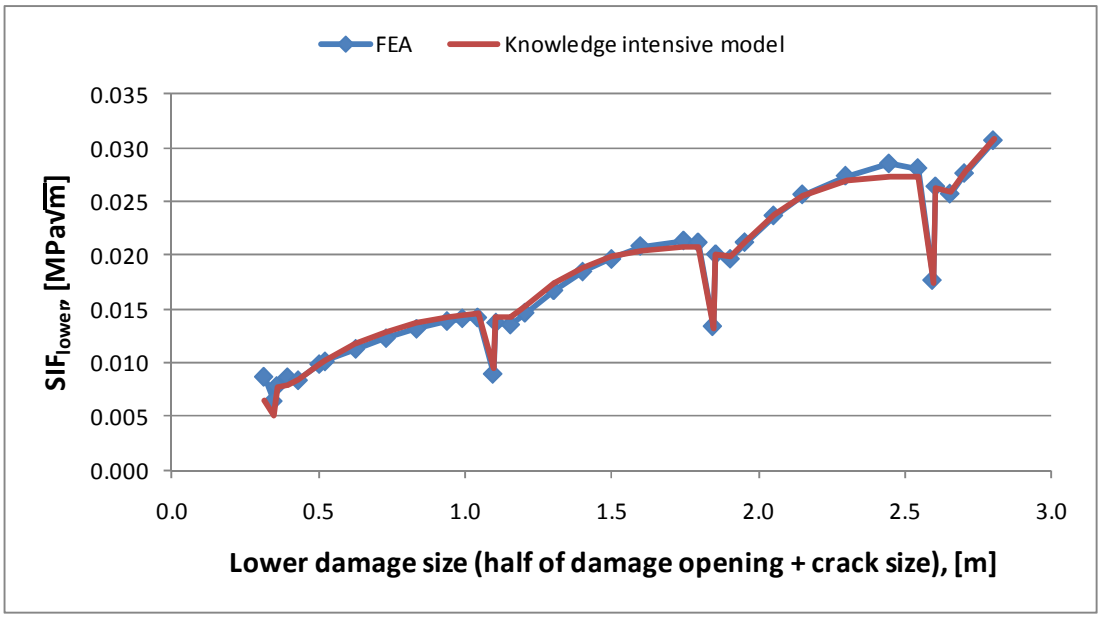

Figure 6-50: SIF curves obtained by the parametric model for lower crack in the side shell damage case and comparison with numerical results

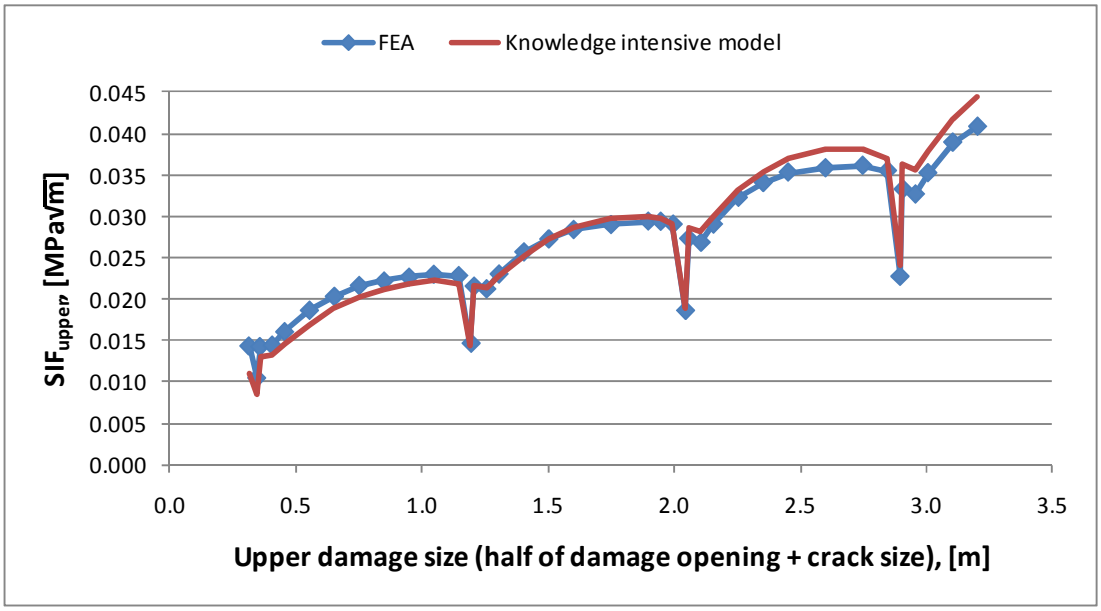

Figure 6-51: SIF curves obtained by the parametric model for upper crack in the side shell damage case and comparison with numerical results

Comparison of the estimated SIF curves with those from the FE analysis is satisfactory.

6.6.4 Wave loads

To evaluate the side shell damage case, two loading conditions are considered: (i) a fully loaded condition, and (ii) a ballast condition, which have been used in the previous two damage cases. The former loading condition, where a sagging bending moment is induced in the still water condition, would accelerate damage propagation in the lower crack tip due to inertia effects, while the opposite would occur for the ballast condition.

The dynamic wave bending moments in time domain for each loading condition are taken from the results shown in Figure 6-17 and Figure 6-34, which are based on the wave data for a period of 6 days as shown in Figure 6-16.

6.6.5 Damage propagation

The same approach used in the previous damage cases is applied to analysis of the damage propagation of the side shell case. The proposed crack growth model shown in Equation (6-9) is used and the values of the coefficients C and m are decided according to the properties of the plate in which the crack tip is located by use of the

plane strain fracture toughness, K_{IC} = 140 MPa$\sqrt{m}$ and the threshold range of SIF, ΔK_{th0} = 2.45 MPa$\sqrt{m}$.

Under the fully loaded condition, the damage in the lower crack tip is found to propagate very slowly as the range of the SIF is small and the maximum SIF is less than 15 MPa$\sqrt{m}$ during the analysis. Additionally, no damage propagation at the upper crack tip is observed as its maximum SIF is kept below zero for most of the time period. The variation of the maximum SIF is shown in Figure 6-52 and the damage propagation is presented in Figure 6-53.

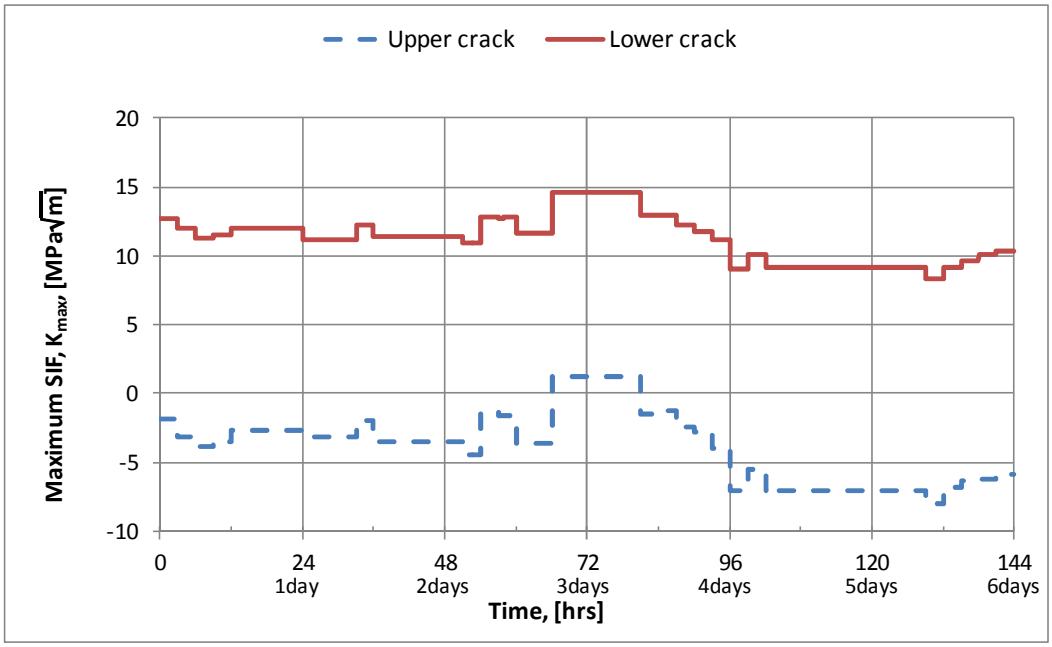

Figure 6-52: Change of the maximum SIFs of cracks on the side shell plate under the fully loaded condition

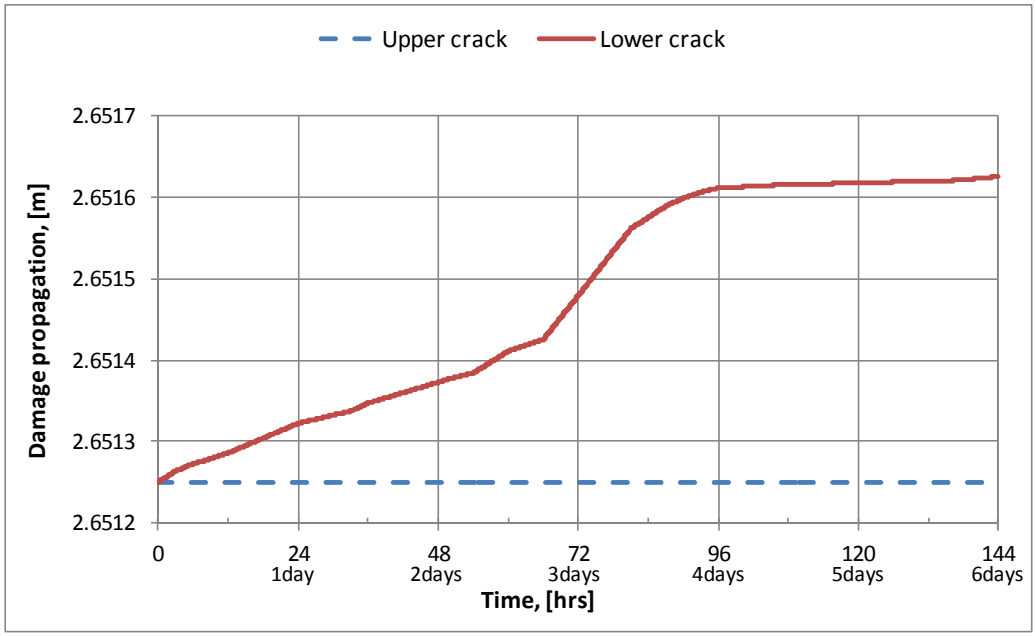

Figure 6-53: Damage propagation of the side shell damage case under the fully loaded condition

A similar result is found in the ballast condition but the behaviour of the lower and upper crack tips are swapped. Crack closure is expected in the lower crack tip while a very slow propagation is estimated in the upper crack tip. The maximum SIFs and damage propagation in time domain are shown in Figure 6-54 and Figure 6-55 respectively. The same reason as that of the fully loaded condition applies.

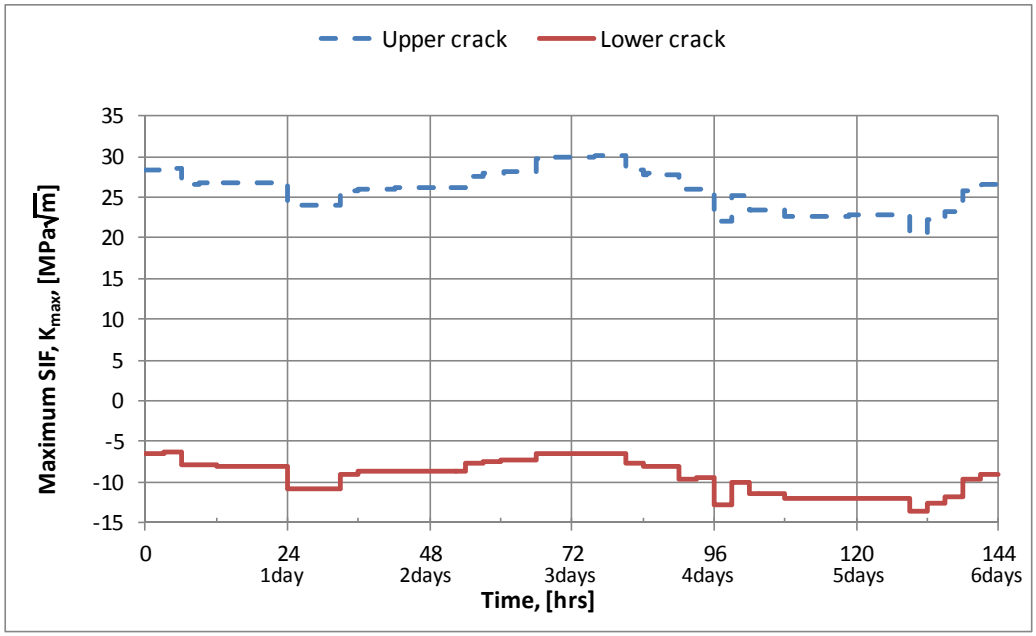

Figure 6-54: Change of the maximum SIFs of cracks on the side shell plate under the ballast condition

The damage propagation of this condition is plotted in Figure 6-55. The larger stress level in the upper crack tip in the ballast condition resulted in the larger damage propagation in comparison to that of the lower crack tip in the fully loaded condition.

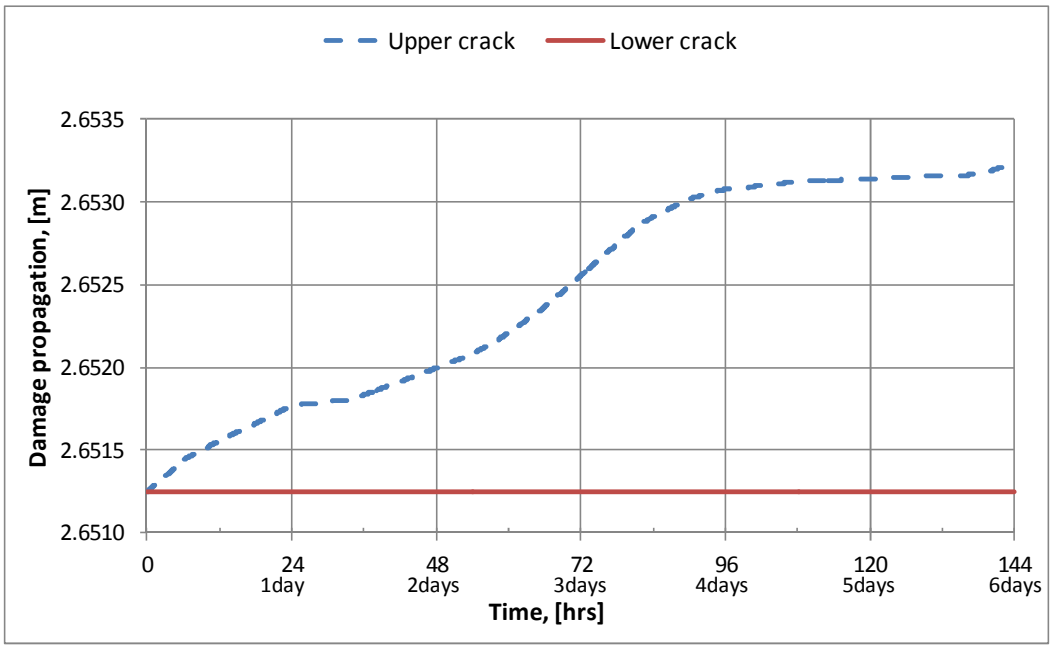

Figure 6-55: Damage propagation of the side shell damage case under the ballast condition

6.6.6 Residual strength

As the damage propagation in the side shell is negligible under the considered loading conditions and the wave data, no structural degradation of the bending moment capacity after the initial damage extent is estimated. Also due to the location of the initial damage near the neutral axis of the cross section, no significant reduction in the bending moment capacity is induced. Comparison of the bending moment capacity between intact and initial damage condition is shown in Figure 6-56.

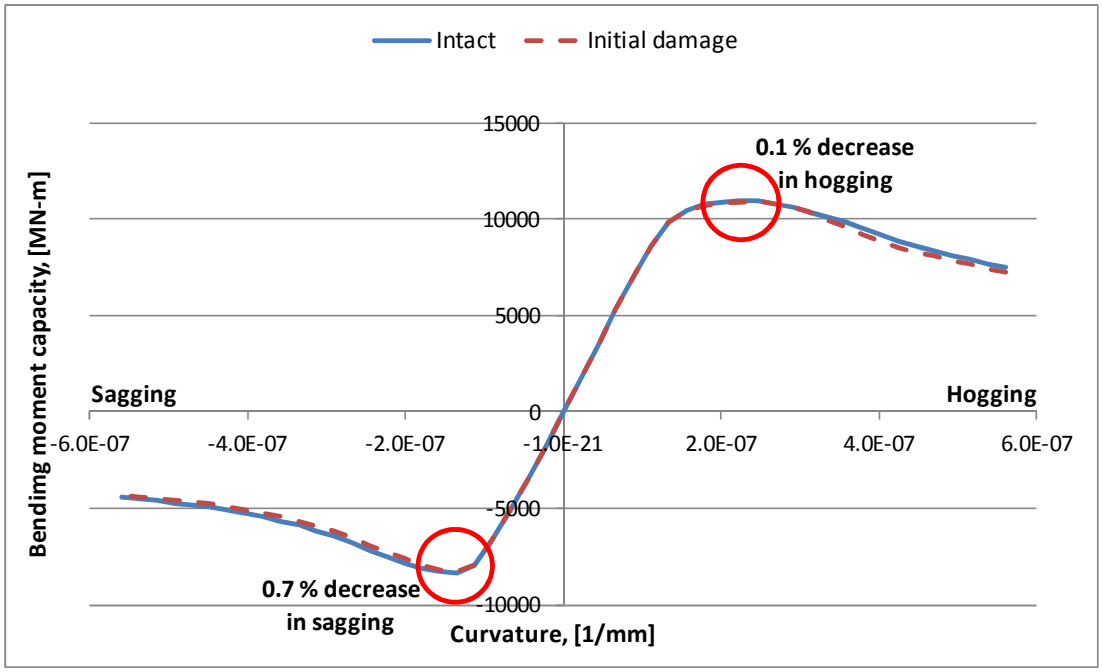

Figure 6-56: Bending moment capacity of the side shell damage case, compared with that in the intact case

6.7 Chapter summary

This chapter has focused on the application of the proposed methodology to an Aframax tanker in order to analyse the damage propagation and resulting residual strength capacity for three hypothetical, albeit realistic, damage cases. Using the tanker, realism is pursued in terms of using the real hull structures, defining damage case with location and extent, and calculating wave loading of the ship from a wave record directly related to a major accident.

The knowledge-intensive models are deployed for the determination of SIFs of cracks in each damage case and compared with those obtained from FE analysis. Correction factors for stiffeners are obtained by ratios between the calculated SIFs from FE analysis and other correction factors and considered specific to each damage case. In this approach the effect of the adjacent structure was taken into consideration.

Although it is understood and appreciated that more research is required in order to define the exact crack growth rate in the unstable propagation region, where the fracture toughness of the material is diminished, the case study of the Aframax

tanker highlights the rationale of the proposed approach in the application to the real ship's hull structures.

In the next chapter, a discussion on the uncertainty associated to various parameters, like the damage location, the initial extent and the initial crack size, is addressed. The developed knowledge-intensive models for Aframax tanker will be an integral part of this analysis and their simplified mathematical nature is highly conducive to this task.

7 SENSITIVITY ANALYSIS AND UNCERTAINTY QUANTIFICATION

7.1 Preamble

Following the applications of the proposed approach to a real ship hull structure, this chapter investigates effects of the variable parameters to the damage propagation by conducting sensitivity analysis and uncertainty quantification. With the models developed in Chapter 6, the calculations are revisited to obtain probabilistic results of the damage propagation as well as the ultimate residual bending strength of the damaged section. Finally, the contribution of the damage propagation in the context of the *risk-based design* methodology is highlighted.

7.2 Analysis process

In the event of accidental collisions or groundings accompanying the initial damage, the damage information is usually difficult to obtain by visual inspection alone. Nonetheless, this is a rather critical input as it was demonstrated in Chapter 6. The precise information on the location, shape and size of as well as the size of crack emanating from the damage opening is hardly available, especially when the damage is under the water. Difficulty also arrives from the estimation of the wave/weather conditions and their variation after the initial damage has occurred.

Hence, an investigation on the variational effects of the wave loading as well as the initial damage conditions on the crack propagation is carried out using the knowledge-intensive (parametric) models developed in the previous chapter for the damage cases under consideration. The work is carried in two directions: (i) identification of the dominant variables of the process by sensitivity analysis, and (ii) quantification of the uncertainty associated with the output of the calculations in relation to the input (e.g. material properties and constants). The former point will lead to the identification of the those variables that have the most significant contribution to the results, and the latter will add confidence in the result, especially taking under consideration that validation data is not available for this methodology.

In order to assess the sensitivity with respect to the considered parameters, Monte Carlo (MC) sampling is carried out for each of the parameters. Each parameter is sampled based on its probabilistic distribution and the mean and the standard deviation of the required time for the damage becomes unstable as well as of the

ultimate residual bending moment capacities is obtained. It should be noted that the time required for the damage to start propagating in an unstable manner is important as it would lead to rapid global failure of the hull girder unless the driving excitation is reduced significantly (e.g. damage propagation on a vertical structural member approaching to the neutral axis of the section or significant decrease of the external wave loading). The MC simulation is performed for 10,000 samples for each parameter.

The parameters for the analysis with respect to the specific damage case in an emergency operation are chosen in order to represent the variation of the damage information (size and location), wave bending moments and material properties pertinent to the crack propagation. For the design study, it is recommended to include design parameters pertaining to ship geometry and structure e.g. plate thickness and stiffener size in the sensitivity analysis as well as those addressed above. Table 7-1 shows the list of parameters investigated and their probabilistic characteristics adopted in the sensitivity analysis. Each parameter is sampled in sequence (according to its mean and standard deviation values) whilst the rest of the parameters are assumed constant and equal to their mean value. It should be noted that the SIF ratio represents the uncertainty associated with the developed parametric models for calculation of the section modulus and the SIFs. That is, any assumption and simplification made during the development of the parametric models affecting the SIFs of the crack tips, and considered indirectly in the calculation of the bending stress in accordance with the section modulus and directly in the calculation of the SIFs using knowledge-intensive models, is taken into account through the variation of the SIF ratio.

Table 7-1: The parameters involved in the sensitivity analysis and their probabilistic values

Parameters		Mean	Std. deviation	Distribution
Distance from centre of damage		0	200 mm	Normal
Bottom damage size	R_{btm}	3665 mm	366.5 mm[1)]	Normal
Deck & side damage size	R_{length}	3780 mm	378 mm[1)]	Normal
	R_{height}	4980 mm	498 mm[1)]	Normal
	R_{depth}	2380 mm	238 mm[1)]	Normal
Side damage size	R_{side}	2625 mm	262.5 mm[1)]	Normal
Crack size ratio (a_0/R)		0.01	0.002[2)]	Normal
Coefficient C		9.5e-12	1.9e-12[2)]	Log Normal
da/dN_{max}		1.0 mm/cycle	0.2 mm/cycle[3)]	Normal
K_{IC}		140 MPa$\sqrt{\text{m}}$	7 MPa$\sqrt{\text{m}}$ [4)]	Normal
ΔK_{th0}		2.45 MPa$\sqrt{\text{m}}$	0.1225 MPa$\sqrt{\text{m}}$ [4)]	Normal
SIF ratio		1.0	0.1[5)]	Normal
Wave bending moment ratio		1.0	0.15[2)]	Normal

1) The coefficient of variation (COV) for the damage sizes is assumed to be 0.1.
2) The standard deviation is based on the COV from Paik et al. (2003b).
3) The COV for the maximum da/dN is chosen as 0.2 in order to allow wider variation.
4) The COV for the material properties is chosen as 0.05 with respond to the COV of 0.03 for the Young's modulus and 0.1 for the yield stress from Paik et al. (2003b).
5) The COV corresponds to the modelling uncertainty is assumed to be 0.1.

7.2.1 Bottom damage

The results of the sensitivity analysis are summarised in Table 7-2 with the mean and standard deviation values for the bottom damage case discussed in the previous chapter. The bar charts of the results are illustrated in Figure 7-1 and Figure 7-2 and show that the responses are most sensitive with respect to (i) the wave bending moment, (ii) the size of the initial damage, and (iii) the estimated SIF followed by the initial crack size.

Table 7-2: Result of the sensitivity analysis in bottom damage case

Parameters	$T_{unstable}$, [hrs]		BM_{hog}, [MN-m]		BM_{sag}, [MN-m]	
	Mean	Std. dev.	Mean	Std. dev.	Mean	Std. dev.
Damage location	69.37 (69.42)	3.30 (3.32)	5973	85	6771	16
Damage size, R_{btm}	80.36	25.51	6616	1505	6971	483
Crack size, a_0	68.36	9.99	6000	520	6785	163
Coefficient C	67.53	4.53	5937	155	6766	44
da/dN_{max}	67.15	0.004	6133	460	6813	110
K_{IC}	67.25	1.00	5911	20	6761	2
ΔK_{th0}	67.15	0.04	5906	0.53	6760	0.06
SIF ratio	71.56	25.32	6360	1302	6901	411
Wave BM	73.35	28.20	6484	1463	6942	462

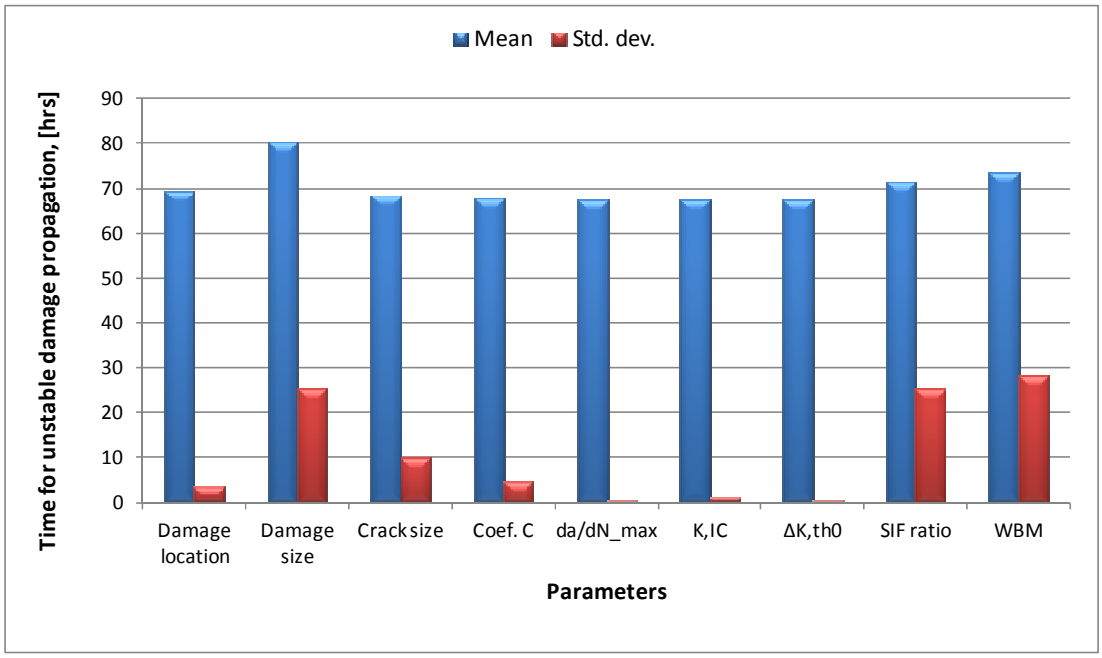

Figure 7-1: The initial damage size, the estimated SIF and the wave bending moment have large effect on the time for unstable damage propagation

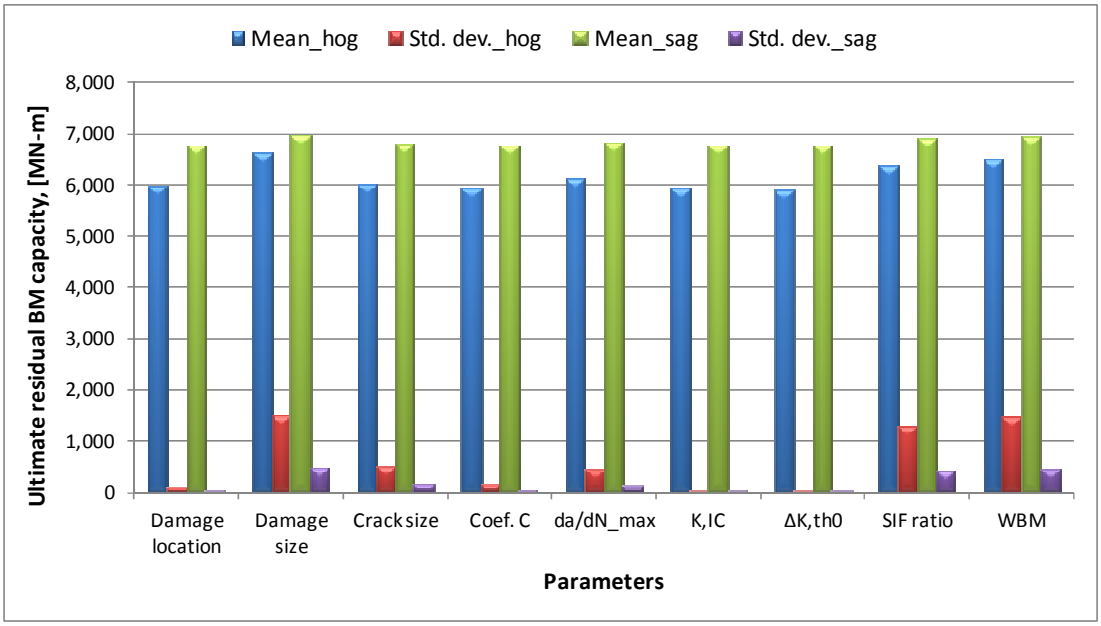

Figure 7-2: The ultimate residual bending moment capacity is also sensitive to the initial damage size, the estimated SIF and the wave bending moment

Further analysis is made to investigate the effect of the wider deviations of the three identified parameters. For each case, the required time for a damage propagation to become unstable is obtained and compared.

Initial damage opening size

The effect of the initial damage opening is investigated by using a wider range of the opening size while other parameters are fixed during the sampling process. The results of the required time for damage propagation become unstable in various damage opening radii are shown in Figure 7-3. The result of 6 days in the graph means that it would take at least 6 days or probably more for the damage case to become unstable. The limit of 6 days arrives from the information of wave data provided for the same duration. The response of the required time against the changes of the initial damage opening size can be divided into three regions and the explanation of each region follows below.

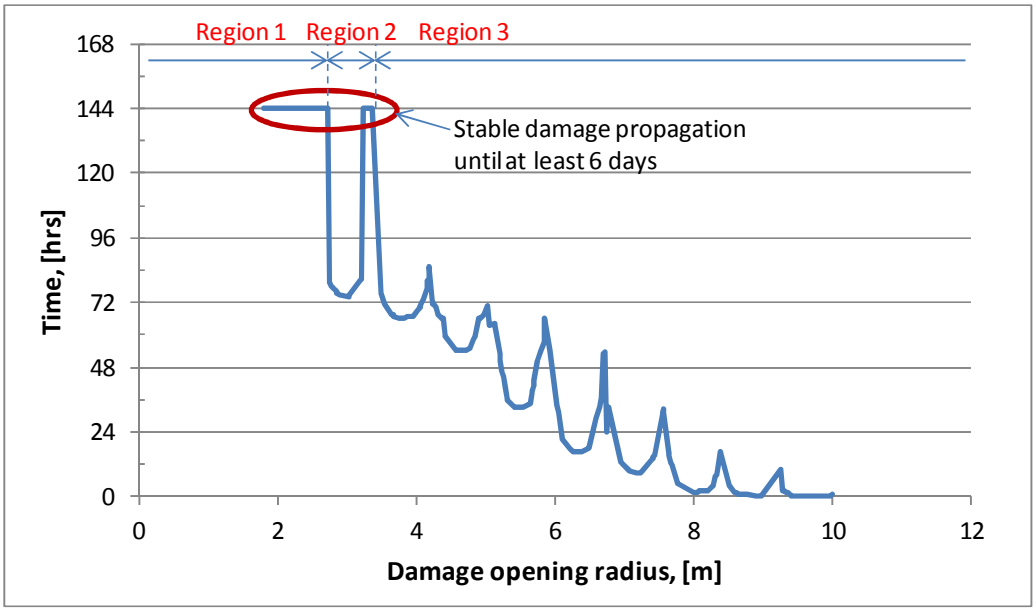

Figure 7-3: The effect of the initial damage opening size on the damage propagation in the bottom damage case of an Aframax tanker

In **Region 1**, no unstable damage propagation is identified within 6 days' simulation. This is attributed to the fact that the initial damage is too small to induce an SIF of sufficient magnitude for meaningful crack propagation. At no time during the corresponding period, the maximum SIF exceeds the material toughness limit.

Region 2 shows a complex response according to the initial size of the damage opening. For some cases in this region, no unstable damage propagation is observed, where the initial crack tips are located in the areas in which the stiffeners' restraint effects exist. As reductions of SIF are experienced while cracks approach stiffeners and during the recovery after severing the stiffeners, the 'U' shaped response is obtained between stiffeners. The absence of the initiating unstable damage propagation after 4 days from the initial damage is contributed to the decreasing trend of the wave loadings (bending moments) applied during the period.

Although the existence of stiffeners defines the line between stable and unstable propagation rate for given initial damage size, there is a point from which damage propagations become unstable regardless of the initial damage size and the initial crack tip location. In **Region 3**, the required time when the damage propagation becomes unstable fluctuates according to the relative location of the initial crack tip between stiffeners but no stable damage propagation has resulted in 6 days of

analysis. The tendency of decreasing in the required time as the initial size of damage opening increases is also evident and observed in the results.

Wave bending moment

The effect of different wave bending moments on the response of damage propagation is tested with the fixed initial damage opening. Various values of the wave bending moment ratio, BM_i/BM_0, where BM_0 is the wave bending moment over time used in Section 6.4.4, are tested and the results of the required time for damage propagation become unstable are shown in Figure 7-4. The result of 6 days in the graph means that it would take at least 6 days, probably more, for the damage to acquire unstable propagation rate. The response of the required time against changes of the bending moment ratio can be divided into two regions, which are explained in the accompanying paragraphs.

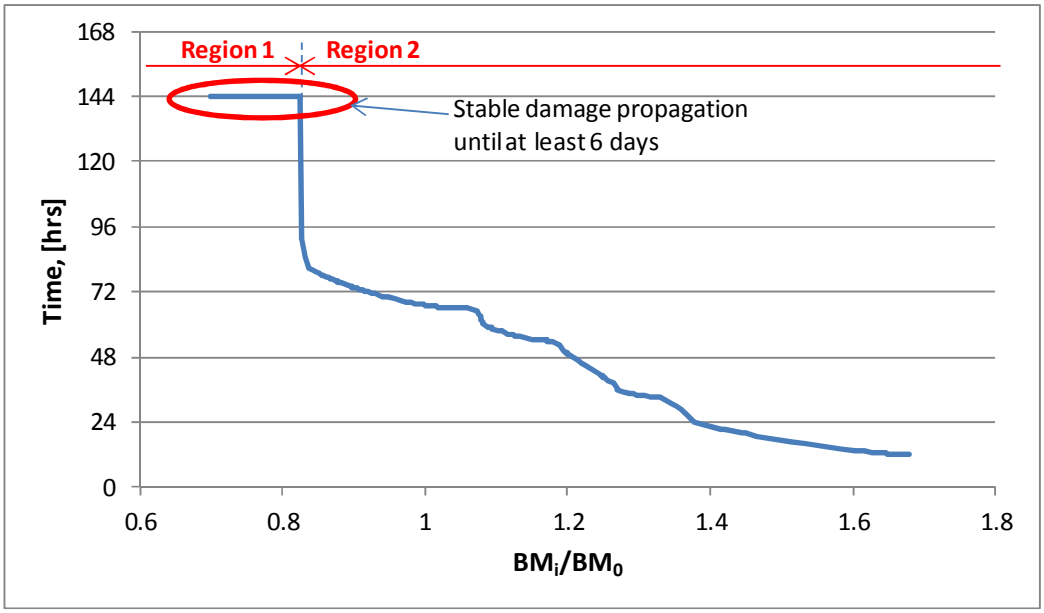

Figure 7-4: The effect of the magnitude of bending moment on the damage propagation in the bottom damage case of an Aframax tanker

Region 2, in which the unstable damage propagation is expected within 4 days from the initial accident, shows that the unstable damage propagation occurs earlier as the applied wave bending moment increases.

However, in **Region 1,** where the wave bending moment decrease, the stable damage propagation is determined under the given wave data. It should be understood that

this implies negligible damage propagation within 6 days of period but not damage arresting. This can be identified in Figure 7-5 where the response of damage propagation with 20% reduction of the wave bending moment is compared to the result obtained in Section 6.4.5. The damage propagation under the reduced wave bending moment becomes unstable after 6 days from the initial damage when the original wave data of 6 days are repeated. It should be noted that the rate of propagation would be different if a different wave data is taken into consideration.

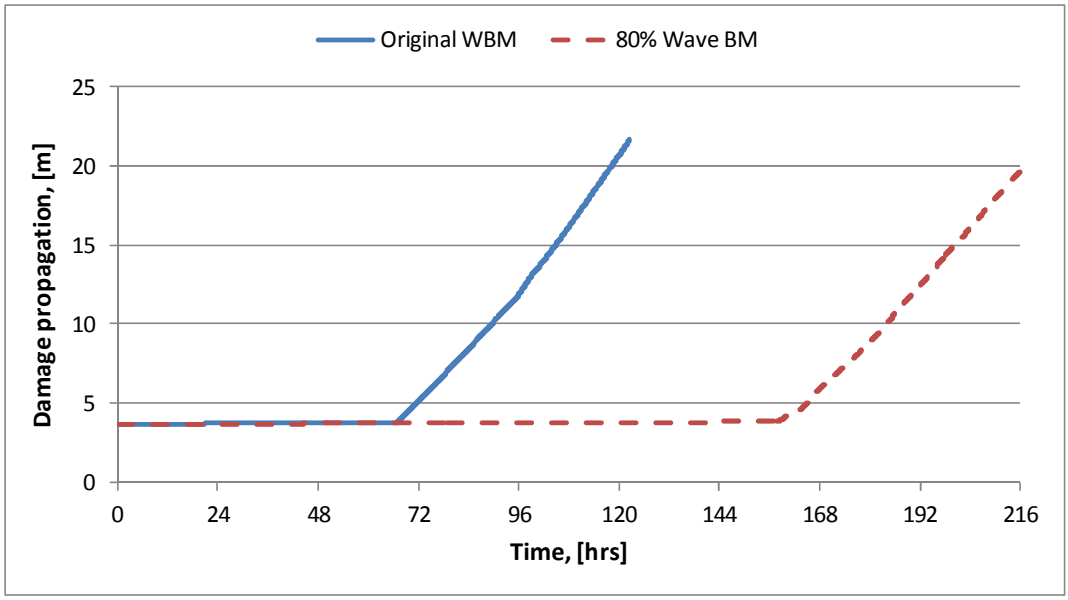

Figure 7-5: Damage propagation of bottom damage case a reduced wave bending moment –the unstable damage propagation is delayed by a reduced wave bending moment (1.0 mm/cycle is applied in the unstable region)

SIF ratio

A similar response to the wave bending moment effect is obtained for SIF as shown in Figure 7-6, where a discontinuity of the response is observed. **Region 1** shows no unstable damage propagation within 6 days. This arises from the fact that the low magnitude of SIF leads to negligible damage propagation for the analysis period. In **Region 2** the required time for the damage propagation to become unstable decreases as SIF increases. The same response from the effect of the wave bending moment is contributed to the fact that the increase of the wave bending moment directly results in the increase of the SIF.

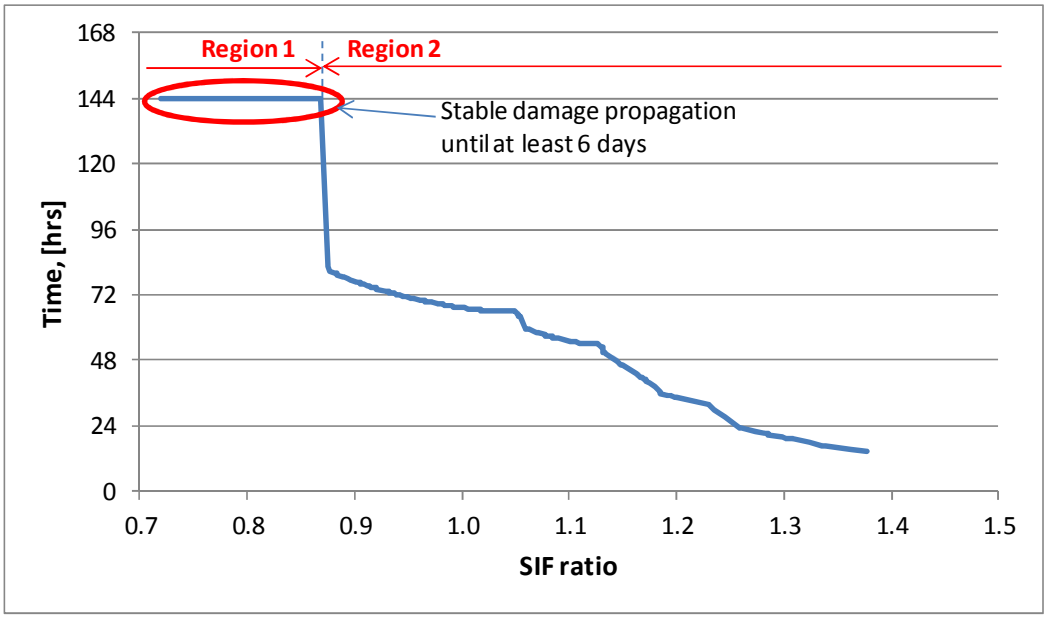

Figure 7-6: The effect of the SIF ratio on the damage propagation in the bottom damage case of an Aframax tanker

7.2.2 Deck and side damage

The results of the sensitivity analysis in the deck and side damage case are summarised in Table 7-3. The bar charts illustrating the sensitivity of the responses are shown in Figure 7-7 and Figure 7-8. In this damage case, the responses are sensitive to the most of the parameters. Among the examined parameters, the estimated SIF and the wave bending moment are the most influential ones on the responses of the damage propagation with a deck and side damage. The responses of the damage propagation are also sensitive to the parameters related to the initial damage opening.

Table 7-3: Results of the sensitivity analysis in deck & side damage case

Parameters		$T_{unstable,}$ deck [hrs]		$T_{unstable,}$ side [hrs]		$BM_{hog,}$ [MN-m]		$BM_{sag,}$ [MN-m]	
		Mean	Std. dev.	Mean	Std. dev.	Mean	Std. dev.	Mean	Std. dev.
Damage location		11.20	3.76	9.07	8.45	3607	172	2145	121
Damage size	R_{length}	30.03	20.59	31.11	20.97	4203	822	2541	569
	R_{height}	13.42	11.54	8.12	13.37	3564	425	2110	289
	R_{depth}	24.88	17.86	21.33	10.97	3972	720	2382	504
Crack size, a_0		28.41	12.58	28.83	10.97	4005	505	2405	349
Coefficient C		29.99	12.95	31.13	12.94	4073	521	2451	359
da/dN_{max}		23.22	0.04	24.13	0.77	4155	886	2512	621
K_{IC}		27.96	13.25	29.03	13.84	4003	502	2403	346
ΔK_{th0}		23.22	0.12	24.23	0.84	3826	3.79	2308	3.74
SIF ratio		36.42	33.02	37.20	33.23	4610	1596	2857	1224
Wave BM		35.90	31.26	36.68	31.30	4546	1517	2808	1162

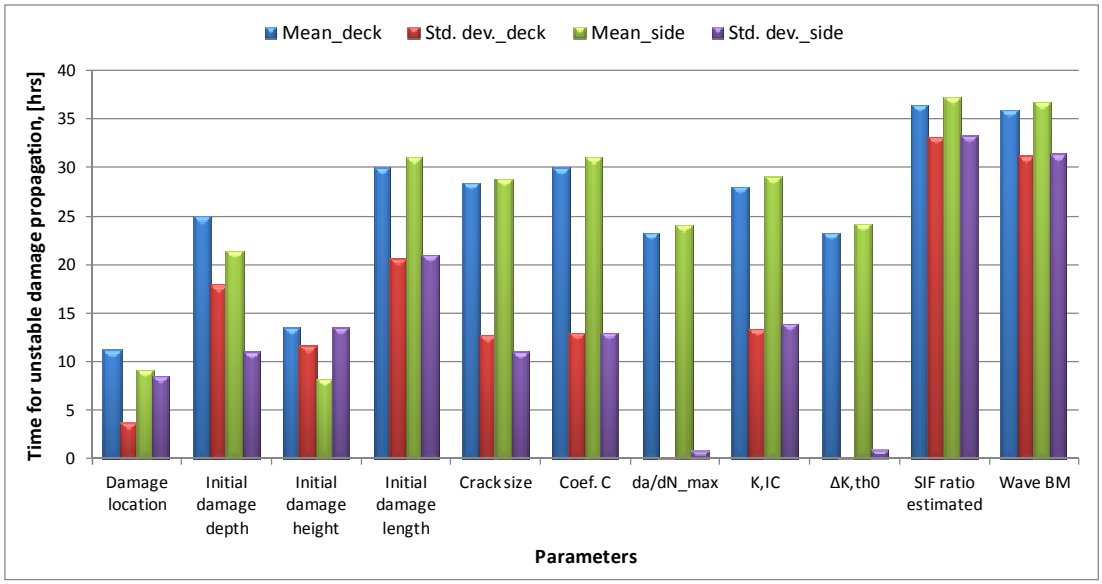

Figure 7-7: The estimated SIF, the wave bending moment and the initial damage conditions have the large effect on the time for unstable damage propagation

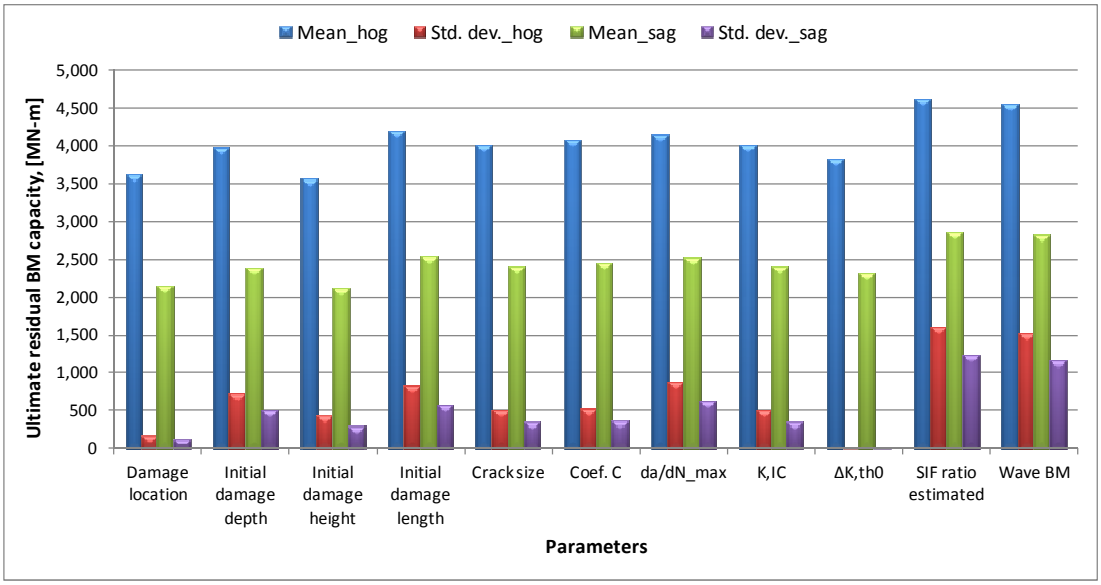

Figure 7-8: The ultimate residual bending moment capacity is sensitive to the SIF, the wave bending moment, and the initial damage conditions

As the effect of the initial damage opening size and the wave bending moment as well as the effect of the SIF ratio are the governing parameters from the sensitivity analysis results, further investigation is focused on their effect on the damage propagation. The required time for a damage to become unstable is obtained and compared for each deviation of the selected parameters. The location of the initial damage opening as well as other parameters is fixed as the concerned damage case is stuck to a preferred location in the section of the ship.

Initial damage opening size

With the developed parametric model of SIFs for the deck and side damage of the Aframax tanker, an in-depth sensitivity analysis is carried out to investigate the effect of the initial opening size on the damage propagations. The depth of damage on deck and the height of damage on side shell as well as the length of the initial damage opening are studied whilst the centre of the damage opening is fixed at the initial location. The effect of different damage opening sizes on the propagation rates is shown in Figure 7-9 ~ Figure 7-11.

The damage propagation with respect to change of depth of the initial opening is shown in Figure 7-9, where both damage propagations seem to become unstable as the size of the opening depth increases. The effect of the stiffener's constraint is seen

in the response of the deck damage propagation with intermittent stable responses when the initial damage opening size is relatively small. It is interesting that the response of the damage on the side shell propagates similarly to the damage on the deck plate.

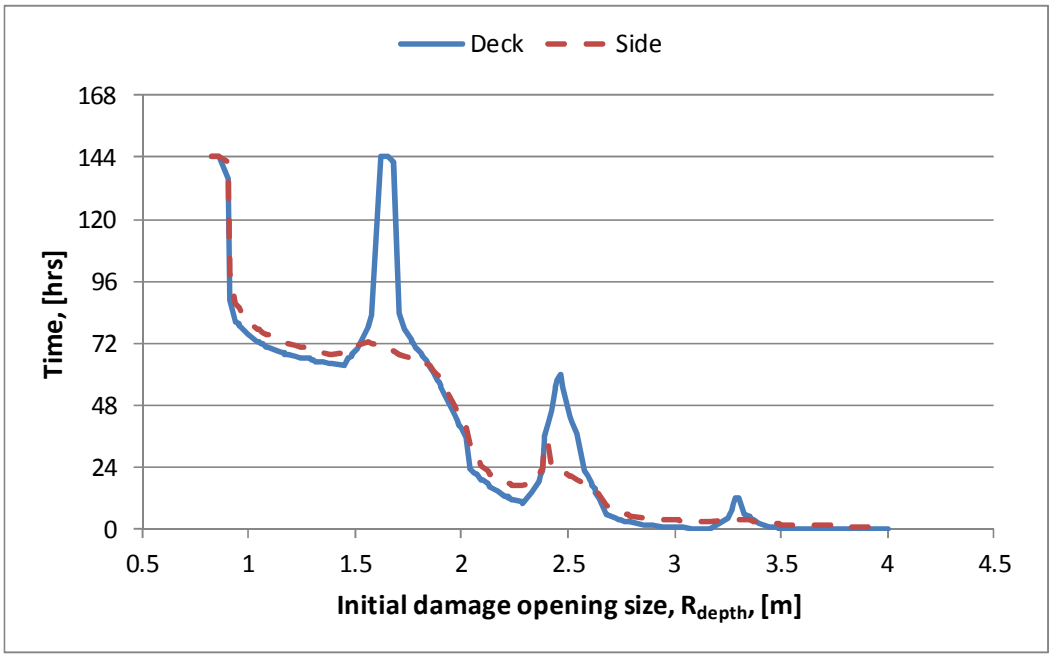

Figure 7-9: The effect of the initial damage depth on the damage propagation in the deck & side damage case of an Aframax tanker

The effect of the different height of the damage opening on the crack propagation in the deck and the side shell is illustrated in Figure 7-10. It is identified that the response of the side shell damage is affected by the stiffeners' restraint effects when the initial location of the crack tip is located in the affected region. The stiffeners' restraint effect may result in stable damage propagation during the given simulation period when the initial damage height is small. As the initial damage height is getting bigger, the unstable damage propagation on the side shell becomes faster in the first half then becomes slower in the second half of the horizontal axis. This phenomenon is explained by that the increased initial opening size induces high level of SIF. However, the location of crack tip in the proximity of the neutral axis of the damaged section delays the unstable damage propagation due to the reduced level of bending stresses.

On the other hand, the response of the damage on the deck plate follows that of the side shell damage, except in region of total instability of which is delayed on the side shell. That is, as the bending stress on the deck plate is getting larger because the neutral axis of the section is getting lower and the distance to the deck plating is increased.

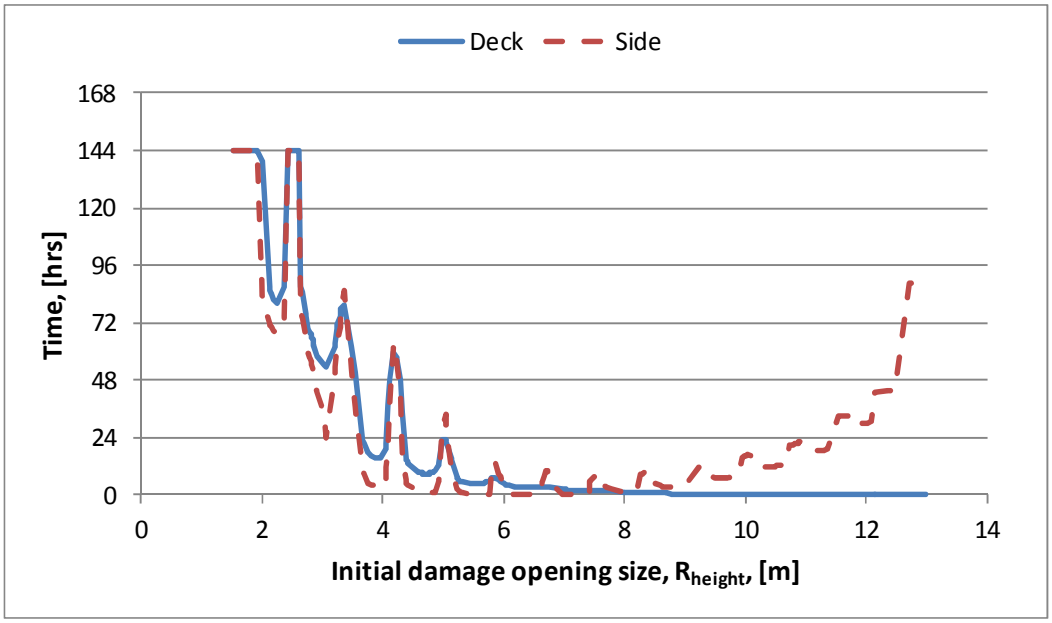

Figure 7-10: The effect of the initial damage height on the damage propagation in the deck & side damage case of an Aframax tanker

When the length of the initial damage opening is changed, the propagation rates are different from those obtained above. That is, as the size of the initial damage opening in the direction of ship's length increases, the unstable damage propagations are delayed and finally the stability is achieved (Figure 7-11). This is attributed to the different correction factors for the elliptical opening induced by the different aspect ratio of the elliptical opening. That is, given the initial crack size and the initial opening size in the direction parallel to the crack propagation, the initial value of the correction factor for an elliptical opening decreases as the size of the elliptical opening in the direction perpendicular to the crack propagation. The higher value of the initial correction factor for an elliptical opening facilitates unstable propagation (Figure 7-12).

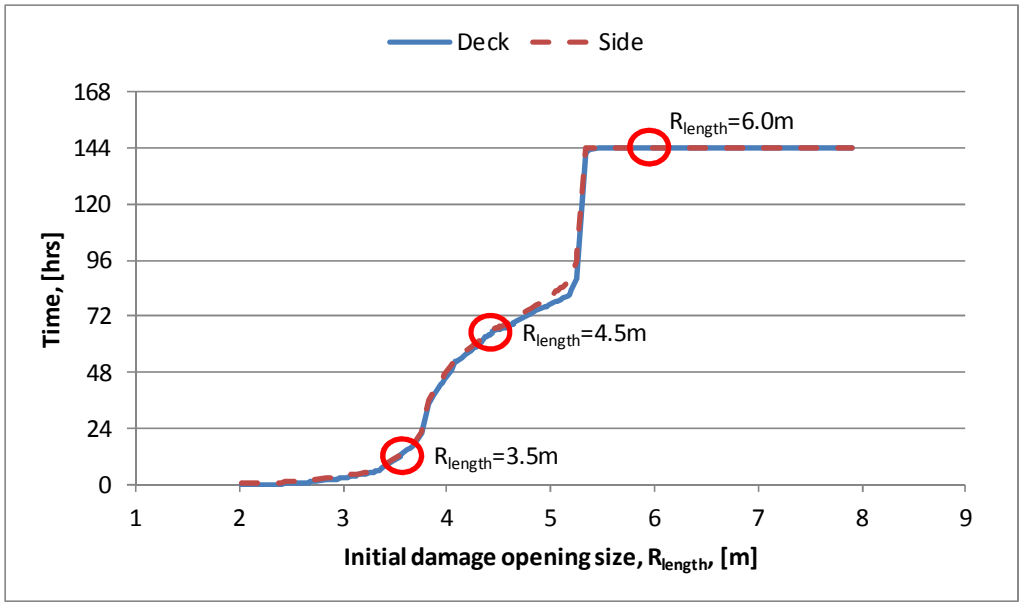

Figure 7-11: The effect of the initial damage length on the damage propagation in the deck & side damage case

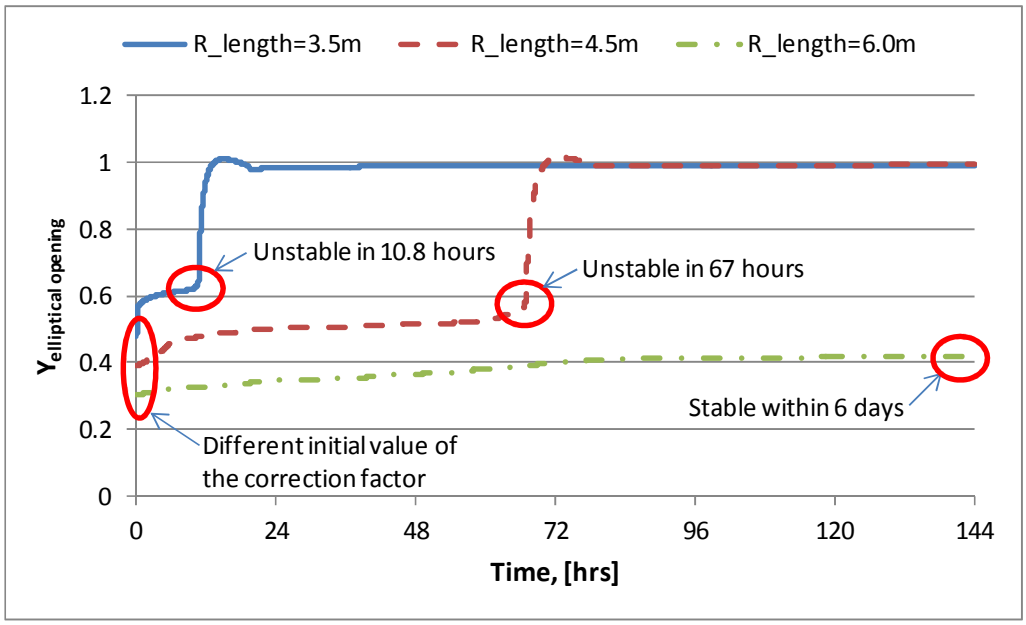

Figure 7-12: The difference of the initial opening length causes different initial correction factor for an elliptical opening, which strongly affects the propagation rate

Wave bending moment

The effect of different levels of the wave bending moments is studied and the similar tendency of response with that of the bottom damage case is obtained as shown Figure 7-13. As expected, the higher magnitude of the wave bending moment applied is the faster unstable condition of the damage propagation becomes. The lower

magnitude of the wave bending moment is found to delay the beginning of the unstable damage propagation. Using the original wave data of 6 days again for the further simulation gives that the damage propagation under the reduced wave bending moment by 30% becomes unstable after approximately 6 days (144 hours) from the initial damage in both deck and side plates (Figure 7-14).

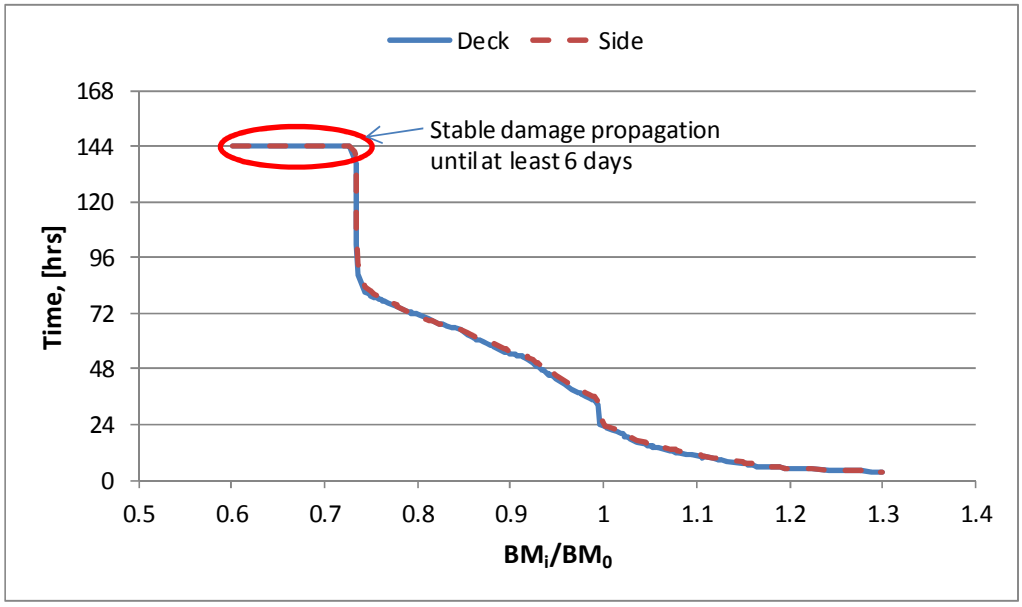

Figure 7-13: The bending moment effect on the damage propagation in the deck and side shell

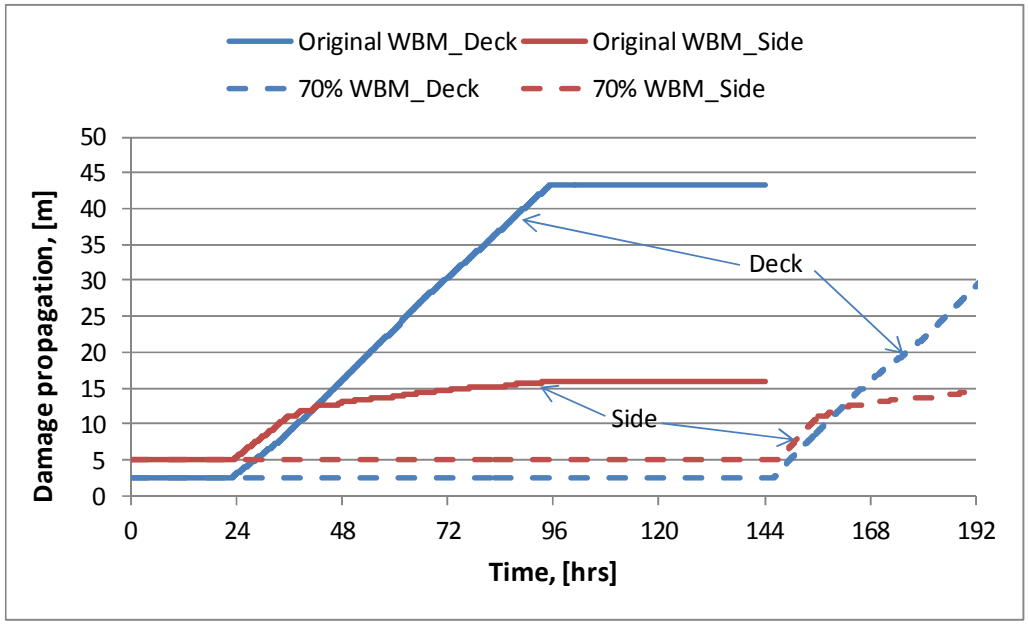

Figure 7-14: Unstable damage propagation of the deck and side damage case is delayed due to the reduced bending moment by 30% (1.0 mm/cycle is applied for the unstable region)

SIF ratio

Various values of the SIF ratio are tested and the results of the required time for damage propagations to become unstable are shown in Figure 7-15. As the case for the bottom damage, the damage propagation against changes of the SIF is almost identical to that of the wave bending moment. With the low value of the SIF ratio, the damage propagation is stable until 6 days while it becomes unstable within 4 days of the initial damage when the SIF ratio increases.

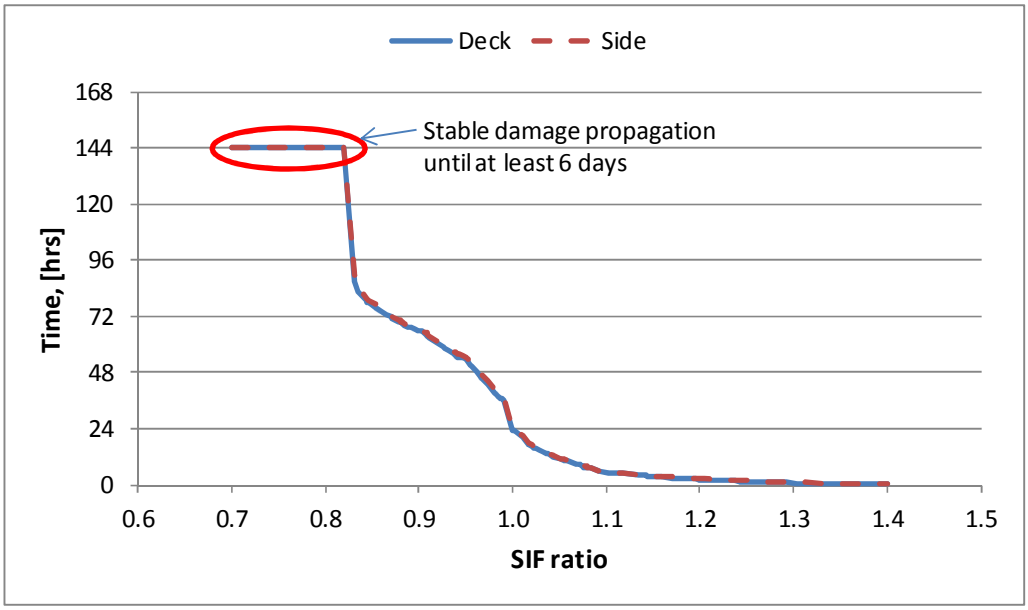

Figure 7-15: The effect of the SIF ratio on the damage propagation in the deck & side damage case of an Aframax tanker

7.2.3 Side shell damage

The sensitivity analysis with the side shell damage case shows a robust result against the examined parameters. With the provided probabilistic characteristics of each parameter, the unstable damage propagation is identified neither at the upper nor lower crack tip both –for the fully loaded and the ballast conditions.

Further analysis is made to investigate the effect of the different initial damage opening size and the wave bending moment. Considering the previous results that the effect of the SIF ratio is almost identical to that of the wave bending moment, the effect of the initial damage location is studied. For each case, the required time for a damage propagation to become unstable is obtained and compared.

Initial damage opening size

Various sizes of the initial circular opening are considered with the centre of each damage opening is fixed. The initial crack size is allowed to change by keeping the ratio of a_0/R constant. The responses of the damage propagation at both crack tips are plotted in Figure 7-16 against the change of the initial damage opening size.

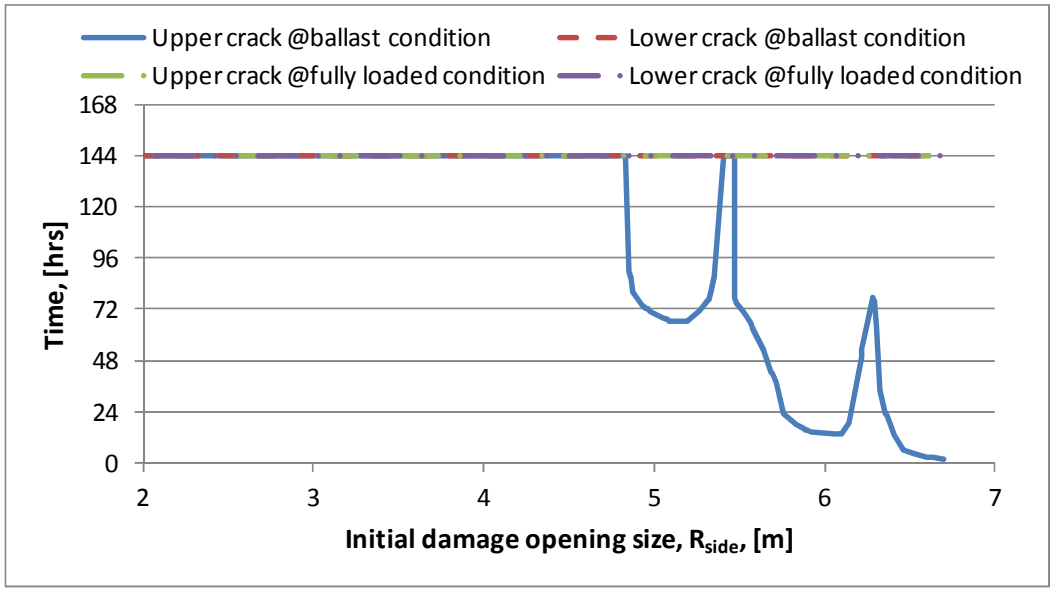

Figure 7-16: The effect of the initial size of the damage opening on the propagation rate in the side shell damage

It is identified that the damage propagation is negligible under the fully loaded condition while the upper crack under the ballast condition is only significantly affected by the change of the initial damage opening size. The response of the upper crack under the ballast condition shows stable damage propagation when the initial damage size is relatively small (less than 4.85 m in this case): the tensile bending stress at the crack tip is not high enough to induce a meaningful SIF. However, as the damage opening size increases the damage propagation of the upper crack becomes unstable with the intermittent influence of the stiffeners' constraint which delays unstable damage propagation. Once the upper crack of side shell plate becomes unstable in the ballast condition, the crack would spread rapidly (Figure 7-17). Finally, it should be noted that the lower crack under the ballast condition as well as the upper crack under the fully loaded condition is exposed to the compressive

bending stress hence the damage would be arrested unless the bending stress turns positive.

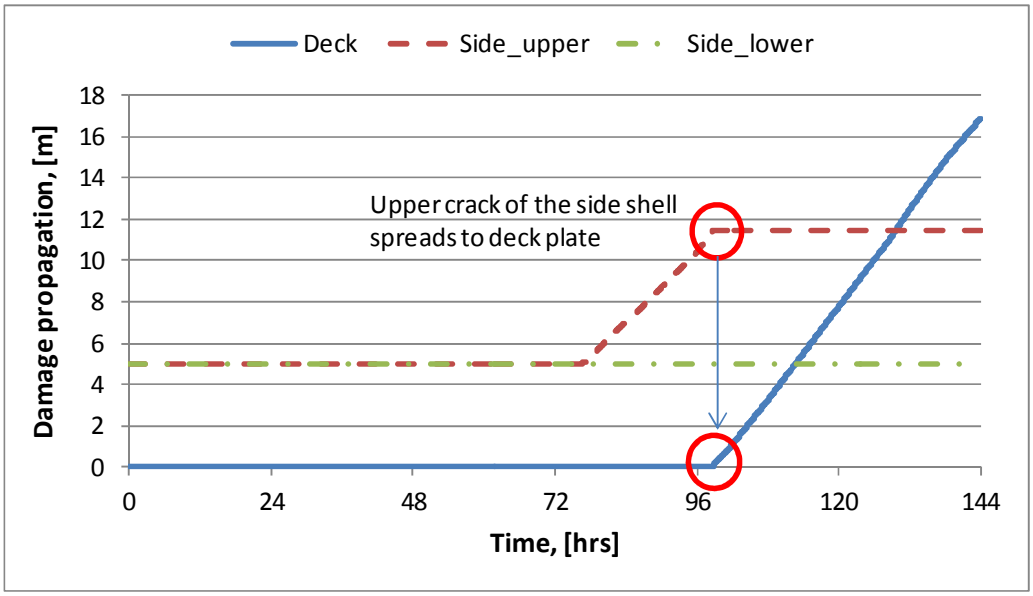

Figure 7-17: Once the upper crack on the side shell becomes unstable, it spreads to deck plate

Wave bending moment

Sensitivity analysis for various levels of bending moment is carried out under the normal ballast condition with the centre of the initial damage opening located 12.9 m above the base line. As this condition initiates unstable damage propagation in the side shell damage case (Figure 7-20), the effect of changing bending moment on the damage propagation would be easily verified in terms of the required time for unstable damage propagation as shown in Figure 7-18, in which the similar tendency of response with those previously obtained from other damage cases is presented. As stressed before, the stable response of damage propagation under small wave bending moment would change according to the subsequent wave conditions.

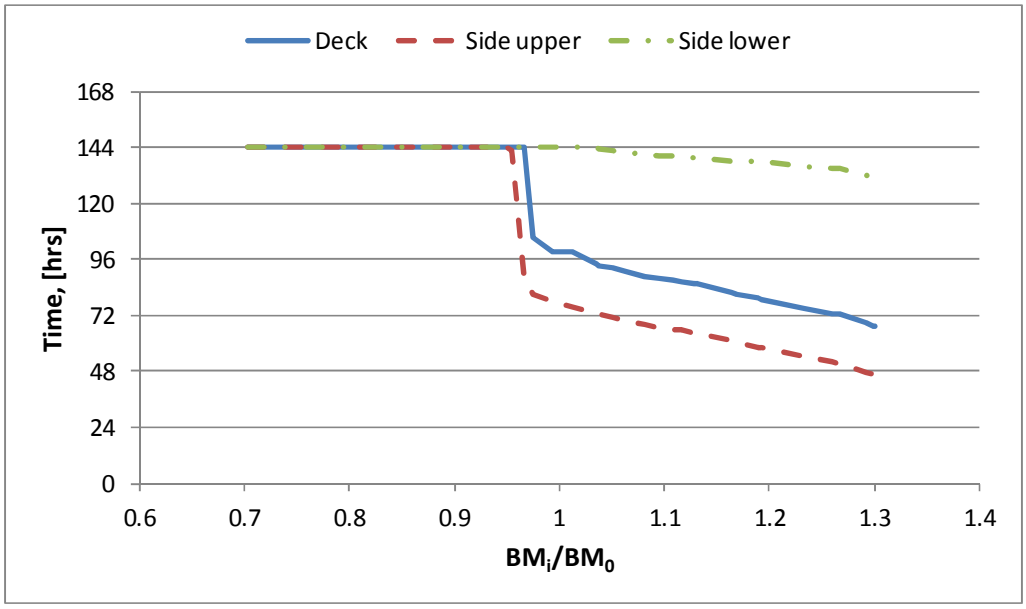

Figure 7-18: Change of bending moment affects the response of damage propagation in the side shell damage case of an Aframax tanker

Initial damage location

Another sensitivity analysis for the various location of the initial damage opening is carried out. In this analysis, the initial sizes of the opening and cracks are fixed but the centre of the initial damage varies. The responses of the cracks are calculated in both loading conditions and plotted in Figure 7-19 against the location of the initial opening.

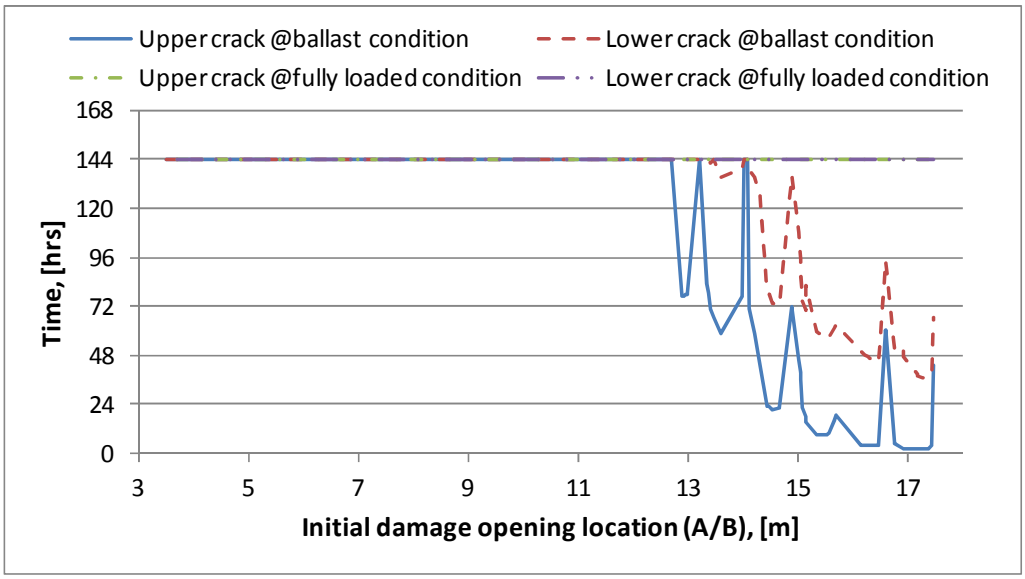

Figure 7-19: The effect of the initial location of opening on the damage propagation in the side shell case

Moving the centre of the initial damage opening downwards is expected to increase the damage propagation of the lower crack with the fully loaded condition but the extended damage is still negligible. Also no unstable damage propagation is identified even in case that the initial damage opening is located near the bilge plate.

On the other hand, moving the initial damage opening upward is identified to affect damage propagation in the normal ballast condition by increasing firstly the damage extension of the upper crack. The damage propagation on the upper crack becomes unstable when the centre of the initial damage opening reaches 12.9 m above the baseline. In this case, the unstable damage propagation enables the upper crack to reach the deck plate in approximately 4 days from the initial damage and to continue on the deck plate (Figure 7-20).

A similar behaviour is identified on the lower damage on side shell under the ballast condition when the bending stress on the lower crack tip turns to positive as the initial damage opening moves upward. The unstable condition of the lower damage propagation becomes stable again as the crack tip approaches the neutral axis of the damaged section (Figure 7-21).

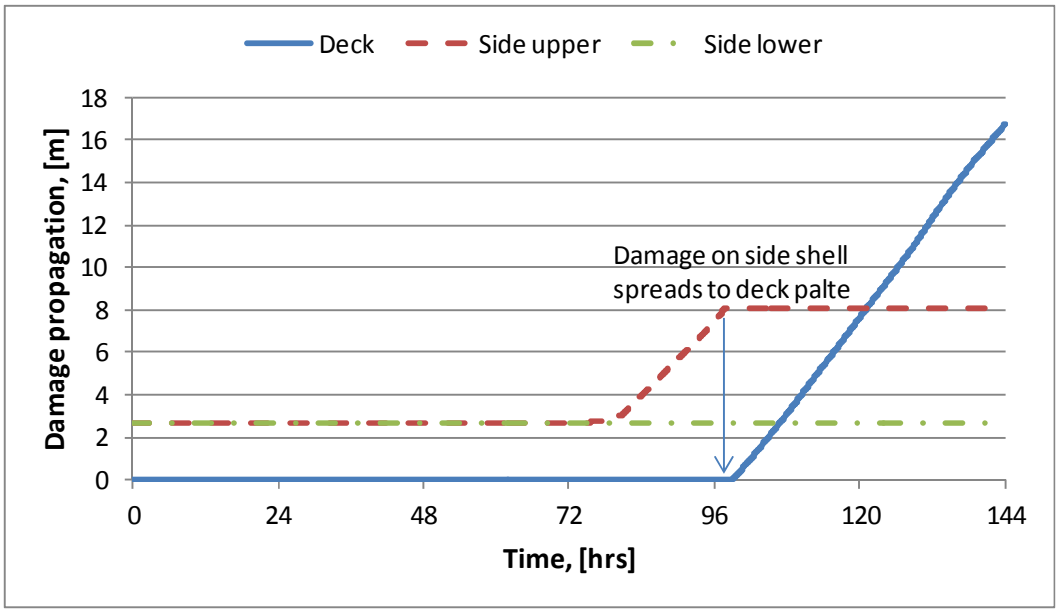

Figure 7-20: The elevated location of the initial damage opening causes unstable damage propagation of the upper crack tip on side shell and results in unstable damage propagation on deck plate (the centre of the damage locates at 12.9 m A/B)

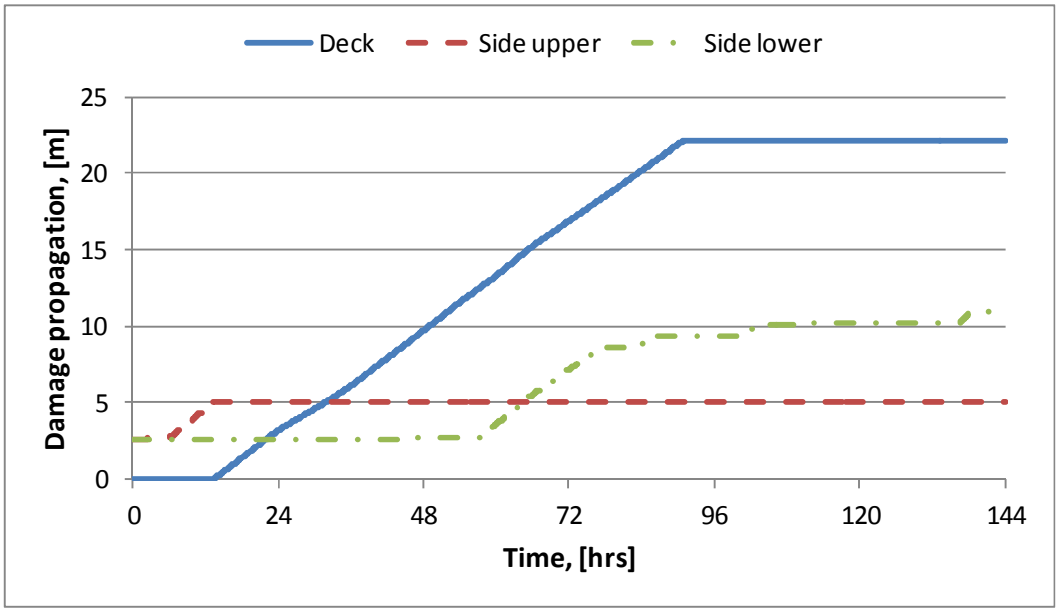

Figure 7-21: Lower damage propagation becomes stable again when the crack tip approaches the neutral axis of the damaged section (the centre of the damage locates at 16.0 m A/B)

7.2.4 Findings of the sensitivity analysis

Prioritisation of the considered parameters in the sensitivity analysis is tabulated in Table 7-4 according to the standard deviation of the required time for unstable damage propagation. The result shows that the response of the damage propagation is most significantly sensitive with respect to the magnitude of wave bending moment, the estimated SIF and the initial damage opening size among the examined parameters. It is recommended that for each damage case, more attention should be paid to the prioritised parameters in order to reduce their variations in the emergency situation. In the design study, the designer should pay attention to the prioritised design parameters in order to control the outcomes and search the optimal design solutions most efficiently with the minimised effort.

Table 7-4: Prioritisation of parameters from the sensitivity analysis

Parameters / Damage case	Damage location	Damage size	Crack size	Coef. C	da/dN_{max}	K_{IC}	ΔK_{th0}	SIF ratio	WBM
Bottom	6	3	4	5	9	7	8	2	1
Deck-side	7	3	6	5	9	4	8	1	2

From the further study with the wider variation of the most important three parameters, the following findings are drawn, which give an outlook on the response of damage propagation engaged with other initial damage conditions:

- In general, the larger opening of the initial damage results in the faster unstable damage propagation under the condition that the initial crack size changes proportional to the size of the damage opening. Even the side shell damage case is estimated to result in unstable damage propagation when the initial damage opening size is large enough.
- Also the initial location of crack tip in the region of the stiffeners' restraint hampers the onset of the unstable damage propagation.
- Large wave bending moment could cause an immediate unstable condition while small wave bending moment could delay the unstable damage propagation for a number of days.
- The variation of the SIF ratio gives the same response as that of the wave bending moment variation.
- The closer of the initial location of damage opening in the side shell plate to the deck plate or bottom plate tends to result in larger damage extension and even unstable damage propagation spreading to the adjacent structures.

7.3 Case studies revisited

In this section, the damage cases analysed in Chapter 6 are re-evaluated in order to obtain probabilistic results by taking into account uncertainty associated with various parameters. The probabilistic distribution of each parameter is adopted as used in the sensitivity analysis (Table 7-1). Among the three case studies, only two damage cases (bottom damage, deck and side damage) are analysed. The side shell case does not develop any significant propagation under the given wave data and it is ignored.

In order to analyse the probabilistic responses of the given damage cases MC sampling is performed again for each set of parameters. Each parameter is sampled according to its probabilistic distribution and each complete set of parameters is an input of the developed parametric models. The analysis is carried out for 10,000 samples for each damage case.

7.3.1 Bottom damage case

The result of the stochastic analysis on the bottom damage case with the given initial damage condition and wave data is summarised in a bar chart (Figure 7-22), which illustrates mean and standards deviation values of the responses with respect to the required time for damage to become unstable and the ultimate residual strength capacity in hogging and sagging. It is identified that the behaviour of both crack tips is almost identical.

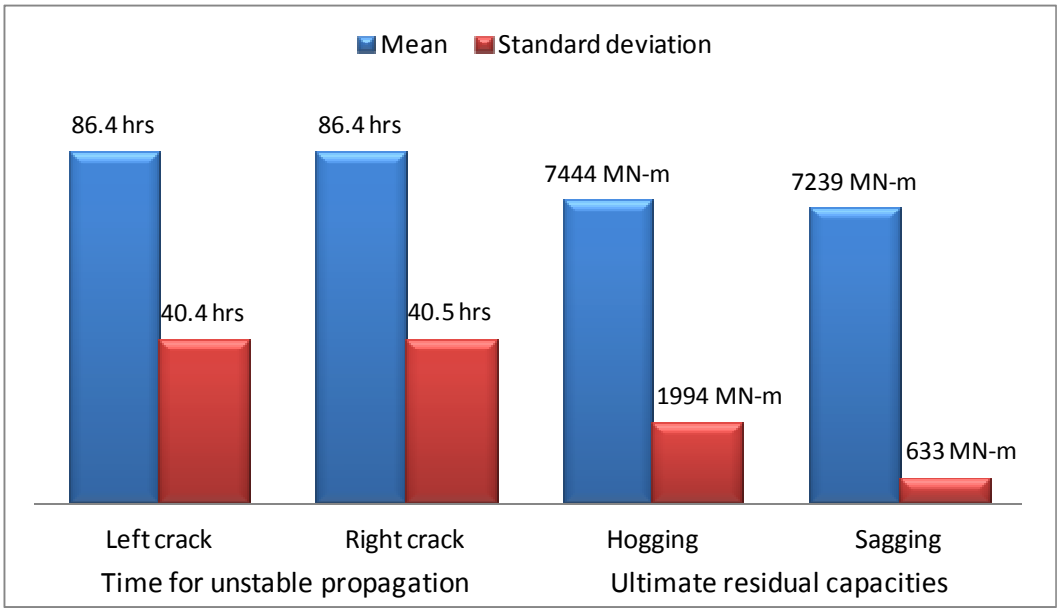

Figure 7-22: Probabilistic properties of responses with the bottom damage case

The probabilistic distribution of the required time for damage propagation to become unstable is shown in Figure 7-23, which contains the cumulative distribution function (CDF) and its upper and lower bound curves. The CDF shows that if the unstable damage propagation occurs, it would start within 4 days (96 hours) from the initial accidental event. More than 70% of the examined samples become unstable within 4 days. This is attributed to the wave loading that reduces significantly after 4days (Figure 6-17) and reduces the chance of unstable damage propagation very much. While the deterministic analysis predicted that the corresponding damage case would become unstable after 67.2 hours, the probabilistic result shows that the probability of the unstable damage propagation within 67.2 hours is only 37%. Assuming that the 50% of the probability is a fair decision-making criterion as it gives the same

chance to the conflicting decision-makers, 72 hours after the initial damage could be more rational in terms of the unstable damage prediction.

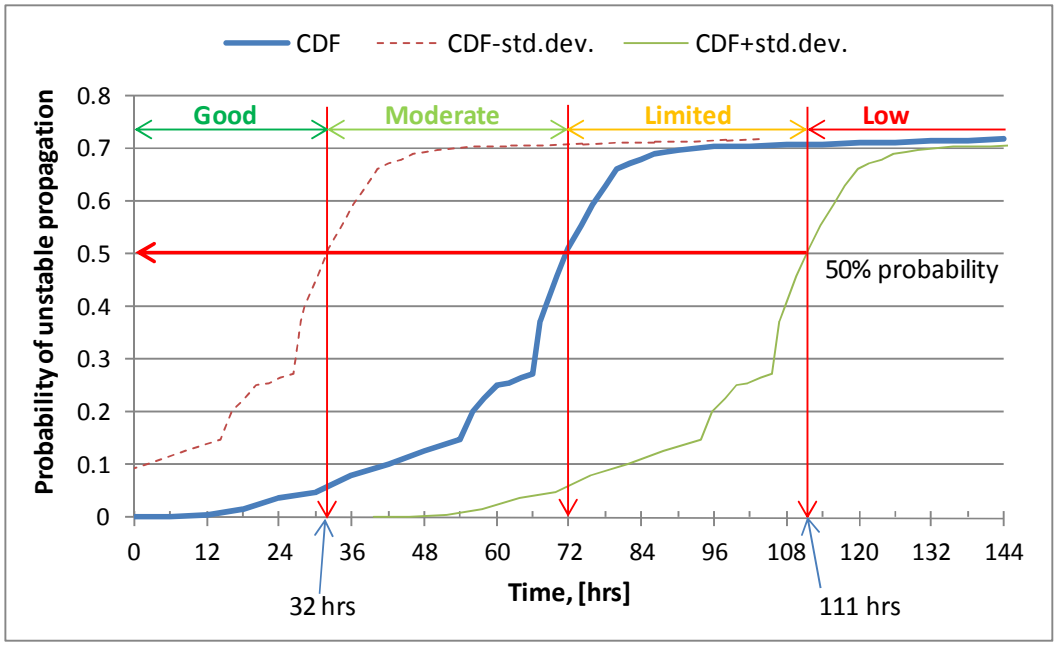

Figure 7-23: Probabilistic distribution of the time for unstable damage propagation in bottom damage case

The upper and lower bounds of CDF curve are obtained in accordance with the standard deviation. In the emergency situation, it is recommended that the rescue and salvage operation should be deployed and managed according to the timeline information that the chart provides. Adopting that 50% of probability is rational for the emergency decision-making (a rather experience-based criterion but valid nonetheless), any intervention would be safely carried out in 32 hours, which is the most preferable situation, while the region between lower bound and CDF curve (32 ~ 72 hours) can be regarded as more uncertain. Any operation beyond the CDF curve (after 72 hours) should be carefully considered as the safe operation would be limited until the upper bound (111 hours), after which any operation should not be carried out as the damage extent is expected to increase rapidly. The probability criterion could be differently chosen by the decision maker - A lower probability could be chosen if the decision maker prefers a conservative approach to safety.

The distributions of probability with respect to the ultimate residual bending moment capacity are plotted in Figure 7-24 for hogging and sagging condition. The horizontal

axis represents the ratio of the ultimate residual bending moment capacity divided by the intact ultimate bending moment capacity in hogging and sagging. The CDFs indicate that, under the given wave data with the specific initial damage condition, the probability that the ultimate residual hogging bending moment strength is less than 63 % of the intact capacity is 0.63 in hogging while the ultimate residual bending moment capacity in sagging would decrease by less than 83.6 % of the intact capacity with the same probability of 0.63.

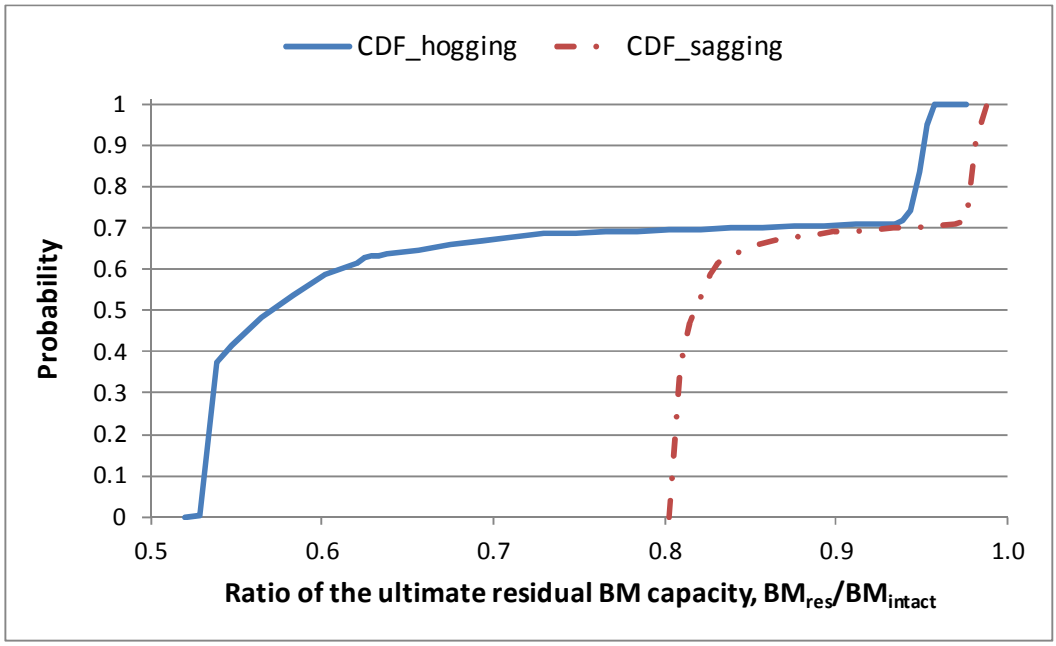

Figure 7-24: Probabilistic distribution of the ultimate residual BM capacity in the bottom damage case

It should be stressed that the results of this analysis is based on the specific initial damage condition under the given wave data hence other damage conditions or other wave conditions would result in different probabilistic conclusions. The intention here is to demonstrate the manner in which the methodology can be used. It is obvious that the analysis for design purposes would require various damage cases to be included as well as all possible wave conditions that the ship is expected to encounter in the planned voyage in order to rationalise its structural configuration.

7.3.2 Deck and side damage case

The mean and standard deviation of responses with respect to the deck and side damage case is summarised in Figure 7-25, where a higher deviation of responses is

obtained compared with that of the bottom damage case. This can be explained according to the fact that the unstable damage propagation takes place dominantly within 24 hours making the mean value low while the stable damage propagation within 6 days has little frequency as shown in Figure 7-26 and Figure 7-27. It is corresponding to the result of the sensitivity analysis.

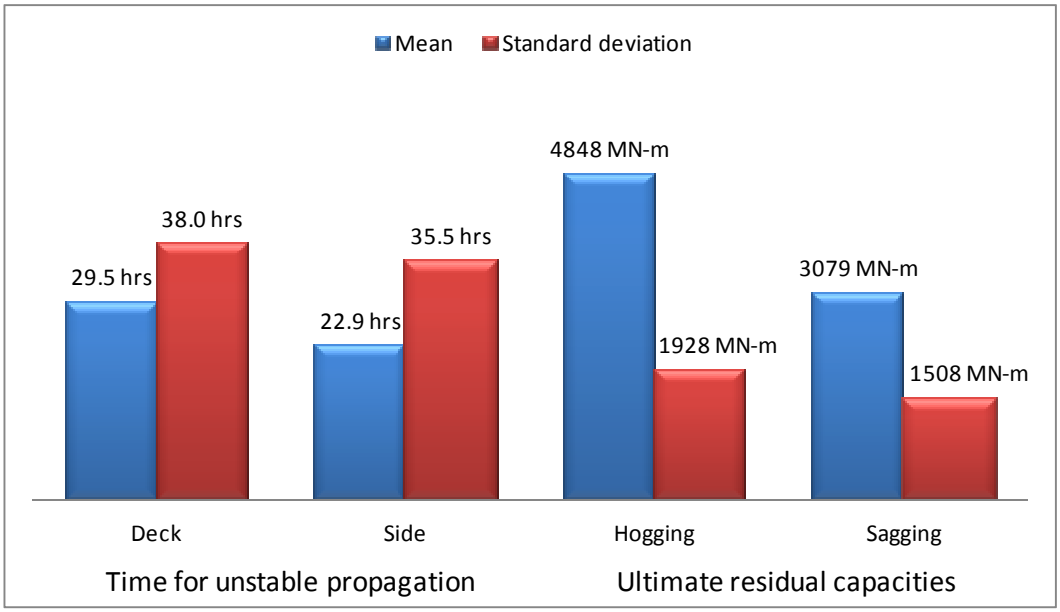

Figure 7-25: Probabilistic properties of responses with the deck & side damage case

The probabilistic distributions of the time when the damage propagation enters the unstable region are shown in Figure 7-26 and Figure 7-27 for deck and side damage respectively. It is interesting that 14.4 % of the samples involve immediate unstable damage propagation on side damage while 1.2 % on deck damage. Investigation on such samples gives the following common findings:

- The vertical damage size on side (R_{height}) is larger than the mean value
- The transverse damage size on deck (R_{depth}) is larger than the mean value
- The longitudinal damage size (R_{length}) is smaller than the mean value
- The initial crack size (a_0) is larger than the mean value
- The plane strain fracture toughness (K_{IC}) is smaller than the mean value
- The SIF ratio is larger than the mean value
- The wave bending moment ratio is larger than the mean value

Considering the deterministic result showing that the unstable damage propagation would start at 23.2 hours and 23.8 hours for deck and side shell respectively, the result from the probabilistic analysis seems corresponding with it as the probability of unstable damage propagation within the time is 66% and 73% for deck and side shell respectively.

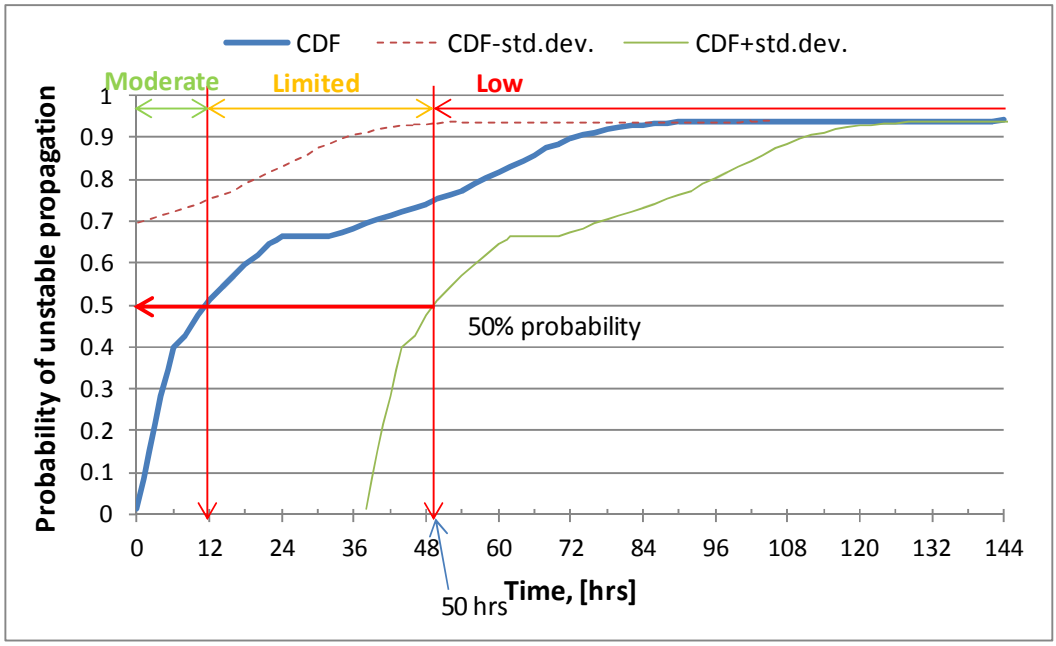

Figure 7-26: Probabilistic distribution of the time for unstable damage propagation in deck

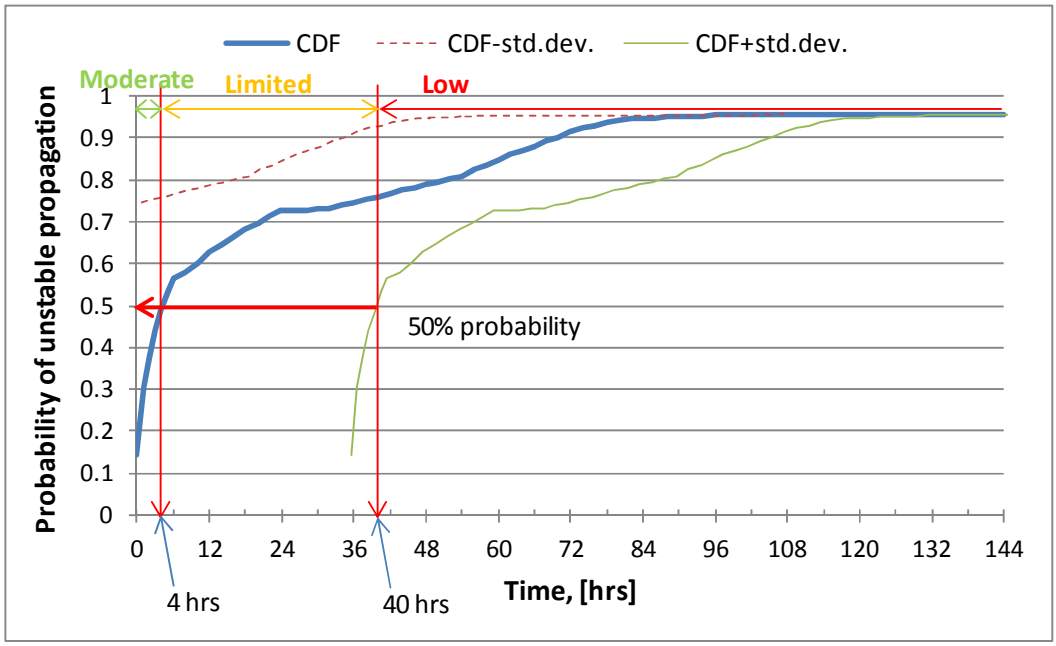

Figure 7-27: Probabilistic distribution of the time for unstable damage propagation in side

The upper and lower bound of the CDF curve indicate that 50% of times sufficient safety is not guaranteed for operation and a narrow zone of moderate safety is expected for the rescue and salvage operation. Although 4 hours of moderately safe operation is recommended from the side shell result, considering that the side shell damage propagation would be limited as the crack tip approaches the instantaneous horizontal neural axis of the cross section, the operational decision *could* be made in accordance with the extended moderately safe operating zone of 12 hours based on the deck result.

The stochastic distributions of the ultimate residual bending moment capacity are illustrated in Figure 7-28 by using the ratio of the ultimate bending moment capacity divided by the intact ultimate bending moment capacity for hogging and sagging respectively. The result is interpreted as that the probability that the ultimate residual bending moment capacity reduces less than 50 % of the intact capacity is 0.75 in hogging while 0.84 in sagging for this specific damage condition under the considered wave data. The probability that the damaged section would lose its intact capacity by 60% is 0.58 for hogging and 0.74 for sagging.

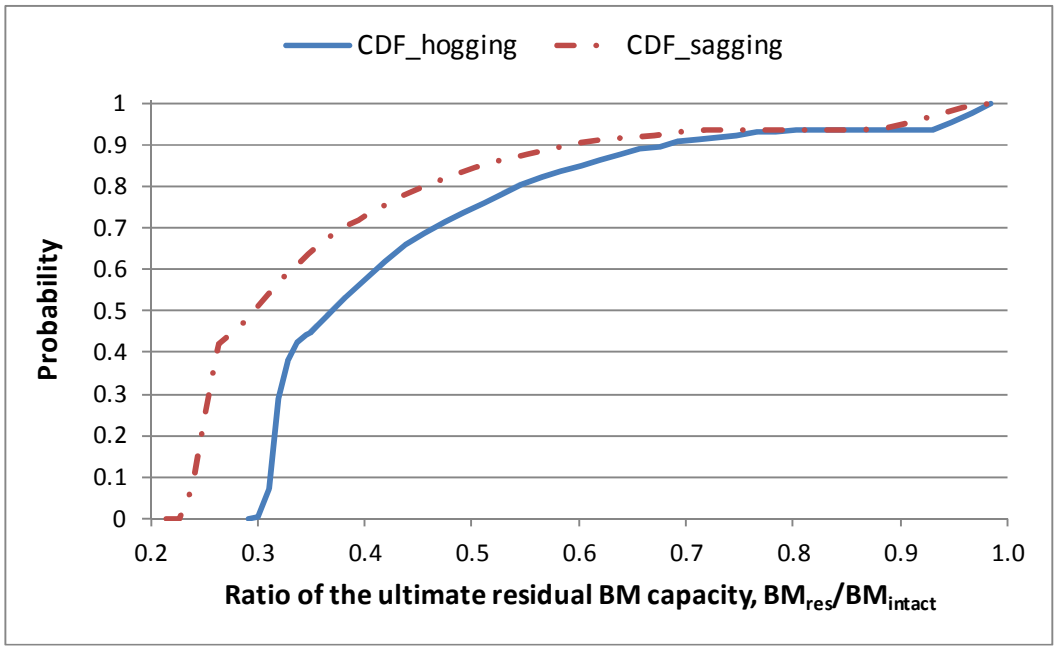

Figure 7-28: Probabilistic distribution of the ultimate residual BM capacity in the deck & side damage case

7.3.3 The effect of the sea state

This section addresses the effect of the different wave data on the probabilistic result and aims to compare and demonstrate how the estimated safe time period for the rescue and salvage operation in the emergency situation would change according the given wave data. It is understood from the sensitivity analysis results that milder sea states would decrease the chance of the unstable damage propagation or at least delay it. However, Figure 7-29 shows how the time for the safe emergency operation is affected by the differently exposed wave data: the original wave data (Figure 6-16) and a 5% and 10% decrease both in the significant wave height and the zero-crossing wave period.

Taking again the 50 % occurrence of the unstable damage propagation as a guide, the graph indicates that the safe emergency operation would be increased by 7 hours, from 32 hours to 39 hours after the initial damage, when the original wave data becomes milder by 5 % even though the same damage configuration on the same ship is considered. The window for safe operation increases sharply to more than 6 days when the 10 % milder wave data of the original one is considered in the analysis.

The above demonstrates that the methodology can provide information pertinent to the decision-making in the management of accidental situations. That is, not only a decision-making on the salvage planning but also a decision-making on whether the damaged ship should be taken to a sheltered area or not can be supported by the produced information based on the predicted wave condition. Furthermore, the various responses from the different wave conditions require a full investigation of the entire wave conditions that the ship would experience during its service at the whole ship level in order to measure and manage the safety performance pertaining to the structural survivability in the implementation of the ship design process.

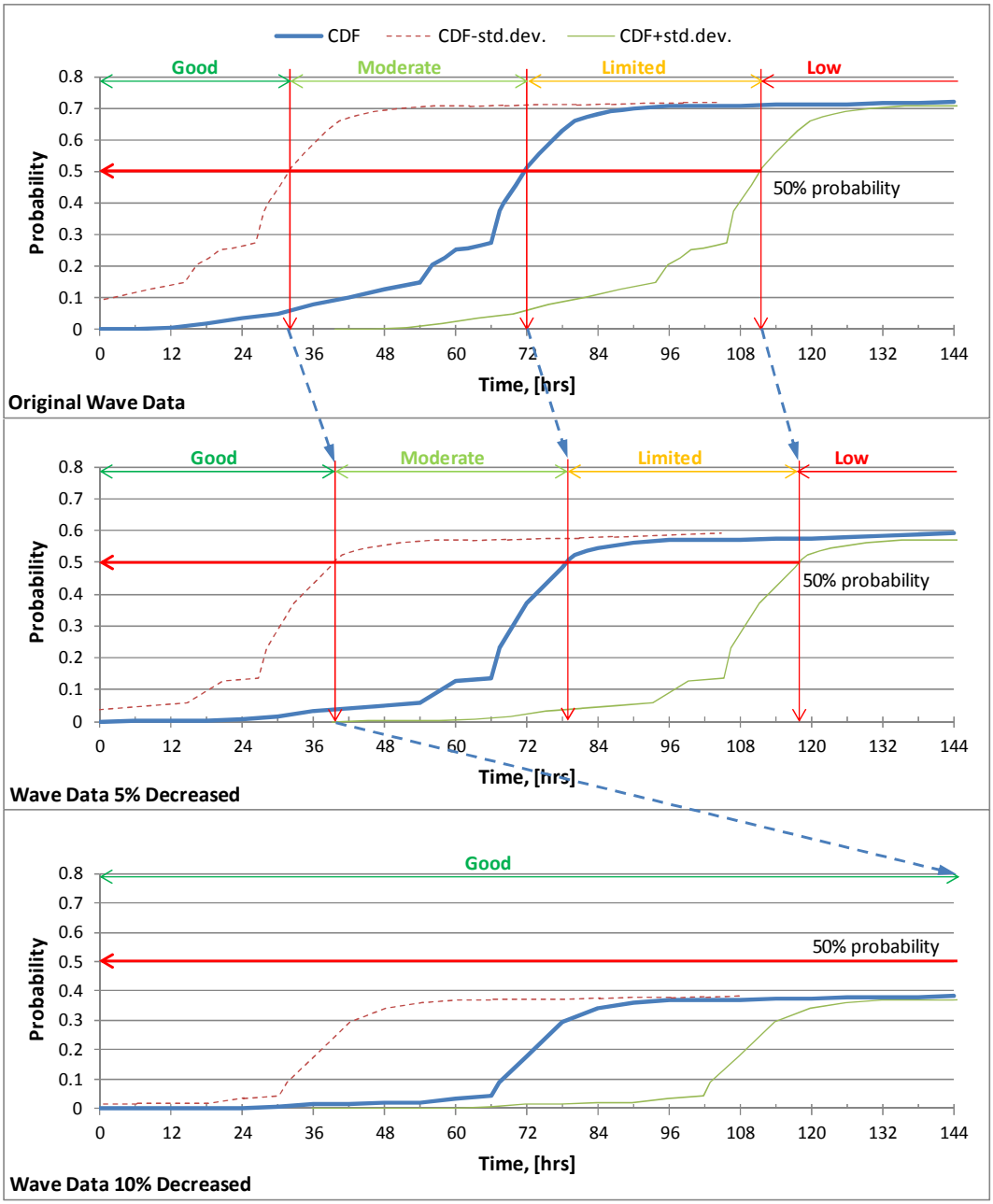

Figure 7-29: The wave data affects the safe emergency operation time (bottom damage case)

7.3.4 Sampling error

In this section, the effect of sampling size is investigated to guide on the required number of samples for the confident analysis result. The examined sampling sizes include 10,000 samples, 5,000 samples, 1,000 samples, 500 samples and 100 samples and for each sampling size the sampling error is calculated in accordance with 99% confidence level based on the Clopper-Pearson confidence interval on the binomial

proportion as addressed in Brown, Cai and DasGupta (2001) and presented by confidence bounds as illustrated in Figure 7-30.

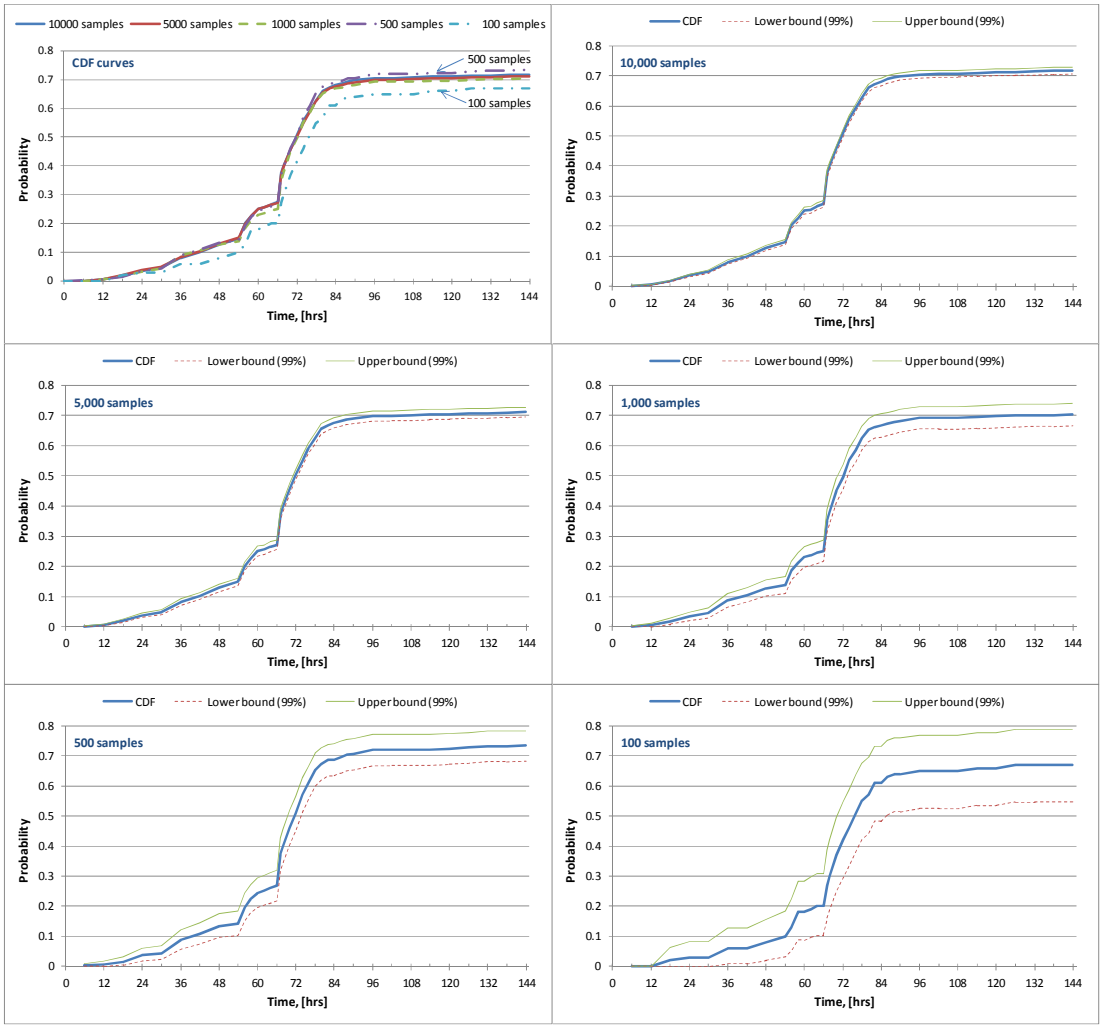

Figure 7-30: The effect of the sampling size on the CDF result (the uppermost left graph) and sampling errors with 99% confidence level for the bottom damage case

From the result, the increasing tendency of the sampling error is identified as the examined sampling number decreases. Considering that the CDF result starts to deviate from the result of the 10,000 MC sampling when the sampling number is as small as 500 or less, it could be said that at least 1,000 MC samples should be used in the probabilistic analysis in order to prevent any sampling error. The same tendency is also confirmed by the result of the deck and side damage case. In the real ship hull's application, the number of samples should be chosen to fit the analysis purposes according to the available time as well as the accuracy tolerance that the result is allowed. For example, the application of the methodology in the early design

stage where as many as damage cases, loading conditions as well as wave data are required for a whole ship level analysis would have benefit from using small sampling size e.g. 100 samples for each design case as the time for analysis is limited during the given design period where, however, the less accuracy is accepted.

7.4 Implementation in the risk-based design context

The application of the developed tool with a specific damage configuration under the predicted wave conditions can be made for an emergency operational aspect. However, with the developed parametric models, all the possible damage cases that a ship could experience can be readily assessed in the early design stage by taking into account the predefined loading conditions as well as various wave conditions which the ship is expected to encounter in the planned routes during its service. That is, the tool developed for the assessment of the progressive structural failure and the ultimate residual strength of a damaged ship in timeline can be integrated in the *risk-based ship design* context to achieve the safety performance i.e. the zero-tolerance of human fatality, the minimum environmental damage and loss of property. In regard with the progressive structural failure, the performance could be attained when the safely operable time zone in the emergency situation is securely guaranteed against the required operation time, which would be different for different ship types.

The risk-based ship design requires multi-objective, multi-criteria optimisation processes allowing trade-off between design parameters. In the optimisation scheme, with other objective functions e.g. stability, speed, minimum weight and etc., the objective functions involved in risk from loss of structural integrity under the action of the progressive structural failure can be expressed as follows:

- Maximise the safely operation time zone
- Maximise the ultimate residual strength

These objectives could be achieved by use of highly fracture-resistant materials in an appropriate locations e.g. around the most probable damage locations, by examining proper alternative arrangements or stiffeners/girder systems.

However, it should be reminded that the purpose of this work is not to perform a design study or an optimisation analysis but rather to develop a tool and methodology for progressive structural failure analysis that can be systematically incorporated in the design process, where the risk-based ship design methodology with the help of optimisation processes is desirably implemented.

7.5 Chapter summary

Following the deterministic analysis of the damage propagation and the corresponding ultimate residual strength assessment, this chapter focuses on the uncertainty that the models are involved with. Sensitivity analysis is performed with the developed parametric models and it is found that the response of damage propagation and the final ultimate residual strengths are strongly sensitive with respect to the magnitude of wave bending moment, the estimated SIF and the initial damage opening size. The probabilistic approach is used to reassess the damage cases of Chapter 6 and the results of the uncertainty propagation are successfully obtained followed by the discussion on the interpretation and use of the probabilistic results in the emergency operational aspect. This chapter finishes with a discussion on the implementation of the developed tools in the *risk-based ship design* context by use of probabilistic schemes.

8 DISCUSSION AND RECOMMENDATIONS FOR FUTURE WORK

8.1 Preamble

The approach proposed in this thesis for the survivability assessment of a damaged ship is the first attempt to take into account the structural degradation in timeline following an accidental event. The key element is the progressive structural failure analysis the concept of which is developed, documented and implemented in conjunction with the residual strength assessment. The developed tool and findings from its application to a real ship structure are summarised in this chapter. Following the discussion on the results, a set of recommendations for future work is made with the intention to enhance the capability of the developed tool and improve the accuracy of the results.

8.2 Discussion

Among the constitutive components of the proposed methodology this thesis elaborates on the progressive structural failure and the residual strength capacity of a damaged hull girder. A summary of findings during the development of the approach and the tool for the focused elements and from the result of its applications are listed in the following paragraphs.

8.2.1 Progressive structural failure

Progressive structural failure is the key component of the proposed methodology as it has received less attention in the literature so far. Moreover, high profile accidents of the recent past like Prestige, clearly define the need for rationalisation of all facets of shipping operations. Although state-of-the-art developments in ship design allow for an effective de-risking during the design process, the remaining risk, often referred as *residual risk*, needs to be managed. Along these lines a methodology for the analysis and assessment of the progressive structural failure of a damaged ship has been developed.

At the core of the methodology lies a crack growth model conjunction with the LEFM approach, the application of which is valid to ductile materials, e.g. steels, as long as the size of the plastic zone around the crack tip is sufficiently small in comparison to the damage size.

A crack growth model that covers slow, medium and accelerated crack growth rates is adopted with some modification in order to take into account the effect of the applied stress ratio. A zero-growth rate is applied in the region below the threshold while a value of the maximum growth rate is set in the region that the maximum SIF exceeds the material fracture toughness. Although the maximum crack growth rate has been found to have little influence on the time for unstable damage propagation, it strongly affects the damage evolution, which in turn is critical to the ultimate residual strength capacity.

The use of the maximum crack growth rate in the unstable region has arisen from the mathematical limitation of the proposed crack growth model, which returns negative values if the maximum SIF exceeds the material's fracture toughness. For the crack propagation enabled in the unstable region, an additional measure is required but unfortunately, no research on the crack growth rate in the unstable region is found. Hence a fixed crack growth rate in the unstable region is introduced. As data from the various experimental tests show that the maximum crack growth rate obtained near the unstable region are in the order of 10^{-3} mm/cycle, which corresponds to the maximum crack growth rate obtained from the proposed crack growth model, the fixed maximum crack growth model is considered in the order of 1 mm/cycle in this analysis. However, as it is believed that the crack growth rate in the unstable region also increases, it is advisable to use a model suitable for this purpose, if it is available in the industry. The alternative way to obtain the crack growth rate in the unstable region is to carry out experiments, but the practical difficulties associated to this approach are obvious. More work is needed in this area.

The SIF magnitude and variation, i.e. the driving force for crack propagation in a complex structure as the ship hull, is obtained with FE analysis. The VCCT for ABAQUS is used in this work and parametric models are developed by use of a superposition concept that combines various correction factors for each damage case under consideration. The correction factors are obtained by handbooks for simple cases and their validity is proved by FE analysis when the complex structure is considered. In the latter case, empirical formulas are developed for the parametric analysis. Although their applicability is analysed in detail, yet they remain specific to

the case of the tanker ship that is exemplified here. More general application would require similar development for other ship sizes and types.

The result of application to a real ship structure for a given wave record shows that the initial damage could propagate to the adjacent structural elements and involves unstable behaviour. It is found that damage in an unstable propagation will hardly stop unless the driving stress is significantly reduced. That is, the environmental excitation changes or the crack encounters a major structural element that will delay it. In addition, the developed cracks on the vertical members e.g. side shell, will stop propagating as they approach the neutral axis of the damaged section (due to the reduction of the bending stresses), contrary to the case of horizontal members (e.g. deck and bottom panels) where non-stop behaviour is observed.

The simulation in the developed model is carried out in the time domain hence the structural degradation can be analysed as a function of time. This information is very useful as it could provide not only the deteriorated geometry that would be used to calculate the residual strength capacity but also the estimated time when the boundaries of flooded compartments would be breached, or when oil outflow (in the case of a tanker) will begin.

Finally, one noticeable inconsistency in the case studies is that the wave loads are calculated using the deep sea conditions, whilst the accidental events assumed to lead the damage cases (i.e. collision and grounding) normally take place in coastal and shallower water. In this respect, wave loading in shallow water needs to be included in the methodology.

8.2.2 Residual strength capacity

An analytical model for the calculation of the ultimate residual strength of a damaged ship is developed based on the beam-column method, which has proved fast and accurate. The particular feature that the developed model has is that it is linked to the progressive structural failure analysis and this enables the assessment of the ultimate residual strength capacity in the time domain, i.e. the deterioration of the hull girder bending capacity.

From the results of the case studies, the progressive structural failure is found to have great effect on the reduction of the residual strength capacity of the damaged section. Although the reduction of the ultimate strength with the initial damage is small, the progressive degradation results in significant reduction in residual strength. For the deck and side damage cases, the initial damage reduces the ultimate strength by less than 4.6 % and 7.8 % for hogging and sagging while the final condition results in reduction by 65.1 % and 72.4 % for hogging and sagging respectively. Similar result is obtained for the bottom damage case while the side damage case results in a negligible reduction of the residual strength capacity.

A point of interest is the loading condition of the ship (in terms of hogging and sagging) at the time of initial damage has a dominant effect on the way the deck and bottom damage will propagate. In this respect, it is expected that bottom damage will be more susceptible in sagging, whereas deck damage will propagate more readily in hogging.

8.2.3 Uncertainty quantification and probabilistic approach

The developed parametric models have enabled probabilistic analysis of the damage propagation and ultimate residual strength. MC sampling is performed using the probabilistic distribution of each parameter (the details of which are obtained from the literature) and sensitivity analysis is carried out. The main findings from the results of the sensitivity analysis are:

i) the most dominant parameters are the wave bending moment, the estimated SIF and the initial damage opening size although the priority of parameters depends on the damage case,
ii) the damage opening at the location where higher tensile bending stress is induced shows faster unstable damage propagation, and
iii) the deeper in deck (beamwise) and the higher on the side (heightwise) the damage opening is, the faster unstable damage propagation occurs, contrary to the longer damage (lengthwise).

The developed parametric models are successfully applied to the damage cases in a probabilistic manner with MC sampling and the probability of time to unstable

damage propagation is quantified. This information can be used in the design and emergency operations.

In the latter case a specific damage is concerned, and the time to unstable propagation can be used to support the decision-making process of the situation. In this context, information regarding the safe intervention time (or window of safe operation) with respect to a certain probability decided by the decision maker is of paramount importance. For the time being the 50% probability is used, primarily because the *50-50* chances of success is a widely accepted measure of an unpredictable outcome when high expectations are at stake and large uncertainty dominates the situation. In this way, a salvage operation should be managed efficiently if appropriate hardware deployed takes place within certain timeframe in order to prevent any loss of human life and to minimise environmental impact, and loss of the cargo and the ship. In the emergency situation, the proposed analysis could be executed regularly (i.e. as new information about the environment or the loading conditions of the ship changes) in order to obtain the most reliable information for the development of the damage.

In practical damage cases, strain gauging a ship in deck and bottom structure would benefit the assessment of damages unless damages take place at the installed area of strain gauges. Change of strains or stresses on deck and bottom between intact and damaged condition of a ship could be used to estimate the damage extent. With the determined loading condition and the approximately examined damage location, the section modulus of the damaged hull could be estimated from the recorded stresses at deck and bottom then the damage extent to the intact section can be calibrated to meet the obtained section modulus in the damaged condition. Furthermore, the history of the stresses would provide an estimated time to unstable propagation if it happens because a sudden increase of the stress on deck or bottom would mean a start of unstable damage propagation as the sudden decrease of the residual strength is observed to coincide with the unstable damage propagation in the case studies.

With respect to the design aspect, the developed model should be applied for all possible damage conditions (opening size and location) that could be experienced in accidental events. This approach refers to a set of predefined loading conditions as

well as the wave conditions that the ship is expected to encounter in the planned routes during its service life. The ship should be designed so as the required safety performance, i.e. zero-tolerance in the loss of human life, the minimal environmental impact and the minimum loss of property, is attained with respect to the considered damage conditions. Otherwise, proper design changes should be sought, increase of plate thickness and/or stiffeners, change of materials and/or stiffener spacing, etc. As the analysis provides safety information for the design decision-making by allowing trade-off among the design parameters, the implementation of the developed tool in the *risk-based ship design* methodology is practicable and highly desirable.

It is expected that the use of tougher steels in ship building would provide benefits in two ways. Under the same range of SIF applied, the tougher steels delay crack propagation as the crack growth rate is smaller. Also the increased fracture toughness of the materials would reduce the chance of unstable crack propagation under the same damage conditions and wave loadings. Although the use of tougher steels would delay crack propagation significantly when the tougher steels are fitted near the initial damages, it should be noted that this benefit could be negligible when the crack has significantly propagated inducing the maximum SIF of the crack tip increased enough to exceed the fracture toughness. The recommended locations are the areas of plate crosses on deck, bottom and side shell including bilge area although the most appropriate location should be selected through broad analysis in order for the maximum benefit to be achieved from using of the tougher steels in ship building. The effect of tougher steels on the crack propagation can be assessed in order to identify the benefits they offer.

Both in the design and the operational context, a number of samples (with the Monte Carlo method) should be obtained (i.e. damage configurations with imposed excitations). The respective discussion shows that the number of samples should be chosen according to the required time and accuracy for the analysis. For example, with regard to the emergency operation, 1,000 samples would give a reasonable result while for the early design stage where as many design cases need to be analysed, 100 samples for each design case is considered reasonable.

Finally, it should be stated that the environmental input in terms of wave period and significant wave height have been considered as a single set in this current stage of work. However, this does not have to be the case and the variability of the sea states (forecasted *Vs* observed conditions) can be readily taken into account either by an MC sampling process or in a deterministic (worst case scenario) manner so that the different results obtained from the different sea states can support decision-making on planning the route of towing or sheltering. The analysis procedure for this work is the same as that used in the sensitivity analysis.

8.3 Recommendations for future work

The methodology proposed in this thesis is new in the field hence further research and enhancement are truly desired and appreciated. The following sections describe the areas where comprehensive investigation is required in order to enhance the accuracy and applicability of the models.

8.3.1 Correction factors for extended applications

The parametric models developed in the current study have limited application as they are aimed for the specific damage cases discussed in the case studies. For the extended applications of the parametric models, the priority is in development of correction factors for the relevant damage features. This could be achieved by using FE analysis and the derivation of relevant empirical equations from the results. The investigation on the following list is recommended for further developments of the parametric models with respect to hull structures:

- Other opening shapes e.g. inverse triangle for striking bow
- Multi openings due to bow and bulb's bow
- The effect of curved plate e.g. bilge area
- The effect of girders and stringers

8.3.2 Inclusion of other loadings

It is known that the compressive residual stress on plates between stiffeners decreases the hull girder strength by reducing its buckling capacity and its effect can be taken into account in the residual strength analysis by reducing the effective width of the plate in accordance with an approximate method proposed by Gordo and

Soares (1993). On the other hand, the compressive residual stress is believed to delay crack propagation while the tensile one increases it. Its effect on the crack propagation analysis can be included by taking into consideration the effective range of stress intensity factor. However as the highly scattered distribution of the residual stress even under the same welding procedure is discussed by Dexter and Pilarski (2000) and further more the high possibility of stress re-distribution is expected during accidental impact from collision and grounding, the estimation of the residual stress distribution becomes more difficult.

It is understood that the effects of shear and torsion on the residual strength and crack propagation should be considered in the case of open-top ships e.g. container carriers. Otherwise they are small compared with those of vertical and horizontal bending moment. However, it is desirable to include them in the analysis for various waves and loading conditions that could dominantly increase their effects.

The effect of water pressure should be included in the residual strength analysis as a form of a resultant lateral deformation (imperfection) if it is obtained due to the pressure. The importance of the water pressure effect on the crack propagation is the reason why the proposed methodology includes the flooding simulation. However, although its importance in the total analysis is obvious, further elaboration on it for its full utilisation in the process is required as it is discussed in the Chapter 3.

8.3.3 Interaction with other tools

This has not been addressed in this thesis but it is strongly required for the completion of the proposed methodology. A platform that would enable the tool for the progressive structural failure analysis to interact systematically (in every time step) with tools for flooding simulation and damage stability analysis is necessary.

In this respect,

- The flooding pressure on the damage opening obtained from the simulation in time domain can be another driving force for cracks around the opening to propagate. The effect of the flooding pressure, though it would be locally induced, on the damage propagation needs to be investigated properly. Also any extended damage opening should be fed back for flooding simulation.

- The behaviour of a damaged ship is different from that of an intact ship hence the damage stability has been the major subject for the survivability assessment of damaged ships. This means that more accurate global wave loadings should be obtained (both for deep and shallow water) by taking into account the complex but real behaviour of damaged ship dynamics.

8.3.4 Direct use of wave spectrums

The current approach deals with the recorded or expected wave data by transforming to an equivalent wave height and the corresponding period within each observed time window rather than deploying a direct wave spectrum in the analysis. The reasons for the current approach is adopted are that (i) the equivalent loading method is simple though it gives conservative results, and most importantly (ii) no method which enables effective analysis of the response of every single loading range is properly applicable yet even though the single loading range can be easily obtained from the combination of a spectral analysis and any counting method.

The effects of overload and underload *during a constant loading* on the crack propagation are known to delay and accelerate its propagation respectively. An analytical model for the former effect is available however research on latter has not been enough and no analytical model is available. Most of all, their application to wave loadings, where different loading ranges are mixed, requires more work as wave loadings are irregular rather than regular with some single overload or underload.

8.3.5 Onboard system integration

The tool developed in this thesis has the capability to support emergency situation as a fast and fully parametric analysis is enabled with the associated uncertainty quantification. In an emergency situation, proper emergency decision may be instructed by a shore-based support team however the best decision can still be made by the hands of crews. The most desirable and effective provision is to provide a decision support system onboard that can provide easy operation by crews at needs. For the purpose, the tool should provide reliable, timely and useful information and a user friendly graphical user interface (GUI) should be developed for an easy operation.

9 CONCLUSIONS

9.1 Conclusions

On the basis of the results obtained from the application of the methodology proposed in this thesis, the following conclusions can be drawn:

- A methodology is proposed to evaluate the survivability of the damaged ship with respect to the progressive structural failure due to time-varying environmental loading.
- A finite element method for the analysis is proposed by use of the VCCT in conjunction with the developed crack growth model. In this way the foundation for the analysis of any complex structure has been set.
- As an alternative to the FE method, a set of knowledge-intensive (parametric) models are developed with the concept of superposition of correction factors to calculate the SIFs for specific damage cases. A tool developed for the use of the parametric models is successfully applied for the progressive structural failure analysis of a real ship structure with a succession of time varying wave data.
- A tool for the assessment of the ultimate residual strength capacity of damaged ship is developed based on the beam-column method. The tool is applied to a real ship structure by taking into account the result of the progressive structural failure in time domain.
- As the developed tool is based on the fully parametric models, they can be implemented in the *risk-based design* methodology as well as in the emergency response service in order to support decision-making.

10 REFERENCES

Aamodt, B. and Bergan, P. G., On the Principle of Superposition for Stress Intensity Factors, Engineering Fracture Mechanics, Vol. 8, Issue 2, pp. 437-440, 1976

ABAQUS, Industrial Applications of New Features in ABAQUS, ABAQUS Central Users' Conference, 2005

ABS, Guide for Assessing Hull Girder Residual Strength, American Bureau of Shipping, 1995

Adamchak, J. C., An Approximate Method for Estimating the Collapse of a Ship's Hull in Preliminary Design, Proceedings of Ship Structure Symposium of the Society of Naval Architects and Marine Engineers (SNAME), pp. 37-61, 1984

ANSYS, ANSYS Release 13.0: Release Notes, 2010

Bahamas Maritime Authority, Report of the Investigation into the Loss of the Bahamian Registered Tanker "Prestige" off the Northwest Coast of Spain on 19th November 2002, The Bahamas Maritime Authority, 2004

Bai, Y., Bendiksen, Y. B. and Pedersen, P. T., Collapse Analysis of Ship Hulls, Marine Structures, Vol. 6, pp. 485-507, 1993

Barsom, J. M., Fatigue-Crack Propagation in Steels of Various Yield Strengths, Transactions of the ASME, Journal of Engineering for Industry, Vol. 93, pp. 1190-1196, 1971

Barsom, J. M. and Rolfe S. T., Fracture and Fatigue Control in Structures, Englewood Cliffs, Prentice Hall, 1987

Bowie, O.L., Analysis of an Infinite Plate Containing Radial Cracks Originating at the Boundary of an Internal Circular Hole. Journal of Mathematics and Physics, Vol. 35, pp. 60-71, 1956

Brown, L. D., Cai, T. T. and DasGupta, A., Interval Estimation for a Binomial Proportion, Statistical Science, Vol. 16, No. 2, pp. 101-117, 2001

BS 7910, Guide on Methods for Assessing the Acceptability of Flaws in Metallic Structures, British Standards Institute, 1999

BS PD6493, Fatigue Design and Assessment for Steel Structures, British Standards Institute, 1993

Burnside, O.H., Hudak, S.J., Oelkers, E., Chan, K. and Dexter, R.J., SSC-326: Long-Term Corrosion Fatigue of Welded Marine Steels, Ship Structure Committee, 1984

Caldwell, J. B., Ultimate Longitudinal Strength, Transactions of the Royal Institution of Naval Architects (RINA), Vol. 107, pp. 411-430, 1965

Cartwright, D. J. and Rooke, D. P., Approximate Stress Intensity Factors Compounded from Known Solutions, Engineering Fracture Mechanics, Vol. 6, pp. 563-571, 1974

Chang, Y. S., Choi, J. B., Kim, Y. J. and Yagawa, G. Numerical Calculation of Energy Release Rates by Virtual Crack Closure Technique, The Korean Society of Mechanical Engineers International Journal, Vol. 18, No. 11, pp. 1996-2008, 2004

Chell, G.G., The Stress Intensity Factors and Crack Profiles for Centre and Edge Cracks in Plates Subjected to Arbitrary Stresses, International Journal of Fracture, Vol. 12, No. 1, 1976

Davenport, R.T. and Brook, R., The Threshold Stress Intensity Range in Fatigue, Fatigue of Engineering Materials and Structures, Vol. 1, pp. 151-158, 1979

Dexter, R.J. and Mahmoud, H.N., SSC-435: Predicting Stable Fatigue Crack Propagation in Stiffened Panels, Ship Structure Committee, 2004

Dexter, R.J., Norris, E.B., Schick, W.R. and Watson, P.D., SSC-335: Performance of Underwater Weldments, Ship Structure Committee, 1990

Dexter, R.J. and Pilarski, P.J., SSC-413: Effect of Welded Stiffeners on Fatigue Crack Growth Rate, Ship Structure Committee, 2000

DEXTREMEL, Design for Structural Safety under Extreme Loads, Final Technical Report, 2001

Donahue, R. J., Clark, H. M., Atanmo, P., Kumble, R. and McEvily, A. J., Crack Opening Displacement and the Rate of Fatigue Crack Growth, International Journal of Fracture Mechanics, Vol. 8, No. 2, 1972

Dow, R. S., Testing and Analysis of 1/3-Scale Welded Steel Frigate Model, Proceedings of the 2nd International Conference on Advances in Marine Structures, pp. 749-973, 1991

Dow, R. S., Hugill, R. C., Clark, J. D. and Smith, C. S., Evaluation of Ultimate Ship Hull Strength, Proceedings of Extreme Loads Response Symposium of the Society of Naval Architects and Marine Engineers (SNAME), pp. 133-148, 1981

Dowling, P. J., Chatterjee, S., Frieze, P. A. and Moolani, F. M., The Experimental and Predicted Collapse Behaviour of Rectangular Stiffened Steel Box Girder, Proceeding of International Conference on Steel Box Girder Bridges, Institute of Civil Engineers, pp. 77~94, 1973

Dowling, P. J., Moolani, F. M. and Frieze, P. A., The effect of shear lag on the ultimate strength of box girders, International Congress on Steel Plated Structures, Imperial College of London, pp. 108–147, 1976

Elber, W., Fatigue Crack Closure under Cyclic Tension, Engineering Fracture Mechanics, Vol. 2, pp. 37-40, 1970

Farahmand, B., Saff, C., Xie, D. and Abdi, F., Estimation of Fatigue and Fracture Allowables for Metallic Materials under Cyclic Loading, Proceedings of the 48th of the American Institute of Aeronautics and Astronautics, AIAA-2007-2381, 2007

Faulkner, D., Adamchak, J. C., Snyder, G. J. and Vetter, M. F., Synthesis of Welded Grillages to Withstand Compression and Normal Loads, Computers and Structures, Vol. 3, pp. 221-246, 1973

Faulkner, D. and Sadden, J. A., Toward a Unified Approach to Ship Structural Safety, Transactions of the Royal Institution of Naval Architects, Vol. 121, pp. 1-38, 1979

Fisher, J. W., Dexterm, R. J., Roberts, R., Yen, B. T., Decorges, G., Pessike, S. P., Nussbaumerm, A. C., Tarquinio, J. E., Kober, G. R., Gentilcore, M. L. and Derrah, S.

M., Structural Failure Modes: Final Report – Development of Advanced Double Hull Concepts, Final Report for Cooperative Agreement N00014-91-CA-001, Vol. 3a, 1993

Foreman, R. G., Kearney, V. E. and Engle, R. M., Numerical Analysis of Crack Propagation in Cyclic-Loaded Structures, Journal of Basic Engineering, Vol. 89, pp. 459-464, 1967

Frieze, P. A. and Lin, Y. T., Ship Longitudinal Strength Modelling for Reliability Analysis, Proceedings of the Marine Structural Inspection, Maintenance and Monitoring Symposium, the Society of Naval Architects and Marine Engineers (SNAME), pp. III.C.1-III.C.20, 1991

Gao, Z., Vassalos, D. and Gao, Q., Numerical Simulation of Water Flooding into a Damaged Vessel's Compartment by the Volume of Fluid Method, Ocean Engineering, Vol. 37, pp. 1428-1442, 2010

Ghose, D. J., Nappi, N. S. and Wiernicki, C. J., SSC-318: Residual Strength of Damaged Marine Structures, Ship Structural Committee, 1994

Gordo, J. M. and Soares, C. G., Approximate Load Shortening Curves for Stiffened Plates under Uniaxial Compression, Integrity of Offshore Structures-5, Edited by D. Faulkner et al., pp. 189-211, 1993

Gordo, J. M. and Soares, C. G., Approximate Method of Evaluate the Hull Girder Collapse Strength, Marine Structures, Vol. 9, pp. 449-470, 1996

Gordo, J. M. and Soares, C. G., Residual Strength of Damaged Ship Hulls, Proceedings of the 9th International Marine association of the Mediterranean Conference (IMAM), Vol. 2, pp. 79-86, 2000

Gordo, J. M. and Soares, C. G., Experimental Evaluation of the Ultimate Bending Moment of a Box Girder, Marine Systems & Ocean Technology, Vol. 1, pp. 33–46, 2004

Gordo, J. M. and Soares, C. G., Experimental Evaluation of the Behaviour of a Mild Steel Box Girder under Bending Moment, Ships and Offshore Structures, Vol. 3. No. 4, pp. 347-358, 2008

Gordo, J. M. and Soares, C. G., Tests on Ultimate Strength of Hull Box Girders Made of High Tensile Steel, Marine Structures, Vol. 22, pp. 770-790, 2009

Gordo, J. M., Soares, C. G. and Faulkner, D., Approximate Assessment of the Ultimate Longitudinal Strength of the Hull Girder, Journal of Ship Research, Vol. 40, No. 1, pp. 60-69, 1996

Grandt, A. F. Jr. and Kullgren, T. E., Tabulated Stress Intensity Factor Solutions for Flawed Fastener Holes, Engineering Fracture Mechanics, Vol. 18, Issue 2, pp. 435-451, 1983

Gross, B., Srawley, J.E. and Brown, W.F., Stress-Intensity Factors for Single-Edge Notch Tension Specimen by Boundary Collocation of a Stress Function, NASA TN-D-2395. 1964

Hirt, M. A. and Fisher, J. W., Fatigue Crack Growth in Welded Beams, Engineering Fracture Machanics, Vol. 5, pp. 415-429, 1973

Hoffmann, G. H., Analysis of Sir John Biles's Experiment on H.M.S. Wolf in the Light of Piazker's Theory, Transactions of the Institute of Naval Architects, Vol. 67, pp. 41-65, 1925

IACS, Common Structural Rules for Double Hull Oil Tankers, International Association of Classification Societies, 2008

IACS, Common Structural Rules for Bulk Carriers, International Association of Classification Societies, 2009

ISSC, Report of Technical Committee III.1: Ductile Collapse, Proceedings of the 12th International Ship and Offshore Structures Congress (ISSC), Vol. 1, pp. 299-388, 1994a

ISSC, Report of Technical Committee V.1: Applied Design – Strength Limit States Formulations, Proceedings of the 12th International Ship and Offshore Structures Congress (ISSC), Vol. 2, pp. 1-58, 1994b

IMO, Report of the Maritime Safety Committee on its Seventy-eighth Session, MSC 78/26, May 2004

Irwin, G. R., Analysis of Stresses and Strains near the End of a Crack Traversing a Plate, Transactions of the ASME, Journal of Applied Mechanics, Vol. E24, pp. 361-364, 1957

Isida, M., Analysis of Stress Intensity Factors for the Tension of a Centrally Cracked Strip with Stiffened Edges, Engineering Fracture Mechanics, Vol. 5, pp. 647-665, 1973

Jasionowski, A., An Integrated Approach to Damage Ship Survivability Assessment, PhD Thesis, University of Strathclyde, 2001

Kanninen, M. F. and Popelar, C. H., Advanced Fracture Mechanics, Oxford University Press, 1985

Karvinen, K. G. and Pegg, N. G., A Simplified Method for Nonlinear Failure Analysis of Stiffened Plates, Marine Structures, Vol. 19, pp. 97-109, 2006

Kato, A., Kurihara, M. and Kawahara M., An Expression of Fatigue Crack Propagation Rates under Wide-Ranged Stress Ratios, Journal of the Society of Naval Architects of Japan, Vol. 153, pp.336-343, 1983

Kell, C. O., Investigation of Structural Characteristics of Destroyers “Preston” and “Bruce”: Part I- Description, Transactions of the Society of Naval Architects and Marine Engineers (SNAME), Vol. 39, pp. 35-64, 1931

Kell, C.O., Investigation of Structural Characteristics of Destroyers “Preston” and “Bruce”: Part II- Analysis of Data and Results, Transactions of the Society of Naval Architects and Marine Engineers (SNAME)., Vol. 48, pp. 125-172, 1940

Klingerman, D. J., Threshold Crack Growth in A36 Steel, A Thesis for the Degree of MSc., Department of Civil Engineering, Lehigh University, Bethlehem, Pennsylvania, 1973

Konovessis, D., A Risk-based Design Framework for Damage Survivability of Passenger Ro-Ro Vessels, PhD Thesis, University of Strathclyde, 2001

Kuo, H. C. and Chang, J. R., A Simplified Approach to Estimate the Ultimate Longitudinal Strength of Ship Hull, Journal of Marine Science and Technology, Vol. 11, No. 3, pp. 130-148, 2003

Kwon, S., Xie, N., Calvez, A. L. and Hodgson, B. System Simulation, Deliverable D3.5 (Technical Report) of the EU-funded Research Project Surfacing System (www.su-sy.eu), 2011

Lai, J., Zhang, X. and Schijve, J., An Investigation of a Hole-Edge Crack Problem by a Combined Complex Variable and Least Square Method, Engineering Fracture Mechanics, Vol. 39, No. 4, pp. 713-737, 1991

Lang, D. W. and Warren, W. G., Structural Strength Investigation of Destroyer Albuera, Transactions of the Institute of Naval Architects, Vol.94, pp. 243-286, 1952

Lee, D., Lee, S. S., Park, B. J. and Kim, S. Y., A Study on the Framework for Survivability Assessment System of Damaged Ships, Ocean Engineering, Vol. 32, pp. 1122-1132, 2005

Leski, A., Implementation of the Virtual Crack Closure Technique in Engineering FE Calculations, Finite Elements in Analysis and Design, Vol. 43, pp. 261-268, 2007

Makabe, C., Purnowidodo, A. and McEvily, A. J., Effects of Surface Deformation and Crack Closure on Fatigue Crack Propagation after Overloading and Underloading, International Journal of Fatigue, Vol. 26, pp. 1341-1348, 2004

Mansour, A. E. and Faulkner, D., On Applying the Statistical Approach to Extreme Sea Loads and Ship Hull Strength, Transactions of the Royal Institution of Naval Architects (RINA), Vol. 115, pp. 277-313, 1973

Mansour, A. E. and Thayamballi, A., SSC-299: Ultimate Strength of a Ship's Hull Girder in Plastic and Buckling Modes, Ship Structure Committee, 1980

Mansour, A. E., Lee, J. M. and Thayamballi, A., An experimental Investigation of ship hull ultimate strength, Transactions of the Society of Naval Architects and Marine Engineers (SNAME), Vol. 98, pp. 411–439, 1990

Mansour, M. A., El-Kilani, H. S. and Abdel-Malek, I. S., Residual Strength of Ships after Grounding, Alexandria Engineering Journal, Vol. 42, No. 5, pp. 517-525, 2003

McEvily, A. J. and Groeger, J., On the Threshold for Fatigue-Crack Growth, Proceedings of the 4th International Conference on Fracture, Vol. 2, pp. 1293-1298, 1977

McEvily, A. J. and Yang, Z., The Nature of the Two Opening Levels Following an Overload in Fatigue Crack growth. Metallurgical Transactions, 21A, pp. 2717-2727, 1990

MSC Software, Nastran 2008 r1 Documentation, 2008

Murakami, Y., Stress Intensity Factors Handbook, Third Edition, Elsevier Science Ltd, 2005

Naar, H., Ultimate Strength of Hull Girder for Passenger Ships, Doctoral Dissertation, Ship Laboratory, Department of Mechanical Engineering, Helsinki University of Technology, 2006

Newman, J. C. Jr., An Improved Method of Collocation for the Stress Analysis of Cracked Plates with Various Shaped Boundaries, NASA Report TN D-6376, 1971

Nishihara, S., Ultimate Longitudinal Strength of Mid-ship Cross Section. Naval Architecture & Ocean Engineering, Vol. 22, pp. 200-214, 1984

Nussbaumer, A. C., Dexter, R. J., Fisher, J. W. and Kaufmann, E. J., Propagation of Very Long Fatigue Cracks in a Cellular Box Beam, Fracture Mechanics, Vol. 25, Edited by Erdogan, F. American Society for Testing and Materials Special Technical Publication, No. 1220, pp. 518-532, 1995

Ozguc, O., Das, P. K. and Barltrop, N., A Comparative Study on the Structural Integrity of Single and Double Side Skin Bulk Carriers under Collision Damage, Marine Structures, Vol. 18, pp. 511-547, 2005

Paik, J. K., Residual Ultimate Strength of Steel Plates with Longitudinal Cracks under Axial Compression-Experiments, Journal of Ocean Engineering, Vol. 35, pp. 1775-1783, 2008

Paik, J. K. and Kim, B. J., Progressive Collapse Analysis of Thin-Walled Box Columns, Thin-Walled Structures, Vol. 48, pp. 541-550, 2008

Paik, J. K., Kumar, Y. V. S. and Lee, J. M., Ultimate Strength of Cracked Plate Elements under Axial Compression or Tension, Thin-Walled Structures, Vol. 43, pp. 237-272, 2005

Paik, J. K., Lee, J. M., Park, Y. I., Hwang, J. S. and Kim, C. W., Time-Variant Ultimate Longitudinal Strength of Corroded Bulk Carriers, Marine Structures, Vol. 16, pp. 567-600, 2003a

Paik, J. K. and Mansour, A. E., A Simple Formulation for Predicting the Ultimate Strength of Ships, Journal of Marine Science and Technology, Vol. 1, pp. 52-62, 1995

Paik, J. K., Thayamballi, A. K. and Yang, S. H., Residual Strength Assessment of Ships after Collision and Grounding, Marine Technology, Vol. 35. No. 1, pp. 38-54, 1998

Paik, J. K., Wang, G., Kim, B. J. and Thayamballi, A. K., Ultimate Limit State Design of Ship Hulls, Transaction of the Society of Naval Architects and Marine Engineers (SNAME), Vol. 110, 2002

Paik, J. K., Wang, G., Thayamballi, A. K., Lee, J. M. and Park, Y. I., Time-Dependent Risk Assessment of Aging Ships Accounting for General/Pit Corrosion, Fatigue Cracking and Local Denting Damage, Transactions of the Society of Naval Architects and Marine Engineers (SNAME), Vol. 111, pp. 159-197, 2003b

Paris, P. and Erdogan, F., A Critical Analysis of Crack Propagation Laws, Journal of Basic Engineering, Vol. 85, Issue 4, pp. 528-534, 1963

Paris, P.C. and Sih, G.C., Stress Analysis of Cracks, Fracture Toughness Testing and Its Applications, Special Technical Publish, American Society of Testing and Materials (ASTM), No. 381, pp. 30-83, 1965

Poe, C. C., Fatigue Crack Propagation in Stiffened Panels, Damage Tolerance in Aircraft Structures, American Society for Testing and Materials, ASTM STP 486, pp. 79-97, 1971

Qi, E., Cui, W. and Wan, Z., Comparative Study of Ultimate Hull Girder Strength of Large Double Hull Tankers, Marine Structures, Vol. 18, pp. 227-249, 2005

Ritchie, D., A Superposition Approach to the Calculation of Stress Intensity Factors of Cracks Growing from Stress Concentrations, International Journal of Fracture, Vol. 30, pp. 29-32, 1986

Rutherford, S. E. and Caldwell, J. B., Ultimate Longitudinal Strength of Ships: A Case Study, Transaction of the Society of Naval Architects and Marine Engineers (SNAME), Vol. 98, pp. 441-471, 1990

Rybicki, E. F. and Kanninen, M. F., A Finite Element Calculation of Stress Intensity Factors by a Modified Crack Closure Integral, Engineering Fracture Mechanics, Vol. 9, pp. 931-938, 1977

SAFEDOR, Probabilistic Models for Collapse Limit State, SAFEDOR-D-2.2.2-2006-07-31-IST-rev-4, 2006

Shivakumar, K. N., Tan, P. W. and Newman, J. C., A Virtual Crack-Closure Technique for Calculating Stress Intensity Factors for Cracked Three Dimensional Bodies, International Journal of Fracture, Vol. 36, pp. 43–50, 1988

Simulia, ABAQUS Analysis User's Manual ver. 6.8, 2008

Smith, C. S., Influence of Local Compression Failure on Ultimate Longitudinal Strength of a Ship's Hull, Proceedings of the International Symposium on Practical Design in Shipbuilding (PRADS), pp. 73-79, 1977

Smith, C. S. and Dow, R. S., Residual Strength of Damaged Steel Ships and Offshore Structures, Journal of Constructional Steel Research, Vol. 1, No. 4, pp. 2-15, 1981

Soares, C. G., Luis, R. M., Nikolov, P., Downes, J., Taczala, M., Modiga, M., Quesnel, T., Toderan, C. and Samuelides, M., Benchmark Study on the Use of Simplified Structural Codes to Predict the Ultimate Strength of a Damaged Ship Hull, International Shipbuilding Progress, Vol. 55, pp. 87-107, 2008

Spanos, D., Papanikolaou, A., Numerical Study of the Damage Stability of Ships in Intermediate Stages of Flooding, Proceedings of the 5th International Workshop on Stability and Operational Safety of Ships, 2001

Stefanescu, D., Edwards, L. and Fitzpatrick, M. E., Stress Intensity Factor Correction for Asymmetric Through-Thickness Fatigue Cracks at Holes, International Journal of Fatigue, Vol. 25, pp. 569-576, 2003

Sumi, Y., Iyama, H., Bozic, Z. and Kawamura, Y., Multiple Fatigue Cracks Propagating in a Stiffened Panel, Journal of the Society of Naval Architects of Japan, Vol. 179, pp. 407-412, 1996

Sumi, Y., Fatigue Crack Propagation and Computational Remaining Life Assessment of Ship Structures, Journal of Marine Science and Technology, Vol. 3, pp. 102-112, 1998

Tada, H., Paris, P. C. and Irwin, G., The Stress Analysis of Cracks Handbook, Third Edition, ASME Press, 2000

Tweed, J. and Rooke, D. P., The Distribution of Stress Near the Tip of a Radical Crack at the Edge of a Circular Hole, International Journal of Engineering Science, Vol. 11, pp. 1185-1195, 1973

Ueda, Y. and Rashed, S. M. H., The Idealized Structural Unit Method and Its Application to Deep Girder Structures, Computers and Structures, Vol. 18, No. 2, pp. 277-293, 1984

Valsgard, S. and Steen, E., Ultimate Hull Girder Strength Margins in Present Class Requirements, The Marine Structural Inspection, Maintenance and Monitoring Symposium, Society of Naval Architects and Marine Engineers (SNAME), pp. III.B.1-III.B.19, 1991

Vanem, E., Rusas, S., Skjong, R. and Olufsen, O., Collision Damage Stability of Passenger Ships: Holistic and Risk-Based Approach, International Shipbuilding Progress, Vol. 54, pp. 323-337, 2007

Vassalos, D., Shaping Ship Safety: The Face of the Future, Marine Technology, Vol. 36, No. 2, pp. 61-76, 1999

Vassalos, D., Risk-Based Ship Design, In: Papanikolaou, A. (Ed.), Risk-Based Ship Design: Methods, Tools and Applications, Chapter 2, Springer, 2009

Vassalos, D., Guarin, L., Konovessis, D., Risk-Based Ship Design Implementation – Riding the Learning Curve, Proceedings of the 9th International Marine Design Conference (IMDC), 2006

Vassalos, D., Jasionowski, A. and Guarin, L., Passenger Ship Safety – Science Paving the Way, Proceedings of the 8th International Ship Stability Workshop, Istanbul, October 2005

Vassalos, D., Konovessis, D., An Implementation of a Life-Cycle Risk-Based Design for Safety Methodology, Safety and Reliability Proceedings of the ESREL 2003 Conference, 2003

Vassalos, D., Konovessis, D., Guarin, L., Fundamental Concepts of Risk-Based Ship Design, Proceedings of the 11th International Congress of the International Maritime Association of the Mediterranean (IMAM), 2005

Vassalos, D., Konovessis, D., Vassalos, G. C., A Risk-Based Framework on Ship Design for Safety, Proceedings of the 8th International Marine Design Conference (IMDC), pp. 225-239, 2003

Vassalos, D., Oestvik, I., Konovessis, D., Recent Development and Application of a Formalized Design for Safety Methodology in an Integrated Environment, SNAME Transactions, Vol. 108, pp. 419-442, 2000a

Vassalos, D., Oestvik, I., Konovessis, D., Design for Safety: Development and Application of a Formalized Methodology, Proceedings of the 7th International Marine Design Conference (IMDC), Kyongju, Korea, pp. 151-165, 2000b

Vasta, J., Lessons Learned from Full-Scale Ship Structural Tests, Transactions of the Society of Naval Architects and Mariner Engineers (SNAME), Vol. 66, pp. 165-243, 1958

Wang, C. E., Grondin, G. Y. and Elwi, A. E., Interaction Buckling Failure of Stiffened Steel Plates, Structural Engineering Report No. 264, University of Alberta, 2006

Wang, G., Chen, Y., Zhang, H. and Peng, H., Longitudinal Strength of Ships with Accidental Damages, Marine Structures, Vol. 15, pp. 119-138, 2002

Wang, G., Chen, Y., Zhang, H. and Shin, Y., Residual Strength of Damaged Ship Hull, Ship Structure Symposium 2000 - Ship Structures for the New Millennium: Supporting Quality in Shipbuilding, 2000

Wang, G., Lee, A. K., Ivanov, L., Lynch, T. J., Serratella, C. and Basu, R., A Statistical Investigation of Time-Variant Hull Girder Strength of Aging Ships and Coating Life, Journal of Marine Structures, Vol. 21, pp. 240-256, 2008

Wang, G., Spencer, J. and Sun, H., Assessment of Corrosion Risks to Aging Ships Using an Experience Database, Proceedings of the 22nd International Conference on Offshore Mechanics and Arctic Engineering (OMAE), pp. 149-159, 2003

Wang, X., Sun, H., Yao, T., Fujkubo, M. and Basu, R., Methodologies on Hull Girder Ultimate Strength Assessment of FPSOs, Proceedings of the 27th

International Conference on Offshore Mechanics and Arctic Engineering (OMAE), pp. 199-205, 2008

Wang, Y. H., Cheung, Y. K. and Woo, C. W., The Stress Intensity Factor of a Crack Emanating from a Circular Hole in a Finite Plate by Boundary Collocation Method, International Journal of Fracture, Vol. 43, pp. 97-108, 1990

Watanabe, M., Yajima, H. and Kawano, H., Analysis of the Crack Strength of a Stiffened Panel in a Ship Hull Structure, Journal of the Society of Naval Architects of Japan, Vol. 146, pp. 314-320, 1979

Xie, D. and Biggers Jr. S. B., Progressive Crack Growth Analysis Using Interface Element Based on the Virtual Crack Closure Technique, Finite Elements in Analysis and Design, Vol. 42, pp. 977-984, 2006

Xie, N., A Numerical Prediction of Global Wave Loads for Intact and Damaged Ships, Ship Stability Research Centre, Internal Report, 2011

Yazdani, N. and Albrecht, P., Crack Growth Rates of Structural Steel in Air and Aqueous Environments, Engineering Fracture Mechanics, Vol. 32, No. 6, pp. 997-1007, 1989

Zhang, S., Yu, Q. and Mu, Y. A., Semi-Analytical Method of Assessing the Residual Longitudinal Strength of Damaged Ship Hull, Proceeding of the International Society of Offshore and Polar Engineers (ISOPE), Vol. 4, pp. 510-516, 1996

Ziha, K. and Pedisic, M., Tracing the Ultimate Longitudinal Strength of a Damaged Ship Hull Girder, International Shipbuilding Progress, Vol. 49, No. 3, pp. 161-176, 2002

APPENDIX A. DAMAGE STABILITY ASSESSMENT

A component that constitutes the ship survivability assessment but is not dealt in current research is the damage stability assessment. The time to sink and/or capsize following damage is a critical factor in determining the survivability of a damaged ship. The dynamic motion response of a damaged vessel and the progressive flooding of its compartments in a random seaway form a highly non-linear dynamic system, the behaviour of which can only be captured by time domain simulation. This is carried out using explicit dynamic flooding simulation tools like PROTEUS (Figure A-1), Jasionowski (2001). The main elements of PROTEUS can be summarised as follows:

- The ship hydrodynamics are derived from properties of the intact hull, and they are based either on asymmetrical strip theory formulation with Rankine source distribution or a 3D panel code, both accounting for the non-linearities arising from instantaneous variation of the mean ship attitude and large amplitude motions.
- The effects of floodwater dynamics are described by a full set of non-linear equations that is derived from rigid-body theory.
- The floodwater motions are modelled as a Free-Mass-on-Potential-Surface (FMPS) de-coupled system in an acceleration field.
- The water ingress/egress is based on Bernoulli's equation.

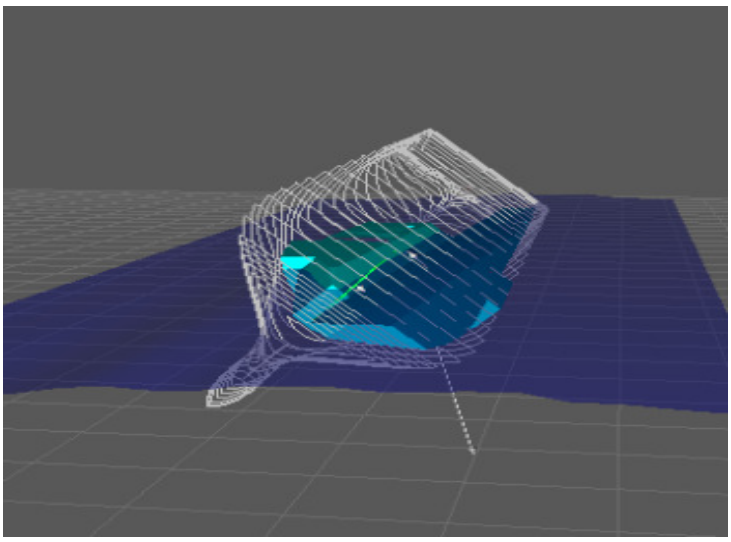

Figure A-1: A captured image of PROTEUS during simulation of damage stability, Safety at Sea (www.safety-at-sea.co.uk)

The ship geometry is defined in sections both for the hull and the internal compartments. The necessary environmental conditions for the simulations are generated by wave spectra (JONSWAP or Pierson-Moskowitz). The output of the calculation concerns ship motions, floodwater mass variation and motion, flow of floodwater through openings, environmental forces, etc. These time domain results support crucial information needed for the survivability of the damaged ship with metrics like *time to capsize* as shown in Figure A-2, which informs that the probability that the vessel capsizes within 1 hour is 0.8. In case of passenger ships, the stability performance dominates structural degradation as the ship could capsize within 1 hour, which is not the case for tankers. This is a tangible demonstration of how matured the damage stability research is.

Input

- Ship geometry (hull & internal compartments)
- Damage size & location
- Wave condition

Output

- Ship motions
- Floodwater mass & motions
- Flow of floodwater through opening
- Environmental forces

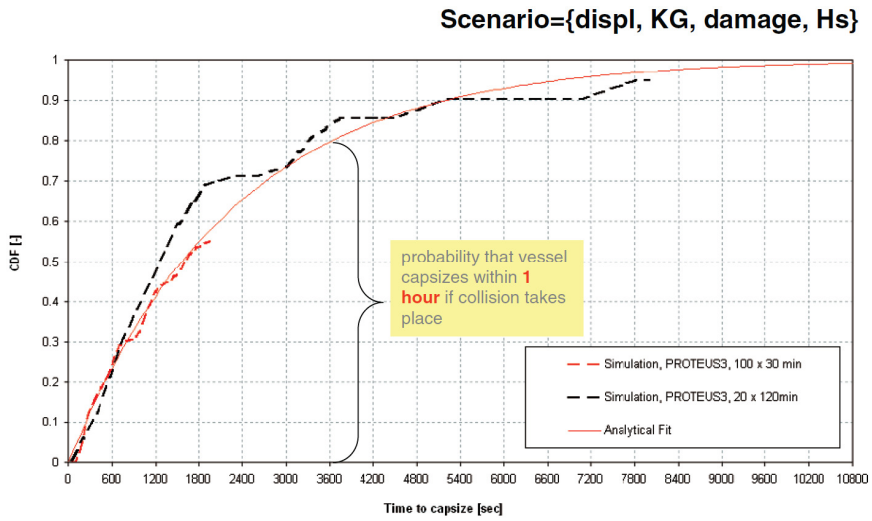

Figure A-2: An example of CDF for time to capsize in scenario level, Vassalos (2009)

Considering that the study on the flooding and damage stability has matured over the past 30 years and that tools that can predict and simulate damage stability have been developed and already used in the industry e.g. PROTEUS (Jasionowski, 2001), CAPSIM (Spanos and Papanikolaou, 2001), etc., it is justifiable in the context of the current research to focus on the most demanding, unexploited area where the development of a tool enabling the progressive structural failure analysis and the structural survivability assessment is strongly required. Therefore, integration of this component is out of the current work scope but constitutes a recommended topic for future work.

APPENDIX B. CRACK GROWTH MODELS

B.1 Models with the effective range of SIF

B.1.1 Yazdani's model

A modified Paris Law proposed by Yazdani and Albrecht (1989) substitutes the range of SIF, ΔK, with an effective range of SIF, ΔK_{eff}, expressed as below equation in which the effect of the stress ratio as well as the yield strength of the material are included.

$$\Delta K_{eff} = \frac{\Delta K}{1 - R_\sigma / Q} \tag{B-1}$$

where, R_σ is the stress ratio, $R_\sigma = \sigma_{min} / \sigma_{max}$

Q is a parameter related with the yield strength of the material, 4.0 for A36 steels, 4.6 for A588 steels and 9.1 for A514 steels are recommended.

Hence the crack growth model is expressed as follow.

$$\frac{da}{dN} = C \times {\Delta K_{eff}}^m = C \times \left(\frac{\Delta K}{1 - R_\sigma / Q}\right)^m \tag{B-2}$$

Adopting Q = 4.0 for A36 steels, the change of Yazdani's model according to various stress ratios is plotted in Figure B-1, where the effect of stress ratio is shown clearly; crack growth rate increases as the stress ratio is increasing.

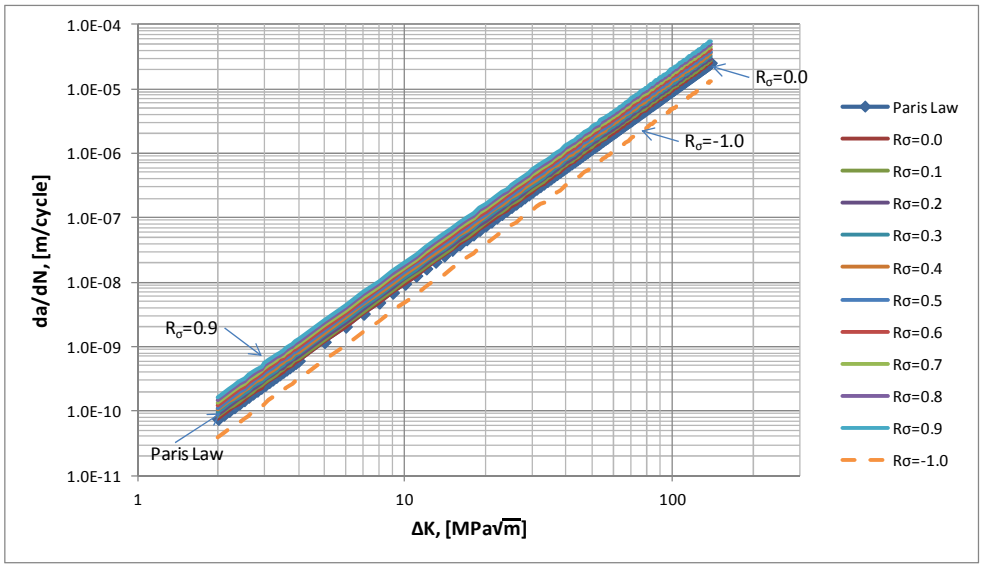

Figure B-1: Crack growth model of Yazdani and Albretcht (1989)

B.1.2 Dexter's model

Another effective range of SIF has been proposed by Dexter and Pilarski (2000) who has included the crack closure effect due to plasticity and residual stress by introducing a crack opening SIF, K_{op} to the following effective range of SIF.

$$\Delta K_{eff} = K_{max} - Max\left(K_{op}, K_{min}\right) \quad \textbf{(B-3)}$$

where, K_{max} and K_{min} are the maximum and minimum applied SIFs

K_{op} is the crack opening SIF,

$$K_{op} = Min\left(\frac{0.2}{(1-R_{\sigma,eff})}, 0.28\right) \cdot (K_{max} + K_R) - K_R$$

K_R is the stress intensity factor due to residual stress σ_{res}

$R_{\sigma,eff}$ is the effective stress ratio, $R_{\sigma,eff} = (\sigma_{min}+\sigma_{res})/(\sigma_{max}+\sigma_{res})$

Hence the corresponding crack growth model is expressed as below.

$$\frac{da}{dN} = C \times \Delta K_{eff}{}^{m} = C \times \left[K_{max} - Max\left(K_{op}, K_{min}\right)\right]^{m} \quad \textbf{(B-4)}$$

For the simplicity of drawing the above relationship, no residual stress is assumed in the model and the following graph of Figure B-2 is obtained.

It is noticeable from the graph that Dexter's model gives lower crack growth rate with low stress ratio when compared with *Paris Law*. This is contributed to the effect of the crack opening SIF. However from the fact that the crack growth rate curves with the stress ratio of 0.3 and above are coincide with *Paris Law*, it is found that this effect is no more taken into account when the stress ratio is equal to or larger than 0.3.

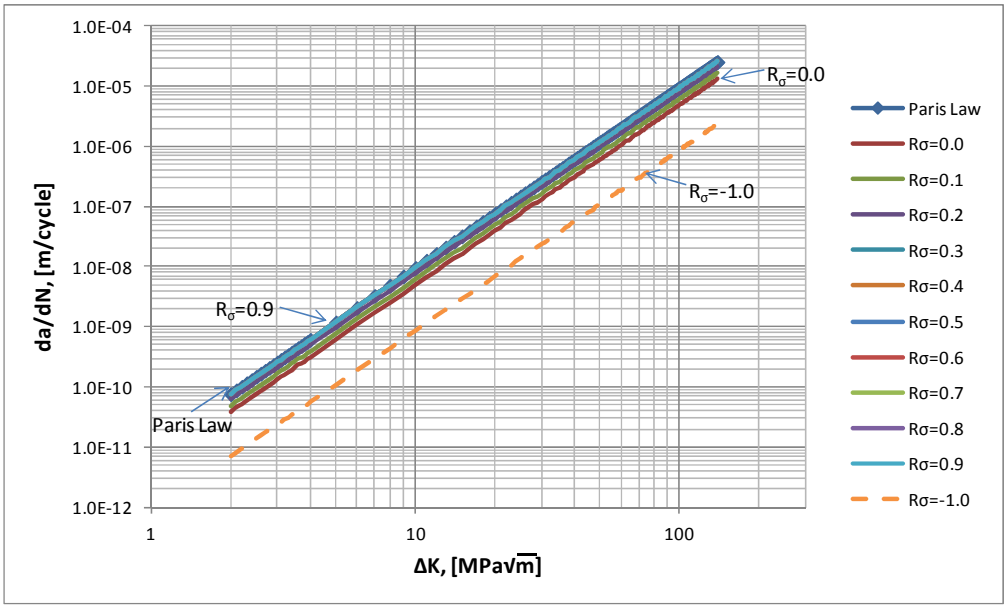

Figure B-2: Crack growth model of Dexter and Pilarski (2000)

B.2 Models with the threshold range of SIF

B.2.1 Donahue's model

A crack growth model with various experimental data at the stress ratio $R_\sigma \approx 0.0$ is suggested by Donahue et al. (1972) by incorporating the threshold range of SIF to cover the low and medium range of SIF.

$$\frac{da}{dN} = C \times \left(\Delta K^2 - \Delta {K_{th}}^2\right) \quad \textbf{(B-5)}$$

where, ΔK is the range of SIF

ΔK_{th} is the threshold range of SIF

As the above equation was developed based on a zero stress ratio, with a constant threshold range of SIF assumed as 2.45 MPa$\sqrt{\text{m}}$ (Sumi, 1998), the crack growth model of Donahue et al. (1972) can be plotted as shown in Figure B-3.

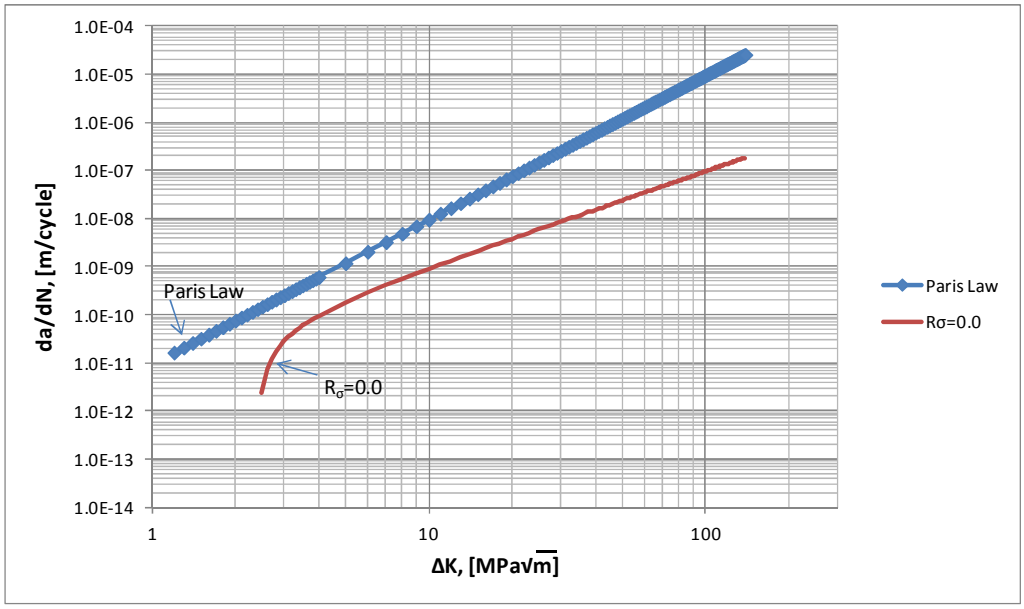

Figure B-3: Crack growth model of Donahue et al. (1972)

B.2.2 Sumi's model

A modified *Paris Law* suggested by Sumi (1998) has taken into account the effect of the threshold SIF as well as the effect of stress ratios including compressive residual stresses.

$$\frac{da}{dN} = C \times [(U\Delta K)^m - \Delta K_{th0}{}^m] \qquad \textbf{(B-6)}$$

where, U is the effective crack opening ratio,

$$U = \begin{cases} 1/(1.5 - R_\sigma), & for\ 0 < R_\sigma \leq 0.5 \\ 1.0, & for\ R_\sigma > 0.5 \end{cases}$$

$$\Delta K = \begin{cases} K_{max} - K_{min}, & K_{min} + K_R \geq 0 \\ K_{max} + K_R, & K_{max} + K_R \geq 0\ and\ K_{min} + K_R \leq 0 \\ 0, & otherwise \end{cases}$$

K_{max} and K_{min} represent the maximum and minimum stress intensity factors

K_R is the stress intensity factor due to residual stress

ΔK_{th0} is the threshold range of the SIF at $R_\sigma = 0$, $\Delta K_{th0} = 2.45\ \text{MPa}\sqrt{\text{m}}$

With the assumption of no residual stress, the equation above is plotted in Figure B-4 for various stress ratios except for zero and negative values, with which the effective crack opening ratio is not defined.

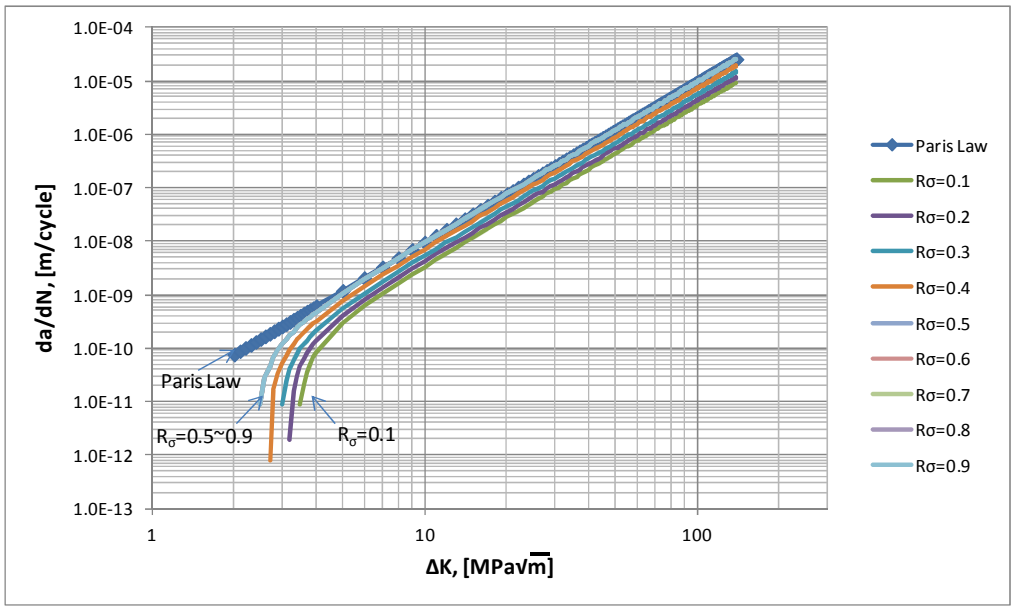

Figure B-4: Crack growth model of Sumi (1998)

In the graph, both of effects from the threshold range of SIF and change of the stress ratio is clearly identified.

B.3 Models with Unstable growth

B.3.1 Foreman's model

An equation to represent a curve covering medium and high range of the SIF to include an unstable condition of crack growth is proposed by Foreman, Kearney and Engle (1967) as below.

$$\frac{da}{dN} = \frac{C \times \Delta K^m}{(1 - R_\sigma)K_C - \Delta K} \quad \textbf{(B-7)}$$

where, ΔK is the range of the SIF

R_σ is the stress ratio

K_C is the fracture toughness of the material

In the Figure B-5 below, the fracture toughness is defined as 140 MPa$\sqrt{m}$ assuming materials of mild steels according to Engineering Fundamentals' Data[3].

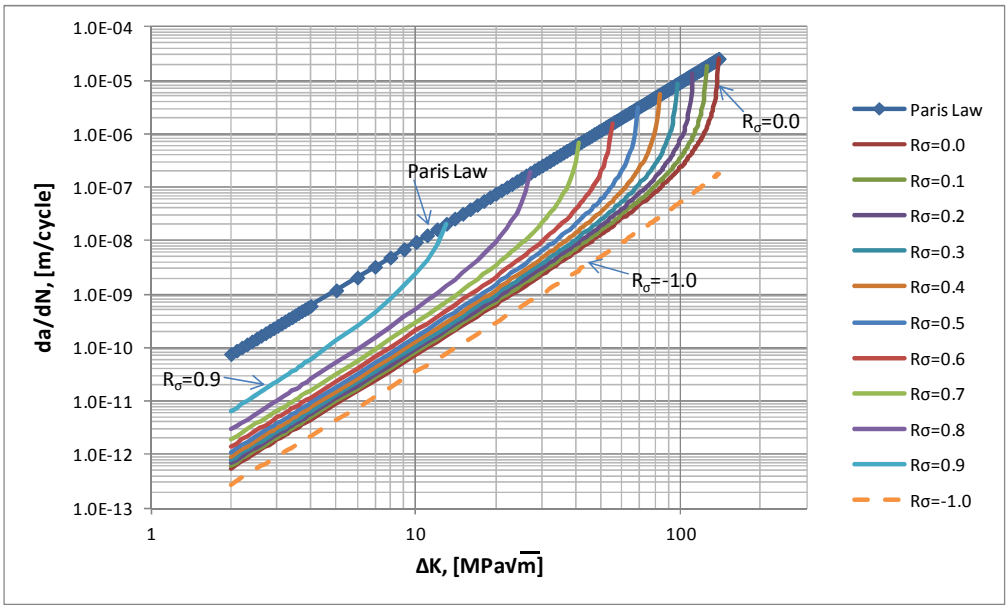

Figure B-5: Crack growth model of Foreman, Kearney and Engle (1967)

B.4 Models including threshold and unstable regions

B.4.1 McEvily's model

A model which combines low, medium and high range of the SIF has been proposed by McEvily and Groeger (1977) including the threshold range of SIF and the material fracture toughness:

$$\frac{da}{dN} = C \times (\Delta K - \Delta K_{th})^2 \times \left[1 + \frac{\Delta K}{K_C - K_{max}}\right] \quad \textbf{(B-8)}$$

where, ΔK is the range of the SIF due to applied loading

ΔK_{th} is the threshold range of the SIF

K_C is the fracture toughness of the material

K_{max} is the maximum SIF due to the maximum loading

[3] http://www.efunda.com/formulae/solid_mechanics/fracture_mechanics/fm_lefm_Kc_Matl.cfm

In the above equation, the threshold range of SIF, ΔK_{th}, is considered to vary as the stress ratio changes. According to Davenport and Brook (1979), the threshold range of SIF is approximated as a function of the stress ratio and the threshold range of SIF at $R_\sigma = 0.0$ as follow. Hence the crack growth model of McEvily and Groeger (1977) can be plotted as shown in Figure B-6.

$$\Delta K_{th} \approx \Delta K_{th0} \cdot \sqrt[3]{(1 - R_\sigma)} \qquad \textbf{(B-9)}$$

The threshold range of SIF at $R_\sigma = 0.0$, ΔK_{th0}, is defined as 2.45 MPa$\sqrt{\text{m}}$ according to Sumi (1998) and the fracture toughness, K_C, is defined as 140 MPa$\sqrt{\text{m}}$ assuming mild steels as in the Foreman's model.

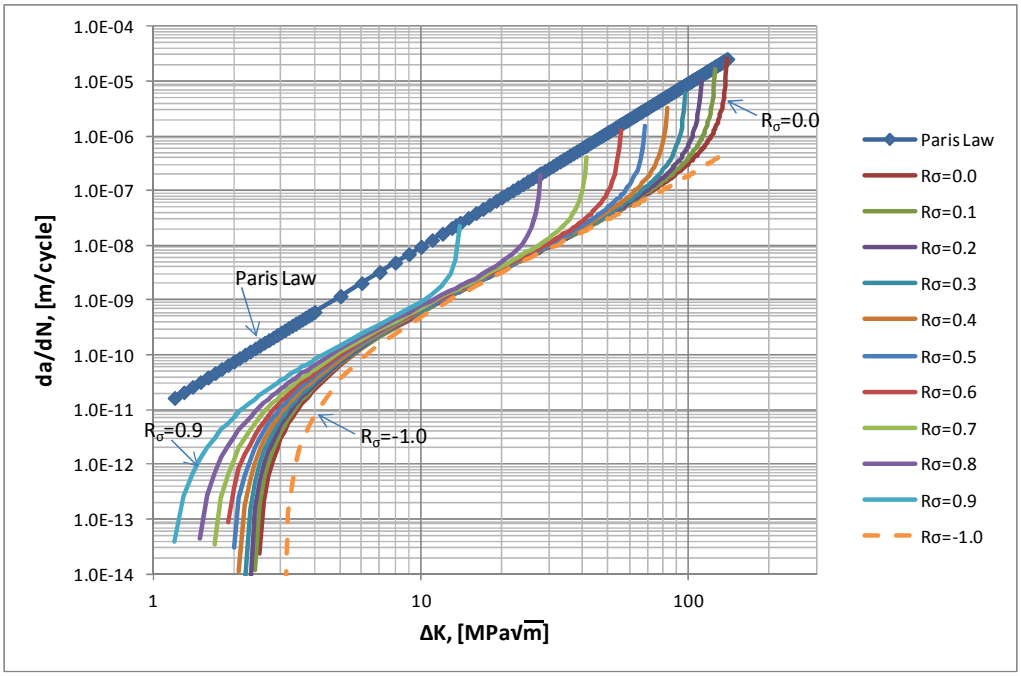

Figure B-6: Crack growth model of McEvily and Groeger (1977)

APPENDIX C. ABAQUS KEY EDITING FOR VCCT

The key editing for implementation of VCCT in ABAQUS should include definition of contact pair of surfaces, definition of initial condition for contact, debonding command in the static analysis with a set of fracture criterion as shown below. A command line start with a single asterisk (*) while a line starts with double asterisk (**) is for comment.

*** INTERACTION PROPERTIES**
***Initial Conditions, type=contact**
***Slave_surf, Master_surf, Slave_nodes**
Surface Interaction, name=IntProp-1
1.,
Friction, rough
**
** BOUNDARY CONDITIONS*
** INTERACTIONS*
** Interaction: Int-1*
***Contact Pair, interaction=IntProp-1, small sliding**
***Slave_surf, Master_surf**
**
** STEP: Step-1*
Step, name=Step-1, inc=1000
Static
0.05, 1.0, 1e-06, 1.0
***Debond, Slave=Slave_surf, Master=Master_surf**
***Fracture Criterion, Type=VCCT, Mixed Mode Behavior=Reeder**
***9.0e4, 9.0e4, 9.0e4, 1.75**

These lines should be added in Interaction Properties section in order to define initial conditions for contact

These lines define a contact pair of surfaces between which a crack would

These lines should be added in Step (static) section in order to allow debonding w.r.t. the defined fracture criterion

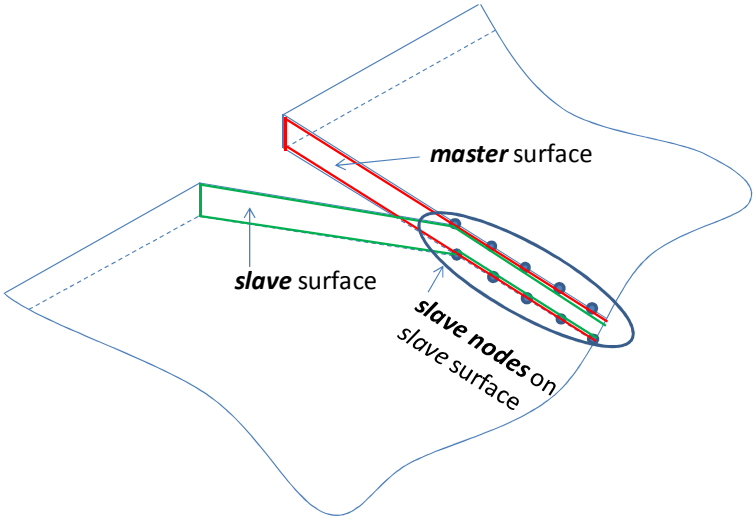

Figure C-1: Defining contact surfaces (master and slave) and slave nodes